Therapeutic Efficacy of a Co-Q10 Analogue in Combating Cachexia and Mortality Induced by Gold-Standard Paediatric Chemotherapy Regimens

By

James Sorensen

BSc (Hons)

Victoria University

A thesis presented in total fulfilment for the Degree of Doctor of Philosophy

College and institute details

Victoria university

Melbourne, Australia

Submitted July 2020

Abstract

Chemotherapy is an effective first-line treatment against cancer; however, it induces a myriad of serious sequalae, including skeletal muscle dysfunction and wasting (SMDW) and fatigue, which we hypothesise is underpinned by mitochondrial dysfunction. When chemotherapy-induced (CI) SMDW is instigated in childhood, it often endures and manifests over the lifespan resulting in exacerbated morbidity and, in some cases, mortality. Despite much research having investigated individual chemotherapeutic agents and their effect on the skeletal muscle in mice (including our own), these models failed to evaluate the potential interactions between agents in a poly-pharmaceutical regimen, or, the effects of long-term and multi-staged chemotherapy regimens like that used in hospitals world-wide. Therefore, this thesis investigated the impact that gold-standard chemotherapy regimens used to combat the three common childhood cancers: acute lymphoblastic leukaemia (ALL), non-Hodgkin's Burkitt lymphoma (NHBL) and medulloblastoma, on the skeletal muscle system in healthy juvenile mice and monitored the effects of treatment endured over the lifespan.

After establishing pre-clinical animal models for three gold-standard chemotherapy regimens, we showed that, regardless of regimen, eight weeks of treatment to four-week-old mice induced considerable skeletal muscle dysfunction which was characterised by significant muscle weakness, fatigability and, in 2 of the 3 regimens, lean mass loss. Although the age of onset of these sequalae were variable (varying between eight-weeks and 30-weeks of life), mitochondrial dysfunction was evident, identifying a point for therapeutic intervention. As such, we investigated the efficacy of daily Idebenone treatment (a powerful antioxidant and mitochondrial Co-Q10 analogue) against mitochondrial dysfunction and thus CI-SMDW. Idebenone co-therapy greatly improved mitochondrial performance in chemotherapy-treated mice, as well as protecting against lean mass loss and improving overall strength in the more aggressive chemotherapy regimen used against NHBL. Moreover, Idebenone co-therapy was shown to completely abate chemotherapy-induced mortality in the NHBL regimen, reducing mortality from 77% to zero.

This thesis shows that childhood chemotherapy, regardless of the aggressiveness of the regimen or the classes of drugs used, induces life-long SMDW which is likely contributed to by mitochondrial dysfunction. The mitochondrial targeting therapeutic, Idebenone, shows

promising potential for clinical application against the SMDW sequalae and mortality induced by some regimens, with the potential to improve childhood chemotherapy patient outcomes and survivability.

Declaration

I, James Sorensen, declare that the PhD thesis entitled “Therapeutic Efficacy of a Co-Q10 Analogue in Combating Cachexia and Mortality Induced by Gold-Standard Paediatric Chemotherapy Regimens” is no more than 100,000 words in length including quotes and exclusive of tables, figures, appendices, bibliography, references and footnotes. This thesis contains no material that has been submitted previously, in whole or in part, for the award of any other academic degree or diploma. Except where otherwise indicated, this thesis is my own work.

James Sorensen

July 2020

Acknowledgements

After writing close to 400 pages to encompass the achievements of over 4 years of work, the words required to express the level of gratitude and thanks that I have for a few are difficult to come by – as there is nothing I could write here which would adequately express my level of appreciation and thanks. But, I'll give it a go.

First, to my supervisors Doctor Emma Rybalka and Professor Alan Hayes, it seems like an age ago that I was sitting in your undergraduate classes in the Biomedical Science course out in Building 4. The journey you have both guided me on since then is astounding and is something I would have never dreamt possible only 10 years ago. Your on-going professional and emotional support, unwavering encouragement and belief, inspirational wisdom and valued friendship has made the near infinite number of impossible challenges (which always managed to arrive at the most inconvenient time); possible. You have made the whole process exceedingly rewarding, enjoyable, character defining and unforgettable. I feel incredibly privileged to have learnt from the both of you. Thank-you.

Secondly, to my friends and colleagues Doctor Cara Timpani and soon-to-be-doctors Dean Campelj and Danielle Debruin, the shared coffees, early mornings and late nights, mouse bites, failing seahorses, temperamental myographs and westerns, laughs and tears, and enduring friendships; we've shared all the low's and high's that research has to offer and I thank you from the bottom of my heart – you have made this possible.

Thirdly, I would like to thank Victoria University for not only giving me the opportunity to undertake my PhD, but also for funding both my research and my top-up scholarship. To the Australian Institute for Musculoskeletal Sciences (AIMSS) for generously providing on-going support as well as funding through their seed grant scheme, and to Santhera Pharmaceuticals for their substantial donation of Idebenone. Without these organisations and institutes, this thesis would not have been possible.

I would also like to acknowledge and thank the Institute for Health and Sport, and the Office for Researcher Training, Quality and Integrity for the on-going administrative, financial and educational support that you have given myself and my supervision team over the years. I would also like to thank the staff at the Australian Institute for Musculoskeletal Sciences and

the Western Centre for Health Research and Education for their on-going support and friendship – it has been a remarkable experience working with you all. I would also like to offer a special thank you to Associate Professor Neuri Gueven from the University of Tasmania, Doctor Joshua Johnson from Victoria University, and Associate Professor Rachel Davey's laboratory group and Doctor Craig Goodman at the University of Melbourne for their varying levels of support in developing and/or performing the methods used within this thesis.

To my friends, and family, who nodded encouragingly every time I have waffled on about my research and supported me every time I've skipped a family event, or been unable to attend any one of the 1000 things that I've missed to finish this thesis – thank you, I have treasured your support, understanding and encouragement every step of the way. Last, but certainly not least, to my love, best friend and fiancé Charlotte, I cannot thank you enough for your support. From me postponing our first ever date on the night of, because one of my mice was dying, to the countless dinners you've brought me in the study whilst I've worked away into the early hours of the night, how you've supported me when I've been unable to do things with you (even though I'm sure you wished otherwise), the supportive shoulder, the understanding nods, the incredible advice and support, the sacrifices you've made to help me on my way, and how you continue to support me through my medical degree (it's almost over I promise!!); I could not imagine what my life would be without you. You make me better in every way.

Table of Contents

List of Figures

List of Tables

List of Abbreviations

ΔΨ	mitochondrial membrane potential
µCT	micro-computed tomography
[ ]	concentration
AIHW	Australian Institute of Health and Welfare
ALL	acute lymphoblastic leukaemia
ALL-POMP	ALL-indicated purinethol, oncovin, methotrexate and prednisone combination therapy
ALT	alanine transaminase
ANOVA	analysis of variance
AST	aspartate transaminase
ATP	adenosine triphosphate
AUC	area under the curve
AWO	animal welfare officer
BL-CHOP	NHBL-indicated cyclophosphamide, doxorubicin (Hydroxydaunorubicin), vincristine (oncovin) and prednisone combination therapy
BMI	body mass index
CCG	Children's Cancer Group
CCNU	lomustine
CDDP	cisplatin
CI	chemotherapy-induced
CPM	cyclophosphamide
D	day
DI	delayed intensification
DiH2O	de-ionised water
DNA	deoxyribonucleic acid
DOX	doxorubicin
DPX	Dibutylphthalate Polystyrene Xylene
DSM	dissociation media
EFS	event-free survival
ETC	electron transport chain
FBE	full blood examination
FBS	foetal bovine serum
FCCP	carbonyl cyanide 4-(trifluoromethoxy)phenylhydrazone
FDA	Food and Drug Administration (United States of America)
FDB	flexor digitorum brevis muscle
H&E	Haematoxylin and Eosin
IAMDF	Intervention animal model development framework
IM	incubation media
IMM	inner mitochondrial membrane
IPGTT	intraperitoneal glucose tolerance test

LCV	lomustine, cisplatin and vincristine combination therapy
LFT	liver function test
m.	muscle
MB	medulloblastoma
MB-LCV	MB-indicated lomustine, cisplatin and vincristine combination therapy
MCH	mean corpuscular haemoglobin
MCHC	mean corpuscular haemoglobin concentration
MCV	mean corpuscular volume
mtDNA	mitochondrial deoxyribonucleic acid
mtROS	mitochondrially produced reactive oxygen species
n.c	not calculatable
n.s	not statistically significant
NADPH	nicotinamide adenine dinucleotide phosphate
nDNA	nuclear deoxyribonucleic acid
NHBL	Non-Hodgkin's Burkitt Lymphoma
OCR	oxygen consumption rate
OCT	optimal cutting temperature
OXA	oxaliplatin
PARPs	Poly-ADP-ribose polymerases
PCR	polymerase chain reaction
PLA	plantaris muscle
PRED	prednisone
PTA	phosphotungstic acid
QUAD	quadricep muscles
RBC	red blood cell
RMANOVA	repeated measures analysis of variance
ROS	reactive oxygen species
RR	relative risk
SD	standard deviation
SFOP	*Française d'Oncologie Pédiatrique*
SMDW	skeletal muscle dysfunction and wasting
SOL	soleus muscle
TA	tibialis anterior muscle
UA	unavailable
UKCCSG	United Kingdom Childhood Cancer Study Group
V or VEH	vehicle treatment group
VCR	vincristine
VEH	vehicle
w/v	weight to volume ratio
WBC	white blood cell
WCC	white cell count

Chapter 1

Chemotherapy-Induced Skeletal Muscle Dysfunction and Wasting in the Paediatric population

Sections of this chapter has been published in The Journal of Cancer, Chemotherapy and Pharmacology [1]

1.1 Introduction

With a mortality rate of approximately 58%, cancer is one of the leading causes of death worldwide resulting in the loss of over 8 million lives a year [2]. Within Australia, 1 in 2 persons will develop cancer before the age of 85 with an estimated 150,000 cases to be diagnosed per year in 2020 [3,4]. Although less than 1% of these cases will be children aged 1-14 [3], cancer is still the leading cause of non-accidental death within this subgroup [5]. Over the past 20 years, the 5-year relative survival rate for children for all cancer types has improved from 68% for 1983-1989 to 81% for 2004-2010 with survival rates continuing to improve to this day [6]. This improvement in survival can be directly attributed to advancements in early detection and more advanced treatment methods, such as individualised supportive care and more efficacious anti-cancer drugs to name a few. However, although immediate side effects of these treatments are well categorised, the long-term side-effects of these newer treatments are not well understood [7]. Of these, chemotherapy is the leading intervention and the most effective aside from surgical resection when a completely resectable tumour is identifiable [8,9]. Chemotherapy elicits its anticancer effect by attacking replicating cells, generally by halting DNA replication [10]. But, due to their non-specific mode of action, chemotherapeutics also attack healthy cells, halting the cellular replication process and hindering normal growth [11] which is of particular detriment to the growing child.

To fully appreciate the broader health risks incurred by childhood chemotherapy and its negative effect on the normal physical growth of a child (described in more depth in *S1.3*), three long-term health outcomes have been identified for use: health status, mortality and morbidity [12]. Of these, both health status and mortality have been well investigated [12-16]. For example, a 2003 study investigating the health status of 9535 U.S. adult childhood cancer

survivors showed 44% of survivors indicated 1 or more health domain(s) (general health, mental health, functional status, activity limitations, cancer-related pain, and cancer-related anxiety/fears) being moderately or severely affected [16]. For mortality, a 2012 study by the Australian Government showed that the 5 year survival rate of Australian children between 0-14 years of age was 81% from date of diagnosis, compared to 99.99% for the healthy cohort [6] highlighting a severe decline in the survivability of childhood chemotherapy patients. Of those that survive chemotherapy treatment, morbidity within this cohort is greatly increased, with 70% of survivors developing chronic disease later in life [17]. Survivors are also 8 times more likely than their siblings to develop severe or life-threatening chronic health conditions, such as myocardial infarction, congestive heart failure, premature gonadal failure, secondary cancers and severe cognitive dysfunction [7,12,18-20]. Growing evidence also suggests that normal skeletal muscle growth and repair processes are compromised by chemotherapeutic treatment, which can manifest into chronic chemotherapy-induced skeletal muscle dysfunction and wasting (CI-SMDW) throughout the lifespan, culminating in reduced strength, endurance and mobility [18,19,21,22]. Early childhood skeletal muscle growth is hyperplastic (i.e. new muscle fibres are generated by mitosis), with the final muscle fibre number set by approximately 7 years of age, after which muscle fibres only grow in size (i.e. hypertrophy) through the absorption of newly divided muscle precursor cells (refer to *S1.3.2*). Our research group has previously hypothesised that mitotically active skeletal muscle growth, whether hyperplastic or hypertrophic, is inadvertently targeted by chemotherapeutics to reduce or completely arrest cellular proliferation and thereby reduce the overall mass, quality and function of the skeletal muscle system for life [11,18,19,22,23]. These long-term dysfunctions greatly reduce the child's capacity to respond successfully to future treatments – or be fit enough to receive treatment at all – if indeed the cancer relapses (due

to a reduction in lean tissue mass). Moreover, a loss of lean mass is directly linked to reductions in quality of life both during and after treatment; which is attributable to the child's shortcomings of muscle strength, endurance and recovery [11,22,24].

Currently, CI-SMDW is "treated" in the clinic via maintenance of a higher dietary protein intake [25,26], although this is not possible in all patients and has not been established experimentally as being protective against this form of skeletal muscle mass loss. Overall, the current recommended treatment protocols to combat CI-SMDW are far from clear – such as exercise and pharmacological recommendations by key opinion holders which vary greatly in their approach [27-32] – and are underscored by the lack of understanding of the mechanisms that underpin it. This lack of understanding is exacerbated by the complexity of, and variance in, the types and locations of cancer that exist and the children that the cancers exist within. Complicating efforts to isolate the sequalae associated with CI-SMDW is the complex pathology of cancer cachexia itself, which, through its own means, induces lean mass loss [33] (refer *S1.2.3*). Further, as there is no one gold standard of chemotherapy drug or treatment regimen, physicians use a plethora of different chemotherapeutic agents with differing modes of action and toxicity, in varying combinations, dosages, administrative timings and delivery methods, and in combination with or separately from radiotherapy and/or surgical resection; with all of these variations having the capacity to affect the body (refer *S1.2.2*). Compared to adults, children also experience the most severe levels of detriment to the musculature from chemotherapy when administered during their childhood, suggesting that their active-growth status primes their susceptibility to chemotherapy toxicity [34]. As such, an understanding of the mechanisms that lead to paediatric CI-SMDW would be beneficial for the development of therapies that could be applied to patients during chemotherapy, regardless of the regimen they receive.

This chapter will first explore the aetiology of paediatric cancer and the most common cancers that plague children. The known physical side-effects of cancer treatments will then be explored, concentrating on the detrimental effects that chemotherapy has on the skeletal muscle. Key areas of research interest within this area will then be discussed with the aim of summarising the known mechanisms which underpin CI-SMDW in the childhood cancer patient and survivor. Afterwards, prospective areas for therapeutic intervention against CI-SMDW will be reviewed, followed by an evaluation of previously published experimental models within which their efficacy against CI-SMDW can be investigated. For this thesis, children who have been diagnosed with cancer or who are undergoing treatment for cancer will be referred to as patients. Patients who have survived the original cancer incident (defined as a 5-year event free survival (EFS) and inclusive of relapse patients) will be referred to as a survivor.

1.2 Paediatric Cancer and Cancer Cachexia

1.2.1 Endogenous and exogenous causes of paediatric cancer

A large majority of cancers today are linked to risk factors associated with lifestyle choices – such as obesity, smoking, alcohol and sedentariness – and involuntary carcinogenic exposure [35]. These associations with cancer development serve to assist our understanding of why adults develop cancer at a rate of close to 1 in 2 [35]. However, most paediatric cancer patients have rarely had the opportunity to experience these risk factors. Behind these environmental oncogenic perpetrators, lay a more complex and hidden landscape of cancer inducers. With the advancement of genetic science, the interplay between proto-oncogenes, such as *BRCA1*, *MYC*, *RAS* and *WNT* genes, and tumour suppressor genes, such as the *p53* gene, has provided some back story as to why humans are especially susceptible to cancer and, in some cases, why we are destined to develop cancer before we are even born [36-39]. These proto-oncogenes, however, need to be switched on to have an oncogenic effect [40] rather than being oncogenic to begin with [41-43]. Conversely, tumour suppressor genes must also be first switched off for neoplastic growth to be initiated and maintained within the body [44,45]. This theory has been substantiated in congenital twin studies where the major contributing factor for cancer development in this cohort was shown to be environmental factors, rather than by genetically inheritable means [46,47]. Considering that genetically identical twins can have considerably different phenotypic outcomes (which are largely dependent on the environments that they grew up in) [46,47], concentration should lie on the factors that control genetic deciphering, rather than the genetic code itself. These factors are known as epigenetics. Nawrot *et al* [48] eloquently described epigenetics as "the conductor who

interprets the unchanging musical score (our genetics) and then in turn controls its symphonic performance (phenotypic outcome)". In normal circumstances, epigenetic regulation does not lead to oncogenic outcomes, rather, it is the combination of anomalous epigenetics in combination with the presence of proto-oncogenes which results in neoplastic growth. Similarly, the presence of oncogenes does not necessarily result in the development of cancer [49,50]. Epigenetics thus play an obligatory role in the development of paediatric cancer. It should be mentioned, however, that regardless of epigenetics, the risk of developing cancer is significantly increased with genetic inheritance of specific proto-oncogenes [51]. Inheritance is only associated with an increased risk and not a definite result. Thus, the question then remains, if proto-oncogenes are required to be activated and tumour suppressor genes deactivated, together with abnormal performance of epigenetics, what mechanisms are causing these alterations? There are two major theories which serve to answer this question: chance [52-55] together with, or independent of, environmental factors [55,56]. In terms of chance, due to the intricacies of biological mechanics and the highly choreographed nature of cellular replication (and indeed the replication of genetic information), there lays a considerable number of opportunities for abnormalities to occur throughout our lifecycle. Endogenous abnormalities can come to fruition in many forms, varying from cellular level errors such as failed protein folding [57,58] and mistakes in DNA replication [59-63] to larger more systemic problems like errors with inflammatory processes [64-66] and the immune system [67-69]. These endogenous blunders are thought to contribute to the alterations which lead to changes within our genetic and epigenetic systems which ultimately enable carcinogenesis to occur independent of exogenous insults. Conversely, exogenous insults from our own surrounding environments can both initiate and exacerbate endogenous abnormalities which can consequently drive carcinogenesis. In terms of childhood cancer, many lifestyle related

diseases that drive carcinogenesis in adults (such as obesity, type-II diabetes, cardiovascular disease, smoking, alcoholism etc.) are generally not developed by children, at least until their adolescent years. Recent studies have made clear indications though that parental lifestyles can negatively affect prenatal development. Parental smoking for example, regardless of whether maternal ingestion of smoke is primary or secondary in nature during pregnancy, has been shown to increase the unborn child's risk of developing cancer [70-73]. A plethora of maternal lifestyle choices have also been linked to increased prenatal cancer risk [74,75], such as alcoholism [76] and meat consumption [77,78]. Further risk factors, such as pre-conception exposure to radiation [79-83], teratogenic and toxic chemicals [84-86] , air pollution[87,88] and low socio-economic status [89] have also been shown to increase the risk of childhood cancer, regardless of which parent is exposed.

With such a complex series of carcinogenic factors, all of which can interact and modify the outcome of the other, the exact cause of paediatric cancer is still elusive. Although a plethora of risk factors have been identified, the cause of paediatric cancer can be said to be generally prenatal – or even preconception – in nature, which, after genetic mutations have been created through endogenous or exogenous means, result in the malfunctioning of vital biological processes which results in cancerous neoplastic growth.

1.2.2 Most common paediatric cancers and their treatments

Although a child in the developed world has a small chance of developing cancer (0.23% in the US before the age of 14) [55], the impact cancer has on a child and their family's life is immense. 1 in 5 children will not survive 5 years from diagnosis [6] and, with most children being diagnosed before the age of 15, the impact of cancer-related morbidity (and mortality) which these children live with for the rest of their life is considerable [55]. In 2009 in the US, 153,390.4 years of potential life was lost due to childhood cancer [90]. Important here is that the most common paediatric cancers: central nervous system (CNS) tumours, leukemias and non-Hodgkin Burkitt lymphomas, accounted for approximately 60% of the total years lost by this demographic [55,91,92]. In the case of survival, 44% of survivors will report serious negative side effects, including a significantly increased relative risk of developing secondary cancers, over the lifespan [16]. Often these morose statistics can be attributed to the interventions used to treat the cancers, rather than the side effects of the cancers themselves [13,22,93-96]. However, the side effect profile of each cancer and its correlated treatment is dependent on the cancer's pathology and the mechanisms which underpin the interventions. Fortunately, if diagnosed early and appropriate treatment commenced, most non-invasive paediatric cancers can be effectively managed.

Aside from surgical resection, chemotherapy is the leading treatment against cancer [97] with distinctive chemotherapeutics required to treat different cancers, due to their unique mechanisms of anti-mitotic action and the differing physiological profiles of the cancers themselves (refer Table 1.1). For example, alkylating agents irreversibly damage cellular DNA (either nuclear or mitochondrial) by interfering with base pairing, preventing repair and

replication, arresting the cell-cycle and inducing cell-death [98,99]. Whereas antimetabolite agents block the formation of DNA building blocks, thus, blocking the DNA replication process resulting in the same outcome [100-102]. Mitotic inhibitors such as vinca alkaloids, on the other hand, interfere with cellular mitotic machinery blocking the cell division process and inducing cell death: for example, vincristine inhibits centromere action inhibiting cytokinesis [103,104]. Moreover, the anti-tumour antibiotics, for example, have been used for over 50 years to treat a number of different cancers including leukaemia, prostate, ovarian, lung and breast [105,106], with doxorubicin hydrochloride (Adriamycin®)— an anthracycline with limited therapeutic tolerability and efficacy due to its highly toxic effects on the heart—used extensively to treat solid tumours [107,108]. Being one of the oldest and most widely used of the chemotherapeutics, Doxorubicin's mechanism of action and side-effects are widely researched and reported. A number of mechanisms of action have been proposed to explain the effective neoplastic, cytotoxic and cytostatic nature of doxorubicin, which include: (1) DNA intercalation thus inhibiting protein biosynthesis and affecting transcription processes [109,110]; (2) free radical formation resulting in cellular damage and apoptosis signalling and/or necrosis [111-113]; (3) inhibition of topoisomerase II [114], an important nuclear DNA transcription enzyme; and (4) intrinsic mitochondrial apoptotic signalling [115].

Due to the uncontrolled replicative nature of cancer, agents which inhibit replication offer high therapeutic yield and, as such, chemotherapy is often the only required anti-neoplastic intervention when multiple chemotherapies are used in combination. An exception to this is CNS tumours, where radiotherapy is often used in conjunction with chemotherapy and surgical resection to abolish the tumour. CNS tumours are extremely variable in location and cell-line origin and can be either benign or malignant [116]. Medulloblastoma is the most common malignant childhood CNS tumour [116-119] and is an

abnormal embryonal manifestation of neuronal cell differentiation which often metastasises via the cerebral spinal fluid [120]. The majority of medulloblastomas manifest from the inferior cerebellar vermis, in the posterior fossa of the cranium, where it typically spreads through to and fills the fourth ventricle [116,121,122]. Due to the accessible location of this type of cancer, surgical resection is the front-line treatment, usually followed by cranial irradiation and/or chemotherapy which can cross the blood brain barrier, such as lomustine (a nitroureas alkylating agent), to consolidate removal of the primary tumour and metastases [123,124]. Comparably, surgical resection is a front-line treatment for non-Hodgkin's Burkitt lymphoma (NHBL) as this form of cancer often manifests as a large single tumour [125]. Paediatric NHBL is a rapidly growing cancer of mature B-lymphocytes, with patients usually presenting with high-grade abdominal, head or neck tumours [126]. Due to the aggressive nature of this typically paediatric cancer, suitably aggressive short-cycle high-dose chemotherapy regimens, sometimes supported by targeted irradiation therapy, are used for treatment [127,128]. Similarly, acute lymphoblastic leukaemia (ALL) is a malignant disease of the immune system – in this case genetic mutations of B- and T-cell progenitors resulting in proliferation of immature leukemic blast cells – which peaks in incidence in children between 2-5 years of age [129-131]. As the ALL pathology involves blood cell precursors, chemotherapy is the front-line treatment, with the aim of abolishing all leukemic blasts prior to their maturation [132]. Until recently, in instances where CNS involvement was present, cranial and spinal irradiation was used with promising effects, however, significant impact on the long-term neurological health of the patient was prominent [133-135]. Further advancements in paediatric-ALL treatment (particularly through the work of St Jude's Children's Research Hospital [136]) has since seen irradiation largely replaced by intrathecal chemotherapeutic administration which offers improved long-term patient outcomes. Regardless of cancer, however, the alkylating agents, anti-tumour

antibiotics and antimetabolites usually form the basis upon which combination chemotherapeutic regimens are built, as all cancer cells require DNA replication for neoplastic growth to occur and these agents target that process.

Anti-cancer intervention, however, is not without the risk of significant side-effects. Surgical resection, for example, has its obvious potential for sequalae (such as nosocomial infection, surgical error, anaesthetic complications etc). Especially when used against CNS cancers, cranial and spinal irradiation too poses significant risks. Irradiation is similar to chemotherapy in that it causes irreparable and indiscriminate cellular DNA damage in its target field [137]. As such, it damages all cells, both healthy and malignant, within the line of therapy. CNS radiation has been observed to induce lifelong neurological and intellectual disabilities even at the lowest effective doses [138,139], with rates of close to 100% when irradiation is used in children under 7 years of age [140]. Chemotherapeutics, on the other hand, are the gold-standard where multiple or systemically homogenous targets exist, such as malignant metastasis, non-tumour cancers (such as haematological cancers) or multi-loci cancers (such as those which involve the lymphatic system), due to their indiscriminate action and systemic mode of delivery. As malignant cancers often have the capacity to metastasise, whether they are observable or not, chemotherapy is often used to 'mop up' any unobserved metastasis', blood born or systemic cancers, or any residual cancer cells which remain in the primary loci after surgical removal of the tumour.

Although effective, chemotherapies exert a multiplicity of acute and chronic side effects that greatly increase both morbidity and mortality in the paediatric cancer patient. As the primary mode of action of these agents are to inhibit the cell-cycle, any healthy cells undergoing cellular replication during their administration will also be inadvertently targeted.

The skeletal muscle, particularly that in children, falls under this highly replicative category as the organ relies on specialised cells which replicate to achieve muscle growth, muscle mass maintenance and muscle repair. Any anti-mitotic insult here results in devastating effects to the patient. Although the more detailed components of the chemotherapy-muscle relationship will be discussed in *S1.3* below, it is important to recognise CI-SMDW as a devastating side effect of chemotherapeutic treatment on multiple organ systems with significant long-term clinical implications (for more refer to [11,18,93,141-145]). Although body surface area is used to determine initial dosage, measures of lean mass are often used as a determining factor for chemotherapy dosage, frequency and overall patient survival, a loss of muscle mass diminishes treatment options for the patient and considerably reduces patient outcomes [146-149]. Moreover, chemotherapy-induced loss of muscle mass strongly and negatively impacts patient quality of life through the loss of muscle strength, endurance and recovery capacities and, ultimately, patient independence [14,18,22,93,150,151]. Unfortunately, for the patient, cancer, and the very therapy that is used to treat it, have both been shown to initiate the loss of skeletal muscle, further exacerbating the CI-SMDW phenotype.

Table 1.1: Mode of action and reported side effects of chemotherapy agents from various drug classes

Class of agent	Common drugs	Common treatment	Mode of action	Side effects
Alkylating agents	• Nitrogen mustards (mechlorethamine, chlorambucil, cyclophosphamide, ifosfamide, melphalan) • Nitroureas (including streptozocin, carmustine, lomustine) • Alkyl sulfonates (busulfan) • Triazines (including dacarbazine & temozolomide) • Ethylenimines (including thiotepa and altretamine) • Platinum-based (oxaliplatin, cisplatin, carboplatin)	• Leukemia • Lymphoma • Multiple Myeloma • Sarcoma • Cancers of the breast, ovary, lung and colorectum	Interfere with DNA base pairing, causing strand breaks and preventing replication: • DNA lesion formation • Arrest of DNA synthesis • Inhibition of RNA synthesis	• Anaemia • Impaired spermatogenesis and gonadal function • Nausea and vomiting • General weakness
Anti-tumour antibiotics	• Anthracyclines (daunorubicin, doxorubicin, epirubicin, idarubicin) • Actinomycin-D • Bleomycin • Mitomycin-C • Mitoxantrone	• Wide variety of cancers	Interfere with enzymes involved in DNA replication, preventing replication: • Works at all phases of the cell cycle	• Cardiac dysfunction & toxicity • Nausea and vomiting • Muscle weak
Antimetabolites	• 5-fluorouracil • 6-marcaptopurine • Capecitabine • Cytarabine • Floxuridine • Fludarabine • Gemcitabine • Hydroxyurea • Methotrexate • Pemetrexed	• Leukemias • Cancers of the breast, ovary and GI tract	Block the formation and use of nucleic acids required for DNA replication: • Substitute for nucleic acids of DNA and RNA • Interfere with DNA and RNA growth • Damage occurs during S phase	• Hair loss • General weakness • Nausea and diarrhoea
Topoisomerase inhibitors	• Topoisomerase I inhibitors (topotecan & irinotecan) • Topoisomerase II inhibitors (etoposide, tiliroside, mitoxantrone)	• Leukemias • Cancer of the lung, ovary & GI tract	Interfere with Topoisomerase I and II: • Block DNA separation • Block DNA replication	• Nausea and vomiting • Hair loss • General weakness
Mitotic inhibitors	• Taxanes (paclitaxel & docetaxel) • Epothiolones (ixabepilone) • Vinca alkaloids (vinblastine, vincristine, vinorelbine) • Estramustine	• Leukemia • Lymphoma • Myeloma • Sarcoma • Cancers of the breast & lung	• Interfere with mitosis in the M stage of the cell cycle	• Peripheral and central neuropathy

1.2.3 Cancer cachexia vs chemotherapy-induced lean muscle mass loss

An important distinction needs to be made between the muscle mass loss from cancer versus the loss induced by chemotherapy. On the one hand, muscle mass loss as a sequalae of a pathology, such as cancer, is currently understood as a complex metabolic syndrome characterised by systemic inflammation, on-going loss of muscle and a negative protein and energy balance with or without the loss of fat mass. This pathology is currently described as cachexia (see Figure 1.1). What makes cachexia different from anorexia is that even with nutritional therapy, the loss of muscle mass cannot be completely reversed and irreparable functional impairment of the muscle is often observed [33,152-158]. A key opinion paper by Fearon *et al* [33] has quantified the amount of muscle mass loss in cachexia as a 5% reduction in lean mass with or without the loss of body fat, or a loss of >2% of lean mass when the patient's body mass index (BMI, calculated as weight (kg)/height(m)^2) is below 20 [33]. On the other hand, chemotherapy-induced muscle mass loss has no such clinical definition aside from being a side effect of chemotherapeutic treatment or being misdiagnosed all together and being categorised as cancer cachexia. For example, Fearon *et al* [33] outlined that cancer cachexia should be seen as a continuum, with patients moving from pre-cachexia, to cachexia and then refractory cachexia, with various risk factors exacerbating progression through the stages (refer Figure 1.1). Important here is that the lack of response to anticancer therapy has been identified as a key risk factor to the progression of cachexia, as, if the anti-cancer treatment is successful, treatment will be reduced or ceased all together, the cancer reduced in size or eradicated, and the combined overall cachectic effect of both the cancer and chemotherapy either reduced or abolished. But, if interventions fail, the cancer continues to remain, and treatments (like chemotherapy) increased in dosage and frequency, ultimately exposing the

patient to greater drug toxicities and a greater, overall, combined cachectic effect. In terms of the cachectic effects of treatments, chemotherapy is of the greatest concern due to its systemic mode of administration. An increase in chemotherapy dose will increase the severity (or even presence) of its associated side effects; such as lean muscle mass loss (for a plethora of reasons ranging from the cellular level with induction of muscle cell and organelle damage and/or impairment of cellular energy and signalling systems to impairment of abrogation of systemic growth mediators such as gonadal function and thus sex hormones production) [11,24,141,143,144,159-163] and food intake reduction [164,165]; the very sequalae associated with cancer cachexia.

There is no question that cancer itself can result in a reduction of muscle mass independent of chemotherapy [166]. For example, in one multicentred study; more than 50% of patients diagnosed with non-small cell lung carcinoma were classified as cachectic at the time of diagnosis [167] suggesting considerable body mass loss had occurred prior to any interventions commencing. However, herein lies the problem: cancer cachexia can be investigated independently from treatment in patients, but the side effects of cancer treatment cannot be independently investigated in patients without the cancer being present for obvious ethical reasons. Thus, we are restricted in our capacity to investigate the true effect that chemotherapeutics have on the lean muscle mass in human patients. Of course, it can be argued that any change to the cachectic phenotype once chemotherapy commences could be attributed to the chemotherapy itself. However, this rudimentary reasoning does not answer several key questions; does chemotherapy exacerbate cancer cachexia, or does it induce muscle mass loss via a separate pathway? Is the life-long skeletal muscle dysfunction and mass reduction seen in chemotherapy survivors a result of this exacerbation, or is it a sequalae of the chemotherapy? Pin *et al* aim to answer some of these questions by

investigating the difference in effect of cancer- versus chemotherapy-induced (twice a week combination of 5-fluorouracil (50 mg/kg), leucovorin (90 mg/kg), and CPT-11 (24 mg/kg) via intraperitoneal injection for) cachexia in 8-week adult old mice [168]. Using comprehensive metabolomic investigations, they showed clear differences in system energy substrate utilisation between each of the groups (cancer, cancer+chemotherapy and chemotherapy alone) as well as differing changes in amino acid and fatty acid metabolism. Although an important study which highlights potential differences that underpin cancer- versus chemotherapy-induced muscle mass loss, the model used for these investigations has its shortfalls. Notably, the FOLFIRI regimen used was delivered to mice in combination through injection twice weekly, where, clinically, patients would receive these drugs over the course of 48 hours once per fortnight. Moreover, mice were sacrificed once they had lost 10% of their body weight which is ideal for investigating the molecular changes of the induced cachexia, but not for the long-term mechanisms of CI-SMDW. In any case, a vast number of resources are currently being employed to understand the underlying mechanisms behind cancer cachexia in order to complete the cancer cachexia side of the equation, including preclinical animal models reviewed by Ballarò *et al* from University of Torino which aim to investigate the cancer cachexia (refer [169] for further reading). However, limited efforts have been undertaken to develop our understanding of the mechanisms behind CI-SMDW. As CI-SMDW greatly impacts patient survivability and quality of life, it is important to understand how chemotherapy impacts the muscle which, in doing so, may unlock the answers to treating not only CI-SMDW, but cachexia and other muscle wasting diseases as well.

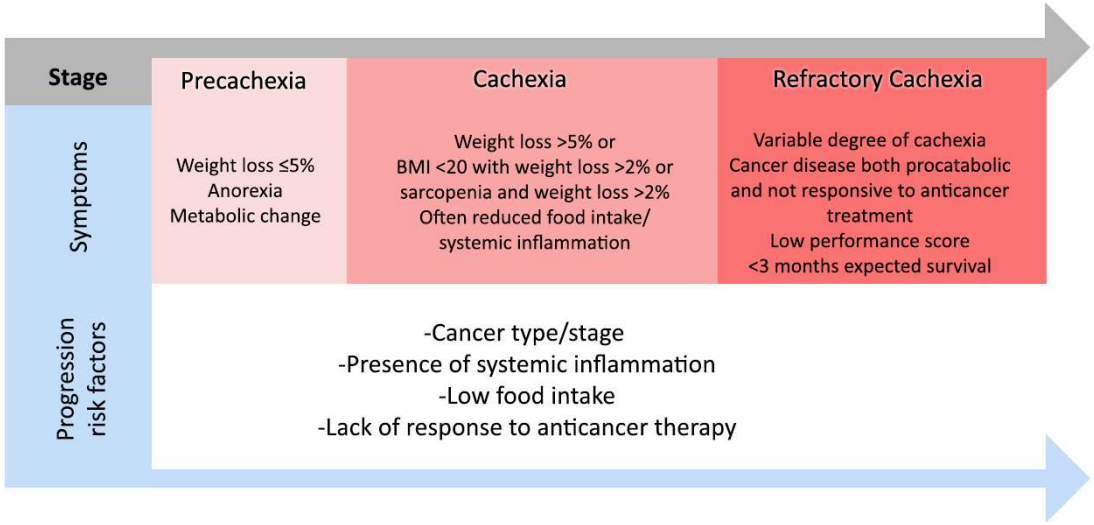

***Figure 1.1: Stages of cancer cachexia*:** Cancer cachexia is a multifaceted pathology which lacks definitive biomarkers to define progression. Clinical signs such as weight loss and muscle mass loss are used as diagnostic factors, however, stage progression is thought to be exacerbated by risk factors such as anticancer therapy. *Adapted from Fearon et al.*[34].

1.3 Chemotherapy, skeletal muscle and the mitochondria: the CI-SMDW pathology

1.3.1 Basic skeletal muscle anatomy and physiology

The skeletal muscle system is a highly plastic and dynamic arrangement which comprises 15-40% of a child's body composition and is continuously undertaking cellular replication to both promote, maintain and repair muscle [170,171]. This is in contrast to adult muscle tissue which is not as highly plastic, and only undertakes replication to repair damaged muscle. [170,171] The primary function of the skeletal muscle system is the production of movement, with secondary functions including temperature regulation, amino acid storage (up to 70% of the body's protein stores) and myokine production [172]. Skeletal muscle is primarily composed of muscle fibres which are bound together by connective tissue. Muscle fibres are contained by a plasma membrane known as the sarcolemma and are comprised of smaller myofibrils which contain the functional component of the muscle, the sarcomere (see Figure 1.2). Myofibrils consist of an array of functional and structural proteins, such as actin, myosin, troponin and tropomyosin, which lay parallel to each other and create contractional force through the intricately choreographed sequence of connecting, pulling and releasing by functional proteins – known as cross bridge cycling (see Figure 1.2) [173-175]. Skeletal muscle contains a homogenous mixture of fast-contracting (oxidative) and slow-contracting (glycolytic) fibres [176]. This variance in fibre type allows a diversity in performance, such as high explosive force, slow maintained force or fine motor skills, with particular performance type being favoured by the increase in one fibre-type over another [177,178]. It is the combination of fibre types, fibre length, total fibre number and fibre size that give variation in overall muscle

performance and function. Throughout the lifespan the demands and stresses on the skeletal muscle system can change in response to a plethora of stressors, stimuli and environmental variables. Thus, skeletal muscle is continuously remodelled, by way of total muscle mass, size, fibre type ratio, vascular supply etc., to adapt to these new demands [178,179]. The amount of total muscle mass, or lean mass, is a key wellness factor positively correlated with good health, survivability and quality of life [1,180]. Lean mass is regulated by several factors, which will be discussed in more depth in later sections, but include nutritional status, physical activity levels, hormonal balance, disease state and other compounding external factors such as drug interactions, which alter the balance between protein synthesis (muscle growth) and protein degradation (muscle wasting).

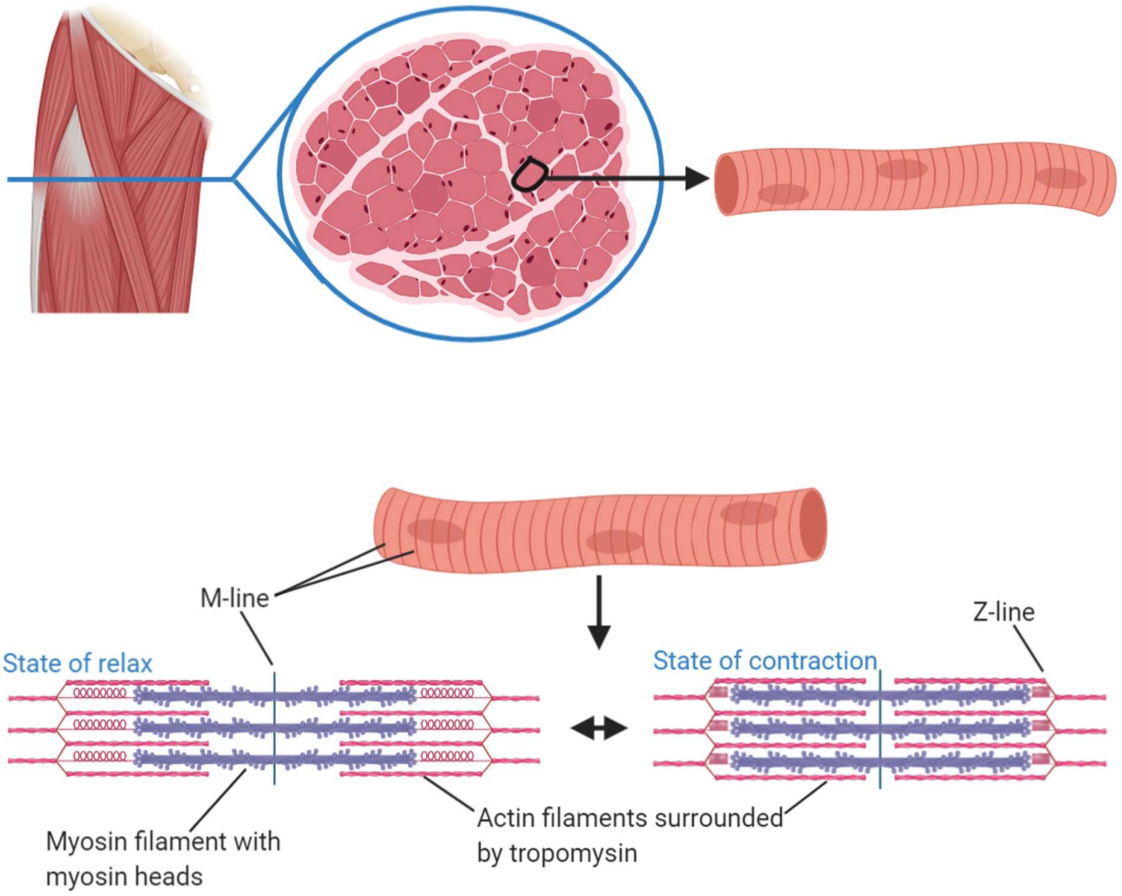

Figure 1.2: Representative image of the skeletal muscle and the muscle contractile unit. *A cross section of skeletal muscle showing its constituent smaller muscle fibres being made up of muscle fascicles. These then contain numerous (middle) individual myofibrils (right) which are contained within connective tissue. Upon contraction, tropomyosin undergoes a conformational change, exposing binding sites on the actin filaments. Myosin heads bind to these binding sites and complete a power stroke essentially pulling the actin filaments (and attached Z-line towards the M-line of the myofibril. This is repeated successively until the contraction stimulus is revoked and is referred to as cross bridge cycling.* [177]

1.3.2 Paediatric muscle: Growth, development and repair

During the formative years of growth, children triple their weight within the first 2 years of life [182] with the greatest rate of skeletal muscle development occurring during these years as new muscle fibres are created [183,184]. It is also during this period that children will experience one of the highest incidence rates of developing cancer in their lifetime, resulting in exposure to anti-mitotic therapies as treatment [185]. This is of considerable clinical significance as skeletal muscle growth is a complex process which is founded on mitotic activity, the very process chemotherapy is designed to stop. Mitotic skeletal muscle growth begins within somites of the newly conceived embryo where the continuous influx and fusion of myoblasts results in an increase in myofibres and myonuclei [186,187]. This process of new myofibre creation is referred to as hyperplastic growth. Briefly, undifferentiated stem cells undergo differentiation into myoblasts (myogenic stem cell) which initially fuse together to create primary myotubes. After this formation occurs, unfused myoblasts begin to aggregate and fuse together to create a secondary myotube using the first as a scaffold. Myoblasts then begin to fuse into the terminal ends of the primary and secondary myotubes, elongating both tubes into myofibres. Lengthening continues as the myofibres are filled with contractile proteins, which inadvertently push the nuclei to the periphery of the myofibre [176,188]. Myofibres continue to lengthen until they attach to tendon cells signifying the appropriate length has been reached – this process is guided by mechanical tension sensed by the structural components of the fibre [189]. Myoblasts stop fusing at the ends of the fibres and instead either begin to create other myotubes or attach to the exterior of the newly built myofibres (more specifically between the sarcolemma and basal lamina [190]) and lay dormant (now referred to as satellite cells) until repair, regeneration or hypertrophic growth is

required [175,191-193] (these processes are explored in more depth in section 1.4.1). For muscle growth to occur at normal rates, suitable numbers of undifferentiated stem cells need to be available. For this to occur, stem cells throughout the ancestral line must complete mitotic replication to maintain the population. Although satellite cells appear to be critical in muscle development, the actual number of quiescent satellite cells vary between fibre types and whole muscles. In general, oxidative fibres express an increased density of satellite cells compared to glycolytic fibres [194]. This process is accompanied by axonal growth, synaptic formation and the creation of neuromuscular junctions all of which are critical for nervous control of muscle growth and function and occurs largely prenatally [195-197].

As chemotherapy halts cellular replication, it is important here to highlight how growth over this period is linked to cellular replication as high levels of satellite cell mediated growth could be severely limited by chemotherapeutic treatment. Several studies have shown that musculoskeletal growth within the first few months of life involves significant increases in cross-sectional myofibre area (through the addition of new myofilaments [198,199]), and longitudinal area (through satellite cell fusion [200,201]). Gokhin *et al* quantified this increase in mice showing a two-fold myofibre number increase, a seven-fold increase in myofibre cross-sectional area, and a four-fold increase in muscle mass within the first 28 days of postnatal life [188,202]. During this initial growth spurt however, a reduction in satellite cell population is observed. Shultz *et al.* [203] measured this reduction in the mouse lumbar muscle showing an immediate decline to approximately 30% of the number of nuclei of the muscle tissue soon after birth, with further reduction occurring until a steady state of 5-6% of the nuclei population is achieved later [203]. This decline continues with age until the final years of the lifespan [188,204,205]. These findings were supported by Oustanina *et al.* [206] who showed that knocking down *Pax7*, a key satellite cell developmental protein, in mice caused a 90%

decrease in satellite cell population during maturation and severely diminished muscle injury repair (as compared to control). Interestingly however, hypertrophic growth in response to mechanical overload has been shown to be largely independent of satellite cell presence [207] indicating that this model of growth may be regulated by other means. These findings, that muscle repair as well as hyperplastic muscle growth are almost entirely satellite cell dependent, give insight into the CI-SMDW pathology, particularly into why symptoms are heightened when experienced in childhood where growth is largely hyperplastic and satellite cell dependent.

As with any growth occurring within the body, environmental factors such as nutritional status, exercise participation, genetics and disease status play pivotal roles on the growth of paediatric muscle [208,209]. The defined risk factors and symptoms for cachexia progression are the antithesis of growth, with poor caloric intake, increased fatigue and increased systemic inflammation all highly detrimental to proper development. With extended bed rest encouraging disuse atrophy and chemotherapy arresting mitotic growth, the paediatric musculoskeletal system stands little chance to develop in cancer patients. Another factor which fuels this multipronged insult is how these treatments and their sequalae interact with the prime energy supplier to the muscle: the mitochondria. As muscle tissue is one of the largest consumers of Adenosine Tri-Phosphate (ATP, the energy currency of the body), the mitochondria play an essential role in skeletal muscle function with the intricacies of this relationship, together with the effects of chemotherapy, being explored in the next section.

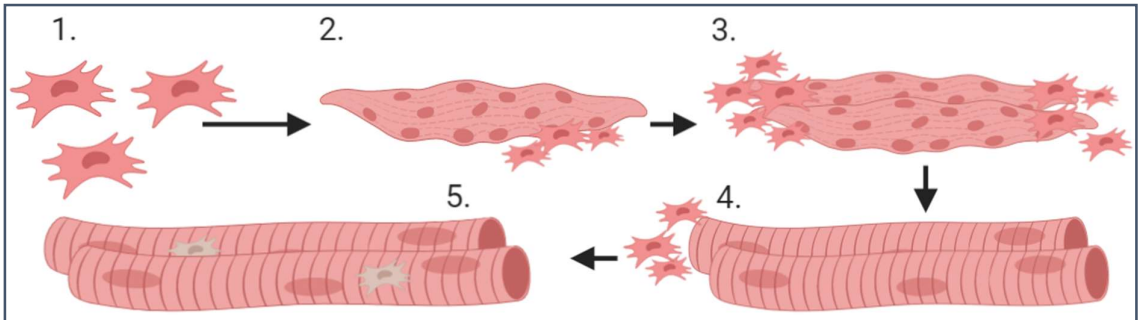

Figure 1.3: Cartoon representation of myofibre development from myoblasts. ***1)*** *Differentiated myoblasts fuse together to form primary myotube 2) Myoblasts begin to fuse together to develop a secondary myotube using the primary myotube as a scaffold 3) myoblasts fuse at the terminal ends of the primary and secondary myotubes which elongates the myotubes into myofibre's 4) Under-sized myofibre's continue to lengthen through addition of myoblasts to terminal ends until the myofibre attaches to tendon cells (not shown) and the intra-fibre mechanical tension increases as a result 5) Once appropriate length has been reached, myoblasts will either create more myofibre's or fuse to the surface of existing myofibre's and lay dormant as satellite cells.*

1.3.3 Basic mitochondrial physiology

The mitochondria are dynamically shaped organelles, capable of forming complex networks, that consist of an inner and outer membrane, with the inner membrane folding in on itself to create a rolling structure with peaks and troughs known as cristae [210-212]. The inner mitochondrial membrane houses numerous respiratory proteins which function together to perform oxidative phosphorylation (OXPHOS). This oxidative process involves the stripping of high energy substrates, such as $NADH^{+}$ and $FADH^{+}$, of their additional electrons which are then used to pump protons across the inner membrane against their electrochemical gradient. The return of protons back across the membrane down the electrochemical gradient then drives the mitochondrial machinery which create cellular energy (see Figure 1.4) [213]. Often referred to as the 'powerhouse' of the cell, the mitochondria play a pivotal role in the

functioning of all living human cells through the creation of this energy in the form of ATP. Even though the mitochondria are essential to cellular physiology, they are only partly controlled by the nucleus of the cell. The mitochondria house their own 16,569 nucleotide pairs in the form of a circular plasmid, which form 37 coding genes and a regulatory region [214,215]. These genes, together with several nuclear genes, encode for all functional mitochondrial proteins, including those which make up the OXPHOS machinery, making mitochondrial function dependent on both systems of DNA. Although a highly important aspect of mitochondrial function, energy production accounts for only a small component of the vast number of functions that the mitochondria have within the cell. In the most recent decade of research, the intricate nature of the mitochondrial-cellular relationship has come to light, highlighting a plethora of two-way interactions between the mitochondria and other cellular organelles and physiological processes. Of these, ATP and ROS production rates [216-219], Ca^{2+} handling and storage [220-222], enzyme function [223-225] and apoptosis [111,226,227] are often mediated by and, at times, completely controlled by the mitochondria [1,220,228,229]. The mitochondria are greatly susceptible to chemotherapeutic-induced DNA damage as the mitochondria rely on single-stranded DNA which does not have the capacity to repair itself. As these mitochondrial functions are innate to skeletal muscle physiology and pathology, the mitochondria share an intricate relationship with skeletal muscle, including regulatory roles of both performance and wasting, which we hypothesise is greatly affected by chemotherapy [1]. These hypotheses will form the foundation of later experimental chapters which will aim to establish and categorise this relationship.

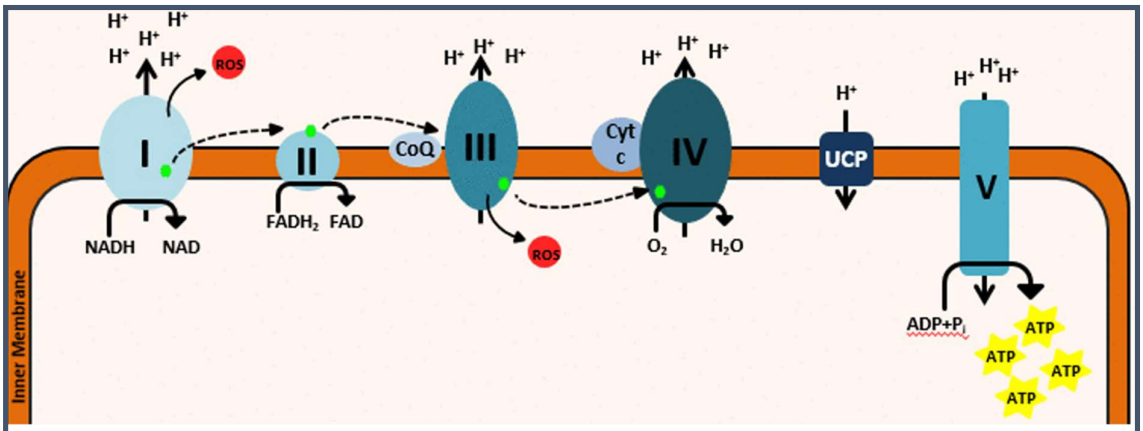

Figure 1.4: **Normal physiological functioning of the mitochondrial electron transport chain (ETC).** Electron carriers NADH and $FADH_2$ deliver high energy electrons to protein complexes 1 and 2 respectively. These electrons then travel down the ETC (with assistance from CoQ10 shuttling electrons from Complex II to Complex III) before being accepted by oxygen at Complex IV which is then converted to water. Proteins I through IV utilise the high energy state of the electrons to drive proton movement from the inner mitochondrial space to the outer mitochondrial space with a small by-product of reactive oxygen species (ROS). After creating a proton gradient across the inner membrane, protons travel down their chemical (and electrical) gradient through complex V which utilises the energy created from this movement to form ATP from $ADP+P_i$. Important to mitochondrial physigology is the presence of uncoupling proteins (UCP) which allow the protons to move down their gradient but bypass Complex V, serving to preserve ADP stores and reduce ATP production.

1.3.4 Potential mechanisms of chemotherapy-induced mitochondrial myopathy

Mitochondria are increasingly emerging as key players in the pathogenesis of a variety of diseases. Due to the highly metabolic nature of the skeletal muscle, mitochondrial density is also high [230], and mitochondrial dysfunction and toxicity can therefore manifest as skeletal muscle-specific symptomatology which include fatigue, muscle wasting, impaired regenerative capacity, pain, exercise intolerance, and sometimes, mild-to-severe neurological symptoms. Indeed, these symptoms have been well documented in chemotherapy-treated cancer patients [18,144,231,232] suggesting that anti-cancer chemotherapy may be non-specifically targeting the skeletal musculature, and perhaps even more specifically, the mitochondria to induce a variety of persistent adverse side effects.

A multitude of chemotherapy agents, such as alkylating agents, anti-tumour antibiotics and antimetabolites (previously described in *S1.2.3)*, target DNA as its primary cytotoxic action. Since nuclear DNA (nDNA) is double stranded and multiple modes of repair are employed to maintain it, it has been hypothesised that the circular, single-stranded and covalently closed nature of mtDNA allows easier intercalation of DNA-targeting chemotherapies, and thus an increased rate of transcriptional error leading to mitochondrial dysfunction [115,233]. Mitochondrial function, and perhaps even more so, mitochondrial dysfunction, is physiologically complex and is modulated by a variety of regulators including the mitochondrial (mtDNA) and nDNA, ROS, nuclear and cellular signalling molecules and ATP production amongst others [233,234]. In the first instance, chemotherapy-induced mitochondrial dysfunction has been associated with elevated levels of mitochondrial ROS (mtROS). It is well established that doxorubicin treatment, for example, causes increased ROS production as a by-product of its metabolism via a redox cycling process unique to the anthracycline class of chemotherapeutics [218,235-238]. Doxorubicin, which has a high affinity for the inner mitochondrial membrane (IMM) [239], accumulates on the matrix side and undergoes a single-electron reduction process at complex I (NADH oxidase) of the electron transport chain (ETC) removing electrons vital to ATP production [240]. This process forms the free radical semiquinone species that reduces molecular oxygen to produce the highly reactive superoxide (O_2^-) molecule and subsequently the less reactive hydrogen peroxide (H_2O_2) molecule [106,235,236,238 241,242]. O_2^- and H_2O_2 collectively constitute the mtROS, which directly increase the state of cellular oxidative stress if not buffered effectively by endogenous antioxidants [239,241,243,244]. Thus, doxorubicin acts via a two-hit mode of action on the mitochondria acting as a powerful reducer when stable, depleting ATP production and

available ATP stores, and as an efficient oxidiser in its semiquinone state, producing excess mtROS. In addition to decreasing electron flow through the ETC and thus decreasing ATP production, the single-strand DNA breaks created by doxorubicin (and indeed other chemotherapies that directly damage DNA) induces the activation of enzymes that can, such as glycosylase enzymes, repair such damage albeit to the detriment of ATP stores [245].

As previously mentioned, an increase in chemotherapy-induced mtROS production is strongly linked to mitochondrial dysfunction and damage. However, mtROS are also thought to function as signalling molecules that activate several proteolytic pathways within skeletal muscle, including caspase-3 and calpain [239,246-248]. These pathways in turn catalyse the release of myofilament proteins, allowing activation of the ubiquitin–proteasome system, and resulting in skeletal muscle degradation [248-250]. Activation of the ATP-dependent ubiquitin–proteasome system is responsible for the muscular degradation seen in homeostatic regulation of skeletal muscle mass and is amplified in many chronic diseases including cancer cachexia and diabetes [223,251,252]. Thus, doxorubicin-induced skeletal muscle atrophy is strongly associated with mitochondrial dysfunction. This dysfunction is a direct result of increased ROS production via drug metabolism as well as that due to nonspecific electron leak from the mitochondrial respiratory chain which is likely induced by mtDNA and respiratory chain protein damage. These negative effects have been the basis of several investigations into chemotherapy-induced myopathies. Adachi et al. [253] have demonstrated strong evidence that the prevalence of mtDNA deletions increases with doxorubicin dosage, and exponentially more so with long-term exposure. In cardiomyocytes, mtDNA deletions could be prevented with co-therapy of the antioxidant and electron carrier co-enzyme Q10 [253], suggesting that the aetiology of mtDNA mutation is via doxorubicin-induced mtROS rather than the doxorubicin semiquinone itself. Long-term doxorubicin treatment induces significant

reductions in skeletal muscle mass, strength, and endurance in cancer survivors (for detailed review, refer to [11]). Scheede-Bergdahl et al. [11] postulated that the molecular basis of these effects was due to the progressive amplification and proliferation of mtDNA mutations. Gouspillou et al. [254] have also demonstrated a reduction in muscle mass and function—thought to be due to an increase in mtROS and a reduction in mitochondrial respiration—in female C57BL/6 mice when treated with four cycles of doxorubicin (with one cycle equivalent to two 10 $mg.kg^{-1}$ doses on days one and five with 3 weeks recovery). However, no evidence of mtDNA damage post-doxorubicin therapy (as detected by long range PCR) was found [254].

Another effective class of chemotherapeutics are the alkylating agents, of which the platinum-based agents; oxaliplatin and cisplatin are used in the treatment of a wide variety of cancers such as lymphoma, medulloblastoma, leukemia, colorectal cancer and sarcoma to name a few.[255-257] Oxaliplatin exerts its antibiotic effects by forming platinum–DNA adducts which efficiently block DNA replication forcing cell cycle arrest and ultimately apoptosis in mitotic cells [255-258]. Both doxorubicin and oxaliplatin — although both inhibiting DNA replication but differing in their precise modes of action — have been shown to negatively affect mitochondrial function [111,112] and to induce deleterious effects on skeletal muscle that clinically manifest as muscle weakness [105,144,259] (refer to Figure 1.6). Gourdier et al. [260] demonstrated that oxaliplatin treatment induces mitochondrial and energy homeostasis dysregulation in colorectal cancer cells, potentially through the direct mutation of mtDNA or via mutation of the nuclear-encoded mitochondrial proteins (refer to Figure 1.5). While this effect is of obvious benefit to the induction of cell death pathways in neoplastic cells, suppression of mitochondrial function and the disruption of energy homeostasis would have detrimental consequences to somatic cells, especially in highly metabolic tissues such as the skeletal muscle. Our group has recently demonstrated that oxaliplatin accumulates within the

mitochondria, and that its administration increases mtROS production, and reduces mitochondrial and muscle cell viability when delivered to mice over a 2 week period [159]. Moreover, we showed in a C2C12 myoblast cell study that oxaliplatin seems to exert immediate but reversible inhibition of key respiratory enzymes, as shown by induction of a metabolic shift towards an anaerobic glycolytic phenotype following acute administration [111]. We speculate that this phenotype shift occurs to buffer the acute suppression of respiratory function that occurs during the transport of oxaliplatin into skeletal muscle, and more specifically, the mitochondria. We speculate that oxaliplatin, specifically the platinum component, is competitively substituted for copper (Cu^{2+}) at receptor sites on the copper transporter 1 (CT1), limiting the availability of the transporter to Cu^{2+} and thereby reducing the mitochondrial Cu^{2+} pool, which is essential for normal complex IV function and oxidative phosphorylation. A study by Lutsenko *et al*. [261] suggests that the mitochondrial Cu^{2+} transporter, COX17, transports Cu^{2+} into the mitochondria and, with the assistance of Sco proteins, incorporates the Cu^{2+} molecule into complex IV. Thus in addition to, or instead of, reducing the mitochondrial Cu^{2+} pool, it is possible that the entire oxaliplatin molecule is incorporated into complex IV with the potential to induce malfunction of electron flow and acceptance by molecular oxygen. An acute effect of oxaliplatin administration thus seems to be inhibition of the mitochondrial respiratory chain. The chronic effects of oxaliplatin treatment, however, seem intrinsically related to mtDNA damage and mutation resulting in gene polymorphisms as per the single-stranded breaks induced in nDNA, rather than due to compounding effects of acute respiratory chain inhibition. As mtDNA encodes for the matrix-residing components of the respiratory chain complexes which are responsible for proton pumping and initial electron transfer, a natural consequence of such damage would be reduced mitochondrial function and increased mtROS production leading to skeletal muscle

atrophy, damage and wasting (refer to Figure 1.5). A recent study by Wisnovsky *et al*. [262] highlighted the capacity for oxaliplatin to induce single-stranded breaks in the mtDNA. The group isolated the nDNA damaging component of oxaliplatin and conjugated it with the N terminus of a mitochondrial-penetrating peptide (mPP). When delivered to ovarian cancer lines, the oxaliplatin-mPP molecule localised solely within the mitochondria and induced mtDNA mutation, followed by mitochondrial death, and the induction of cellular apoptosis. Wisnovsky *et al*.'s data, combined with our own, show that oxaliplatin is capable of penetrating the mitochondria in its natural form and, once there, is able to damage mtDNA.

While we are yet to determine the precise mechanisms of oxaliplatin toxicity in skeletal muscle, our data suggests that in addition to the anthracyclines, chemotherapeutic agents from other drug classes that do not necessarily induce mtROS formation as a consequence of drug metabolism (i.e. the platinum-based alkylating agents and the anti-metabolite chemotherapies) are also detrimental to mitochondrial function and myofiber survivability. The molecular mechanisms underlying doxorubicin toxicity in skeletal muscle and the consequential repercussions on physiological function are being increasingly documented [110,163,239,243,253,263,264] and have established that mitochondrial dysfunction and heightened ROS production are key players. However, skeletal myopathy is a common side effect of chemotherapy exposure across all drug classes, and thus, if it has a mitochondrial origin, the initial defect seems not to be intrinsically associated with a particular mode of drug action, i.e. DNA damage versus inhibition of DNA replication. Indeed, our preliminary data in both a myotube culture and mouse model indicate that both increased mitochondrial ROS production and reduced mitochondrial pool viability are consequences of treatment with chemotherapies from various drug classes including the anti-metabolite (5-fluorouracil) and topoisomerase inhibitor (irinotecan) families [111,112]; however, we did not observe functional

deficits in myotubular mitochondrial function following exposure to these drugs as per doxorubicin and oxaliplatin. This highlights that there are both similarities and differences in the precise effects different chemotherapy agents have at the mitochondrial level and warrants further investigation. Indeed, since doxorubicin is the only chemotherapy agent that has been even moderately characterised in the literature with respect to the skeletal muscular system, there is an immediate need for the investigation of all chemotherapeutic agents in current clinical use and whether their toxic effects induce similar levels of myopathy, such that appropriate therapies can be devised to address them.

1.3.5 Consequences of mitochondrial dysfunction and ROS production on skeletal muscle mass

A number of recent studies investigating the molecular origin of skeletal muscle atrophy in various diseases/conditions have concluded that atrophy is almost always preceded in the first instance by increased levels of mtROS [216,217,265-269]. In a 2015 review, Sena *et al.* [270] outlined that mtROS production is a tightly regulated cell signalling pathway that, when excessive, induces mitochondrial and cellular protein damage thus leading to autologous mitochondrial destruction. Termed as mitophagy, this type of targeted autophagy is promoted in an attempt to attenuate elevated mtROS production by stressed mitochondria, which would otherwise inevitably induce oxidative damage, cellular energy depletion, and apoptotic/necrotic cell death. Attaix and Taillandier [271] have demonstrated that skeletal muscle mitophagy, regardless of cause, is a potent inducer of skeletal muscle wasting. Thus our hypothesis that chemotherapeutic agents (irrespective of the chemical class from which they derive) promote skeletal muscle atrophy and wasting via a mtROS/mutation-dependent

mechanism seems pertinent—especially since we have demonstrated elevated mtROS levels following exposure to chemotherapy agents from a variety of drug classes [111,112,272]. Indeed, Gilliam *et al*. [239] have shown that chemotherapy (doxorubicin) treatment causes an immediate increase (16 hours post-treatment) in the established upstream muscular atrophy regulators, E3 ubiquitin ligase and Atrogin-1/ MAFbx, in cardiomyocytes via a mtROS-dependent pathway. The effect mitochondrial dysfunction on skeletal muscle atrophy is well described with two studies showing that mtROS molecules are implicated in the induction of the FoxO family of transcription factors, which have been shown to upregulate Atrogin-1/MAFbx atrophic signals [273,274] (for detailed review see Bonaldo and Sandri [275]). In addition to direct modulation of atrophic signalling pathways, mtROS have the capability to oxidatively modify protein structures [270,276]. As chemotherapeutic agents demonstrably increase mtROS production [111,112,159,239,272,277], it is rational to link the subsequent increase in mtROS concentration with the modification of mitochondrial as well as other cellular proteins. A study by Kurihara *et al*. [219] has linked excessive ROS production with dysfunctional mitochondrial respiratory proteins which perpetuated a positive feedback cycle of increased mtROS production, respiratory chain defects, mtDNA deletion, and ultimately mitophagy. As mitochondrial dysfunction increases, cellular energy depletion occurs which, as demonstrated by Neel *et al.* [278], leads to macroautophagy within the skeletal muscle in an attempt to increase substrate availability to oxidative phosphorylation and restore energy homeostasis—albeit a futile effort in the event of respiratory chain inhibition and/or defects/dysfunction. As conclusively established by Argilés *et al*., negative alterations in energy balance act as a potent stimulus of muscle atrophy; including cachexia [231,279]. Furthermore, Maccarrone *et al.* [280] have implicated increased ROS levels with the propagation of lipoxygenases which induce structural defects within the cell leading to necrosis-induced

cell death, with others associating ROS-induced necrosis with organelle or plasma membrane modification [281]. With these findings reinforcing a number of previous studies [267,282,283], targeting mitochondrial dysfunction to reduce mtROS production is a logical intervention point through which to attenuate the initiation of muscular atrophy, macroautophagy, necrosis, and apoptosis signalling pathways, all of which have been strongly associated with chemotherapy treatment [10,244,284,285].

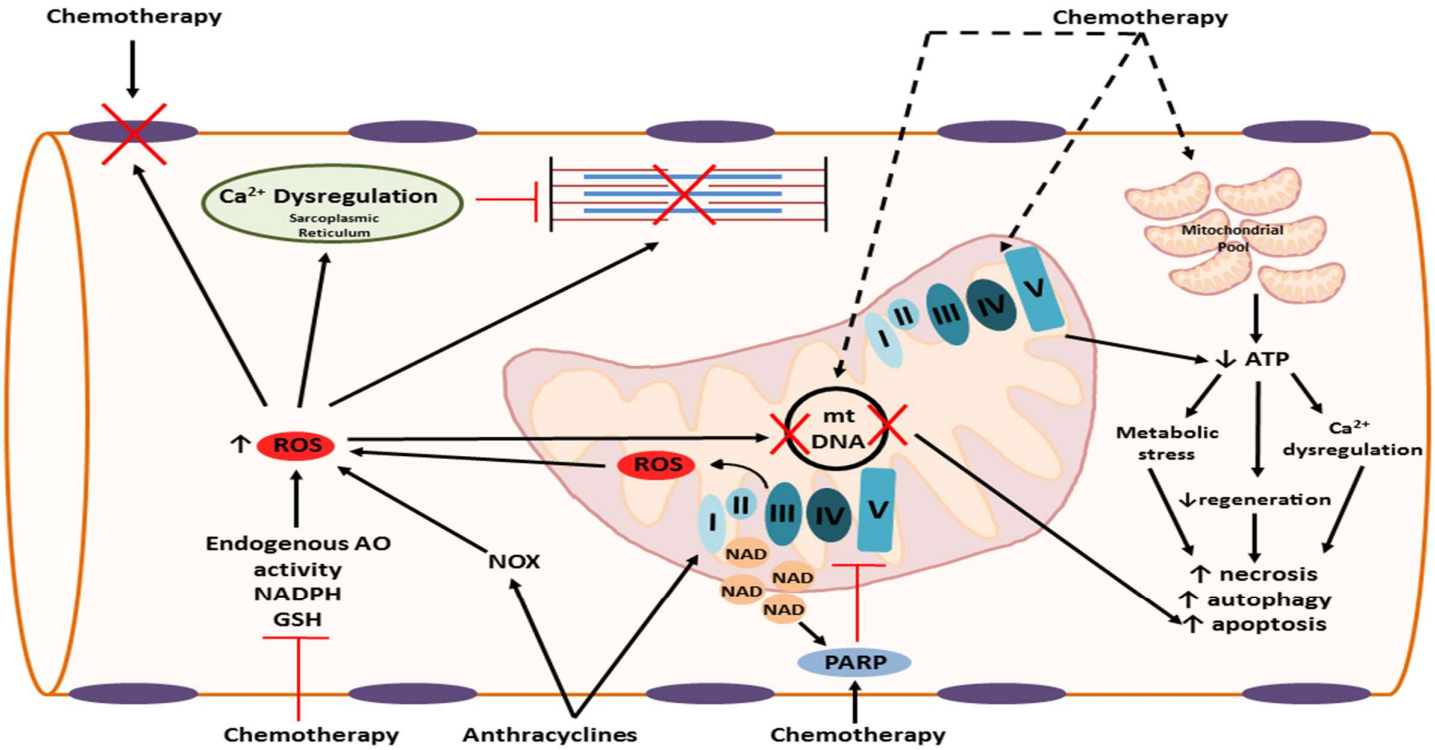

Figure 1.5: ***Effects of chemotherapeutic agents on mitochondria and the promotion of skeletal muscle wasting.*** *(A) The metabolism of anthracycline chemotherapies occurs at Complex I of the electron transport chain (ETC) within the mitochondria. The anthracycline molecule is reduced by Complex I, removing vital electrons from the ETC and transforming the anthracycline into its oxidative semiquinone, which reduces molecular oxygen to superoxide. This final reduction process returns the anthracycline to its non-semiquinone state. (B) Chemotherapy-induced nuclear DNA (nDNA) damage stimulates PARP-1 activity, which consumes NAD^+ (a vital mitochondrial substrate) to repair the nDNA damage. In doing so, the NAD^+ pool is rapidly depleted. This loss of NAD^+ negatively effects ATP production as well as negatively impacting various metabolic pathways including glycolysis and TCA cycle. (C) While the precise mechanism of oxaliplatin toxicity is unknown, likely mechanisms are intercalation of the platinum derivative into the mtDNA and the ETC complexes, and depletion of the mitochondrial Cu^{2+} pool. (D) mtDNA encodes for multiple components of the ETC and as such damage to the mtDNA through chemotherapy treatment and increased ROS levels perpetuates a positive-feedback loop of damage and dysfunction to the mtDNA and cellular components of the mitochondria. (E) mtROS can oxidise the mitochondrial membranes and damage the proteins of the ETC resulting in electron leak and an increase in mtROS production. As ROS levels increase within the cell, they upregulate atrophic pathways leading to muscle cell degradation, necrosis due to oxidative damage, autophagy and macroautophagy. (F) As a result of ROS-induced (and possibly chemotherapy-induced) mitochondrial dysfunction and mtDNA damage, mitophagic pathways are stimulated in order to curb the number of dysfunctional and mutated mitochondria within the total mitochondrial pool. As dysfunctional mitochondria are destroyed, the capacity of the mitochondrial pool to produce ATP is reduced resulting in depletion of the cellular ATP pool and thus induction of various autophagic, necrotic and apoptotic pathways. Figure reference* [1]

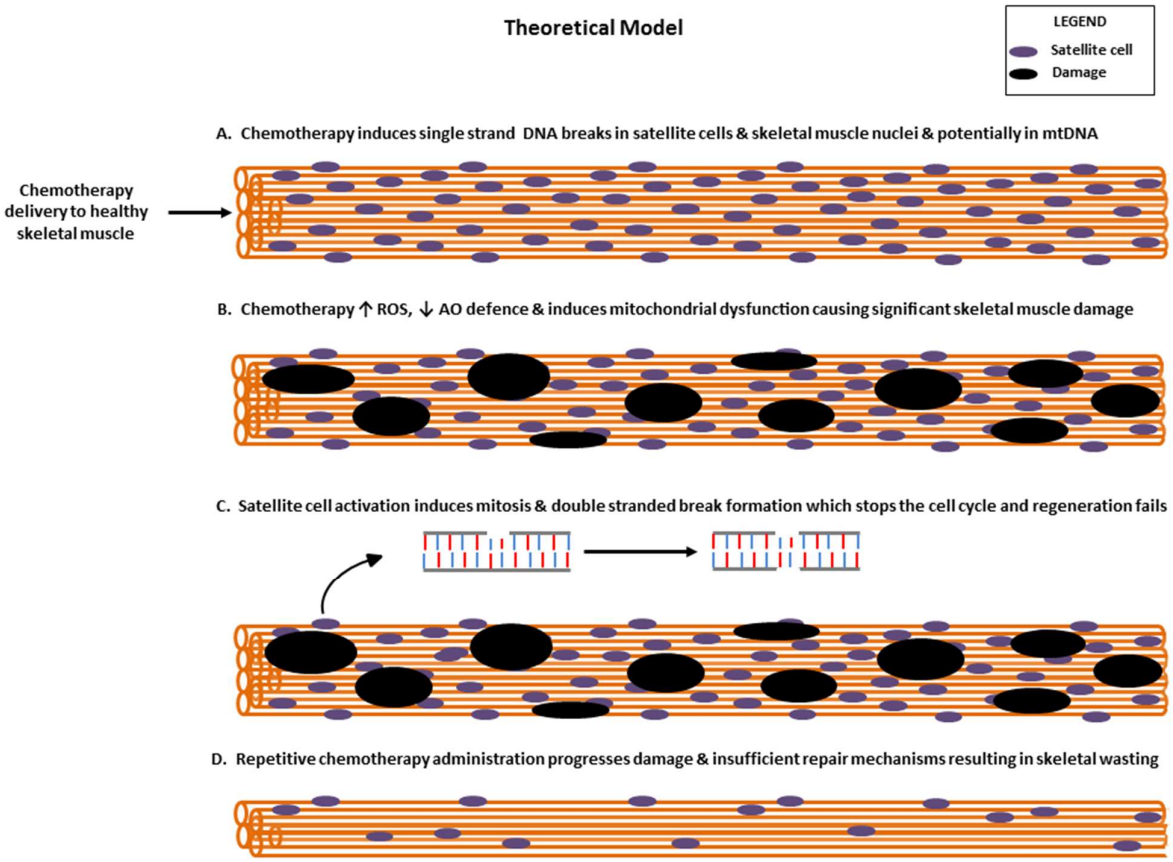

Figure 1.6: ***Hypothetical model of chemotherapy-induced myopathy in skeletal muscle.*** *(A) Chemotherapy is delivered to skeletal muscle which detrimentally effects nuclear DNA and potentially mtDNA.* ***(B)*** *Chemotherapy induces mitochondrial dysfunction resulting in increased mtROS production leading to damage of the skeletal muscle.* ***(C)*** *Damage sustained to the nuclear DNA is exemplified during mitosis causing a failure of satellite cell replication, and therefore, of regeneration mechanisms.* ***(D)*** *Long-term chemotherapy treatment results in progressive skeletal muscle damage and dysfunction due to blunted repair mechanisms. Figure reference* [1]

1.3.6 Protecting the mitochondria to combat CI-SMDW

Chemotherapy-induced mtROS production and DNA damage has been implicated in mitochondrial dysfunction, energy homeostasis dysregulation, mitophagy, and subsequently skeletal muscle atrophy and wasting. As a result, cancer survivors are prone to low muscle mass, poor function and heightened fatigue. Thus, therapeutic interventions to ameliorate these unwanted side effects are greatly needed. We propose that the precise mechanisms through which chemotherapeutic agents induce mitochondrial and skeletal muscle toxicity and wasting be carefully characterised—particularly for those that are in current widespread clinical use—in the first instance. Further, while no single treatment has been identified to clearly ameliorate chemotherapy-induced mitochondrial dysfunction, a number of treatments have been used to treat other myopathies with similar symptomatology and which are specifically underscored by mitophagy [286,287] . Thus, targeting the mitochondria with either established or novel mitochondrial targeted therapeutics could provide a therapeutic avenue through which to provide the skeletal musculature with protection against chemotherapy-induced toxicity.

The antioxidants endogenous CoQ10, Idebenone (IDEB) and SS-31 have been actively investigated as potential ameliorators of excess mtROS production and mitochondrial dysfunctions. Originally supplementation of CoQ10, an endogenous compound within the mitochondria which shuttles electrons between complexes I and III, has been used to increase electron transport within the mitochondria, with some promising results. A number of studies have shown that supra-physiological supplementation of endogenous CoQ10 increases the

shuttling of electrons between Complexes I and III to drive the pumping of protons from the mitochondrial matrix into the IMM space, restoring the mitochondrial membrane potential and thus the drive for mitochondrial ATP synthesis [288-290]. The synthetic CoQ10 analogue Idebenone (IDEB) has most recently been touted as a more potent treatment option for mitochondrial dysfunctions, especially those with characteristic Complex I involvement, when compared to CoQ10 (refer to Figure 1.7) [291,292].

Importantly, IDEB is currently being used in a number of clinical trials for disease states such as Mitochondrial Encephalopathy with Lactic Acidosis and Stroke-like episodes (MELAS), Leber Hereditary Optic Neuropathy (LHON), Duchenne Muscular Dystrophy, Friedreich's Ataxia, Alzheimer's and general cardiomyopathy, with some promising results [286,293-295]. IDEB therapy also has significant advantages over natural CoQ10 supplementation due to its lower molecular weight allowing easier up-take into the mitochondria. Due to its smaller physical size, IDEB has also been shown to be more readily incorporated functionally into the ETC, as well as being able to positively complete with natural CoQ10 [296]. As IDEB mimics CoQ10 actions, treatment with IDEB has been shown to increase transfer of electrons in isolated mitochondria and further avert electron leak from complex I that would normally produce mitochondrial ROS [297]. Although protective effects for IDEB with respect to chemotherapy-induced mitochondrial dysfunction are not yet known, IDEB has been shown in a recent study to restore electron transfer to Complex III in cells with genetically-induced complex I dysfunction [298]. IDEB is currently being used mainly to protect against neurodegenerative disorders, however, the mechanisms behind its protective nature have not been established although no side-effects from IDEB treatment has been noted. These data suggest that co-

administration of IDEB with chemotherapeutic agents that induce ROS formation at Complex I (particularly DOX) could ameliorate mitochondrial dysfunction caused by oxidative stress in healthy tissues without affecting antineoplastic mechanisms in cancer cells, and as such should be considered for future research as a viable co-therapy (refer to Figure 1.7 for hypothetical schematic).

While no other study has examined whether IDEB can afford benefit to chemotherapy-induced myopathy, other free radical scavengers such as the cell-permeable antioxidant peptide SS31, have shown promising results. Gilliam et al [239] showed that treatment with SS31 effectively scavenged excess hydrogen peroxide in the mitochondria which was induced by DOX therapy. The group also showed that post-chemotherapy treatment with the peptide improved mitochondrial function to increase ATP synthesis, decrease electron leak and thus inadvertently reduce ROS production. However, the study failed to identify whether this level of function was maintained when treatment with the peptide ceased or if the treatment was effective against long-term chemotherapy treatment as only one single dose of the peptide and the chemotherapy was administered. Other earlier studies [299-301] have shown that SS31 with repeated daily doses of between 3-5mg/kg reduced markers for oxidative stress and protected from Ca^{2+} mediated mitophagy as well as cellular necrosis as a result of energy depletion. These earlier findings suggest that SS31 could have therapeutic advantages against chemotherapy induced oxidative stress, however, there is no current research providing insight into whether the peptide will have any negative effects on chemotherapy anti-neoplasticity, positive effects on neoplastic growth or deleterious effects to the host if

combined with other drugs. Thus, due to the advanced nature of clinical trials with IDEB, co-administration of IDEB seems to have the greatest potential against CI-SMDW.

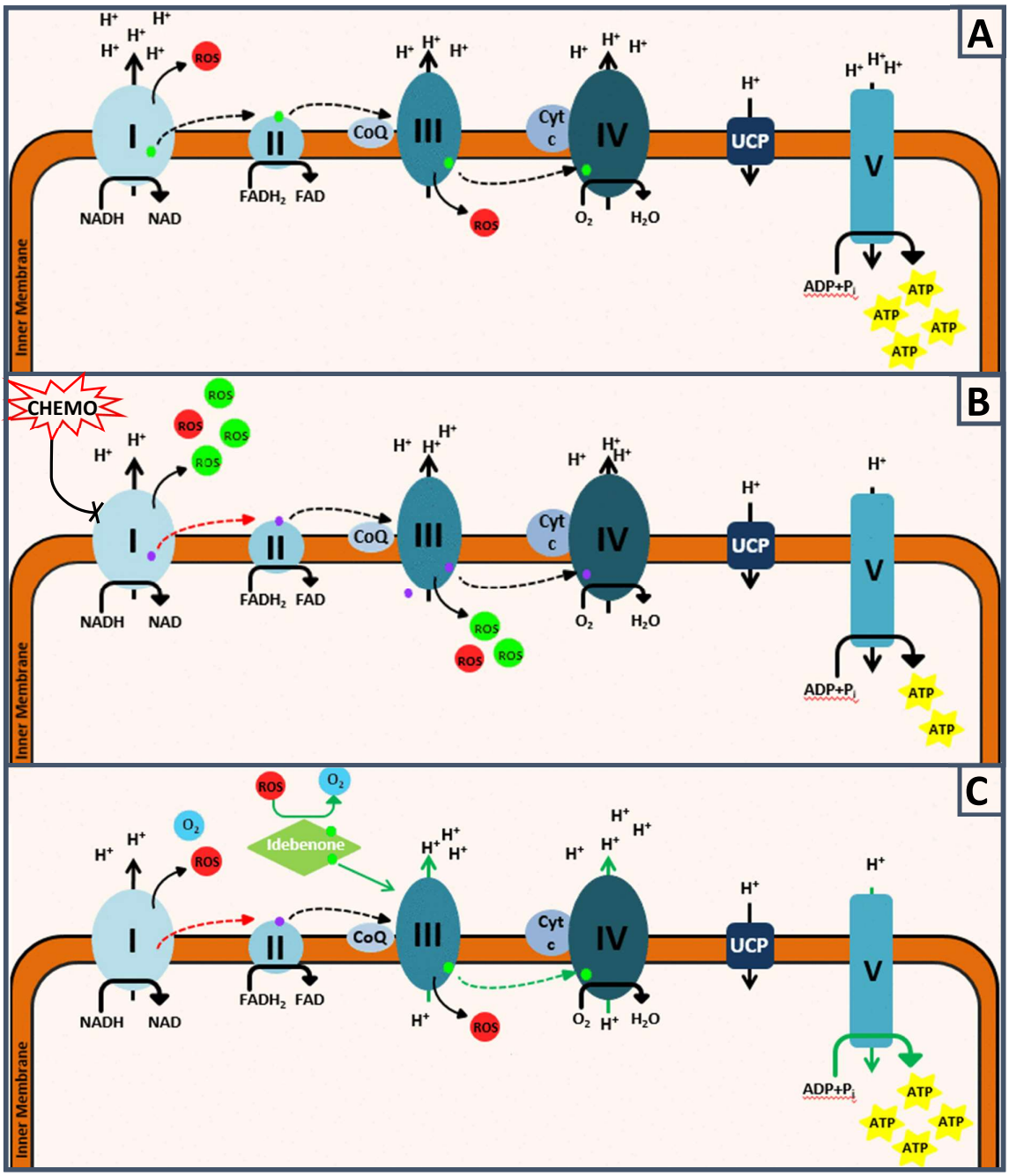

Figure 1.7: Effect of chemotherapy and Idebenone on the mitochondrial ETC. **A)** normal physiological functioning of the mitochondrial electron transport chain (ETC) (as described in *Figure 1.4*) **B)** In the presence of chemotherapy, we propose these agents inadvertently damage mitochondrial DNA (refer chapter 1) resulting in dysfunctional protein production and thus dysfunctional ETC complexes. These dysfunctional complexes, through normal activity, allow the escape of electrons from the ETC which then bind oxygen creating elevated amounts of ROS which can go on to further damage mitochondrial DNA and proteins creating a positive feedback loop of damage. As less electrons are available to travel through the ETC, a weaker proton gradient is created and thus less ATP is produced per unit of oxygen consumed (due to both elevated ROS production). **C)** We hypothesise that the co-administration of IDEB with chemotherapy can offer protection against elevated ROS by forcing a redox reduction of the ROS molecules and then delivering these electrons to Complex III; essentially reducing the amount of damaging ROS whilst returning electrons to the ETC, restoring ATP production.

1.4 Potential models to investigate CI-SMDW and potential co-therapies

Considerable efforts have been made over the previous half century to improve clinical evaluation of anti-cancer treatment; and with impressive results. These improvements can be directly correlated to improved treatments and clinical management of both the presenting cancer and the developed sequalae from both cancer and treatment. These advancements, although impressive and vital for survivability, have not addressed the incredible and often life-threatening side-effects which endure after the 5-year relative survival measurement has been surpassed. With patients being plagued by cancer relapse, chronic disease and pain, and reduced quality of life, a definitive answer as to where these sequalae originate is required. Research has shown definitively for close to 30 years that wholly untreated cancers induce cachexia [302,303], although for ethical reasons these studies have only occurred in animal models. Likewise, for investigations of the effects of chemotherapy independent of cancer, a plethora of cell and animal studies within this field are published every year [(as previously cited)]. Though informative for mechanisms of singular and sometimes multiple chemotherapies, these cancer-independent studies often fail to investigate chemotherapy regimens in a clinical context. Studies into chemotherapeutic agents also neglect to investigate their long-term effects and, with clinical 5-year event free survival rates pushing 90%, the problem lies after 5 years where 70% of survivors develop co-morbidities as a result of anti-cancer treatment [7,12,18-20]. For example, Riad *et al* [304] studying the therapeutic effects of statins against cardiotoxicity induced by doxorubicin in mice used a single once off intraperitoneal (IP) injection at 20mg/kg. Mice were culled 5 days later, and analysis showed that statins were effective at attenuating cardiotoxicity [304]. Unfortunately,

there is little evidence that single dose doxorubicin is used within the clinical arena on its own. Further, this study only investigated the acute effects of doxorubicin treatment and failed to measure long term effects. A study by Fardell *et al.* [305] fell into the same short comings. Stoeltzing *et al* [306] considered the effects of longer-term treatment by using osmotic pumps which delivered 5-FU (50mg.kg.week^{-1}) over 14 days. Although an improvement on many studies, mice were administered 5-FU alone, even though clinical usage of the drug is generally done so in the FOLFOX or FOLFIRI regimen which normally extends over a considerably larger time frame [307,308]. Mice were again culled for analysis within a short period of time after treatment (in this case 7 days after cessation of treatment) offering little insight into the long-term effects of chemotherapeutic treatment. Contrastingly, some investigations considered the long-term effects of singular cytotoxic agents [309,310] including one into CI-SMDW [277]. The studies treated mice with one of several common chemotherapeutics (cyclophosphamide, docetaxel, doxorubicin, 5-fluorouracil, methotrexate, or topotecan) individually. Animals were then culled at varying timepoints after treatment cessation and effects of individual chemotherapeutics compared. Although an improvement on prior papers, drugs were administered individually, and the teams failed to acknowledge that, once given in combination, pharmaco-interactions between the agents could produce markedly different results. A systematic search of the literature (refer to Figure 1.8 for process) uncovered only one original research paper which investigated a clinically relevant chemotherapy regimen and its effects (on cognitive function) over the long-term [311]. Still, no papers appropriately accounted for clinical treatment timeframes (such as the use of induction, remission, maintenance cycles etc.) or ascertained the long-term effects on sequalae development and survival within the surviving organism.

These studies indisputably play a critical role in developing our understanding of chemotherapeutic mechanisms and their devastating effects on the body. However, to further our understanding of the CI-SMDW, it is now of critical importance to advance research models to be capable of investigating the wholistic and complex nature of combination-chemotherapeutic interventions. By developing clinically relevant, pre-clinical animal models upon which these investigations can take place, appropriate research can then be conducted which can elucidate the mechanisms of CI-SMDW and, then, assess the therapeutic efficacy of co-therapies which can ameliorate the pathology.

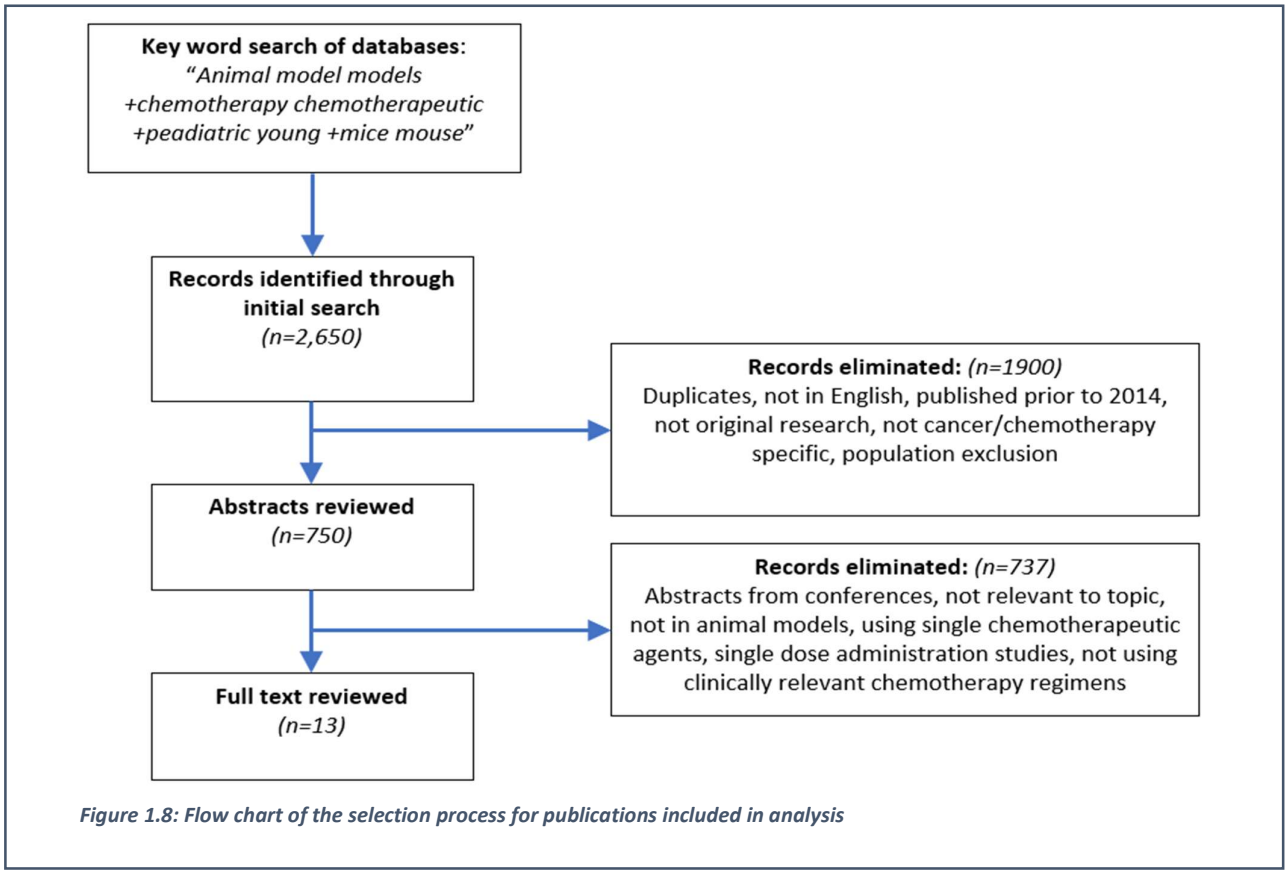

Figure 1.8: Flow chart of the selection process for publications included in analysis

1.5 Chapter Summary

The clinical repercussions of chemotherapy-induced skeletal muscle toxicity range from reduced participation in activities of daily living, chronic fatigue, exercise intolerance, depression and treatment discontinuation, to an increased risk of morbidity and mortality from myopathy-related disease [144,312]. These chemotherapy-induced pathologies are exacerbated when administered in children due to their high levels of mitotic growth. We have presented compelling evidence to suggest that the mitochondria are an etiological pharmacotoxic target of chemotherapy treatment which induces various co-morbidities that are overwhelmingly manifested in the skeletal muscular system. Given the persistent and severe nature of these co-morbidities, we stress the importance for a concerted research effort to develop appropriate (co-)/therapeutics, such as IDEB, to address the deleterious effects of chemotherapy-based anti-cancer therapy on the mitochondria to mitigate impacts on the skeletal muscular system (IDEB and potential alternatives are discussed in more depth in the next Chapter). However, before launching investigations into the efficacy of such therapeutics, we first need to properly understand both cachexia and CI-SMDW. Therefore, animal models upon which clinically relevant chemotherapy regimens over realistic time frames, with and without the cancer they aim to treat, must be developed. By doing so, the true acute and chronic sequalae associated with chemotherapeutic intervention can be isolated from the sequalae associated with the original cancer pathology. After an appropriate model of the pathology has been developed, targeted therapeutics against these chemotherapy-induced pathologies, such as CI-SMDW, can be properly developed and tested in a clinically relevant arena.

1.5.1 Thesis aims and hypotheses

The broad aim of this thesis is to determine whether mitochondrial targeting therapies, specifically IDEB, can prevent acute and/or long-term skeletal muscle dysfunction and wasting induced by juvenile gold-standard chemotherapy treatment in clinically relevant mouse models. We hypothesise that the mitochondria are inadvertent targets of systemic chemotherapy treatment and that damage to these organelles likely underpins the CI-SMDW phenotype. Further, we hypothesise that systemic paediatric chemotherapy induces both acute and chronic mitochondrial and skeletal muscle dysfunction and that by using IDEB we can afford protection to both the mitochondria and the skeletal muscle, thus, ameliorating the CI-SMDW pathology.

To complete these investigations, we will aim to:

1. Develop clinically relevant animal models which accurately replicate the CI-SMDW sequalae induced by gold-standard paediatric chemotherapy regimens used against the most common childhood cancers; ALL, medulloblastoma and NHBL

2. Determine whether the gold-standard paediatric chemotherapy regimens used against the most common childhood cancers; ALL, medulloblastoma and NHBL induce CI-SMDW both acutely and chronically, and whether this is underpinned by mitochondrial dysfunction

3. To determine whether co-delivery with IDEB can protect mitochondria, and thus the skeletal muscle, against CI-SMDW when given in combination with the gold-standard paediatric chemotherapy regimens used against the most common childhood cancers; acute lymphoblastic leukemia, medulloblastoma and non-Hodgkin's Burkitt lymphoma

Chapter 2

Intervention Animal Model Development Framework and Animal Model Creation

2.1 Introduction

No animal models to date are capable of investigating the CI-SMDW sequalae in mice in a clinically relevant manner. As such, development of an appropriate framework was required to facilitate the creation of these animal models. The Intervention Animal Model Development Framework (IAMDF) presented here has been created as both a structure to develop the required animal models specifically required in this thesis to investigate CI-SMDW but has also been broadened for application in other areas. The framework aims to provide a systematic process to develop a healthy animal model upon which investigations into a specific clinical intervention can be launched – regardless of the area of biomedical research.

As a foreword for the use of this framework in areas other than the requirements of this thesis; this framework assumes that standard scientific animal guidelines and metrics have been followed; such as ethical considerations and committee approval, budget, scope etc. Considering that this model of investigation is primarily in healthy animals, the framework is limited in its ability to foresee contraindications when combined with the pathology until the later steps in the framework. It should therefore be considered whether the intervention or the pathology is of key interest. For example, it must be determined whether the primary goal is to investigate the pathology independent from the intervention first (in scenarios where the pathology is not yet understood), or, whether the pathology is used as a variable after the viability of the intervention has been assessed (as laid out in this framework). Moreover, if the purpose of the animal research being developed is to transition findings into human trials, which it ethically should be, it is highly recommended that the reader follows appropriate drug development guidelines of the country that they wish to complete the trials in conjunction with this framework.

With that disclosed, each step of the framework will be presented (the structure of which is laid out in Figure 2.1 below), followed by how it was applied to develop the models which will be used later in this thesis to investigate our central research question; whether mitochondrial targeting therapies can prevent acute and/or long-term skeletal muscle dysfunction and wasting induced by juvenile gold-standard chemotherapy treatment. Thus, the aims of this chapter is to, first, develop a viable and robust framework which can be used to investigate specific clinical interventions in a healthy animal model and, second, to use this framework to develop investigatory mouse models by which the chemotherapy regimens used against the three most common paediatric cancers (as discussed in the previous chapter) ALL, medulloblastoma and NHBL can be launched.

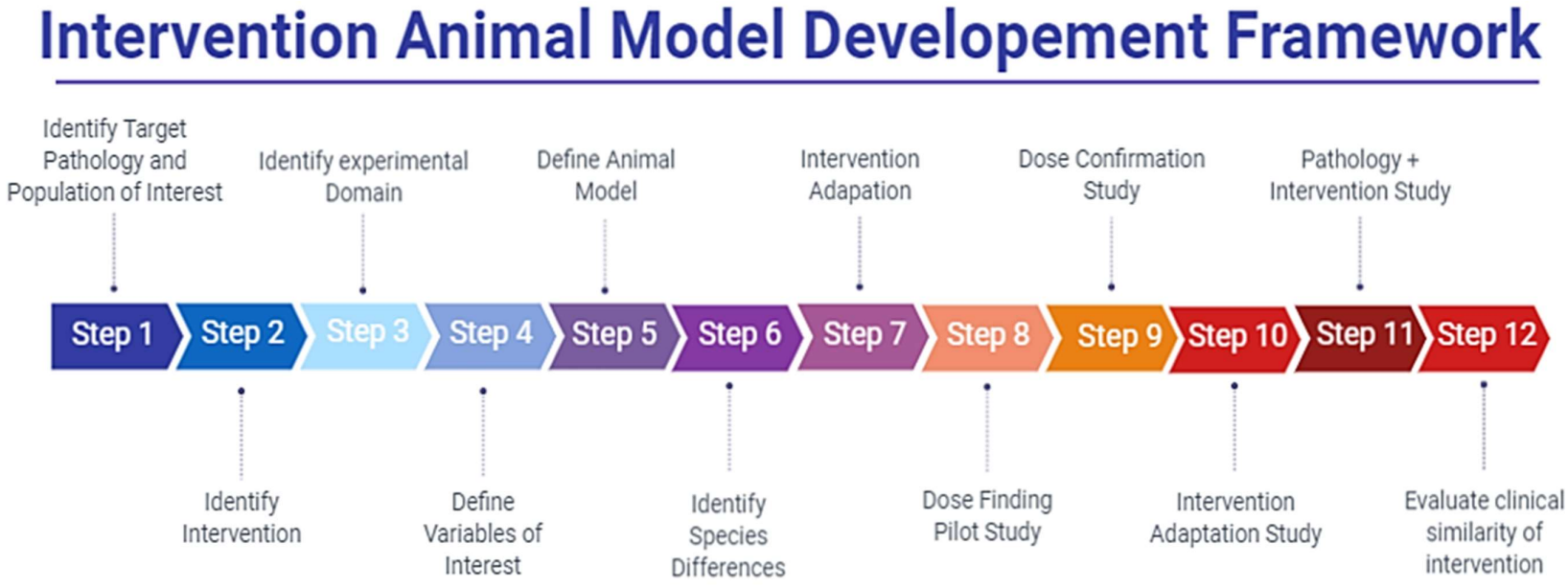

Figure 2.1: Flow-diagram of Intervention Animal Model Development Framework (IAMDF)

2.2 Intervention Animal Model Development Framework

Step 1: Identify target pathology and population of interest

In most cases the development of an intervention focused on animal models will be underpinned by a pathology of interest and thus the selection of the pathology normally precedes the selection of the intervention. For example, a research department or laboratory may already be investigating pathological outcomes of a disease state and are interested in developing a more robust and favourable intervention to improve patient outcomes. In this case, the pathology and the population have previously been defined and the selection of a viable intervention can follow by moving on to Step 2. Alternatively, in circumstances where this is not the case (i.e. where a specific pathology and population has not been defined, but an intervention with therapeutic potential has), the pathology and target population must be defined to develop and refine the scope of the animal model. Thus, a sound understanding of how the intervention works is needed in order to match the mechanism of action to the processes of the pathology. For the most case, where an intervention has been shown to have therapeutic efficacy, and is of therapeutic interest, its mechanism of action will have already been established and a simple process of matching intervention to pathology will ensue. Regardless of whether the intervention or pathology has been selected first, a sound review of the literature must be made to canvas the current knowledge of the pathology and its effects on patient outcomes. This is important to clearly establish a solid understanding of baseline values, so changes from interventions can be accurately quantified.

Step 1: Application

This step has been discussed at length in the first introductory chapter of this thesis. In brevity, however, adult survivors of anti-cancer chemotherapeutic intervention during their formative years often suffer from considerable long-term sequalae. We hypothesise that anti-mitotic interruptions to the paediatric skeletal muscle lifecycle induced by childhood chemotherapy underpin the dramatic reductions in QOL (due to CI-SMDW) that these patients face after the therapy ceases and the cancer subdued. We also hypothesise that due to the single stranded and largely unprotected nature of the mitochondria, inadvertent damage to these essential energy-producing organelles during therapy further exacerbates the CI-SMDW phenotype. The target pathology and population chosen for this framework is, first, paediatric patients diagnosed with cancer who receive(d) chemotherapy as a first line response to childhood cancers before the age of 10, which is identified as a child's greatest period of growth. [6] Secondly, due to the life-long nature of CI-SMDW, the age range of our target population will extend from childhood (approximately from 2 years of age) through to middle adulthood demarcated by the cessation of overall growth and the onset of ageing (i.e. a sarcopenic phenotype) which typically occurs after the age of 50. [313-316]

Step 2: Identify intervention

As interventions generally target a specific pathology, the outcome of Step 1 will guide the selection of the intervention in this step. As previously discussed, it may be more beneficial to complete this step first prior to completing Step 1, though the interventions used within this thesis were developed by following the steps in sequential order. As an in-depth review of the mechanisms which both underpin the pathology's initiation and progression was completed in the previous step, potential therapeutic interventions need to now be identified. A search of the literature which aim to canvas potential interventions which target the pathways that underpin the pathology (or the symptoms of the pathology if symptom treatment is the goal) is now required – with a list of candidate interventions accrued. From this short-list, the most viable intervention should be selected, considering factors such as availability, cost, available safety and toxicity data etc. Moreover, some broad-spectrum factors that should be considered when selecting the intervention are: that clear mechanistic targets have been established and that the intervention can reliably and consistently target them; that a specific population and/or geographic location that the pathology affects is identified and that the intervention will be viable for use within this population; and lastly, that the intended research has not been conducted previously (and if it has, that this project will improve upon it).

Step 2: Application

Most paediatric cancers are treated with systemic chemotherapy interventions, thus, to narrow the scope of this study, the gold standard chemotherapy regimens employed against the most common paediatric cancers will be selected for investigation. According to the World Health Organisation, leukemia, CNS and NHBL are of the highest prevalence cancers in children, with ALL being the most common of the leukemia's and medulloblastoma, the most common CNS cancer. [116-119,317-320] As such, gold standard (the most widely used and effective) chemotherapeutic interventions against ALL, medulloblastoma and NHBL were selected as the interventions of choice for this thesis.

ALL intervention selection

Due to the systemic nature of ALL, surgical resection and radiotherapy are not viable options as there is not specific tumour to target. For this reason, chemotherapy is the only viable treatment option, which consists of a large battery of chemotherapeutic agents given in conjunction with other co-therapeutics and supportive therapies. Presented by the Berlin Frankfurt Munster (BFM) group in 1976, the delayed intensification method involving intensifying the postinduction phase of the chemotherapy regimen showed promise in improving survivorship in paediatric ALL patients [321]. This procedure, involving 5 separate phases, induction, consolidation, interim maintenance, delayed intensification and maintenance covering 24 weeks of treatment with continuing maintenance for 2 years for

girls and 3 years for boys, was later reviewed comprehensively over the following 25 years by the Children's Cancer Group (CCG) [322]. The CCG review showed that a single delayed intensification (DI) process increased five-year event free survival (EFS) from 61% (without DI) to 77% (with DI, *p*=0.001). The CCG further investigated the efficacy of a double delayed intensification process which was shown to improve relative risk ([RR]=1.38) as well as improve 6-year survival estimates from 87%±2% to 91%±2%. These rates, at the time of review, were found to be the highest survival rates offered by any intervention for this type of cancer and risk profile. The intervention is considered the gold standard intervention recommended by one of the key opinion leaders in the field [323,324] and thus was selected for this study.

ALL chemotherapy agents, timings, and dosages:

The regimen outlined by Children's Cancer Group (CCG-1891) was selected for this study [322]. This section will outline the regimen in its entirety as used in human patients (refer *Figure 2.2* for diagrammatic representation). This regimen will be referred to as ALL-indicated 6-mercaptopurine (Purinethol), vincristine (Oncovin), methotrexate and prednisone (POMP) modified combination therapy, or ALL-POMP for short.

Induction phase (Week 1-4)

Prednisone (40 mg/m^2 per day for 28 days); vincristine (1.5 mg/m^2 per week × 4); L-asparaginase (6000 IU/m^2 intramuscularly [IM] × 9); and age-adjusted intrathecal methotrexate (age 1 through 1.99 years, 8 mg; age 2 through 2.99 years, 10 mg; age at least

3 years, 12 mg on days 0 and 14). Patients with CNS disease at diagnosis also received intrathecal methotrexate on days 7 and 21.

Consolidation phase (Week 5-8)

Daily oral 6-mercaptopurine (75 mg/m^2 per day); vincristine (1.5 mg/m^2 on day 0); and age-adjusted intrathecal methotrexate (doses as given above) weekly × 4.

Interim maintenance phase (week 9 to 16)

Daily oral 6-mercaptopurine (75 mg/m^2 per day); weekly oral methotrexate (20 mg/m^2 per week); intravenous vincristine (1.5 mg/m^2 on days 0 and 28); oral prednisone (40 mg/m^2 on days 0 through 4 and 28 through 32); and intrathecal methotrexate (age-adjusted doses, as above) on day 0.

Delayed Intensification phase (week 16 to 24)

Intravenous vincristine (1.5 mg/m^2 on days 0, 7, and 14); dexamethasone (10 mg/m^2 per day for 21 days with 7-day taper); doxorubicin (25 mg/m^2 intravenously bolus on days 0, 7, and 14); L-asparaginase (6000 IU/m^2 IM 3 times a week for 6 doses); cyclophosphamide (1 g/m^2 on day 28); cytosine arabinoside (75 mg/m^2 IV or subcutaneously on days 29 through 32 and 36 through 39); oral 6-thioguanine (60 mg/m^2 on days 28 through 41); and age-adjusted intrathecal methotrexate (doses as above on days 28 and 35).

Maintenance phase (week 24 onwards)

Intravenous vincristine (1.5 mg/m^2 on days 0, 28, and 56); oral prednisone (40 mg/m^2 on days 0 through 4, 28 through 32, and 56 through 60); daily oral 6-mercaptopurine (75 mg/m^2 per day); weekly oral methotrexate (20 mg/m^2 per week); and age-adjusted intrathecal methotrexate (doses given as above on day 0 of each course).

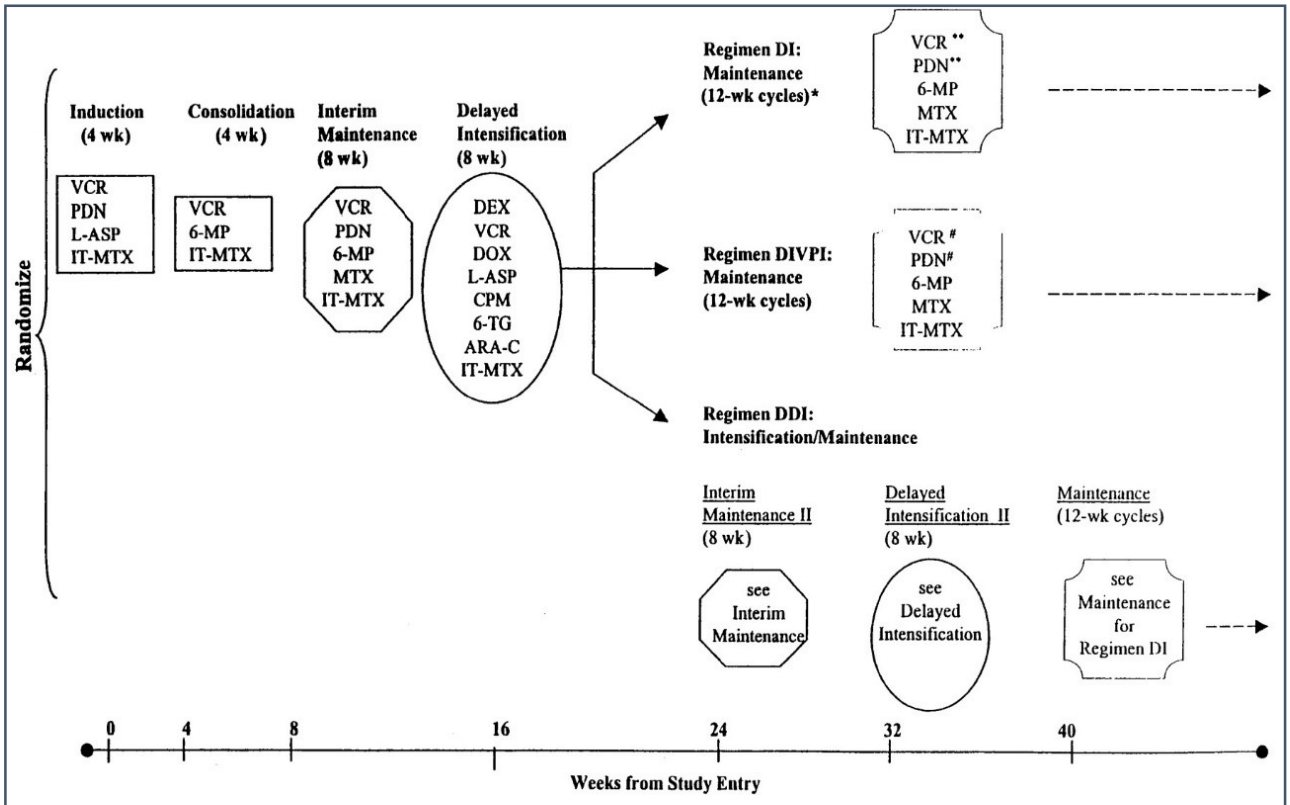

Figure 2.2: Regimen used in CCG report investigating efficacy of delayed intensification and double delayed intensification regimens for treatment of intermediate risk paediatric acute lymphoblastic leukaemia (ALL). Abbreviations: VCR, Vincristine; PDN, Prednisone; L-ASP, L-Asparaginase; IT, Intrathecal; MTX, Methotrexate; 6-MP, 6-Mercaptopurine; DEX, Dexamethasone; DOX, Doxorubicin; CPM, Cyclophosphamide; 6-TG, 6-Thioguanine; ARA-C, Cytosine-Arabinoside; *, maintenance cycles continued for 2 years for girls and 3 years for boys on all regimens; **, pulses of VCR and PDN given in 4 week intervals; #, pulses given in 3 week intervals. Image source: Lange *et al.* [316]

Medulloblastoma intervention selection

Medulloblastoma is the most prevalent form of malignant brain tumour in children and is treated with targeted radiotherapy (doses generally ranging from 54-56 Gy) with or without chemotherapy [325-329]. However, investigations into the longer-term effects of high-level cranial radiation revealed a high incidence of intellectual dysfunction from radiation treatment [326-329]. More recent studies introducing chemotherapy as a front-line defence against medulloblastoma have shown a significant increase in EFS, particularly against metastatic variations of the cancer [330,331]. With survival rates continuing to improve, long-term sequalae are of considerable concern as they greatly affect the patient's long-term quality of life [330]. Although separate sequalae exist for radio- and chemo-therapy, chemotherapy regimens offer a greater opportunity for therapeutic manipulation due to their non-specific mode of pharmacological administration and their more physical interactions within the body.

Although multiple ideations exist of which drug combination is the most effective; the Children's Cancer Group (CCG) has consistently used a combination of the staple cranio-chemotherapeutic lomustine (which can cross the blood-brain barrier due to its lipid soluble nature), together with vincristine and either a platinum based chemotherapeutic (carboplatin or cisplatin) or corticosteroid compound (pregnenolone, prednisolone, prednisone etc.) [124,331-334]. Using these chemotherapy regimens prior to radiation (or in combination with reduced levels of radiotherapy in some instances [25-27]) resulted in an unmatched improvement in progression-free survival (PFS). Other studies also presented similar, although slightly reduced survival and EFS/PFS rates, when replacing the platinum based chemotherapeutic with prednisone. The regimen used in CCG-9892 (which does not include

this replacement) was thus selected as it, at the time of this thesis, is associated with improved survival (>80% with cis/carboplatin vs <80% with prednisone) and EFS/PFS rates in the target population [318,331,332,335,336].

MB chemotherapy agents, timings, and dosages:

The regimen outlined by Children's Cancer Group (CCG-9382); [124,331-334] was selected for this study. This section will outline the regimen in its entirety as used in human patients. This regimen will be referred to as medulloblastoma-indicated lomustine, cisplatin and vincristine combination therapy, or MB-LCV for short.

Induction Phase (week 1-8)

Radiotherapy + intravenous vincristine (1.5mg/m^2 at ≤2mg weekly from day 1) for 8 weeks.

Consolidation/Maintenance Phase (week 14-62)

Oral lomustine (75mg/m^2 once per 6 weeks), intravenous cisplatin (75mg/m^2 once per 6 weeks) and intravenous vincristine (1.5mg/m^2 at ≤2mg once per week, 3 weeks on 3 weeks off for duration of phase)

NHBL intervention selection

Historically, survival rates for chemotherapy and/or radiotherapy treated NHBL were as low as 10% in 1975 [337]. Since then, NHBL has progressed to become considered one of the most curable malignancies in children, with survival rates surpassing 90% in both older (FAB/LMB 96, 2008) [338] and more recent (FAB/LMB 96, 2019) [339] studies. *The French American-British Lymphome Malins de Burkitt* (FAB LMB) 96 study [338,339] was an international collaboration between *the Française d'Oncologie Pédiatrique* (SFOP), the CCG, and the *United Kingdom Childhood Cancer Study Group* (UKCCSG) and has been credited with developing the widely accepted, gold standard CHOP therapy. Moreover, the FAB/LMB 96 associated CHOP therapy (with and without rituximab) is attributed with the impressive success against childhood NHBL [340-350] which has also seen success in adults [351].

Although praised for its success in resource-rich nations, the success of the therapy largely relies on an intensive and high-dose strategy which is inextricably reliant on equally intensive support-therapy regimen. This is highlighted by the large discrepancy in the regimens success in low-income nations, such as the sub-Saharan region where overall survival for lymphoma which was treated with low to medium intensity CHOP varied from 30-50% (2005-2016) [352-357]. This discrepancy highlights the severe toxicity induced by the regimen which can be largely overcome with adequate supportive care. Together with the severe long-term and highly characteristic sequalae of anthracycline therapy (discussed in *Chapter 1; S1.2.2, S1.3.4*), these shortcomings, together with its heavy reliance on supportive therapies, highlight areas which even the slightest improvement could have profound benefits to patient outcomes. With this in mind, and that the FAB/LMB 96 CHOP regimen [338] is widely considered

the gold standard therapy against childhood NHBL, the CHOP regimen was a natural choice for this study.

NHBL chemotherapy agents, timings, and dosages:

The regimen outlined by *FAB/LMB 96 CHOP regimen* [338] was selected for this study. This section will outline the regimen in its entirety as used in human patients. This regimen will be referred to as NHBL-indicated cyclophosphamide, doxorubicin (Hydroxydaunorubicin), vincristine (oncovin) and prednisone combination therapy, or BL-CHOP for short.

Regimen 1 & 2 given 21 days apart

Cyclophosphamide (250mg/m^2) given per IV twice daily for days 1-3 (for a total dose of 500mg/m^2 per day), doxorubicin (hydroxydaunorubicin, 60mg/m^2) given per IV on day 1, vincristine (oncovin, 2mg/m^2) given per IV on days 1 and 6 and prednisone (30mg/m^2) given orally twice daily on days 1-6 (for a total of 60mg/m^2 per day). The course is repeated 21 days after commencement.

Step 3: Identify experimental domain

Having now identified the pathology, population and intervention, it is now appropriate to categorise the project to appropriately guide its design. As the primary purpose of establishing an animal model is to investigate an intervention - initially independent of the pathology that the intervention is designed to combat, to ensure its safety and efficacy - the category the study is defined in plays an important role in its development. Biomedical therapeutic and intervention research is generally categorised into one of three domains: 1) fundamental discovery 2) feasibility testing and 3) clinical modelling and efficacy prediction [358], with the experimental design of the study being greatly moulded by the domain selected.

Fundamental discovery

Testing a novel intervention, which has not been previously investigated against a human pathology, in an animal model would qualify the study for the fundamental discovery architype. In general, the fundamental discovery aims to establish a novel protocol for a novel intervention against a known pathology of interest. This is done either by instigating a holistic physiological response by using a systemic intervention to resolve the pathology; occasioning an effect using an intervention which either actively or passively targets a specific target. These targets, e.g. a gene, protein or cell type, may be targeted to elicit a favourable pathway response in the organism, or, by physically altering the organism to either remove, add or

adapt physical structures to overcome the pathology [359]. It should be considered here that multiple methods are available to alter an organism including genetic modification (genetic knock-down, over-expression etc.), surgical and pharmacologic to name a few. This methodology and thesis will concentrate on those which are currently available for use in human patients to maintain as much clinical relevancy within the animal model as possible. As such, detailed consideration of genetic modifications, such as knock-down models, are outside the scope of this thesis.

Feasibility testing

Testing an intervention which has been previously established, either against a pathology that is has not been established for or employed in a different manner than originally designed, would qualify the study for a feasibility testing architype. Feasibility testing aims to test an established intervention against a pathology where it is not considered the gold standard treatment. The purpose here is to either modify the intervention from its original design to target a different pathology, or, improve its original design to enhance its efficacy to (re)establish its use as the standard of care.

Clinical modelling or efficacy prediction

Testing an intervention which has been previously established in a human model against a pathology it was originally designed for, but in a species other than humans, would qualify the study for the clinical modelling or efficacy prediction domain. For clinical modelling; the intervention must be the standard of care currently being used clinically to

ensure the projects outcomes are relevant and translatable. If this is not the case, the study should be designed as a feasibility study. The clinical modelling architype aims to develop an animal model to investigate a gold standard intervention, currently used in humans, to define the mechanisms of action which underpins its therapeutic efficacy, its side effect profile, or both. For the efficacy prediction architype, the intervention used must be a modified version of the gold standard intervention used clinically, with the aim of improving efficacy, tolerability, and/or survivability. The testing of the gold standard intervention in combination with a co-intervention or -therapeutic will also be categorised as an efficacy prediction architype as the addition of a variable is seen as a modification to the gold standard intervention. However, it is recommended that an appropriate animal model be established using one of the prior domains, or the clinical modelling architype, prior to commencement. This is to ensure that the feasibility of the co-therapeutic is ascertained and the gold standard intervention has been clinically modelled to ensure its clinical similarity.

Step 3: Application

The chemotherapy regimens identified for use in these investigations are commonly referred to as the gold standard to treatment against the pathologies they are indicated to treat. Thus, the experimental domains of these models primarily within the clinical modelling architype. However, in later steps (i.e. *Step 10*) the models which have achieved acceptable levels of clinical similarity will be adapted through the addition of a co-therapeutic in an attempt to improve clinical outcomes. Thus, the later steps will then fall into the efficacy prediction architype.

Step 4: Define variables of interest

Although the side effect profile will largely drive this step, it is still important to outline the expected therapeutic effects of the intervention as well, as these will be used to authenticate the animal equivalent doses of the intervention in later steps. In most cases, the variables of interest will be those that show benefit to the patient as these will measure the efficacy of the intervention. It is still prudent, though, to measure negative variables as a therapeutic may not be beneficial when these are considered. For example, a therapeutic that improves a specific condition but induces another worse-off pathology would not be worthwhile pursuing. Even still, an induction of any pathology may not be viable though it could be argued that, for instance, a therapy that improves survival by a significant amount but induces mild type II diabetes may still be worthwhile. Nevertheless, this is a screening exercise of sorts, and a wide net should be cast to catch unforeseen contraindications. For example, simple variables such as changes in body weight, food and water intake, wet organ weights, and blood profiles are relatively simple to measure but in combination offer a considerable insight into the health of the animal.

Considering the purpose of this framework and resulting model, it is important to consider how well the model replicates the pathology seen in humans. Out of the defined variables, at least one variable should have been previously used and defined in a human model of the pathology that the intervention targets for a clear direct comparison between species; i.e. overall survival or event free survival in cancer studies, bone mineral density (BMD) in osteoporosis studies, creatinine kinase levels in Duchenne's muscular dystrophy etc. with these variables being measured in both the control, pathology only and pathology +

intervention groups. This is an important aspect of the variable design to allow for direct comparisons between the species (generally the pathology only group vs. the disease in a human model) and thus the relevancy of the animal equivalent intervention model. For example, a model studying the efficacy of Vitamin D therapy to ameliorate BMD loss in an older osteoporotic human population would first need to ensure that Vitamin D does not reduce BMD in a healthy animal model and does not induce a more severe pathology than what it is aimed to treat. Further, when the pathology is added to the model as a variable, it is essential that the osteoporotic phenotype in the animal corresponds to the osteoporotic phenotype in humans for the pathology model to be viable. It is for these reasons that variables that measure the pathology's phenotypes should be included, together with the variables that measure the efficacy, or lack-thereof, of the intervention.

Step 4: Application

With *Chapter 1* discussing the CI-SMDW pathology in depth, this step will succinctly outline the proposed variables of interest, why they are of interest and the methods by which they will be measured. First and foremost, the basis of this framework is to develop animal models which mimic clinical outcomes as closely as possible. Therefore, animal weight changes and food intake monitoring are of primary importance as these are common and important predictors of overall patient health in the clinic. However, recent reviews of cancer patient management suggest that the monitoring of weight-loss alone does not offer significant prognostic value as significant weight-loss is more indicative of late stage cachexia,

rather than an indication that the sequalae is beginning [360]. Thus, more importance is placed on overall body composition and function rather than pure caloric intake vs output (and thus weight maintenance) [33,361]. Although these variables are often used to measure the cachectic phenotype, they are important measures of treatment toxicity, and thus the CI-SMDW sequalae, as well. Lean muscle mass and strength are two of the most important predictors of chemotherapy toxicity [148,362-366]. Moreover, due to the systemic and infiltrative nature of chemotherapy, measures of systemic inflammation and its effect on highly mitotic cells (such as blood cell lineages) are routinely utilised as measures of toxicity [367-372], particularly in blood cancers like ALL [373-376].

With these clinically used protocols in mind, the intricacies of animal model investigations need to be considered to choose and develop methods to measure these variables. Bodyweight changes and food intake monitoring are simple measures to perform, however, body composition scans are far more tedious. Computed tomography, for example, is completed with relative ease in human patients as replicate scans and values are not required for clinical diagnoses. Body composition analysis in mice requires highly specialised machinery, such as the SkyScan 1276 micro-CT, and often takes in excess of 45min per whole animal to scan, which is unable to be automated. In a study such as this one which will likely see the use of over 100 mice, this quickly renders whole mouse body analysis via micro-CT scanning laborious and costly. Although likely feasible in a larger, more well-funded study (both with financial and human resources), this option was outside the finite resource capacity of this thesis. However, the SkyScan 1272 micro-CT scanner allows for 16 smaller samples (such as a whole limb) to be automatically scanned in approximately 4 hours. Although whole body analysis would offer more information, automated CT analysis of mouse

hind limbs alone would allow sufficient analysis of body composition in a timely and financially affordable manner [377,378].

As mentioned previously, however, body composition and mass is only one portion of CI-SMDW sequalae. Skeletal muscle function, or lack thereof, significantly impacts patient quality of life and survival and is a positive predictor of treatment toxicity [18,34,151,379-381]. Grip strength is often used in clinical trials to assess muscle strength and is a diagnostic tool used in many muscle wasting diseases, such as sarcopenia [313,382,383], Duchenne's Muscular Dystrophy [384-386] and of course cachexia [387,388]. Therefore, to measure the clinical progression of the CI-SMDW phenotype, daily body weight and food intake will be measured, together with time point specific full blood examinations and measures of body composition (via hind-limb micro-CT analysis) and grip strength.

To further understand the muscle dysfunction component of the CI-SMDW phenotype, it is important to investigate which components of function (fatigue, strength, endurance, recovery capacity etc.) are affected. Fortunately, our lab has extensive experience in contractile function testing in isolated mouse muscle [389-393]. As discussed in *Chapter 1; S1.4*, the mitochondria play an important role in the regulation of muscle mass and functional capacity. Their involvement in the CI-SMDW underpins the basis of our investigations and present a novel and potentially viable therapeutic target to combat the CI-SMDW pathology. To further characterise the underlying pathology of CI-SMDW and whether the mitochondria are implicated, investigations of mitochondrial function using the Seahorse XF24 flux analyser will be also be completed.

Analysis of these variables will serve to characterise the presence and progression of the CI-SMDW phenotype via methods that's are in-line with current clinical practice, thus

ensuring data is more closely comparable to the human cohort of CI-SMDW sufferers. By further investigating muscle and mitochondrial function *ex vivo,* we hope to further characterise the CI-SMDW phenotype and identify potential co-therapeutic targets to improve clinical outcomes associated with the ALL-, medulloblastoma- and NHBL-indicated chemotherapy regimens.

Step 5: Define animal model

The pathology that the nominated intervention is used against will mostly drive the selection of the animal model which should be used. Particular focus on the variables of interest are needed as different animal models express different phenotypes which can be used for the researchers benefit (more in Step 11). The resultant model will, in general, be either of the induced, spontaneous, transgenic, negative, or orphan disease categories, depending on the pathology of interest (for further breakdown of categories see *Rand* [394]) and be categorised in one of four categories which define the required level of similarity between the animal and human models, these are: 1) Fidelity. A scale measure of physical and biological similarity between model and human. 2) Homologous. Symptoms observed in the animal model are identical, both genetic and physiological, to those observed in humans. 3) Isomorphic. Symptoms and or anatomy are like those in humans although aetiology or genetic character are different. 4) Partial. The animal model does not mimic the human model exactly, either physiological or phenotypical, but there exists enough similarity between the two to study some aspects of the intervention or disease [395,396]. For example, a model aiming

to investigate the effects of a female contraceptive pill which alters progesterone production will require a high fidelity, homologous model, if investigating the systemic and contraceptive effects of the intervention. In contrast, a model investigating a surgical knee replacement may only require an isomorphic or partial model. Levels of similarity should be chosen based on clinical relevancy requirement before selecting an animal species and genus. There is a plethora of informative databases (such as the International Mouse Strain Resource [397,398] and the Mouse Genome Database [399]), publications [400-410], and guidelines and frameworks [411-414] outlining appropriate animal models for particular pathologies, which should be used to guide the selection of the animal model for this step. Although outside the scope of this thesis and framework to outline all the considerations that are needed for appropriate selection, the model should primarily aim to minimise confounding experimental variables whilst maximising experimental replicability and clinical human similarity. As different species have been shown to be more analogous with humans (dependent on the variable measured), careful consideration should be taken regarding this component. The use of transgenic or genetically modified (GM) animals can be used as an isomorphic model as both improve pathological and physiological similarity between human and animal [415-417]. Consequently though, transgenic and GM models also introduce unnatural genetic shifts which can have considerable unmeasurable and unknown effects to the model [416,418] and should only be used in proof of concept models.

These models can, however, provide excellent additive value if used in conjunction with other animal models from other species. In considering studies that target specific physiological mechanisms, one can only speculate on the transferability of the interventions success in one species compared to its success in another. Evolutionary biologists have combated this in their field by studying the effect of one mechanisms in multiple distant

species, for example Tatar *et al* [419] investigated the cell-signalling pathways and genetic regulation of insulin-like peptides and their effect on ageing in three highly distinct species; namely house mice, round worms and fruit flies. By doing so, the group showed that manipulations of endocrine function can slow ageing without altering reproductive capacity. By replicating their study across three separate phyla, the group can conclude that the investigated mechanisms are highly conserved between evolutionary groups and thus can more confidently infer that humans share the same physiological characteristics. If we utilise this approach here, models which aim to investigate novel pathways and mechanisms could be greatly improved in their robustness by exploring these variables in separate, evolutionarily distant species. Conversely, where available, the use of species that are highly similar to humans (like our relatives the chimpanzee) can by-pass the requirement for multiple animal studies. Of course, this is not always possible due to various limitations (time, finance, resources etc.) in which case the best available must suffice.

The selection of the animal model(s) that are used, forms in many but not all ways, the study's capacity for transferability. Simply choosing a model that is traditionally used within a laboratory or collaborative group, or one that is commonly used in a field of research, may not always result in the most robust scientific design being created. If planning on sticking to the *status quo*, following the directives in this step to test the veracity of that decision is recommended. Furthermore, if designing the animal model with a pre-clinical aim and the goal is to establish an intervention for human use or progression into human clinical trials, following approved country specific guidelines for the development for such drugs should be followed. For example, the U.S Food and Drug Administration outlines these requirements for the transferability of pre-clinical animal models to human use [420]:

1. There is a reasonably well-understood pathophysiological mechanism of the toxicity of the substance and its prevention or substantial reduction by the product;
2. The effect is demonstrated in more than one animal species expected to react with a response predictive for humans, unless the effect is demonstrated in a single animal species that represents a sufficiently well-characterized animal model for predicting the response in humans;
3. The animal study endpoint is clearly related to the desired benefit in humans, generally the enhancement of survival or prevention of major morbidity;
4. The data or information on the kinetics and pharmacodynamics of the product or other relevant data or information, in animals and humans, allows selection of an effective dose in humans.

Step 5: Application

For obvious reasons, the species which are of the highest fidelity are of the primate genus, which are almost perfectly homologous to humans. However, considering the ethical implications concerning the use of primates in research, the housing and resource requirements that they require (and that we have access to), and the large number of animals required in pre-clinical studies, mice will be used for this study. As this is a pre-clinical investigation and ultimately a proof of concept study, large animal numbers are required to satisfy statistical power requirements. As there are no previous studies to base the expected

effect size on, a power analysis to determine the appropriate sample size cannot be reliably completed. Although we hypothesis a negative impact on the animals used, the effects of drugs can vary greatly from patient to patient and we expect this to translate to the animal model as well. Other studies in the chemotherapy toxicity area [1,159,160,272,421,422] have used group numbers between 10-12 for lean weight measurements, 10-11 for lean muscle mass measurement with echoMRI [423], 15-21 in a survival based cancer xenograft model [424], 12-20 in cancer genetic investigations [425] and 6-20 [426-428] for CT analysis of cachexia. Importantly, though, these studies have not included an 8-week regimen of cytotoxic drugs. Due to the nature of chemotherapy, and considering over 70% of childhood cancer survivors develop a severe secondary chronic illness over their lifespan[7,13,16,18,93,150], it is reasonable to suggest a larger group of animals is necessary (15-20). For this reason, that this is a pre-clinical proof-of-concept study, our previous experience with mice, as mice are frequently used in cancer, cachexia and muscle disorder research, and due to the capacity of our animal facility, we have selected mice as our species of investigation.

Step 6: Identify species differences

In the prior step, similarities between the selected animal model and humans were reviewed. Conversely, clinically relevant differences that exist between the two models should also be identified. Differences which are not identified and acknowledged may occasion an unknown shift of results, causing a skew in the perception of the intervention's

success (or lack thereof) within the animal model. Moreover, without acknowledging and accounting for these differences, efficacy in the animal model may be unknowingly inflated or truncated due to nuances within that animal. This could ultimately compromise the study and result in a mistakenly 'successful' intervention transitioned to clinical trials where they shouldn't be, or mistakenly 'unsuccessful' interventions abandoned. As such, these differences comprise limitations within the study and are important aspects to acknowledge prior to moving forward. For example, variables which may impact intervention tolerability, toxicity and mortality – such as pharmacokinetics, body surface area, anatomical differences in organ or musculoskeletal mass, behaviour or animal social requirements which may be impacted upon when experimentally housed, inflammatory responses to implants etc. – should be considered and accounted for. Differences in known spontaneous development of pathologies should also be noted if they are significantly different to their human counterparts. For example, the OF-1 out bred strain of mouse exhibits a 35% frequency of occurrence for osteoma's, which is significantly higher than the average 1% seen in most other mouse strains [429] and less than 0.1% in humans [430]. A study that failed to recognise this nuance of the OF-1 strain may falsely abandon their study due to concerns that the intervention may be cancerogenic. Notwithstanding the above, it does come to a point where this process becomes a process of diminishing returns, where to identify all limitations of a model could easily eventuate into a complete study on its own. The amount of resources spent here is directly proportional to the level of homologous-ness required and the use of multiple animal models may be required (as outlined in the previous step).

Step 6: Application

As human CI-SMDW is endured over the lifespan, investigations into the mechanisms that underscore them must be completed in a model that can replicate the complex nature of ageing and metabolism. Furthermore, chemotherapy is only administered to humans after cancer has been diagnosed. As cancer elicits compounding variables which exacerbates skeletal muscle wasting, such as cancer cachexia, this has the potential to mask the underlying pathology of CI-SMDW. As we are investigating skeletal muscle dysfunction and wasting induced by paediatric chemotherapeutic administration, healthy, cancer-free paediatric mice will be used. The balb/c strain of mice have been chosen for use within these studies for two major reasons, the first being that balb/c mice are commonly used (including by us) in pre-clinical models of cancer. Secondly, balb/c mice are easily available to us in their natural (albeit inbred), severe combined immunodeficiency (SCID) and in a genetically modified state (for the induction of medulloblastoma), allowing for the same strain of mouse to be used in different in modes of investigation (refer to Step 11 for more details). Notably, however, this strain of mice are reported as having a low mammary tumour incidence but do develop other types of cancers in later life, most commonly reticular neoplasms, lung tumours, and renal tumours as compared to other strains – a likely result of inbreeding. As we are using mice throughout the lifespan, a larger number of mice will be used to combat this. Further, a control group will also be used to ensure that any progression of the CI-SMDW phenotype, can be identified as being due to the treatment received and not due to secondary and naturally occurring pathologies such as cancer.

Step 7: Intervention adaption

Treatment methods for interventions are required to be altered between patients to accommodate for physiological differences, such as weight, body surface area, lean mass and age. These same changes must be implemented to accommodate for the differences between human and the animal model selected. With the differences outlined in Step 6, the intervention must now be modified to accommodate for these to maintain clinical relevancy. Although not an exhaustive list, outlined here are four categories which aim to account for common misalignments between species and, if required, to modify the chosen intervention from its human dose to the animal equivalent dose and to consider clinically relevant supportive therapies.

7a: Time and age discrepancies between species

Adapting an intervention which uses a short-term, quantifiable end (such as a singular dose/application or two weeks of dietary modification), may not require any adaptions to time points due to the acute nature of the intervention. On the other hand, due to lifespan differences between species, conducting a full-length intervention where a long-term time frame defines the end point (such as 12 weeks of daily intervention or monthly follow up testing), may not be possible. Prime examples of this are chemotherapeutic regimens that span from months to years to achieve remission of cancer, which in humans is achievable, but

when investigated in small rodents for instance - whose lifespan may only be two years - the full study may not fit within its natural life. To overcome this discrepancy, considerations into metabolic rates can be made. For example, the mouse has a metabolic rate some 7 times higher than humans [431,432], thus experimental time frames in mouse studies may need to be shorter in comparison to human studies to achieve the same clinical effects. In some cases, like dietary modifications, hormonal changes or immune suppression where a specific level of change is required (i.e. 10% reduction in fat mass, 5% increase in circulating lymphocytes) this may not be the case, although these goals may be reached faster in animals with a higher metabolic rate.

7b: Intervention amount

Having previously identified the experimental domain and the intervention of interest, it is likely that the intervention amounts have also inadvertently been ascertained. It is, however, uncommon that a human dose will also be used as the animal equivalent dose, except in circumstances where the intervention is physical in nature (i.e. isomorphic biomechanical implants) in which case this step is unnecessary. In cases where pharmacokinetics, physiological processes and metabolism are involved (such as pharmaco-interventions or dietary modifications) this step is essential to maintaining clinical relevancy, as important modifications to the human dose need to be made. From here on and throughout this thesis, the human dose and/or 'dose' refers to the dose, amount, application

or level of intervention decided upon in Step 3. Further reading on drug dose comparisons can be done so here (Goldsmith *et al* [433])

A human dose should be adapted to an animal equivalent dose with the following criteria:

1) Directly converted from the clinically relevant human dose to the appropriate animal equivalent dose for the selected species; taking into consideration and proportionally modifying for, at the very least, metabolic rate and body surface area differences using modified FDA guidelines[434] (see Table 2.1). These guidelines take into consideration differences in metabolic rate, size and body distribution for pharmacological interventions.

Table 2.1: FDA guidelines to modify human dose (HD) to animal equivalent dose

Species	**Reference body weight (kg)**	**Working weight range (kg)**	**Body Surface area (m^2)**	**To convert dose in mg/m^2 to dose in mg/kg to divide by K_m**	**To convert HD dose in mg/kg to animal dose in mg/kg, either:**	
					Multiply human dose by	Divide human dose by
Human	60	-	1.62	37	-	-
Child	40	-	1.09	25	-	-
Mouse	0.02	0.011-0.034	0.007	3	12.3	0.081
Hamster	0.08	0.047-0.157	0.016	5	7.4	0.135
Rat	0.15	0.08-0.27	0.025	6	6.2	0.162
Rabbit	1.8	0.90-3.0	0.15	12	3.1	0.324
Dog	10	5-17	0.50	20	1.8	0.541
Rhesus Monkey	3	1.4-4.9	0.25	12	3.1	0.324

*Data adapted and modified from 2005 FDA guidelines[434]

2) Ensure the new animal equivalent dose does not exceed previously published animal tolerability or toxicity data. If it does, the dose should be lowered to published tolerable doses if these were exceeded to abate animal welfare concerns.

2a) Where only single dose tolerability data is found, and multiple doses or applications of the intervention are required, the maximum tolerable published single dose should be used as the maximum cumulative dose. This assumption is limited in its ability to predict cumulative effects (or lack thereof) and opportunities will be available to refine these doses later based on the side effect profile observed (see Step 8: Dose finding pilot).

2b) Where only tolerability data for cumulative doses are found, and a single dose is required, the pharmacokinetic and bioavailability data from cumulative dose toxicology studies need to be considered, and the dose appropriately modified to ensure undesired levels of toxicity (and more importantly; lethality) are avoided. In the case where these data are not available or appropriate for the intervention selected, single dose data should be used, and dose levels refined (see Step 8: Dose finding pilot).

7c: Toxicity and side effect profile

Aside from effectivity, toxicity is the major limiting factor for the success of an intervention. To ensure that the intervention tested throughout this study is safe for use, it is equally important to measure both its efficacy and toxicity. Thus, this step aims to obtain biochemical, physiological and morphological information indicative of toxicity that is reproducible, reliable, and dose-related and which can be interpreted and extended to assess the risks in humans. Measures of toxicity will of course change between interventions and should be adapted to meet the requirements of each intervention. Monitoring of body mass and food consumption should always be included due to their ease of measure and their powerful predicative nature.

7d: Supportive therapies

Many interventions against human pathologies are generally multifaceted in nature with multiple supportive therapies revolving around a central intervention. These supportive therapies are often used clinically to support survival and treatment tolerability (such as antibiotics for infection concerns, forced entero-feeding or I.V lines for supportive therapy of fluids or treatments). A classic example is the systemic treatment of cancer. A patient could receive multiple regimens of chemotherapy and radiotherapy, combined with surgical intervention to reduce the size of and remove their cancer. Moreover, patients receive a multitude of supportive therapies including intravenous fluid drips, nutritional supplementation, exercise interventions, immune and blood cell transfusions, bone marrow transplants, pain management, depression therapy, counselling and so on. Within this step it

is important to define all supportive therapies relevant to the intervention being trialled (if used previously – if not, hypothetical considerations are to be made) and consider their purpose and their effects on the patient and the intervention at hand. In doing so, a decision can be made to include the supportive therapy(ies) that are deemed essential to the success of the intervention and disregard those that aren't.

Considerations of feasibility to add supportive therapies should be made as some will either be impossible or extremely resource intensive to include, and thus may not be viable options. For example, a neutrophil blood infusion for those undergoing systemic methotrexate chemotherapy may be crucial in humans but, for mice in an experimental sterile environment, the increase in clinical similarity may not be worth the resources used to marginally improve clinical similarity. This largely becomes an exercise of executing a cost/benefit analysis which will be unique to each laboratory and dependent on financial, equipment and human resources.

Step 7: Application

Step *7a application: Time and age discrepancies between species*

Each of the regimens stated in Step 2 of this chapter span considerably different timeframes. For example, the ALL-POMP regimen involves an initial 24-week chemotherapy assault, before a two- to three-year maintenance period is commenced, the MB-LCV regimen for at least 62 weeks, and the BL-CHOP regimen for at least 42 days. As stated in the

framework, the natural lifespan of a balb/C mouse is approximately two-years, meaning that the ratio of treatment to lifespan is some anywhere from 1:4 to 1:1. When compared to humans, even the longest treatment regimens, such as ALL-POMP, would only achieve a 1:20 ratio. If indeed metabolic rates were accounted for and the length of these regimens shorted by 7x, this would provide a clinically relevant modification for the treatment time course. However, this would not consider the mouse's xenobiotic clearance capacity which may greatly elevate chemotherapeutic toxicity and thus reduce the clinical relevancy of the study. Considering the pathology that these interventions are designed to combat are usually administered in the first 15 years of life [55,435], another modification option is to match the developmental milestones between mouse and children (specifically sex characteristic development and sexual maturity). Of course, both options have their merit, and implementing both would be ideal. However, without preliminary drug clearance investigations (of which are out of the scope of this thesis), the ramifications of shortening regimen timeframes present too much uncertainty. Due to this uncertainty, regimens will be administered using the same timing as in humans with the starting age adapted to ensure similarity exists between the mice used here, and the children who receive these regimens.

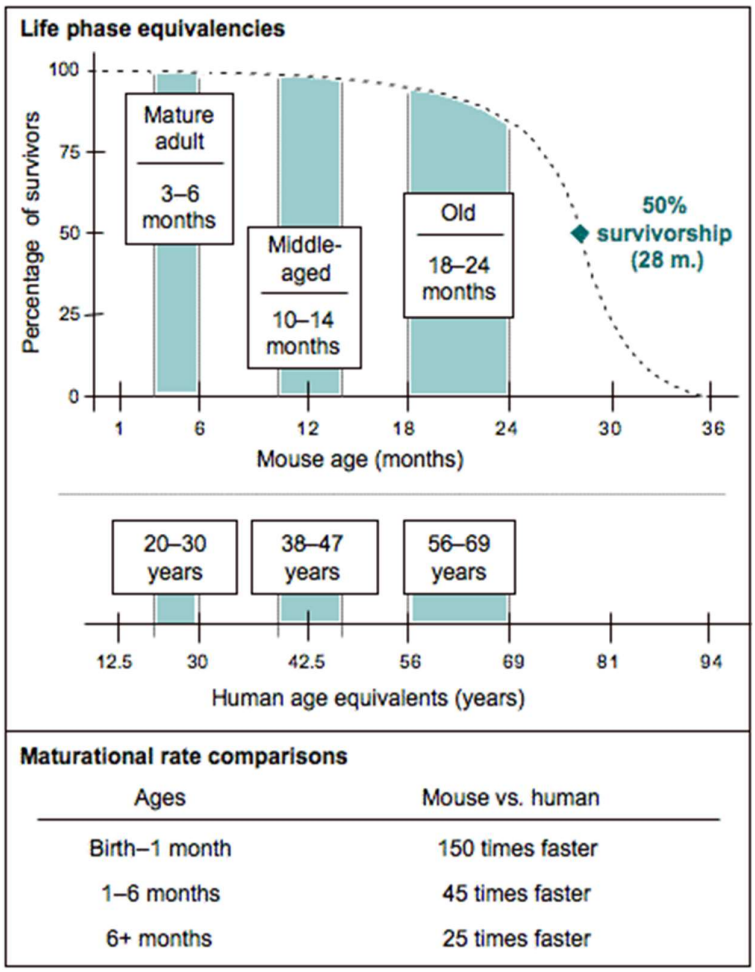

Maturational rate comparisons

Ages	Mouse vs. human
Birth–1 month	150 times faster
1–6 months	45 times faster
6+ months	25 times faster

Figure 2.3: Representative age ranges for life phase equivalents between rodent and human beings. *Image source: Life as a biomarker, The Jackson Laboratory, USA* [421].

Mice mature at a rate 150 times faster than humans in the first month of life and, as such, reach the sexual maturity of a 12 year human by 1 month of age [437]. This suggests that the optimal time to commence treatment for these regimens would be 2-3 weeks of age as the greatest incidence rate of all three cancers are below the age of 5 years [55,435] (refer Figure 2.3). However, due to welfare considerations for the mice, mice under the age of 3 weeks must be transported with their mother as the pups are still dependent on maternal feeding. Due to ethical (as we, nor our collaborators, had any scientific use for older female mice) financial reasons (due to a 1:4 mum:pup shipping ratio requirement), and due to the technical difficulty in handling and treating 2-3 weeks old mouse pups, it was decided that 24 days of age was an appropriate time point to commence treatment which would still maintain as much clinical similarity as possible. This allowed for the mice to be delivered at 21 days (3 weeks) with 3 days acclimatisation, before treatment commenced. Moreover, due to the short lifespan of the mouse and the limitations of resources, alterations made to each of the regimens will be are as follows:

ALL-POMP

As the full regimen spans 3-4 years, only the first 8 weeks of the regimen will be used. As such, only the induction phase (using vincristine, prednisone, L-asparaginase and methotrexate) and the consolidation phase (using vincristine, 6-mercaptopurine and methotrexate) will be administered. Importantly, in this regimen, methotrexate in humans is delivered intrathecally. Due to the high degree of difficulty of this technique, methotrexate

will be delivered via intraperitoneal injection instead. The regimen used is outlined in Figure 2.4.

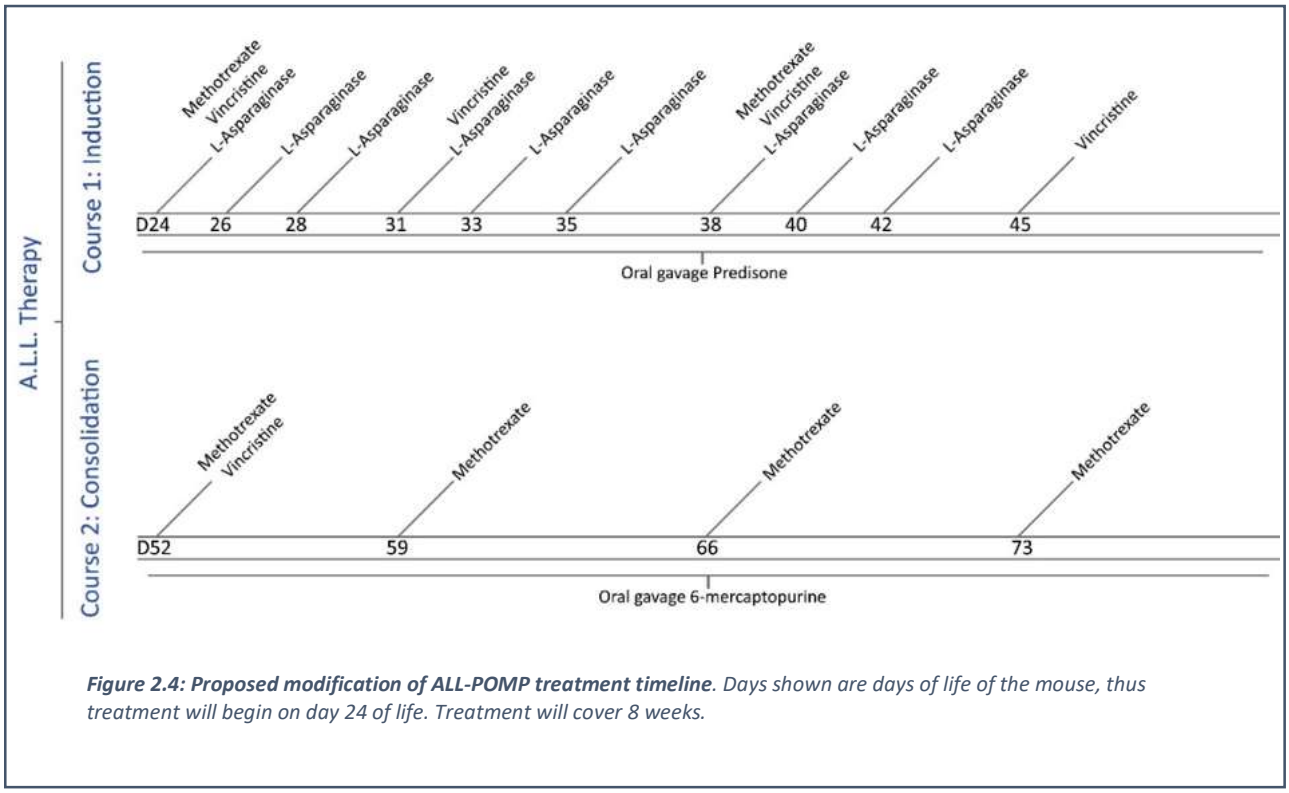

Figure 2.4: Proposed modification of ALL-POMP treatment timeline*. Days shown are days of life of the mouse, thus treatment will begin on day 24 of life. Treatment will cover 8 weeks.*

MB-LCV

Following a similar modification method as ALL-POMP, only 8 weeks of the MB-LCV regimen will be used. As the induction phase centralises around cranial radiation and vincristine use for 8 weeks, it was decided that the chemotherapy-centric consolidation phase would be used instead. This phase utilises repeating cycles of lomustine, cisplatin and vincristine. The regimen used is outlined in Figure 2.5.

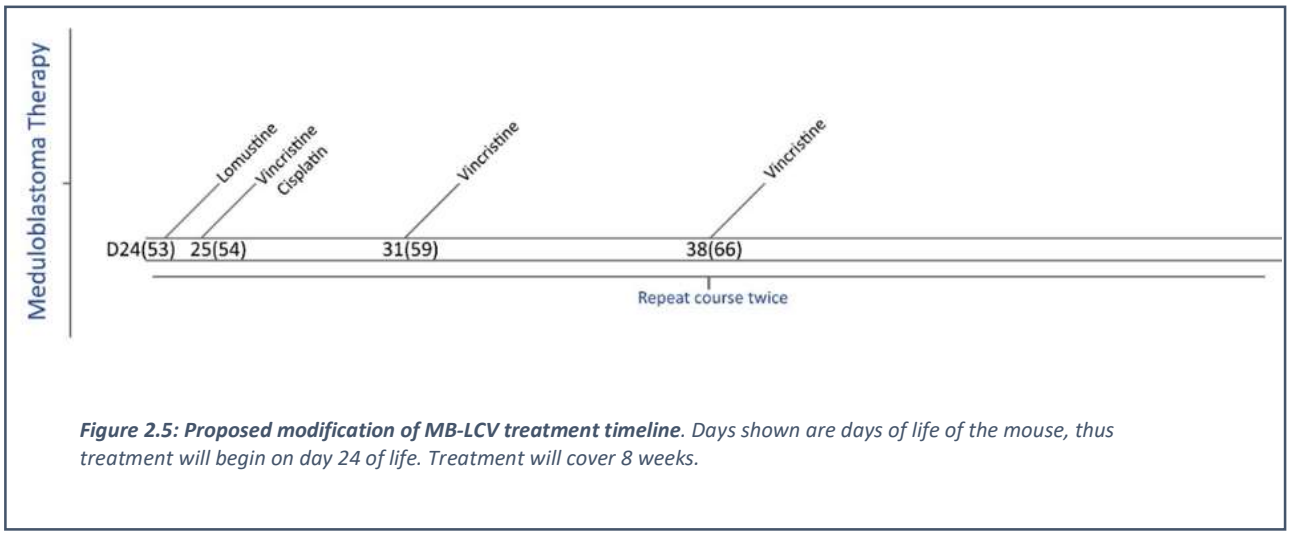

***Figure 2.5: Proposed modification of MB-LCV treatment timeline**. Days shown are days of life of the mouse, thus treatment will begin on day 24 of life. Treatment will cover 8 weeks.*

BL-CHOP

In line with modifications made to the previous regimens, the *FAB/LMB 96 CHOP regimen* was altered to a 4-week cycle. No other alterations were made aside from changes to dose (outlined in the next step). The regimen used is outlined in Figure 2.6.

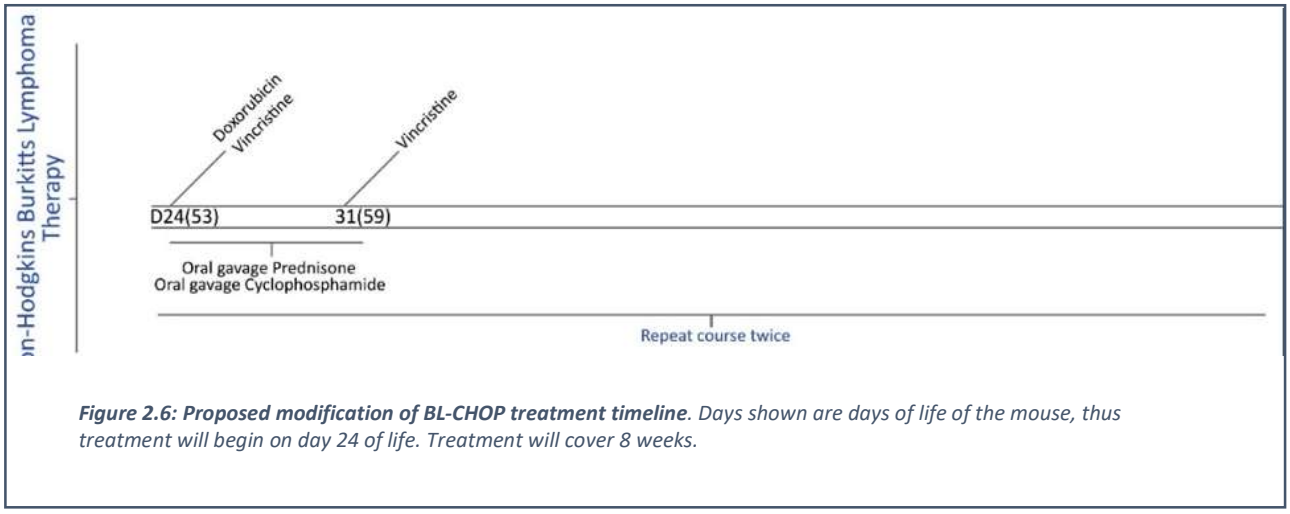

***Figure 2.6: Proposed modification of BL-CHOP treatment timeline**. Days shown are days of life of the mouse, thus treatment will begin on day 24 of life. Treatment will cover 8 weeks.*

Step 7b application: Intervention amount

The dosages that will be used have been selected from the gold-standard regimens selected in Step 2. These human dosages have been converted to an animal equivalent dose based on the guidelines in *Step 7b.1*. Where these dosages were above the published tolerable doses for mice, they were reduced to lowest therapeutically viable dose previously reported in the literature, as per *Step 7b.2a*. Where tolerable doses are of a single, once off treatment, and in the case where treatment in this project requires multiple treatments on successive days, the previous publications showing tolerable cumulative doses of individual chemotherapies (i.e. cumulative maximal tolerable dose = 45mg/kg over 7 days, thus 15mg/kg administered on D1,3,5) will be used (refer Table 2.2). It should be noted that these regimens are expected to induce acute toxic side-effects and have an acute impact on the welfare of the animals, however, these effects are required to ensure the pathology of CI-SMDW is initiated. To ensure that the appropriate doses have been selected, the following step in this framework will establish a dose finding pilot study to ensure maximum clinical relevancy whilst mediating as much toxicity as possible.

Table 2.2 IAMDF-modified ALL-POMP, MB-LCV and BL-CHOP regimen drug doses.

Regimen	Drug	Original daily dose	IAMDF modified daily dose (mg/kg)
ALL-POMP	Prednisone	40mg/m^2	11.81
	Vincristine	1.5 mg/m^2	0.44
	Methotrexate	10 mg	5.47
	L-Asparaginase	6000 IU/m^2	1771.20 U/kg
	6-Mercaptopurine	75 mg/m^2	22.14
MB-LCV	Lomustine	*75mg/m^2*	22.14
	Cisplatin	*75mg/m^2*	22.14
	Vincristine	1.5mg/m^2	0.44
BL-CHOP	Cyclophosphamide	500mg/m^2	450.00
	Vincristine	2mg/m^2	0.98
	Prednisone	30mg/m^2	29.52
	Doxorubicin	60mg/m^2	6.50

Step 7c application: Toxicity and side effect profile

Common clinical sequalae observed in chemotherapy treatment is highly variable between patients. To monitor treatment toxicity, we have adapted an animal welfare scoring system and observation chart from the Victorian Department of Agriculture [438] (refer to Table 2.3 and Table 2.4). By using this observation system, we aim to monitor the impact of the chemotherapy regimens on the mice throughout the study (primarily in the pilot study outlined below in Step 8). Further, and in combination with the variables of interest outlined in Step 4, bodyweight and food intake will be monitored.

Table 2.3: Daily individual animal monitoring form. *This form was used to assess chemotherapy side effects within the pilot study. Observations were recorded in the table; normal clinical signs were recorded as "N" with abnormalities recorded as "A" and severity score in brackets e.g. Breathing: A (3) using the clinical signs severity score (**Table 2.4**). Table adapted from the Victorian Department of Agriculture, Australian Government [438]. Abbreviations: AF, animal facility; AWO, Animal Welfare Officer; g, gram. Clinical monitoring defined as continuous hourly monitoring and reporting until symptoms subside or death/euthanasia occurs.*

CLINICAL OBSERVATION	DATE & OBSERVATION SCORE (N or A)						
DATE:							
UNDISTURBED							
Coat							
Activity							
Breathing							
Movement/gait/trembling							
Eating							
Drinking							
Alert/sleeping							
ON HANDLING							
Alert							
Body condition							
Bodyweight (g)							
Hydration							
Eyes							
Faeces							
Nose							
Breathing							
Urine							
Vocalisation:							

Cumulative Score	Action Required
0	No action required
1-3	Inform AF staff/AWO and place on clinical monitoring
4-7	Inform AF staff/AWO and place on clinical monitoring -may require analgesia or euthanasia
7-10	Inform AF staff/AWO, intervention with analgesia, fluids or humane euthanasia
10+	Inform AF staff/AWO –humane euthanasia immediately

Table 2.4: Clinical Signs Severity Score table. *Adapted from Signs of Severity Score published by the Victorian Department of Agriculture, Australian Government* [438]

CLINICAL SIGNS SEVERITY SCORE TABLE				
SIGNS	**0**	**1**	**2**	**3**
Activity	normal	isolated, abnormal posture	huddled/inactive OR overactive	moribun d OR fitting
Alertness/ sleeping	normal	dull or depressed	little response to handling	unconscious
Body condition	Normal	Thin, loss of body fat and or muscle mass (Body condition score of BC3)	Further loss of body fat and or muscle mass (Body condition score of BC2)	Hunched over, emaciated (Body condition score of BC3)
Body weight	normal weight and growth rate	Some acute weight loss within 48 hours <10% change. Chronic weight loss of <10% within 5 days.	Acute weight loss of >10% but <15% within 48 hours. Chronic weight loss >10% and <15% within 5 days.	Acute weight loss of >15% within 48 hours. Chronic weight loss >15% within 5 days.
Breathing	normal	rapid, shallow	rapid, abdominal breathing	laboured, irregular, skin blue
Coat	normal	coat rough	Unkempt, wounds, hair thinning	bleeding or infected wounds, or severe hair loss or self- mutilation
Dehydration	none	skin less elastic	skin tenting	skin tenting & eyes sunken
Drinking	normal	increased OR decreased intake over 24 hours	increased OR decreased intake over 48 hours	constantly drinking OR not drinking over 24 hours
Eating	normal	increased OR decreased intake over 24 hours	increased OR decreased intake over 48 hours	obese OR in appetence over 48 hours
Eyes	normal	wetness or dullness	discharge	eyelids matted
Faeces	normal	faeces moist	loose, soiled perineum OR abnormally dry +/- mucus	running out on handling OR no faeces for 48 hours OR frank blood on faeces
Movement/ gait	normal	slight incoordination OR abnormal gait	Un-coordinated OR walking on tiptoe OR reluctance to move	staggering OR limb dragging OR paralysis
Nose	normal	wetness	discharge	coagulated
Urine	normal		abnormal colour/volume	no urine 24 hours OR incontinent, soiled perineum
Vocalisation	normal	squeaks when palpated	struggles and squeaks loudly when handled/palpated	abnormal vocalisation

Step 7d application: Supportive therapies

A large variety of supportive therapies are available and recommended for use to combat chemotherapy-induced side effects, such as nausea and vomiting, mucositis, anaemia, neutropenia, osteoporosis and diarrhea to name a few [439]. Due to each chemotherapeutic agent being associated with a different side-effect profile, the supportive therapies used to treat these are often closely associated with certain chemotherapeutic agents. For example, most chemotherapies induce nausea and vomiting and as such it is mostly common practice to treat patients with antiemetics after they commence treatment (aprepitant, ondansetron, etc.) [440-444]. The same is true for other easily treatable side effects like diarrhea, where the treatment has a low toxicity profile itself and, thus, low risk to the patient if administered prophylactically [439,445]. Some chemotherapies, like the anthracycline class, commonly induce cardiotoxicity or renal toxicity which can be partially combated by prophylactic administration of cardioprotective agents (dexrazoxane) or chemoprotectants (amifostine) [446,447]. Other side-effects require a more reactive approach, like that in anaemia, neutropenia, osteoporosis, skin rashes and mucositis, for example, as treatments often require a more invasive (such as blood transfusions) or physiology altering (such as bisphosphonates to combat chemotherapy-induced osteoporosis) supportive interventions which could be contraindicated in some circumstances [448-451]. Other, more simple, supportive therapies are often administered concomitantly with chemotherapy, such as intravenous saline drips and antibiotics to combat chemotherapy toxicity (through dilution, fluid volume maintenance and protection against renal injury) and immune suppression which are common side effects of treatment [452-454].

Other, non-pharmacological, non-haematological interventions often surround improving survival and chemotherapy tolerability by increasing body mass and function. Nutritional supplementation to ensure adequate intake (particularly of protein and vitamin D for lean and bone mass maintenance respectively) is imperative, as is ensuring patients maintain movement and attempt exercise to maintain bodily function and abate disuse atrophy. Interestingly, though, a study by Hyltander *et al.* showed parenteral feeding (where nutrition is delivered directly into the venous system, bypassing the gastrointestinal system) showed no improvement to overall survival, length of stay in hospital, body weight and body composition maintenance [455]. With lean mass positively associated with chemotherapy tolerability, the maintenance of muscle through supportive therapies cannot be understated [456-458].

Although these supportive therapies are offered in a clinical setting, many of these will mask the potential atrophic effect of the chosen chemotherapies and thus the key variable of interest of these studies. Moreover, the financial and resource cost associated with these supportive therapies are not viable for the current study. For example, the administration of blood transfusion to combat anaemia's or neutropenia's, intravenous administration of saline or antibiotics, or customising nutritional intake to individual or all mice would be logistically impossible. For these reasons, some of these supportive therapies, but not all, will be used reactively to combat adverse events. Specifically, antibiotics and nutritional supplementation will be used to combat infections or life-threatening weight-loss as they are observed.

Step 8: Dose finding pilot study

As with standard human clinical trial processes [459], the phase I trial here is used to test the intervention for the first time within the identified animal model to evaluate safety and tolerability. The establishment of whether the selected levels of the intervention are tolerable and viable in the animals selected is needed, together with the production of a side effect profile similar to that seen in the clinical setting. The pilot study is designed to incrementally increase the level of intervention from a known safe point to ensure animals are not subjected to unjust cruelty and to ensure minimal mortality. Based on the Organisation for Economic Cooperation and Development (OECD) Up-Down protocol [460], a dose lower than the previously selected Intervention Animal Model Development Framework (IAMDF) dose is used as a starting dose to ensure absolute tolerability and to establish a baseline side effect profile. Once that animal survives (1-2 days has been previously shown to be sufficient in most cases to capture a majority of treatment related deaths [461]) the dose is then increased to the selected IAMDF dose and the next animal treated with the elevated dose. If that animal survives the initial 1-2 days, a further 14-day observation period should be adhered to and a second animal started on the same dose. Both animals should survive before accepting the IAMDF dose as viable. In the case either animal dies, the dose should be systematically reduced and the trial repeated. This process continues until two animals survive a maximum tolerable dose by increasing and decreasing the intervention amount depending on the outcome of the preceding trial. From this data, pharmacological values (such as therapeutic or lethal doses) can be calculated. Multiple methods for dose reduction could be applied, such as using factors (i.e. 2/10), logarithmic reductions (i.e. 10x), or dose halving, with further explanation of these outlined in the OECD up-down protocol [460]. In some cases, it may be

necessary to alter the interval timing of the intervention rather than the levels of the intervention itself. For example, instead of a starting dose of 0.1mg/kg of body weight before escalating to 1mg/kg of body weight on days 1, 3, 5, 8, 10, 12, a trial more concerned with overdosing due to timing may wish to begin with an intervention regimen of days 1 and 8 before escalating to 1, 3, 5, 8, 10, 12.

The goal here is to, first, establish an intervention level which does not cause significant harm or change to the animal to establish a baseline side effect profile upon which subsequent trials can be compared to. Secondly, to trial using the adapted up-down dose method (or interval timings if that is the case) described above to establish a rudimentary dose response in the animal model to, thirdly, select an intervention level and regimen that best fits the human side effect profile observed clinically. As animals have innate differences, it may be necessary at this stage to alter the originally defined regimen to better match clinical observations and to overcome newly found variables or adverse reactions. This can be done either by altering the current intervention regimen further (such as altering treatments individual treatments or increasing timing intervals) or by adding supportive therapies as outlined in Step 6.

Importantly, these further alterations should not diminish the studies clinical relevance if avoidable. Variables outlined in *Step 4* should be measured throughout the pilot study to create both a variable-of-interest and side-effect-to-dose relationship. This will also provide important data to complete a power analysis for larger studies in the following steps.

Step 8: Application

The application of this step will be presented in the following chapter; Chapter 3, where the dose-finding pilot study (as outlined in this Step) will be performed and the outcomes analysed. This chapter (or step) will then form the basis of the Step 9 and 10.

Step 9: Dose confirmation study

Following the completion of the pilot study, the selected IAMDF dose should now be tested with more scale and veracity. A standard animal experimental model should be employed here whereby an experimental group (healthy animals treated with the intervention at the previously defined dose) is compared to control and vehicle/sham groups over appropriate timeframes with appropriate animal numbers. Using the effects measured in the pilot study, a power analysis can be performed to accurately determine the required sample sizes needed for this step. Variables of interest and side effects defined in *Step 4: Define variables of interest* and are to be measured and compared to hypothesised expectations.

Two main outcomes can occur here. First, the intervention at the IAMDF derived dose elicits the expected effects on the animals (within a reasonable margin of certainty due to the pathology being absent). If this is the case, progression to Step 11 is advised. Secondly, the intervention at the IAMDF derived dose does not elicit the expected effects on the animals. In this latter case, it must be determined whether the effects, or lack thereof, are due to the

pathology, or supportive therapies not being present within the model, and whether these can be accounted for in the next step. If neither of these are viable, it may be in best interest to return to earlier steps and troubleshoot why the outcome was not as expected.

Step 9: Application

Following on from Step 8 and Chapter 3, where the dose finding pilot studies were performed and their outcomes analysed, the outcomes of this step will be presented in later chapters. Due to the relatively quick success of adapting the MB-LCV and BL-CHOP regimens from human to mice in their respective pilot studies, these two regimens were progressed into dose confirmation studies where their CI-SMDW effects could be properly assessed in Chapters 4 and 5 respectively. The ALL-POMP pilot, largely due to significant treatment complications took much longer to finalise and, due to time limitations of this PhD candidacy, was not progressed further.

Step 10: Intervention adaptation study

In Step 7, the selected intervention was modified to better replicate the intervention within the selected animal species. After confirming that the adaption accurately represents the clinical presentation of the intervention in humans in steps 8 and 9, this step concentrates on adapting the intervention to improve outcomes or specific variables. For example, a model

investigating the outcomes of a surgical knee replacement should, for example, now modify the prosthesis to investigate whether the modification is viable, safe and an improvement on the original gold standard setup used in Step 8 and 9. This step will be largely driven by the successes of the previous steps, as the effect of the gold-standard intervention on the variables of interest must be previously established and measured so any improvement, or lack thereof, induced by the adapted intervention can be assessed. Utilising the information obtained in Step 1 and Step 4, a variable (or variables) which significantly impact the outcome of the patient should be selected. Then, after the pathophysiology of the issue is understood, or at the very least a viable physiological target can be identified, then further adaptions to the gold-standard intervention can be made, such as; altered dosing schedules, addition or removal of specific agents or mechanisms, using a different intervention all together or using supportive therapies to name a few. The modification and its effects should be measurable and replicable with relatively clear mechanisms of action allowing for comparisons and future modifications to be reliably made.

Step 10: Application

As highlighted in *Chapter 1*, targeting mitochondrial dysfunction to reduce mtROS production is a logical intervention point through which to attenuate the initiation of muscular atrophy, macroautophagy, necrosis, and apoptosis signalling pathways, all of which have been strongly associated with CI-SMDW [10,244,284,285]. By adapting the gold-standard chemotherapy regimens to include a co-therapy capable of mitigating mitochondrial

dysfunction, we hypothesise that this could ameliorate the CI-SMDW phenotype and improve patient outcomes. Idebenone (IDEB) was identified during the review of literature as the most viable and safe mitochondrial targeting co-therapeutic with the potential to reduce cellular mtROS whilst simultaneously improving mitochondrial function.

A review of the literature, including phase-III trials using IDEB, dosages varied from 450mg to 2250mg per day in humans, with treatment periods of up to 52 weeks. One study, investigating the therapeutic effects of IDEB against the myopathy; Duchenne muscular dystrophy, showed therapeutic promise using 200mg.day^{-1} in 4 week old mice up until the age of 10 months. With this mouse model in mind, after converting therapeutic doses from the above human trials, after consultation with pharmaceutical specialists; it was decided that co-administration of IDEB at 100mg.day^{-1}, for the full 56-days of chemotherapy would offer the best therapeutic potential.

Step 11: Pathology and intervention study

With the IAMDF-derived intervention having been verified and adapted, the addition of the pathology that it aims to treat is an important subsequent step. The level of success of the previous step should be considered and refinement to improve the model should be made before commencing. After any refinements have been made, this step is simply additive to the previous model. As the intervention, control and vehicle/sham groups have already been investigated, the target pathology and its derivatives are investigated instead. Thus, the

experimental groups in this step are pathology and pathology+intervention. It may be necessary to include a pathology sham group, if the pathology is induced into the model by non-genetic means (for example surgical, xenograft, transplant or pharmacological). All analysis made in the previous step, should be maintained in this step for continuity and comparison.

Step 11: Application

Each of the chemotherapy regimens used within this framework is considered as the gold-standard therapy for their associated pathology, namely ALL, medulloblastoma and NHBL at publication of this thesis. Although we were unable to complete this step due to time and financial restraints, to assess the efficacy of Step 10 modifications it was planned to investigate the modified interventions in a xenograft SCID (severe combined immunodeficiency) or genetically engineered mouse models using the same strain (balb/c) as used in previous steps. For the ALL-POMP model, SCID mice would be inoculated with human leukemic cells obtained via therapeutic apheresis of paediatric ALL patients [462]. Similarly, orthotopic xenografts of human NHBL cells into the adrenal or para-adrenal glands (location used due to ease of access and replicability via ultrasound guided needle) would be used as previously described to investigate the therapeutic efficacy of the modified BL-CHOP therapy. [463] To investigate the modified MB-LCV regimen, a genetically engineered knockdown mouse model ($Lig4^{-/-}$ / $p53^{-/-}$) has been shown to have the highest incidence rate

(or take up rate if compared to xenograft transplant models) of medulloblastoma with rates of 100%. [464] It must be conceded, however, that although these pre-clinical models may develop the cancer under investigation, a myriad of variables pull the clinical relevance of these xenograft model under question. The most significant of these is the ability of the tumours to metastasize, as this is one of the main reasons systemic administration of anti-cancer chemotherapeutics are used. [465] The referenced studies have all reported metastases within the chosen models and have reported congruence between their pre-clinical mouse model and the human patient sequalae. As the application of this step was outside the scope of this thesis, further discussion of the importance of this step will be resumed in Chapter 7 where the limitations and future directions of this thesis will be addressed.

Step 12: Evaluate clinical similarity of intervention

From conception, clinical relevancy and similarity have been key through this framework. A comprehensive analysis of the level of similarity that was achieved is paramount to support the translation of the intervention into the clinic. With nine from ten successful pre-clinical projects failing in clinical trials [466,467], more needs to be done to ensure success at these later translational levels. Although there exists a plethora of reasons why most animal models fail to produce successful human treatments, the steps laid out herein aim to improve both the clinical relevancy of the model and the researchers outlook on the

variables and processes that should be considered when aiming for the coveted 'from bench to bedside' achievement.

This step is thus an important step for the improvement of pre-clinical animal models both within individual collaborative groups and the wider scientific community. Reflection on both the success and failures of where the model achieved clinical similarity, in relation to current human models and not from animal standard, will hopefully identify the potential short falls of the interventions translation before it arrives into the clinical area. Proper reflection here serves to act as a filter to stop the promising yet clinically dissimilar models from progressing into expensive and resource hungry trials.

Step 12: Application

The application and success of each of the study's will be discussed in more depth in each of their relevant chapters, with the overall success of this framework discussed in Chapter 7.

2.3 Chapter Summary

This chapter aimed to develop a robust framework which could be used within this thesis, and in future biomedical research, to create animal models with which to investigate the therapeutic efficacy and viability of a human-targeted specific intervention. Using this

framework, three gold standard chemotherapeutic interventions (ALL-POMP, MB-LCV and BL-CHOP) currently used against paediatric malignancies have been modified for use and an animal model for the investigation of each developed. The next chapter of this thesis will utilise these pre-clinical animal models to assess each of the regimen's viability for use in a larger number of mice and assess the clinical similarity of their side-effect profiles, before using them to investigate the chemotherapy-induced skeletal muscle dysfunction and wasting pathology in later chapters.

Chapter 3

Validation of Juvenile CI-SMDW Investigatory Animal model

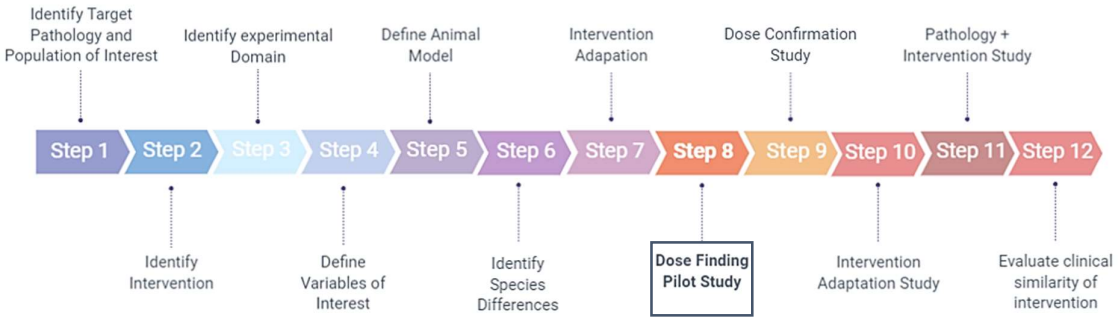

3.1 Introduction

Many of the gold standard chemotherapy regimens that are used today to combat cancer were founded decades ago [368,468-472]. Vast improvements to patient survivability have been achieved since then, and these improvements can be by-in-large attributed to earlier detection methods and greatly improved patient support therapies [6]. Alterations to original chemotherapeutic regimens is largely abated due to, and rightly so, by the health outcome concerns for patients – as only small, incremental changes can be made at any one time out of concern that anything larger may unacceptably increase patient risk. Animal models are thus an essential tool for the development of new treatment methods. However, as outlined in the previous chapter, the development of clinically relevant models can often be difficult due to the physiological and behavioural differences between the species. This chapter will build on the previous chapter which completed the first seven steps of the *Intervention Animal Model Development Framework* (IAMDF) and document the completion of *Step 8: Dose Finding Pilot Study*. This step is crucial to understanding the intricacies of the interventions, particularly the outcome of the interactions between the chemotherapeutic agents used in the various regimens and their subsequent effects on the mouse. This chapter aims to assess the suitability, efficacy and clinical relevancy of the ALL-(referred to heron as ALL-POMP), medulloblastoma- (referred to hereon as MB-LCV) and NHBL- (referred to hereon as BL-CHOP) indicated chemotherapy regimens as created using the Intervention IAMDF presented in *Chapter 2.*

3.2 Methods

3.2.1 Pilot animals

18-day old male, balb/C mice were obtained from the Walter and Eliza Health Institute (Victoria, Australia) and separated into boxes with 3 mice (1 mouse per regimen) per cage upon arrival and allowed to acclimatise for 3 days, before treatment commenced at 21 days of age. Mice were maintained on a 12hr light/dark cycle in a climate-controlled facility (18-23^{oC}, 40-70% humidity) at Sunshine Hospital, Western Centre for Health Research and Education animal facility (Victoria, Australia). Boxes were clad with standard, autoclaved compressed paper pellet bedding. On the day of treatment, mice were administered their respective treatments (as per Figure 3.1, Figure 3.2, and Table 3.1).

3.2.1.1 Pilot specific housing

Pilot mice were housed together in trial groups, with mice receiving respective treatments concurrently. This was done to minimise isolation distress as only one mouse received their respective treatment per trial. As such, food and water consumption was used in conjunction with weight monitoring to rudimentarily measure caloric intake and to assess whether alternative foods (i.e. watered down food paste/mash) were required. Further, due to housing arrangements in the pilot studies, food and water intake data was used as a rudimentary measure of the effect of chemotherapy dosing in general, rather than the effect of specific regimens, due to the inability to distinguish individual mouse intake.

3.2.1.2 Animal welfare monitoring

Mice were monitored constantly for 30min after each treatment and every 30min thereafter for up to 2 hours post treatment for signs of severe impact on welfare, then periodically up to 24 hours post-treatment (but at least 3 times between 4-24 hours). In the 24-48 hours post-treatment, mice were monitored twice daily. Mice were then monitored once daily from 48hours to 14 days after the last treatment of the regimen. Monitoring was completed using Table 2.3 and Table 2.4 from *Chapter 2: Step 7*.

3.2.1.3 Ethical statement

All experimental procedures were approved by the Victoria University Animal Ethics Experimentation Committee (project AEC 17-009) and conformed to the Australian Code of Practice for the Care and Use of Animals for Scientific Purposes.

3.2.2 Pilot chemotherapy regimens and treatments

One mouse per treatment group (ALL-POMP, MB-LCV, BL-CHOP) commenced the first dose trial with its respective chemotherapy regimen at a 10-fold reduced dose (10%) using the IAMDF in Chapter 2. If no severe detriment to welfare (identified as a score of 10 or greater using the forms outlined in *Chapter 2: Step 7*) was observed throughout the trial or at 14 days after completion, the next trial commenced at the IAMDF selected dose (100%) with the next animal. In the case that an animal completed the regimen at the 100% dosage level

with no severe detriment during the regimen or 14 days after completion, then the IAMDF selected dose was selected as the animal equivalent dose for that chemotherapy regimen and the mouse culled and tissues harvested for post-mortem analysis. In the case where the animal exhibited a severe impact to welfare (as outlined in *S3.2.1.2* above) they were anaesthetised with isoflurane (described in *S3.2.3.1* below), culled and a necropsy performed (described in *S3.2.3.3* below). In this instance, the next pilot trial was commenced on the next animal and the regimen repeated at a 10% lowered dose. This process of 10% dose reduction was repeated until an animal completed the pilot without severe detriment. This process was completed for all three regimens: ALL-POMP, MB-LCV and BL-CHOP. Pilot dose levels and IMADF pilot regimen organisation are outlined in Table 3.1 and Table 3.2 respectively in S3.2.2.2 below.

3.2.2.1 Treatment creation

Intraperitoneal injections were created by adding a stock solution of each respective chemotherapy (refer

Table **3.1** below for doses) directly into a sterile syringe under sterile conditions. Where multiple treatments were required, individual treatments were added to the same syringe. Due to the maximum injectable volume (1% of body weight in volume as discussed below in *S3.2.2.2*), it was at times necessary to increase the concentration of the treatments to decrease the volume injected.

3.2.2.2 Treatment administration and supportive therapies

Treatment regimens were designed to be administered back to back, thus 8 weeks of continuous treatment was administered (Course 1 + Course 2 for ALL-POMP and 2x Course 1 for MB-LCV and BL-CHOP, refer to *Chapter 2, Step 7* and Figure 3.1 and Figure 3.2 below for more details). Between 7-9am daily mice were weighed, and food and water consumption monitored, and treated with their respective morning treatment (or daily treatment if only one). Mice were also monitored for complications and toxicity (refer to *S3.2.1.2* above). Between 1-3pm daily, mice were weighed, and their respective PM treatment administered. Mice receiving Doxorubicin, for example, would receive two half dose injections, one between 7-9am and one between 1-3pm, to spread the full dosage over the day, reduce acute toxicity and somewhat mimic the continuous intravenous method of administration used in clinic. For animal welfare reasons, treatment volumes were limited to 1% body weight in volume (i.e. a 30g mouse could receive up to a 300µl I.P. injection). Mice had ad-libitum access to autoclaved water and standard autoclaved rodent chow, with consumption measured as the amount remaining in the hopper/bottle after every 24 hour period. If mice were observed to lose 10% bodyweight for 3 or more consecutive days, these mice were given access to 'chow mash' which was created by adding autoclaved water to approximately 6-7g of standard

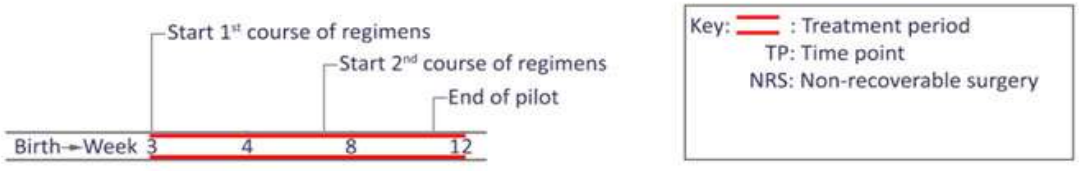

***Figure 3.1 Pilot study timeline**, commencing between 3-4 weeks of age and concluding when one mouse from each regimen successfully complete treatment without undue toxicity (as outlined in text).*

autoclaved rodent chow at a 2:1 ratio to create a smooth paste.

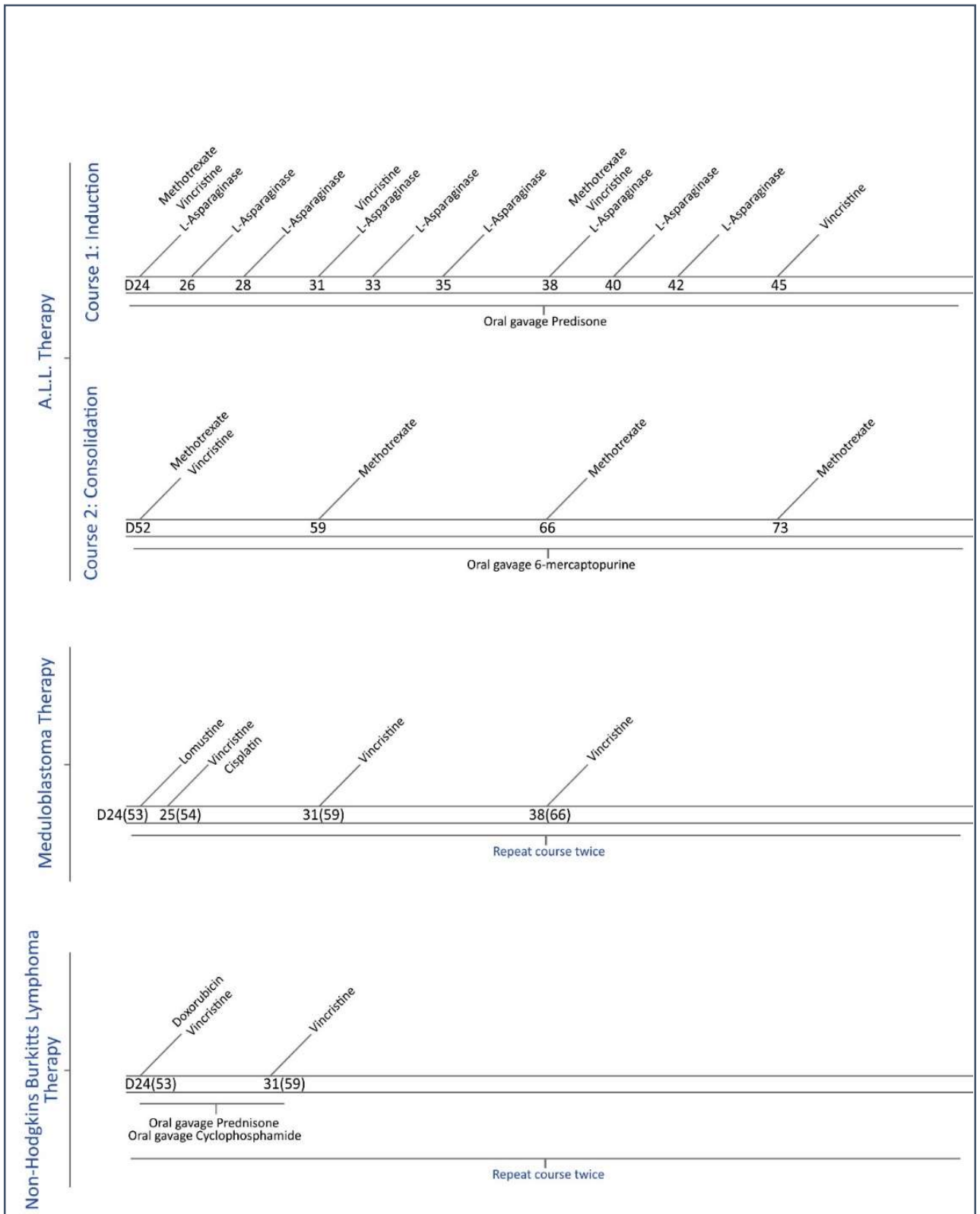

Figure 3.2: Chemotherapy regimens and starting doses for pilot study. *All drugs given via intraperitoneal injection unless otherwise stated. Administration of dosage will occur via 2 injections, or 2 oral gavages (as specified) at 6-hour intervals to reduce acute toxicity and simulate intravenous delivery used in the clinic. Day numbers indicate days of life and those in brackets indicate subsequent courses., refer to Chapter 2, Step 2 for details.*

***Table 3.2: IMADF trials of each dose finding attempt with associated dose percentages used**; (10% is a 10% dose of the IAMDF derived clinically relevant dose). Where individual drug names are used with percentages, the bracketed percentage used is independent of the percentage used for the rest of the regimen (i.e. ALL-POMP80 (6MP*50%) indicates that the ALL-POMP regimen is reduced from 100% to 80% of the clinically relevant IAMDF dose and 6MP is reduced from 100% to 50% of its clinically relevant IAMDF dose). In the instance of 6MP, the 50% reduction is due to a halving of administration from twice daily to once daily and no change to the dose per treatment was made. Abbreviations: CLV: Calcium leucovorin; PT: Prednisone Taper.*

Pilot Run	Regimen(s) trialled	Trial dose %	Additions	Regimen reference ID
T1	ALL-POMP	10%		ALL-POMP10
	MB-LCV	10%		MB-LCV10
	BL-CHOP	10%		BL-CHOP10
T2	ALL-POMP	100%		ALL-POMP100
	MB-LCV	100%		MB-LCV100
	BL-CHOP	100%		BL-CHOP100
T3	ALL-POMP	80% (6MP*50%)		ALL-POMP80
	BL-CHOP	80%		BL-CHOP80
T4	ALL-POMP	100% (MTX*80%, 6MP*50%)	CLVR + PT	ALL-POMP100+CLV MTX80
	ALL-POMP	80% (MTX*60%, 6MP*50%)	CLVR + PT	ALL-POMP80+CLV MTX60
T5	ALL-POMP	60% (6MP*50%)	CLVR + PT	ALL-POMP60+CLV
	ALL-POMP	50% (6MP*50%)	CLVR + PT	ALL-POMP50+CLV
	ALL-POMP	40% (6mp*50%)	CLVR + PT	ALL-POMP40+CLV

3.2.2.2.1 ALL-POMP specific dose finding alterations

Due to severe toxicity induced by the ALL-POMP regimen (refer to S3.3 for details), modifications to the regimen were required to establish its viability. The addition of calcium leucovorin recovery (CLVR) (which was not indicated in the original IAMDF selected regimen [322]) has been shown in similar ALL-POMP treatment regimens to reduce MTX acute nephro- and immune-toxicity by repleting folate and allowing leukocyte and erythrocyte recovery; as well as increasing renal clearance of the drug [473,474]. As such, CLVR was added here. Upon signs of reduced food consumption and lethargy (indications of dehydration and nausea) a liquid diet of food mash was introduced to improve caloric intake and, importantly, hydration to improve MTX clearance [474]. Reductions to MTX dosage was also made in an attempt to improve tolerability and survivability (Table 3.2). To further reduce the regimens toxicity, a 7-day prednisone taper period was added to the regimen whereby prednisone was reduced by 12.5% of its original untapered dose, per day, from day 1 through day 7 of the second phase of the regimen. This taper method has been added to most but not all regimens which contain corticosteroids such as prednisone and dexamethasone [322,475]. Additional reductions to individual drugs within the regimen were made due to observational changes. 6MP is associated with acute liver toxicity in maintenance protocols and, if severe toxicity is noted, the recommendation is for 6MP therapy to be reduced or aborted [476]. Due to the consistent use of 6MP in clinic (and the chosen regimen), it was decided to reduce 6MP therapy to once daily instead of twice daily administration (hence the drop to 6MP*50%, Table 3.2).

3.2.2.2.2 ALL-POMP specific housing alterations

Trials 1, 2 and 3, which included ALL-POMP10, ALL-POMP100 and ALL-POMP80 mice (trial outlines and mouse reference ID's outlined above in *S2.2.2*; Table 3.2) were housed as outlined in previous sections. However, due to leukocyte depletion induced by the ALL-POMP regimen (details presented in S3.3.4) and resultant infection risk, housing conditions were altered for subsequent ALL-POMP trials (trials T4 and T5) to minimise infection risk. Housing alterations for these trials were under instruction by the university animal welfare officer and included bedding changes from standard compressed paper to autoclaved saw dust to reduce irritation and microbial growth within the bedding media. Further, bedding was changed three times per week.

3.2.3 Ex vivo animal analyses

3.2.3.1 Anaesthetics

Mice were placed in a 1L chamber and subjected to an influx of 4% isoflurane in oxygen to induce anaesthesia. The mouse was removed once appropriately anaesthetised and placed on a surgical pad with a nose cone attached to the mouse to continue isoflurane administration at 2-4% concentration and maintain anaesthesia. Anaesthesia success was measured by checking the loss of the mouses foot reflex. This was achieved by pinching the foot with forceps which, under normal circumstances, would initiate a spontaneous

contraction of the hind limb muscles. Surgical procedures commenced after no foot reflex was observed.

3.2.3.2 Contractile property analysis of EDL and SOL muscles

As a loss of skeletal muscle function is a key characteristic of the CI-SMDW phenotype, the aim of contractile analysis was to measure changes to strength and fatiguability due to chemotherapeutic administration.

3.2.3.2.1 Surgical preparation for contractile analyses

The right hind limb was doused with saline fluid to wet the fur before an incision was made bilaterally through the superficial layers of the skin circling the insertion point of the lower limbs, allowing the lower limbs to be de-gloved exposing the musculature. The fascia separating the anterior and posterior compartments of the leg was carefully cut and removed, and the anterior and posterior compartments separated with a blunt dissecting tool from knee to ankle. The proximal tendon of the EDL was then loosened and surrounded fascia removed, before suture (silk, 0.5mm diameter) was passed under the tendon and a double knot created at the end of the tendon (refer Figure 3.3). The same process was then completed for the distal tendon of the EDL. This process was then completed for the proximal and distal tendons of the SOL (refer Figure 3.4). Both muscles were then removed and placed

in a heated (30^{oC}) bath of Krebs-Henseleit Ringer's solution (refer Table 3.3) in individual organ baths (Danish Myo Technology, Hinnerup, Denmark) (analysis procedure detailed later) and bubbled with carbogen (5% CO_2 in O_2; BOC gases, Melbourne, Australia).

Table 3.3: Components and solutions required for Krebs-Henseleit Ringer's solution (Solution A) used in contractile experiments

Solution	Component	Amount
Solution A component solutions		
Krebs Stock (10x concentration) *Total volume = 1.0L*	NaCl	68.96g
	$MgSO_4.7H_2O$	2.465g
	KCl	3.54g
	Na_2HPO_4	1.42g
$CaCl_2$ Stock *Total volume = 0.5L*	$CaCl_2$	9.19g
$NaHCO_3$ Stock *Total volume = 0.5L*	$NaHCO_3$	20.1625g
Solution A method		
Krebs-Henseleit Ringer's solution Total volume = 1.0L pH=7.4	Krebs Stock	100ml
	$CaCl_2$ Stock	20ml
	$NaHCO_3$ Stock	50ml
	Glucose	1.98g

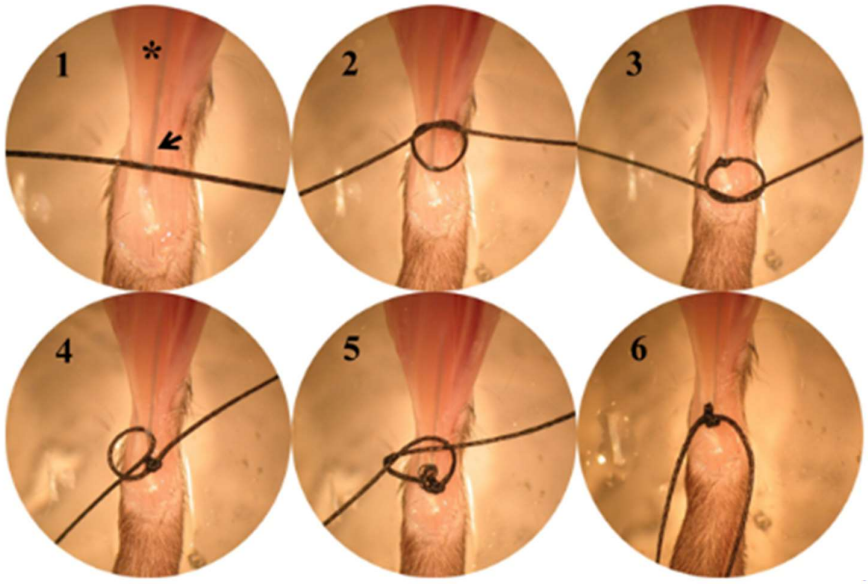

***Figure 3.3*: Knot tying procedure for muscle contractile experiments.** *Suture is passed under the EDL distal tendon (*) and a double knot tied (2-6). The ends of the suture material are then used to attach the muscle to the contractile apparatus (completed on both distal and proximal ends of the muscle).*

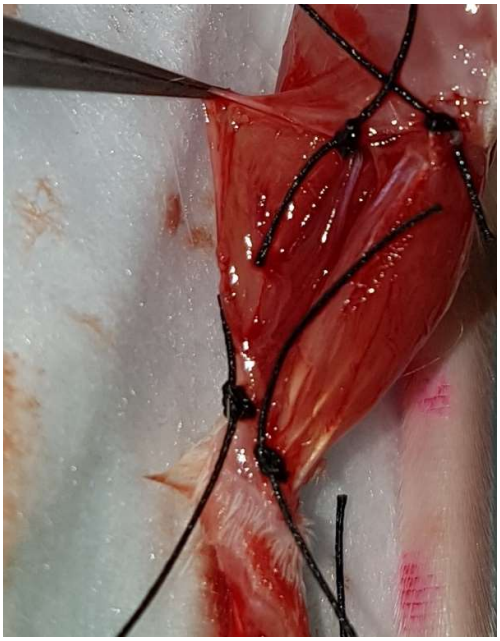

***Figure 3.4*: Example image of suture material attached to both proximal and distal tendons of both the SOL and EDL muscles in the right hind limb of the mouse.**

3.2.3.2.2 Finding muscle optimal length

After excision, both *EDL* (fast twitch) and SOL (slow twitch) muscles were completely submerged in Solution A (contents in Table 3.3) and bubbled with carbogen gas in DMT baths one and two respectively. Muscle optimal length was then established by mechanically lengthening the muscle in small increments and stimulating the muscle with a series of supramaximal twitch contractions (21V, 100Hz, 0.2ms square wave pulse) ensure total recruitment of the motor units. The resulting forces were measured using LabChart Pro 8 software (AD Instruments). These contractions were then measured and, when the contractional force created was at its greatest (established by seeing two successive smaller twitches), the muscle length was returned to what was its optimal length (see Figure 3.5). To ensure robust tying of the suture knots, the muscle was stimulated with a train of impulses to elicit a single tetanic stimulus (100Hz and 350ms train duration, 80Hz and 500ms train duration for *EDL* and SOL respectively). Following this, baseline force was observed for any major decline (which would indicate slipping of the knots) followed by two single electrical pulses to ensure twitch force was the same as previously recorded. With optimal length confirmed, muscle length was then measured with precision metric callipers (see Figure 3.6).

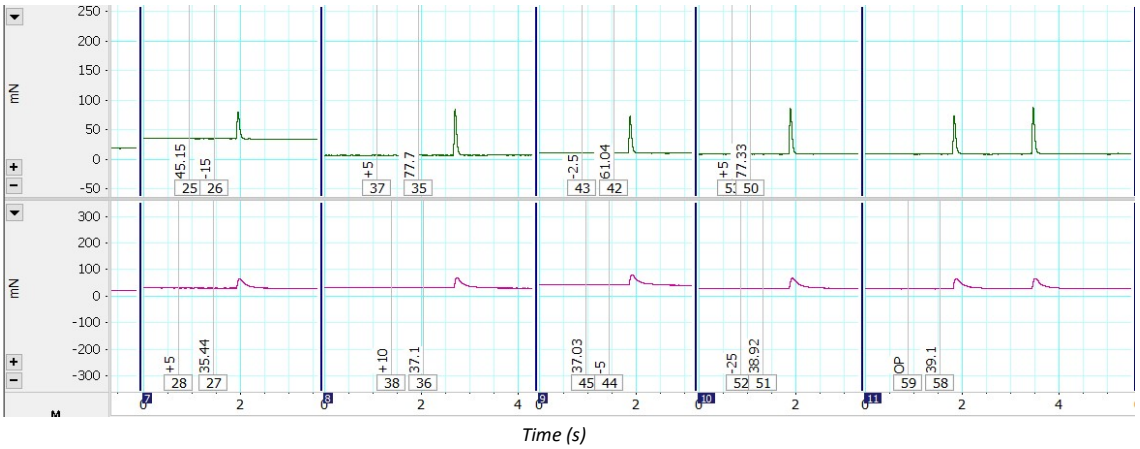

Figure 3.5: Screenshot example from LabChart Reader of optimal length protocol. *Positive and negative numbers (-25 to 25) are indicators of arbitrary measures of required muscle lengthening and shortening with the following larger numbers measures of force production. Green: EDL, Pink: SOL. Abbrev: mN; millinewton, s: seconds, OP: optimal length found.*

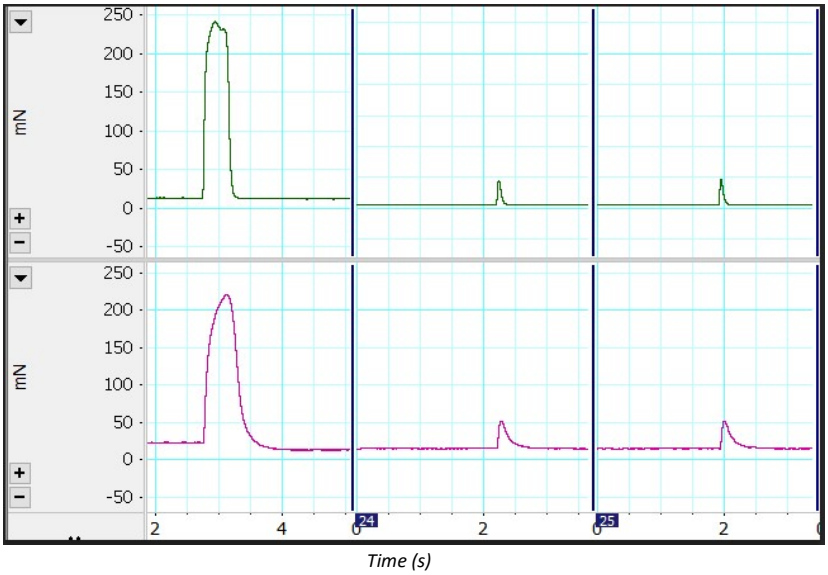

***Figure 3.6*: Screenshot example from LabChart Reader of optimal length confirmation protocol.** *First, a tetanic contraction is shown used to recruit/activate all fibres within the muscle, followed by two separate 'twitch' contractions to at increasing voltage to measure the accuracy and success of the optimal length protocol. Green: EDL, Pink: SOL. Abbreviation: mN: millinewton, s: seconds*

3.2.3.2.3 Force frequency protocol

After the optimal length of the muscles had been found, measurement of the muscles maximal force output was performed. Beginning at 10hz (using previously noted pulse train stimulus parameters) muscles were stimulated at increasing frequencies. The greatest tetanic force produced throughout the protocol was recorded as the peak isometric force for that muscle (see Figure 3.7).

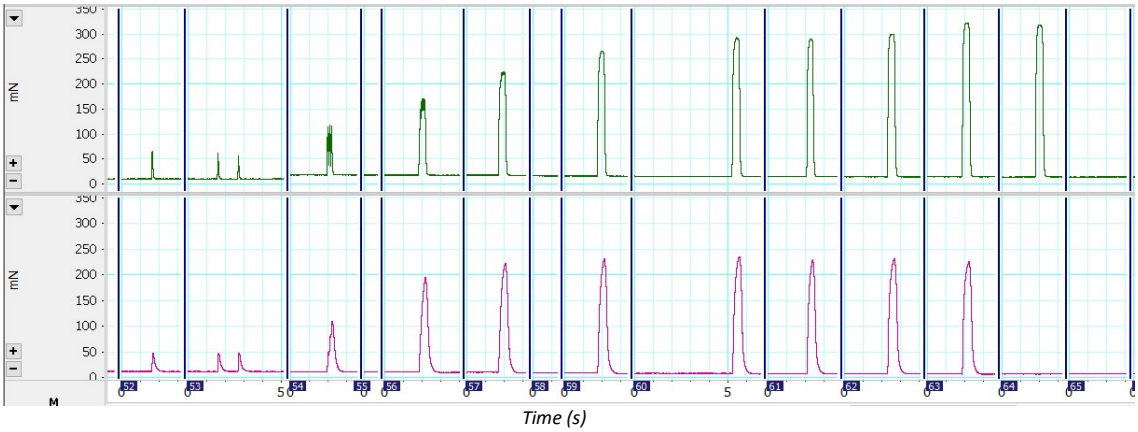

Figure 3.7: Screenshot example from LabChart Reader of force-frequency protocol. *As described in-text, at each step; frequency is increased in intervals to illicit a stronger contraction. At the point of greatest isometric force, an increase in frequency only results in a weaker contraction. Green: EDL, Pink: Sol.Abbreviations: mN (millinewton), s: seconds.*

3.2.3.2.4 Fatigue-recovery protocol

Considering the differences in muscle physiology between the EDL (fast twitch) and the SOL (slow twitch) muscles, fatigue protocols between the muscles differ. Using the 100Hz for EDL and 80Hz for SOL stimulus protocols as they yield close to maximal forces, EDL muscles were stimulated at 4000ms intervals and SOL muscles at 2000ms for 3 min (see Figure 3.8) to elicit fatigue. During recovery, muscles were stimulated using the same tetanic stimulus parameters at minutes 1, 2, 5, 10, 15, 20, 30, 45, 60 and the recovery force produced measured. All forces in the fatigue and recovery protocol were expressed relative to the force developed by the first stimulation.

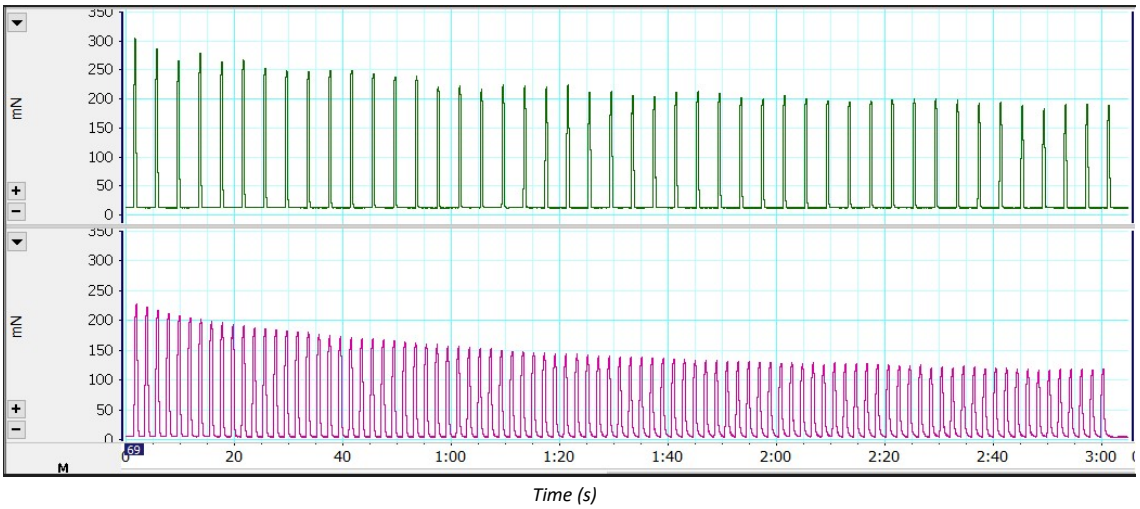

Figure 3.8: Screenshot example from LabChart Reader of force output from fatigue protocol. *As described in-text, muscles are stimulated at defined intervals with a standard electrical stimulation over a 3min period, resulting in a decline in force output over time. Green: EDL, Pink: SOL. Abbreviations: mN (millinewton), s: seconds.*

3.2.3.2.5 Standardisation of force via cross-sectional area and density

After testing, muscles were removed, blotted dry and tendons (and suture) removed and then weighed. Peak force as measured in previous sections was standardised against the cross-sectional area of the muscle which was calculated as previously described [477,478] and as described below:

$$CSA = \frac{wet\ muscle\ mass}{L_o \times R \times muscle\ \rho}$$

Where CSA refers to cross sectional area, L_o refers to optimal length of the muscle, R refers to the fibre:muscle length ratio constant which is equal to 0.71 for SOL and 0.44 for EDL and muscle density (ρ) as 1.06g/cm^3. To normalise the force produced to the mass of the muscle, specific force was also measured which was calculated using the following equation:

$$Specific\ force = \frac{maximal\ force\ produced\ (mN)/1000}{CSA\ (cm^2)}$$

3.2.3.2.6 Pilot specific ex vivo contractile analysis alterations

Unique to this chapter, a control mouse was used for comparison against the chemotherapy treated mice within the contractile analyses. The control mouse here was 47 days old in an attempt to minimise age differences between the groups (ages at time of pilot experimentation due to pilot end point; ALL-POMP=43 days old, BL-CHOP and MB-LCV = 52 days old) and had not received any treatment. Due to the same number of pilot animals used, only the *extensor digitorum longus* muscle was used in analyses as no *soleus* muscle was able to complete the entire protocol. In future chapters, a vehicle group is used instead of the control mouse, the end-point unanimous between groups, and both the *extensor digitorum longus* and *soleus* muscle was analysed.

3.2.3.3 Post-mortem analysis

After muscles were removed for contractile analysis, the remaining muscles of interest were excised, weighed and prepared as per Table 3.4. An incision was then made along the midline of the lower abdomen through to the sternum which pierced all layers of the abdominal wall. Incisions were then made from the terminal ends of the incision laterally to

expose the contents of the thoracic and abdominal cavities. All major organs and tissues of interest were removed (see Table 3.4 below), weighed and frozen in liquid nitrogen and stored in -80^{oC} freezers for future use. The animal was alive until the removal of the heart which was identified as the ethical point of death of the animal.

Table 3.4: A list of tissues taken through non-survival surgery and associated methods in order of excision.

Tissue Collected	Method
***Tibialis Anterior m.* (TA)**	After the EDL was removed the distal insertion of the TA was severed, the TA reflected superiorly and then severed at the origin. The TA was then covered in OCT and snap frozen in liquid nitrogen cooled isopentane.
Plantaris m.	The *calcaneal t.* was severed at the most distal point allowing the posterior musculature to be reflected. The *plantaris m.* was then severed at the origin (proximal end of the femur) and the insertion excised from the lateral head of the *gastrocnemius m*.
Gastrocnemius m.* (gastroc) *& Soleus (SOL) m.	The *gastric m.* was severed at the origin (proximal end of *femur b.*) and both the *gastroc* and *soleus m.* removed. A small incision was then made along the proximal edge of the soleal line to separate the *soleus m*. from the *gastroc*. The *soleus m.* was then separated by light force from the gastroc. Both SOL muscles were then immediately used in contractile function testing, whilst the gastroc was snap frozen and stored for future analysis. After contractile testing, the SOL muscles were snap frozen in OCT and stored for future analysis.
***Quadriceps femoris m.* (quad)**	The *quadriceps femoris t.* was severed at the distal end proximal to the *patella b.* and the quad reflected superiorly. The superficial fat layer was then removed, and an incision made between the *vastus medialis m.* and *sartorius m. to* the *femur b.* with care taken not to sever the *femoral a.* or *femoral v.* The muscle complex was the severed at the origin.
Kidneys	Removed bilaterally via excision.
Spleen	Removed via excision.
Liver	Removed via excision.
Heart	The *diaphragm m.* was severed centrally, and the heart removed via excision

3.2.4 Statistical analysis

As the pilot studies described within this chapter used only 1 mouse per treatment protocol, statistical analysis of results were unable to be calculated.

3.3 Results

3.3.1 Measure of weight loss and survival as indicators of IMADF pilot trial success

Throughout the 8 weeks of treatment, and regardless of regimen, weight loss was proportional to the dose received, in that the higher the dose, the greater the loss in bodyweight. Vehicle (VEH) growth rate percentages from *Chapter 4* have been added to Figure 3.9F for comparison (see *Chapter 4 S4.2.1.2* for further details of VEH regimen), and dosage percentages and changes can be viewed in *S3.2.2*, Table 3.2.

In all cases, the 10% dose of each associated regimen was well tolerated with only moderate failure to thrive observed (percent growth from start; VEH: 191%, MB-LCV10: 162%, BL-CHOP10: 149%, ALL-POMP10: 156%, Figure 3.9A-C & F:). With successful completion of the 10% regimens achieved, doses were increased to the IAMDF derived, clinically relevant 100% dose regimens. At this level, only MB100 was successfully tolerated although the higher dose resulted in a -42% reduction in body weight by the end of the trial (D56 as compared to MB10, Figure 3.9A). Using the IMADF framework outlined in *Chapter 2*,

the MB100 was considered the dose which would provide the greatest clinical relevancy and, as it was tolerated here, was selected for future studies.

At the 100% dose level, the BL-CHOP100 trial induced lethal toxicity (end weight percentages: VEH: 191%, BL-CHOP100: 92% Figure 3.9B). As such, the BL-CHOP dose was reduced to 80% which was successfully tolerated. Due to the severe toxicity observed at the 100% dose it was decided that the 80% dose would be used in future studies as there were significant concerns for animal welfare if the dose was elevated and trialled at 90%.

In regard to the ALL pilot, and due to significant failure to thrive during the ALL100 regimen, alterations in dosage and the regimen itself were made to subsequent ALL trials to improve survivability (as previously described in *S3.2.2.2*). With the dose reduced to 80%, a clear improvement in growth was noticed from the onset of the ALL80 trial (Figure 3.9C). However, continuous weight loss was observed at a similar time point as the ALL100 (a few days after the second administration of MTX) and resulted in death. New trials which incorporated a calcium leucovorin (CLV) recovery post MTX administration with the ALL100 and ALL80, together with reduction in MTX dose to 80% and 60% (respectively for ALL100 and ALL80, Figure 3.9D) showed promise with continuous growth maintained throughout the first 6 weeks (weight peaked at 157% and 149% for ALL80+CLV MTX60 and ALL100+CLV MTX80 respectively), though strong, acute weight loss began from a similar time point as previous trials resulting in death of both animals (weight loss 24% and 26% for ALL80+CLV MTX60 and ALL100+CLV MTX60 respectively). To combat this, further dose reductions were made to 60% and below (in combination with CLV recovery and PRED taper) which were survived, although not without considerable toxicity (described in more depth in *S3.3.4* and *S3.3.5*). Ultimately, the ALL60+CLV was the highest tolerable dose and was selected for use in future studies.

When weight data from each tolerable dose was compared to VEH (Figure 3.9F), all groups showed considerable failure to thrive, indicative that chemotherapy-induced weight loss was present at all dose levels (refer Figure 3.10 for ALL-POMP trial comparison).

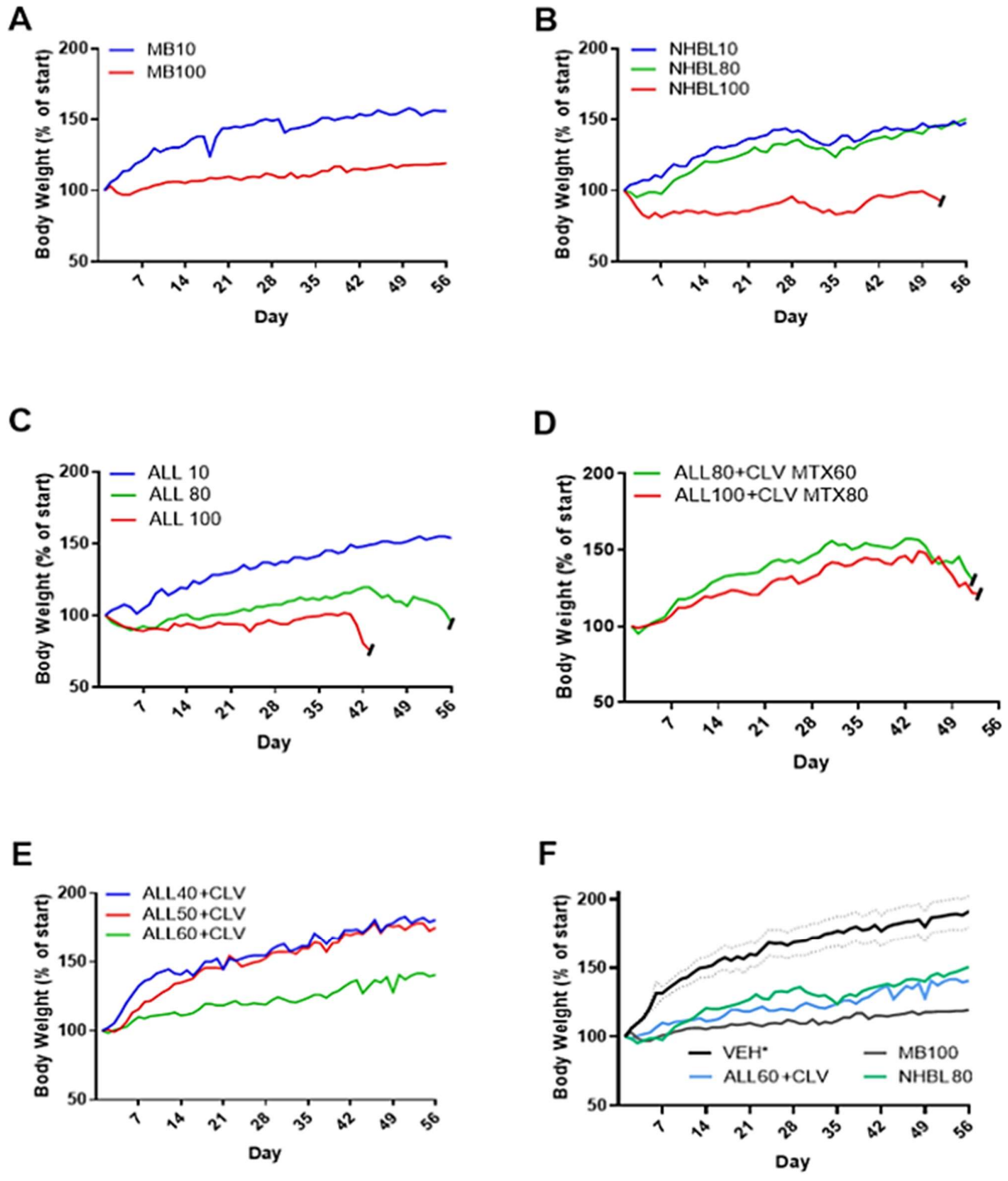

Figure 3.9: Weight percentage change and survival of animals in response to IAMDF dose finding pilots. *(n=1). Considerable changes in weight gain were observed in animals in response to the varying chemotherapy regimens and dose levels with the highest successfully tolerated regimen shown in panel F. VEH* group (n=5) was not conducted as part of this chapter and details of this group can be seen in Chapter 4, S4.2.1.2. Dotted lines in panel F denote standard deviation of results. Diagonal black, diagonal lines indicate death of animal. n=1 for all groups. Weights shown as a percentage of starting weight.*

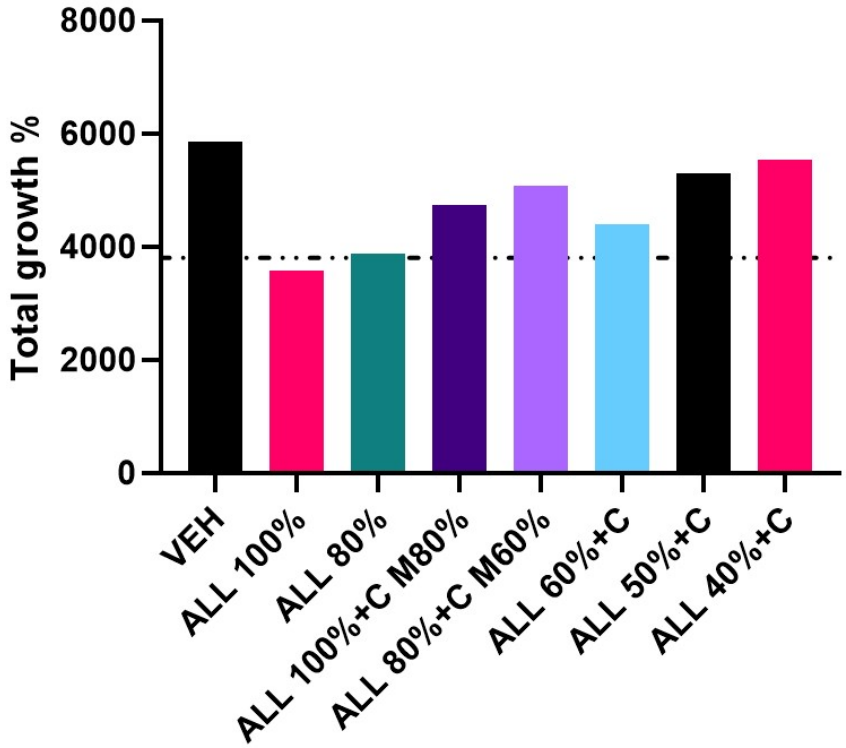

Figure 3.10: Cumulative growth of ALL-POMP treated mice showing increased growth and weight gain as dose was reduced and alterations made. *Data derived from body weight (% of start) data presented in Figure 3.9 as the area under the curve from days 1-39 showing the total weight gained (or lost) over the time period. Day 39 was chosen as a cut-off point to account for the acute decline in bodyweight in the ALL100 trial. A value of 3800 (dotted line) indicates no gain or loss of weight.*

3.3.2 Food and water intake across all trials

Food intake is an important diagnostic tool when monitoring weight-loss associated symptoms. Although cages contained mice being treated with different regimens, trial 1 and trial 2 were housed separately and differed in regimen dose (refer *S3.2.1.1*, for trial alterations) and number of animals up to day 44 of treatment (due to mouse death) and thus were considered comparable up until this time point. Food consumption was lowered in trial 2 (n=3, Day1-44 = total of 120.2g) compared to trial 1 (n=3, Day 1-44 = total of 148.5g) with water consumption increased slightly in trial 1 (n=3, Day1-44 = total of 175.6g) compared to trial 2 (n=3, Day1-44 = total of 158.8g).

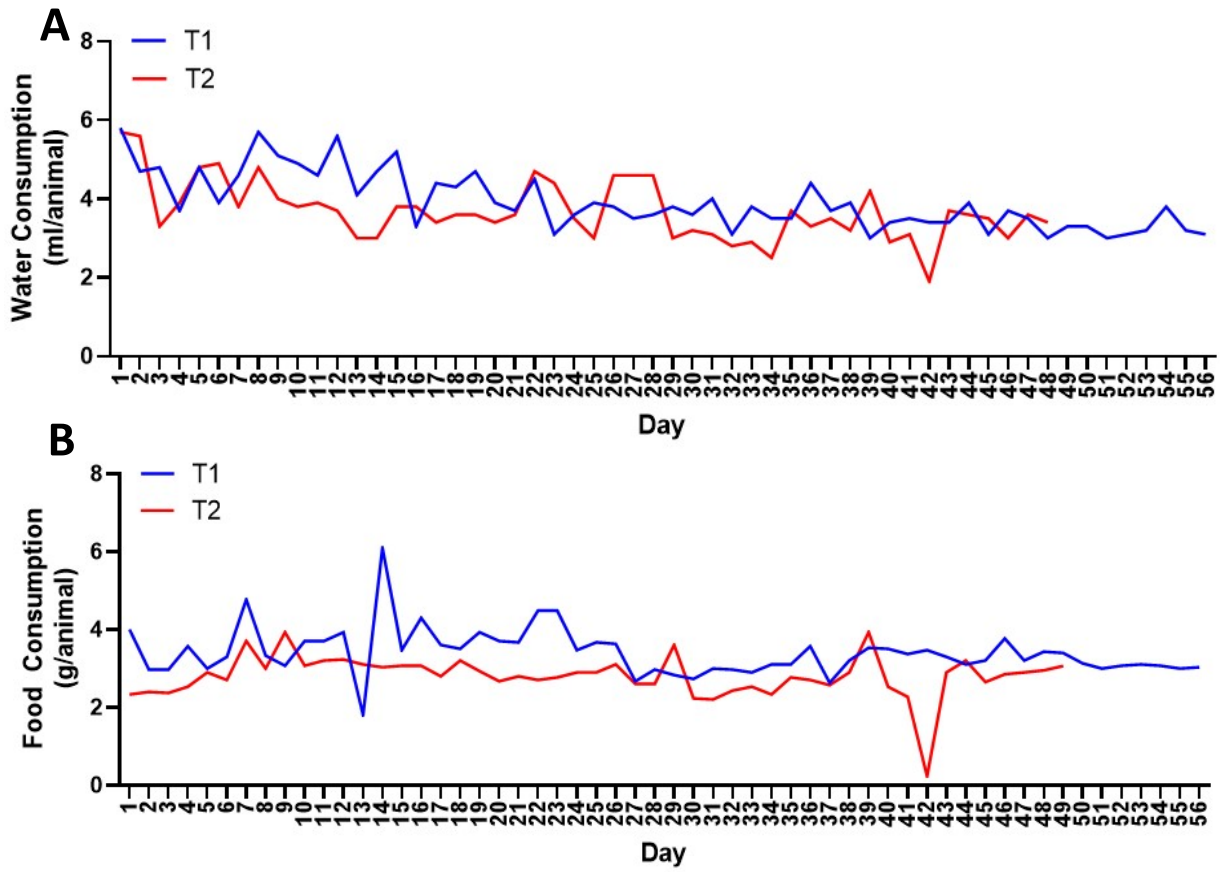

Figure 3.11: Food and water consumption from pilot trials 1 and 2. *Water (A) and food (B) consumption, measured daily, and corrected for number of animals (n=3 day 1-44, n=2 day 44-49). There was no discernible reason for the drop in consumption on D42. Area under the curve D1-44: T1: 148.5g of food consumed per animal, T2: 120.2 g of food consumed per animal.*

3.3.3 Confirmation of chemotherapy induced dysfunction in ALL-POMP, MB-LCV and BL-CHOP chemotherapy treated mice

The *extensor digitorum longus* (EDL) m. from mice treated with the 100% of IAMDF dose underwent muscle endurance and recovery testing. All three chemotherapy treated muscles produced a lower total force output over the endurance phase compared to the control (area under the curve 0s-180s: CON=344.1mN, ALL-POMP=334.2mN, BL-CHOP=294.6mN, MB=268.6mN) with all chemotherapy-treated muscle exhibiting an increased fall in force output over the 180s protocol when compared to VEH (difference in force output between pre-protocol (0s) and post-fatigue protocol (180s): CON=-50.1mN, ALL-POMP=-56.0mN, BL-CHOP=-55.8mN, MB=-61.9mN) as well as considerable decline in performance recovery (difference in force output between end-fatigue protocol (180s) and post recovery protocol (+60m): CON=57.7mN, ALL-POMP=5.5mN, BL-CHOP=-31.4mN, MB=-12.3mN, refer Figure 3.12) . Chemotherapy-treated muscle also failed to recover from the fatigue protocol with all muscle either showing an overall decline or no overall improvement in force output during the fatigue protocol (difference between pre-protocol (0s) force output and post recovery (+60m) force output: CON=+7.6mN, ALL-POMP=-50.5mN, BL-CHOP=-87.2mN, MB-LCV=-74.27mN, refer Figure 3.12).

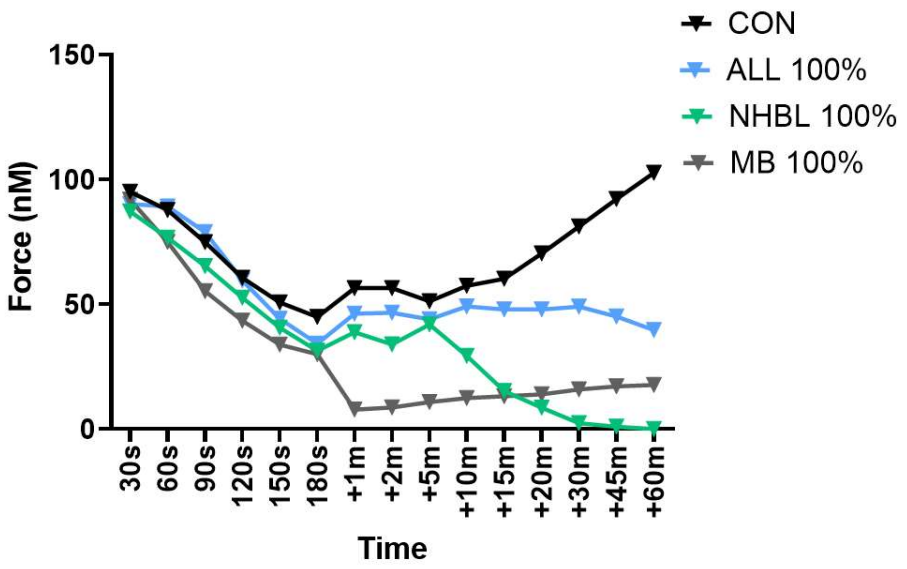

Figure 3.12: Skeletal muscle dysfunction due to chemotherapy treatment regardless of regimen. *(n=1) All treated mice produced a lower force output as compared to CON over the fatigue protocol (0-180s) with ALL-POMP and BL-CHOP treated mice showing a slight post fatigue recovery between the 0 and 5min time points, with the ALL-POMP treated mouse not showing any improvement thereafter and the BL-CHOP mouse showing a considerable decline in force output from 5 minutes onward. The MB-LCV treated mouse showed a considerable decline in force output between the end of the fatigue protocol and the start of the recovery protocol but showed steading, although slight, improvements in recovery thereafter. These observations are in stark contrast to the CON mouse which showed steady improvement in force output from the start of the recovery, with force output ultimately returning pre-fatigue protocol levels. Abbreviations: mN: Millinewtons; s:seconds; m:minutes; CON:control (untreated).*

3.3.4 Immune suppression in ALL-POMP chemotherapy treated mice

An important measure of success for the ALL-POMP regimen is its ability to suppress the white cell profile of the treated animal to eliminate the dysplastic leukocyte precursor, as this is the primary purpose in its application against the progression of ALL [37,129,479-482]. VEH cell counts from *Chapter 4* have been added to Figure 3.13 for comparison (refer to *Chapter 4, S4.3.5* for further details). Examination of peripheral blood smears showed moderate polychromasia with presence of Howell-Jolly bodies and a low to moderate presence of schistocytes in all ALL-POMP treated mice. In comparison to VEH, ALL+CLV treatment afforded a dose related reduction in WCC (where VEH: $4.64x10^9$, ALL-POMP 60+CLV $1.80x10^9$, ALL-POMP50+CLV $2.10x10^9$, ALL-POMP40+CLV $3.60x10^9$) with highest WCC suppression achieved at the highest dose survived (ALL-POMP60+CLV lymphocyte count = $1.5x10^9$). This suppression is an important factor as WCC suppression is central to ALL management. Further, a clear reduction in RCC was observed (albeit not dose proportionate in this instance) with visual observations of the ALL-POMP80 mouse show clear pallor indicative of anaemia (Figure 3.14).

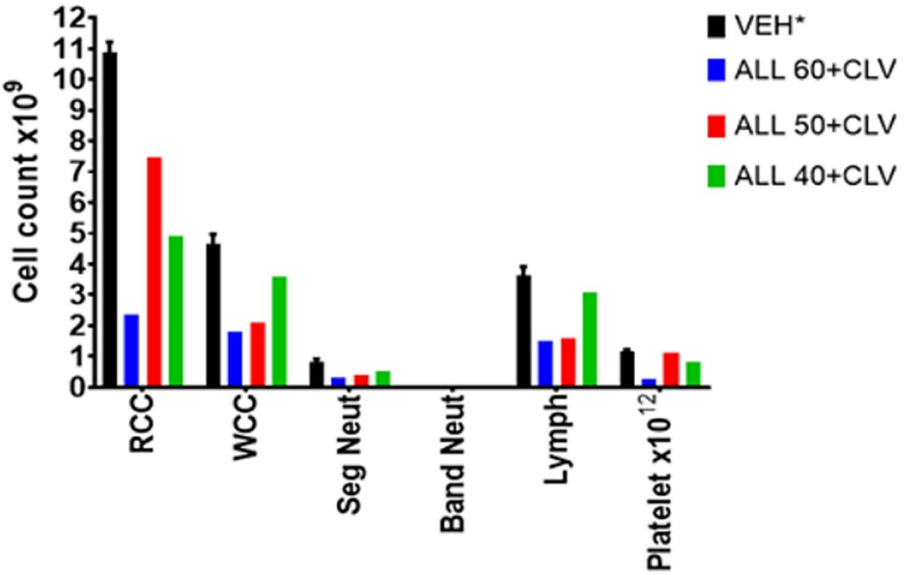

Figure 3.13: Results of full blood examination of mice treated with modified versions of the IAMDF ALL-POMP regimen showing dose dependent pancytopenia. *(n=1) Platelets measured at x10^{12} and is not cumulative with y axis title. VEH* group (n=5) was not conducted as part of this chapter and details of this group can be seen in Chapter 4. Data presented as cell count per litre. Abbreviations: RCC: Red cell count; WCC: White cell count; Seg Neut: Segmented neutrophils; Band neut: Banded neutrophils; Lymph: Overall lymphocyte; mono: monocyte; Eosin: Eosinophil; Baso: Basophil.*

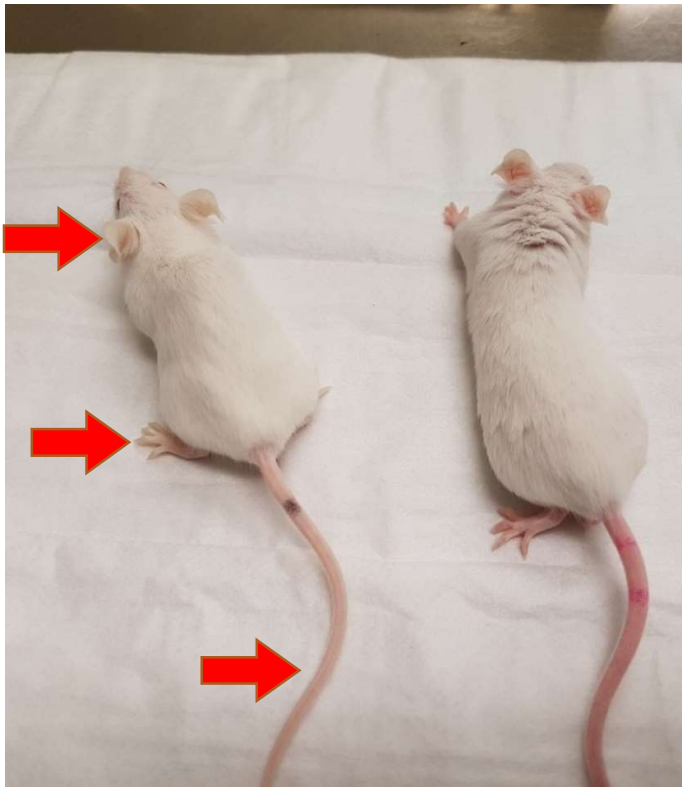

***Figure 3.14**: **Visual pallor in ALL-POMP treated mouse, characteristic of anaemia**: A) ALL80 treated mouse (left) showing signs of pallor at indicated sites when compared to VEH treated mouse (right) of same age. A clear distincition in size is also evident.*

3.3.5 Incidental findings in ALL-POMP treated pilot mice show signs of systemic toxicity

Although the SMDW phenotype is of primary interest, toxicity induced by the regimens are also of critical importance. Toxicity levels here need to be comparable to that seen in the clinic to ensure proportionality between the dose and effect. The ALL-POMP therapy induced several toxic effects in the mouse. Notably, mice treated with 80% or above (ALL-POMP80, ALL-POMP100, ALL-POMP80+CLV MTX60, ALL-POMP100+CLV MTX80) all began to present with penile and testicular inflammation and swelling and apparent nephrotoxicity [474] with 3 of the 4 mice developing solid crystallised urine which remained attached to the penis (Figure 3.15A) until removal was conducted with tweezers. These mice (≥80% dose) also exhibited considerable blood clotting within the cerebellum with occasional clotting within the cerebrum (Figure 3.15B). 6MP and MTX associated hepatotoxicity and atrophy was also clearly evident (Figure 3.15C). The pathogenesis behind the observed gastrointestinal tract damage, which appeared to be skipping necrotic lesions throughout the small and large intestines, remains unclear (Figure 3.15C&D).

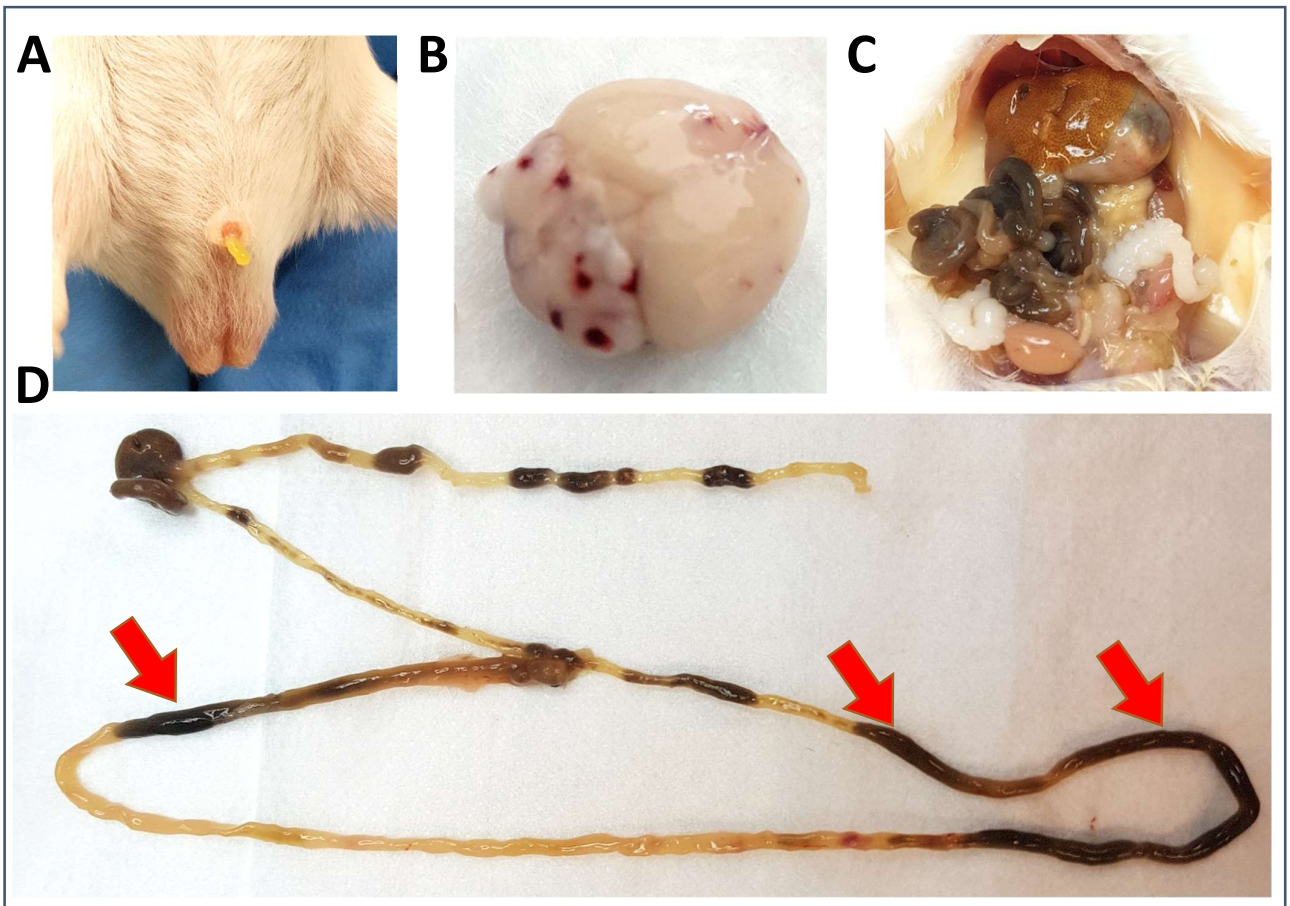

***Figure 3.15*: Observations of systemic toxicity in ALL80 treated mouse.** *A) Crystallised urine with inflamed penis and testis on day 62 of treatment. B) Necropsy observation of blood clots throughout cerebrum and cerebellum C) Gross abdominal image of necropsy showing hepatotoxicity (spotty liver) and atrophy, hyperextended stomach with necrotic fundus and body, and necrotic gastrointestinal tract D) Removed gastrointestinal tract as shown in panel C, showing extent of necrosis throughout both small and large intestines (indicated by arrows).*

3.3.6 Incidental findings in BL-CHOP treated pilot mice show signs of systemic toxicity

Mice treated with the BL-CHOP therapy exhibited a varied array of visual manifestations of chemotherapy-induced toxicity with cardio- and hepato-toxicity being most notable during necropsy (Figure 3.16A,B). Upon examination of the cranium, clear blood spotting on the brain was also evident (Figure 3.16B). As discussed in the previous sections, considerable weight loss was also evident in mice that underwent chemotherapy. The BL-CHOP100 (pictured below in Figure 3.16D) was of no exception. Observationally, all BL-CHOP treated mice experienced gastrointestinal distress, with diarrhea being observed from the second week of treatment.

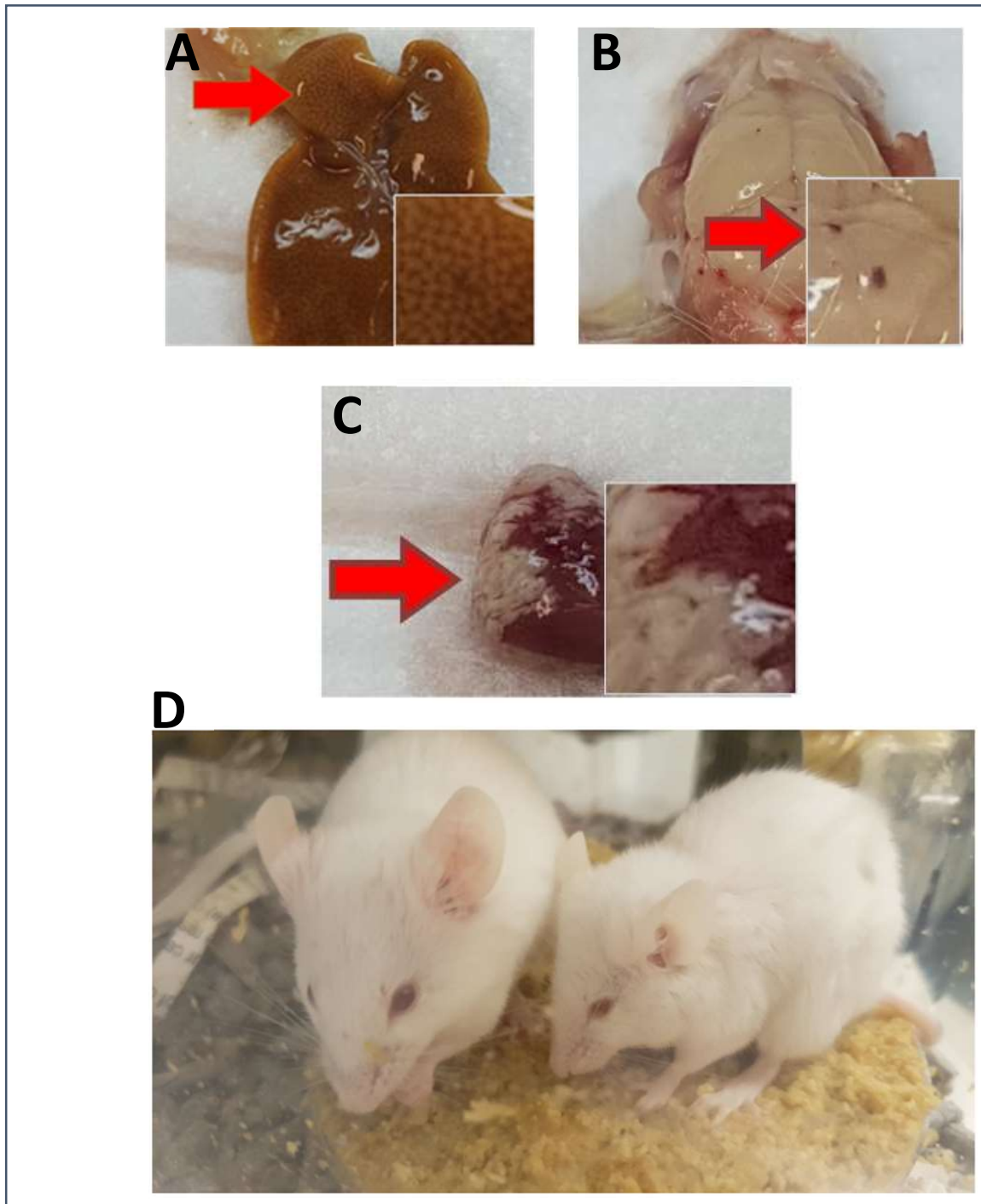

***Figure 3.16**: **Observations of systemic toxicity in necropsy of BL-CHOP80 treated mice.** A) post-mortem prosection of liver showing perfuse hepatotoxicity B) blood clotting on the brain C) cardiomyopathy indicated by pericarditis like deposits D) considerable failure to thrive and visual palor of BL-CHOP100 treated mouse in comparison to its VEH, age matched counterpart.*

3.4 Discussion

Establishing a viable and clinically similar animal model is an essential step to improve laboratory research relevancy against clinically orientated problems. The aim here was to develop animal models capable of replicating gold standard paediatric chemotherapeutic regimens currently used in the clinical setting. To do this, the IAMDF from Chapter 2 was used to identify and alter current gold standard regimens to enable their use in mice. Here, these regimens were tested for their veracity and viability. With SMDW being the primary variable of interest, loss of muscle mass and function were of key interest. Firstly, changes in weight throughout chemotherapy has been used for decades as a rudimentary prognostic factor [483-486]. More recently, weight loss (of 5% or greater) combined with a reduction in BMI (<20 kg/m^2) has also been used to define cachexia [33,152,153,155], highlighting weight loss as a simple yet important macro level observation for diagnosis. As such, mice were monitored daily for weight change and caloric intake (together with a suite of general welfare observations; *S3.2.1.2*). Secondly, survivors of chemotherapy have been shown to exhibit considerable skeletal muscle dysfunction which endures for life [18,19,22]. As such, *ex vivo* assessment of muscle function to assess for this were also completed. Finally, due to the systemic and toxic nature of chemotherapy, general toxicity measures were made to assess the suitability of selected doses. Combined, these measures across the three pilots showed that: 1) all three pilot regimens induced CI-SMDW; 2) The 100% dose of the MB-LCV therapy was viable and was thus selected for the confirmation study; 3) Both the ALL-POMP and BL-CHOP regimens, induced lethal toxicity at higher dose levels; 4) The BL-CHOP regimen was survived at the 80% dose with this dose being selected for the confirmation study; and 5) Multiple dose reductions and modifications to the ALL-POMP regimen was required for tolerability to be achieved . This

discussion will be limited to outlining the efficacy and clinical similarity (or lack thereof) of the pilot studies, the modifications that were required to achieve tolerability, and their suitability for use in the next step of the IAMDF confirmatory study.

3.4.1 Selection of dose for MB-LCV and BL-CHOP regimen

A decline in nutritional status is a well-established complication of chemotherapy treatment; potentially due to nausea related side-effects such as emesis, constipation and diarrhea and/or exacerbated inflammatory status, all compounding to reduce the available energy and nutrients and supress growth in the paediatric patient [487]. Ward *et al* (amongst others) confirm this by showing that together with emesis and constipation, after radiotherapy and 2 courses of chemotherapy, paediatric patients undergoing treatment for medulloblastoma lost on average 8.2% (range 0–21%) of their pre-diagnosis weight over a 2.25 year time period [488]. Of course, it must be conceded that studies in children are done so due to a cancer diagnosis which is absent in most animal models looking at chemotherapy. However, the aforementioned sequalae are consistently concomitant with, and exacerbated by, chemotherapy suggesting a causal link. This weight-loss induced by cancer and/or chemotherapy has been coined cachexia [279]. Here, chemotherapy began at week 4 of life (corresponding to approximately 10-12 years of age in children, see *Chapter 2: Step 7* for further discussion of age comparisons between human and mouse) at 10% of the preferred clinically relevant IAMDF dose which resulted in unremarkable changes to the overall observable wellbeing of the mice (as visually observed and graded as described in S3.2.1.2) in both MB-LCV and BL-CHOP therapies. Acute toxicity was observed (refer Figure 3.9A) in the MB10 regimen with 6.3% bodyweight lost over the course of 24 hours post CCNU oral gavage

on day 28, which took 12 days to recover from. This effect was replicated on day 1 of the MB100 regimen with the mouse losing 3.8% of body weight over 4 days (Day 1-4), although, interestingly, this not seen on the first administration of the drug on day 1 of the 10% regimen suggesting a dose dependent relationship (both cumulatively and acutely). Moreover, mice exhibited depressed activity and were observed to huddle in the corner of their cage for ~60min most oral gavage with CCNU – suggesting the nausea experienced in humans [489,490] was replicated here.

Although the MB10 regimen appears, on the surface, to exact a lesser effect than the MB100 dose, an important concept which will be revisited throughout this thesis is the failure to thrive, which is considered under the cachexia umbrella [279]. Children grow at unprecedented rates in their early years with children gaining close to 20% of their body weight between the age of 5 to 6 years [491]. This growth rate is also seen in mice, who gain 31.6% between the age of 4 to 5 weeks (VEH treated mice, Figure 3.9F, with age approximately comparable to 5-6 years of age in humans). The MB100 mouse, in comparison, only grew 0.9% within the same time frame (week 4-5) which equates to a reduction in growth of 31%. Even with a considerably reduced dose, the MB10% mouse grew only 19% between 4 and 12 weeks of age, a difference of 78% when compared to VEH. This failure to thrive at the start of life occurred without any observable signs of distress (observational data) and survival achieved. These observations highlight that even though growth continued, a considerable suppression of growth was sustained throughout MB-LCV chemotherapy at both the 10% and 100% doses which is similar to that which is seen clinically in paediatric patients treated for MB-LCV [488,492]. These adverse effects were mostly mirrored in the BL-CHOP

therapy (refer Figure 3.9B) with the BL-CHOP10 mouse gaining only 9% body weight in the first week of chemotherapy (Day 1-7 of therapy and week 4 to 5 of life) and 48% over the first 8 week course of chemotherapy (48% less than VEH). At the 100% dose, the mouse failed to achieve a net weight gain over the course of the therapy; which is similar to the growth patterns seen in paediatric patients receiving anti-lymphoma chemotherapy [493,494]. Due to toxicity ultimately inducing death at day 52 of the BL-CHOP100 regimen, the dose of chemotherapeutics were reduced by 20% as a 10% reduction was unlikely to be viable. Surprisingly, with only a 20% dose reduction, the BL-CHOP80 closely mirrored the BL-CHOP10 dose with only an approximate 5% difference in net weight gain (as measured by total area under the curve: refer Figure 3.9B).

Although cachexia is often an underlying cause of morbidity and mortality in patients [152,154,279], the loss of skeletal muscle mass and function is often the cause of the long term morbidity that is so often seen in chemotherapy survivors [19,20,93,94]. Although the exact mechanism behind these dysfunctions are not entirely known, it is speculated that chemotherapy-induced peripheral neuropathy is a major underlying cause [11,495,496]. Moreover, similarities between chemotherapy-induced neuropathy and neuropathies seen in diabetes mellitus or alcohol induced neuropathies have been drawn, as these neuropathies also result in sustained abolition of both muscle function and restorative capacity [496]; a pathological similarity which will become more important in later chapters. Here, both regimens were observed to induce varying levels of skeletal muscle dysfunction (refer Figure 3.12). EDL muscle from the MB100% mouse recorded a 67% reduction in force output over the course of 180 seconds (a further 14% drop compared to CON) (refer Figure 3.12). Contrary

to expectation, after the 60-minute recovery, force output of the MB100 muscle trailed pre-fatigue force by 81% – whereas the control was observed to completely recover. Similar dysfunction was also noted in the BL-CHOP100 mouse muscle with a 64% reduction in force output over the course of 180 seconds (a further 11.26% drop compared to CON) (refer Figure 3.12). Surprisingly, the BL-CHOP100 muscle failed to recover at all during the recovery phase, consistently losing force throughout the recovery period until no force was produced at the 60min mark suggesting complete failure of the muscles contractile apparatus.

Chemotherapy-induced cachexia and a failure to thrive in children is often underpinned by failure of both hyperplastic and hypertrophic muscular growth [497], which is also the case in juvenile mice [498]. The observations seen here in response to chemotherapy can be rudimentarily interpreted as the failure of lean mass growth, rather than muscle loss due to a wasting or atrophic mechanism. Although measurements of mouse organs and tissues were made to confirm this hypothesis, due to singular mice being used, variability was high, and no conclusive deductions could be made from these measurements. A failure which is rectified in later chapters where greater numbers are used. Nevertheless, the reduction in food consumption which was proportionate to chemotherapy dose (Figure 3.11) suggests that weight-loss may have been due to lowered caloric intake, though the accuracy of this will be investigated further in later regimen specific chapters. These across the board reductions in muscle strength, fatiguability and recovery combined with considerable weight loss accurately depicts the SMDW phenotype seen in children within the clinical setting and, as such, both the MB100 and BL-CHOP80 regimens were selected for the confirmation study.

3.4.2 ALL-POMP pilot successes and failures

Due to the normal proliferative nature of lymphoblastic cells within the bone marrow, and the near systemic distribution of them throughout the body, chemotherapeutic regimens used to combat the condition are both enduring and intensive. Although impressive survival rates are seen with the selected regimen in human paediatric patients (91%) [322], considerable toxicity is also observed; including pancreatic and gastrointestinal dysfunction, coagulation abnormalities and persistent and recurrent infections [322]. Here, 10% of the clinically relevant dose was well tolerated with no significant signs of toxicity being noted. The mouse also gained 56.7% of its original body weight (refer Figure 3.9C) although failure to thrive was clearly evident when compared to VEH treated mice, which gained on average 92% of starting weight over the course of the 8-week treatment period – a difference of ~35%. With the survival of the ALL-POMP10 regimen achieved, doses were increased to 100% (and subsequently reduced to 80%) which resulted in lethal toxicity, considerable reduction in growth rates (Figure 3.9C) and indications of nephrotoxicity and acute kidney injury. In fact, toxicity of this regimen created considerable difficulties in establishing the protocols viability. Considerable research was undertaken to ascertain where the toxicity was being created to modify the regimen to improve toxicity. Previous observations in MTX treated patients showed that the MTX treatment induced nephrotoxicity due to the crystallisation of MTX within the kidneys; which served to explain the crystallised excretions seen in patients [474] and which were seen here in MTX treated pilot mice (Figure 3.15A). This likely exacerbated the dehydration status of the mice leading to lower renal output, further reducing renal clearance of MTX and thus intensifying its toxicity and crystallisation. To counter the described MTX kidney injury, the regimen was adapted to include calcium leucovorin recovery and added

hydration through watered-down feed which (increased hydration) is in accordance with clinical practice [474,499-502]. Unfortunately, these trials were not survived, though the 20% reduction in dose (from ALL-POMP100 to ALL-POMP80) increased lifespan by 34%, and increased growth rates by 8% from Day 1 through 39 (Figure 3.9C).

With the added regimen modifications and newfound understanding of high dose MTX therapy in mice, ALL-POMP100 and ALL-POMP80 doses were re-attempted with the addition of the CLV recovery and PRED taper protocols. MTX dose was then reduced by a further 20% for each regimen. With the addition of CLV, and the reduction in both 6MP and MTX doses, total growth between days 1-39 were comparable between ALL-POMP10 and ALL-POMP100+CLV MTX80 suggesting the majority of regimen toxicity lay with these agents (refer Figure 3.10). Ultimately, due to time constraints, ALL-POMP doses were reduced to 60%, 50% and 40% in a final pilot run to ensure a successfully completed ALL-POMP pilot was achieved. All three pilots at these doses were tolerated indicating that the ALL-POMP60+CLV (with once daily 6MP and 7-day PRED taper) was the most viable option for this regimen. Interestingly, the presence of schistocytes in the peripheral blood smears of the ALL-POMP60, 50 and 40 mice lends to support the MTX-induced acute kidney injury hypothesis as schistocytes are characteristic of haemolytic anaemia which can indirectly result from acute kidney injury [503,504]. Additionally, the high presence of reticulocytes (indicated by Howell-Jolly bodies described in S3.3.4) further supports this theory. An interesting finding in the ALL-POMP necropsy (Figure 3.15) was evidence of clotting on the brain which could be interpreted as a complication of acute kidney injury, namely thrombotic microangiopathy, which is commonly associated with thrombocytopenia, kidney injury and anaemia [505]; all of which were seen

here. Although functional muscle data was not obtained from these mice, data from the ALL-POMP100 treated mouse suggests the agents used induced skeletal muscle dysfunction (Figure 3.12). The *EDL* muscle from the ALL-POMP100 mouse was unable to recover after the fatigue and recovery protocol was administered, exhibiting a 43% decline in force output (a -64.5% difference when compared to CON). Although it is possible that the additions of CLV, and the reductions in 6MP may reduce the dysfunction seen, this is speculative at best and is unlikely. Longitudinal studies looking at survivors of paediatric ALL show a decline in both strength [19] and a greatly increased rate of fatigue [18,93] long after the cancer survived and the treatment ended [144]. These studies looked at varying regimens including those that comprised an MTX+CLV recovery, which led to the hypothesis that the addition of CLV is not protective against skeletal muscle dysfunction and that the ALL-POMP60+CLV regimen would indeed induce a SMDW phenotype.

It was important to ascertain that even with reductions in dose, the ALL-POMP regimen could still sufficiently ablate lymphoid cells. Blood investigations into this ability (Figure 3.13) showed that for treatment at 60% of the ALL-POMP IAMDF clinically relevant dose, lymphocyte populations were more than halved (lymphocyte count: VEH $3.62x10^{9}.L^{-1}$, ALL-POMP60+CLV $1.50x10^{9}.L^{-1}$). Although 60% was the highest survivable dose, the red cell count (VEH $10.86x10^{9}.L^{-1}$, ALL-POMP60+CLV $2.36x10^{9}.L^{-1}$) and platelet count (VEH $1.16x10^{12}.L^{-1}$, ALL-POMP60+CLV $0.25x10^{12}.L^{-1}$) in the 60% regimen were both reduced by 78% when compared to VEH. Considering the ALL-POMP50+CLV dose did not suffer from such significant RCC suppression ($7.45x10^{9}.L^{-1}$, a 32% reduction) or platelet suppression ($1.11x10^{9}.L^{-1}$, a 4% reduction), this dose level may be more viable for future investigations if further supportive

therapies are not included (such as blood product transfusions). It must be considered, however, that the addition of such supportive therapies greatly increases both cost and labour for the study and is the primary reason why they were not included in these pilots. Both packed RCC and fresh frozen plasma transfusions are used as supportive therapies in the IAMDF selected regimen in humans, as well as renal dialysis if required [322]. As these supportive therapies were not used here in mice, it is reasonable to suggest that this is one of the major reasons why the dose was required to be reduced to the level it was, and that the calcium leucovorin recovery was required to improve MTX tolerability.

3.5 Chapter Summary

The IAMDF proved a viable process in which gold standard interventions were adapted for investigations in mice. Using this method, the clinically relevant dose of the MB-LCV regimen, and 80% of the BL-CHOP regimens were well tolerated. These doses also successfully induced the CI-SMDW phenotype which is central to the purpose of these investigations. Limitations in the application of the framework also presented themselves in that, for example, the efficacy of regimen replication in mice can be dependent on the laboratory's ability to replicate the supportive therapies co-administered within the clinic. Although these supportive therapies are mainly geared towards improving survivability, the implication of not offering these therapies would likely impede the accurate replication of the chosen intervention. As a result of this, and due to the lack of available resources and time to

appropriately modify the regimen to include these supports, the IMADF derived ALL-POMP regimen was not continued to the confirmation phase of the framework. However, the ALL-POMP60% regimen is a viable regimen which appropriately replicates the CI-SMDW phenotype in mice. Any future studies into CI-SMDW within the ALL-POMP pathology and treatment should consider using the ALL-POMP regimen outlined herein – with or without additive supportive therapies. The BL-CHOP80 and MB100 regimens both presented as viable. As such, both will be investigated in more depth within the following chapters.

Chapter 4

Investigation of CI-SMDW Induced by MB-Indicated LCV Therapy in Juvenile Mice

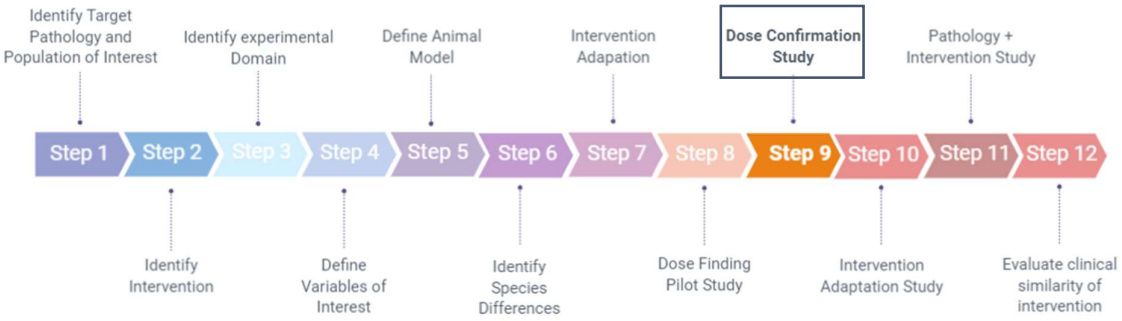

4.1 Introduction

Current treatment regimens for paediatric medulloblastoma offer greater than 70% of children long-term survival against this otherwise lethal disease [506]. Chemotherapy is a frontline treatment against medulloblastoma [507], however, is not without toxicity. Cranial-targeting chemotherapeutics are often linked to neurological toxicity (both peripheral and central) [140,328,473], with long-term sequalae including severe intellectual disability and truncated childhood physical development [508]. Chemotherapy-induced neuropathy, a characteristic feature of medulloblastoma chemotherapy [509], has been shown to impair muscle development in the growing child [18,510]. These neuropathies also lead to motor skill impairment [511,512], and the degree of chemotherapy-induced impairment is thought to escalate with younger intervention in children [513]. Unfortunately, chemotherapy-induced neuropathy and SMDW is not unique to medulloblastoma therapy.

We have previously established that 2 weeks of individual chemotherapy (oxaliplatin) administration induces skeletal muscle wasting, through mitochondrial impairment, excessive ROS production and subsequent inhibition of protein synthesis in 12 week old mice [159,160,272]. In Chapter 3, we further established in pilot models that IAMDF-modified gold standard combination-chemotherapy regimens used against common paediatric cancers – namely MB-LCV, ALL-POMP and BL-CHOP – all induced some level of SMDW and mitochondrial impairment. Since healthy mitochondrial function underpins muscle performance due to a key role in energy production and by regulation of life sustaining cellular functions through ROS signalling, a failure of energy homeostasis could explain the SMDW observed in paediatric patients following chemotherapy. We, and others have shown that various other

chemotherapeutic agents (e.g. doxorubicin and cyclophosphamide) disrupt mitochondrial function in both cell lines and in rodents [110-112,163,239,254,277,514]. Important work by Talvensaari *et al.* [22] showed that long-term survivors of childhood chemotherapy not only manifested declines in muscle mass, strength and endurance capacity, but were also at a significantly higher risk of developing metabolic syndrome later in life, and that this was closely linked to mitochondrial dysfunction [515-520]. Further, when radio- and chemo-therapy were used together against childhood brain cancer, considerable declines in physical and intellectual performance were observed, which greatly hindered patients' ability to live independently [509]. However, the underlying mechanisms causing these sequalae are not well understood since chemotherapy cannot be investigated independent of cancer and other anti-cancer interventions in humans.

Animal models provide the opportunity to investigate the direct effects of chemotherapeutic agents without conflicting variables. However, models which allow appropriate clinical similarity between animal and human treatments have not been established prior to this study, mainly due to the difficulties associated with required human-to-mouse drug dose conversions, modifications in administration methods, and considerable labour associated with regimen delivery (as described in the previous chapters). Here, a gold standard medulloblastoma chemotherapeutic regimen (LCV), using lomustine (CCNU), cisplatin (CDDP) and vincristine (VCR), has been modified for use in animals to investigate the effect of the therapy on the skeletal muscle of juvenile mice as previously described in Chapter 2. With the IAMDF-modified MB-LCV regimen having been established and validated in Chapter 2, the aim of this chapter and study was to: 1) further authenticate the MB-LCV animal model as clinically relevant by showing that IAMDF-modified LCV administration in young mice induces SMDW, which endures over the lifespan; 2) investigate the underlying

mechanisms of MB-LCV-induced SMDW through *in vivo* and *ex vivo* skeletal muscle structure and function analyses and; 3) interrogate the role of the mitochondria in the molecular regulation of SMDW using *ex vivo* extracellular flux analysis. We hypothesise that CI-SMDW is instigated by administration of MB-LCV to juvenile mice and is endured throughout the lifespan. We also hypothesise that CI-SMDW is, at least in part, underpinned by mitochondrial dysfunction.

4.2 Method

Methods were performed as described in Chapter 3 unless otherwise stated below. Methods performed in addition to those described in Chapter 3 are described herein.

4.2.1 Animals

Animal experimentation was performed as outlined in *Chapter 3: Pilot*, and only animal numbers differed in the current study. In this study, 34 mice began treatment housed in cages of five (with one group of four) with group names, numbers and associated cull points outlined in Table 4.1. Fourteen MB-LCV treated mice were culled on the last day of the regimen (D56 of treatment/D84 of life), with the remaining 20 culled at week 30 of life. Sixty mice were treated with the VEH regimen as outlined in S4.2.1.2, with 35 mice being culled at D56/D84 of life and the remainder culled at 30 weeks of age. These time points were chosen

to replicate key post-chemotherapy timeframes in humans, namely adolescence (15-18 in human years) and pre-sarcopenic adulthood (30-40 human) [436].

A power analysis to determine the appropriate sample size could not be reliably completed as there are no previous studies to base the expected effect size on. Although we hypothesised a negative impact on mouse survival, well-being and skeletal muscle function and mass, the effects of individual drugs can vary greatly from patient to patient and we expected this to occur in the mouse model as well. Other studies investigating chemotherapy regimens in rodents (including previous studies by us [1,159,160,272,421-423]) have used group numbers of 10-12 to observe differences in lean muscle mass and body weight measurements. However, the duration of these studies was far less than the 8-week clinically equivalent chemotherapy regimen performed in the current study. Due to the nature of chemotherapy, and considering that: (1) over 70% of childhood cancer survivors develop a severe secondary chronic illness during their lifespan; and (2) balb/c mice are naturally more inclined to develop cancer later in life; we increased the sample size in all groups to account for these variables. As such, we sampled a minimum n =15 for each treatment group.

Table 4.1: Group names and animal numbers with associated cull points

Group	***n* to 12 weeks of age**	***n* to 30 weeks of age**
MB-LCV	34	20
VEH	60	25

4.2.1.1 Chemotherapy summary

Following from the success of the MB-LCV pilot study, the 100% IAMDF dosing schedule was used in this study as outlined below. For more information on how this dose was derived, refer to *Chapters 2 and 3*. Treatments herein were adapted from the Children's Cancer Group, study number: *CCG-9892* by Packer et al [124].

Table 4.2: Drug names, delivery modes and doses for selected medulloblastoma-indicated regimen

Drug	*Mode of delivery*	*Delivery times*	*Dose per delivery*	*Total daily dose*	*Days delivered per regimen*
Lomustine (CCNU)	Oral gavage	7-9am + 1-3pm	11.07 mg/kg	22.14 mg/kg	1
Cisplatin (CDDP)	Intraperitoneal injection	7-9am + 1-3pm	11.07 mg/kg	22.14 mg/kg	2
Vincristine (VCR)	Intraperitoneal injection	7-9am + 1-3pm	0.22 mg/kg	0.44 mg/kg	2,7,14

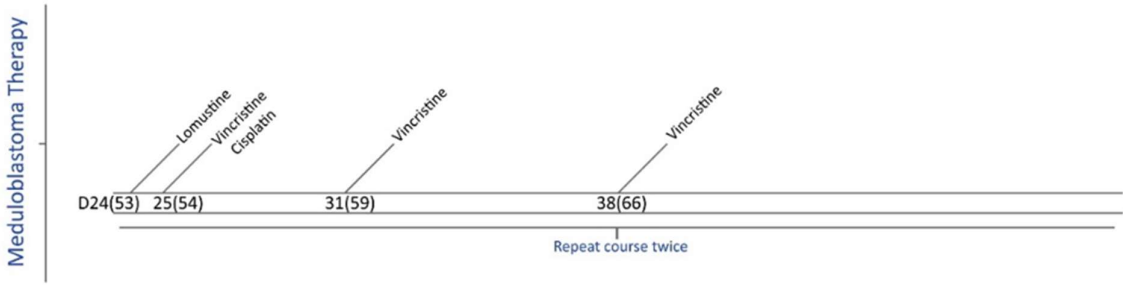

Figure 4.1: MB-LCV regimen outline. Days indicate age of life of treated mice with bracketed numbers indicating days of treatment for the second round of therapy.

4.2.1.2 Vehicle regimen

Due to the complexity of the project and lack of resources (human, financial and time) it was necessary to develop a vehicle group with the capability to be used for all three regimens; ALL-POMP, MB-LCV and BL-CHOP. Although a vehicle group which exactly replicated each of the treatments, their vehicles and modes of administration for each of the regimens investigated in this PhD would have been ideal, this was not realistically possible with our limitations. As the ALL-POMP regimen was considered the most intensive – due to the daily oral gavage for 80 days, thrice weekly injections for the first course and once weekly for the second – it was considered that if any effects were to be seen due to vehicle substances and/or the stress of manual handling and treatment methods, they would manifest greatest in the ALL-POMP regimen. Therefore, the ALL-POMP regimen served as the basis for the VEH regimen used throughout this project. It should then be considered that some, more minor effects of the MB-LCV and BL-CHOP regimens, could have been masked by the severity of the VEH regimen.

4.2.2 Analytical methods

Analytical Methods were performed as outlined in *Chapter 3*, with the addition of the following methods:

4.2.2.1 *Intraperitoneal glucose tolerance test (IPGTT)*

Studies have demonstrated that metabolic syndrome regularly occurs in adults who were treated with chemotherapy during childhood [521-524], and for this reason, we investigated glucose homeostasis/regulation in mice. To do this, we utilised a standard IPGTT protocol [525]. Mice were removed from cages and weighed before topical analgesic cream (25mg.g^{-1} lignocaine, 25mg.g^{-1} prilocaine) was applied liberally to their tails. After 30min, 1-2mm of the end of the tail was removed from each mouse with surgical scissors and a blood glucose reading taken to establish baseline blood glucose levels. Mice were then immediately injected with a 45% glucose solution (D-(+)-Glucose solution 45% in H_2O, Sigma-Aldrich) at 2.2µl.g^{-1} body weight, to achieve a 1g.g^{-1} dose. Following the glucose injection, blood glucose levels were measured by re-opening the tail wound and taking blood glucose readings at 5, 15, 30, 45, 60, 90, and 120 minutes. Base readings and injections were staggered to allow 10 mice to be completed by one operator within 3 hours. An Accu-Chek® Guide glucometer and Accu-Chek® Guide test strips were used to measure blood glucose.

4.2.2.2 *Grip strength*

In the clinical setting, patient grip strength is often measured using a hand-held dynameter. To parallel this measure in mice, an isometric force transducer (Research Grade 60-2999, Harvard Apparatus, South Natich, MA) was engineered to enable attachment of a mouse-friendly grip platform; allowing a mouse to hold on to the mesh with its fore and hind

paws (refer Figure 4.2A). Afterwards, a calibration with weights of known mass was conducted. During testing, the tail of the mouse was gently pulled in the horizontal plane until the pulling force overcame the mouse's ability to hold onto the mesh. The force at which the mouse let go was recorded as maximum grip strength obtained by the mouse. Data was recorded using LabChart Pro 8 software (AD Instruments) with an example force/time trace presented in Figure 4.2B. This was repeated five times per mouse and the average of the replicates was determined and expressed relative to body weight.

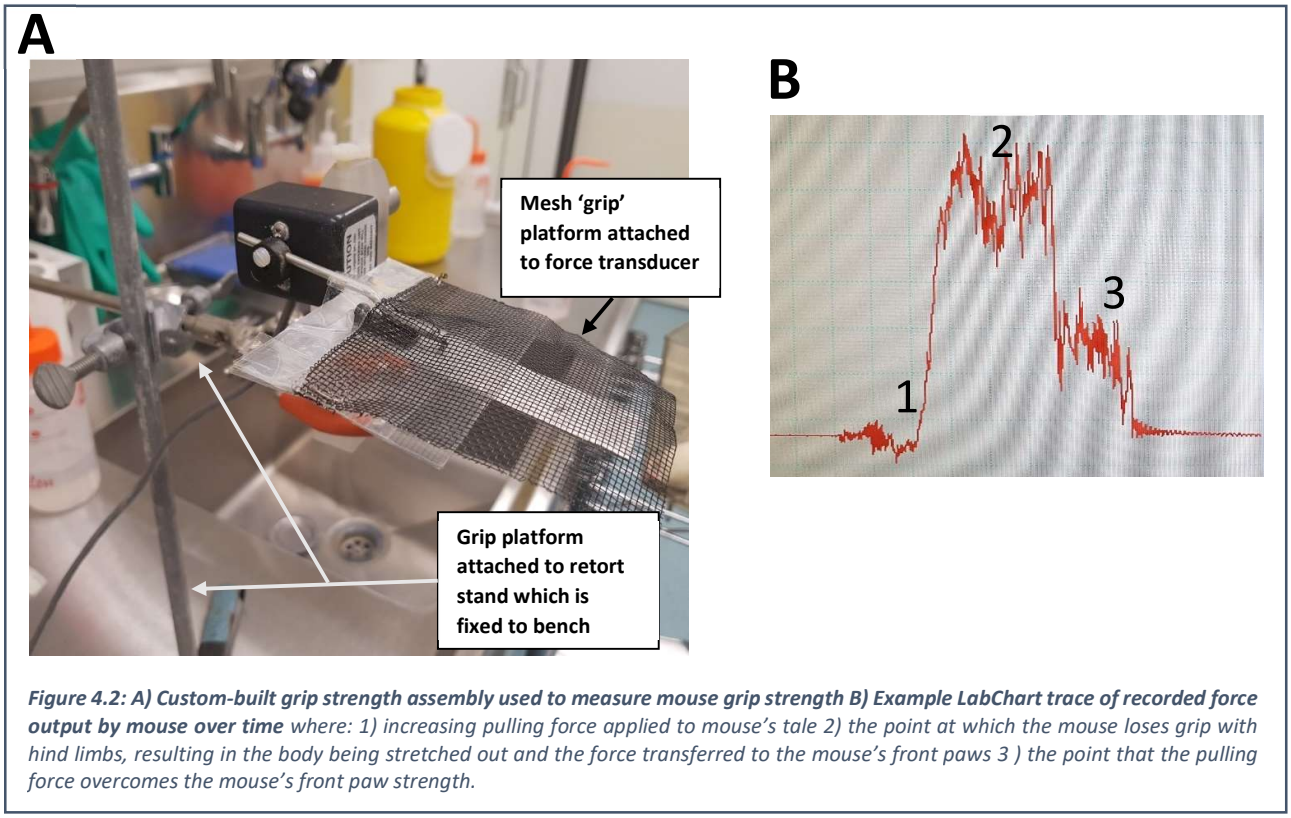

Figure 4.2: A) Custom-built grip strength assembly used to measure mouse grip strength B) Example LabChart trace of recorded force output by mouse over time *where: 1) increasing pulling force applied to mouse's tale 2) the point at which the mouse loses grip with hind limbs, resulting in the body being stretched out and the force transferred to the mouse's front paws 3) the point that the pulling force overcomes the mouse's front paw strength.*

4.2.2.3 Micro-computed tomography

Micro-computed tomography (µCT) is the gold standard imaging modality using in body composition and soft tissue pathology investigations [127,378,426,526]. As lean mass loss is a clear sequalae of CI-SMDW, assessing whether or not chemotherapy reduces skeletal muscle mass or quality through increased intra-muscular fat or connective tissue. To do this, the hind left limb was harvested from anaesthetised mice (as described in *Chapter 3, S3.2.2*) by amputating the leg proximal to the knee joint. Hind-limbs were prepared using previously described protocols [378,527]. Briefly, limbs were skinned and fixed in 10% neutral-buffered formalin (HT501128-4L, Sigma) for 24 hours at room temperature before being blotted clean with 1x phosphate buffer solution and stored in 60% ethanol at 4^{oC}. Multiple trial formulations and staining times were used to derive an optimal staining protocol (as described below in *S4.2.2.3.1*). Ultimately, samples were stained in Na_2WO_4 dissolved in DiH_2O at a 50% w/v concentration for 48 hours prior to imaging. Samples were removed from original storage tubes and scanned in 2ml 0.5mm Eppendorf tubes. Samples were imaged using the Skyscan 1272 (Bruker, Belgium), NRecon software (v1.7.4.2, Bruker, Belgium) and CT Vox (V3.3.0 r1403, 64bit, Bruker, Belgium). The scanning parameters were 9µm pixel size, 50 kV, 200uA, 0.4^{o} step with 450 projections at 1450ms exposure using a 0.5 mm Al filter. Images were assembled in NRecon using 5.0 post alignment compensation, 20% beam-hardening and level 7 ring artefact reduction. Although samples were stained as above, samples were unfortunately overstained and 3D volumetric analysis using various software were unable to differentiate between the different tissue types of the hind limb, namely fat, muscle or bone. As such, a new method of analysis was developed by us where the proximal level of the calculated 1/3 of the tibia was selected as a landmark for analysis. Cross sectional area of the

musculature was measured at this station and at stations 1mm above and below. These results were then combined, together with the distance between the points, to give a measure of muscular volume (see Figure 4.3).

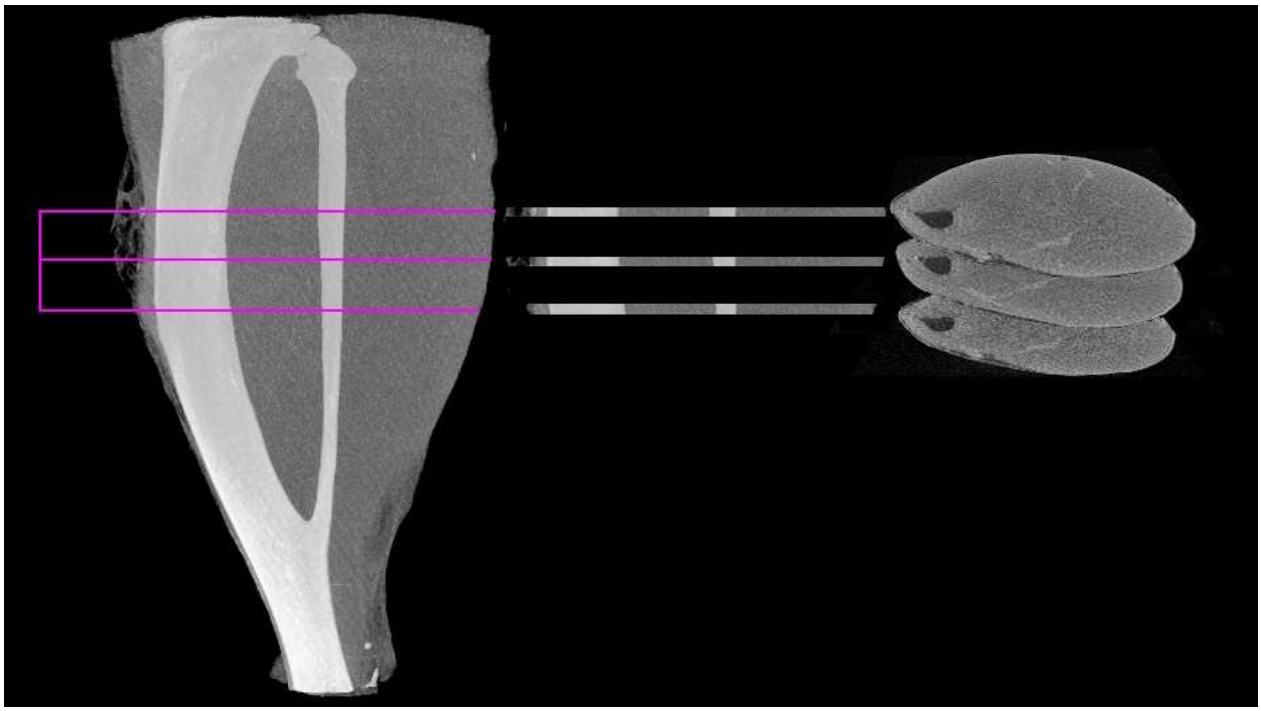

Figure 4.3: Visual representation of µCT volumetric analysis method. *Mouse hind limb's were imaged using Skyscanner 1272 imaging system and 3-dimensially reconstructed using NRecon and CTVox to identify the location of the proximal 1/3 of the tibia. CT slices from this location and 1mm above and below were extracted for extrapolation of muscle volume in this area by manually measuring the cross-sectional area of muscle in each slice and calculating volume.*

4.2.2.3.1 Micro-computed tomography trials

Trials to derive optimal staining protocols were completed on limbs from pilot mice obtained from *Chapter 3* and are described in Table 4.3. Imaging was performed as described

in the previous section. A trial was considered successful if the staining agent completely penetrated and stained all soft tissue (complete muscular penetration through to the bone). Importantly, the stain was required to be of a lower density than that of bone for clear differentiation to be achieved. This was achieved during the final trial.

Table 4.3: Micro-CT contrast staining protocols outlining staining agent, concentration and staining time using imaging parameters outlined in S4.2.2.3.

Trial/Study	Staining agent	Staining solution	Stain time	Resulting contrast
Trial 1	Phosphotungstic acid (PTA)	1% w/v in DiH2O	24 hours	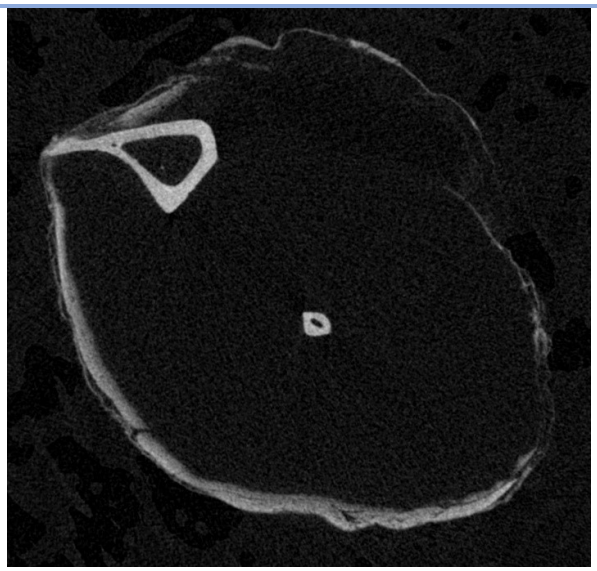

Trial 2	Phosphotungstic acid (PTA)	1% w/v in DiH2O	7 days	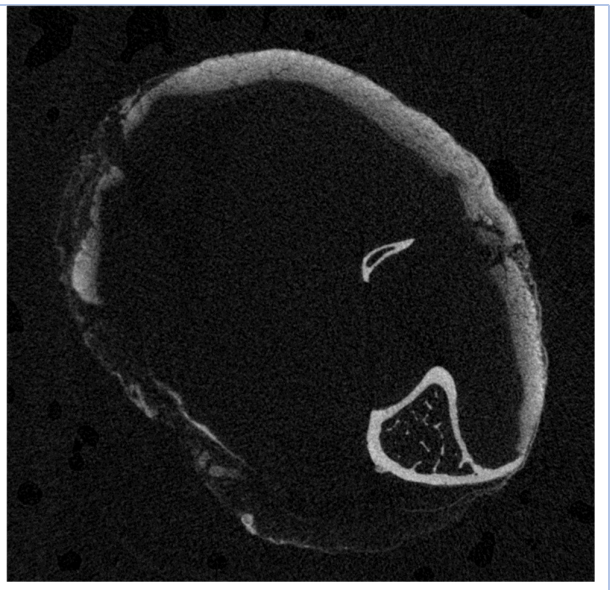
Trial 3	Phosphotungstic acid (PTA)	5% w/v in DiH2O	9days	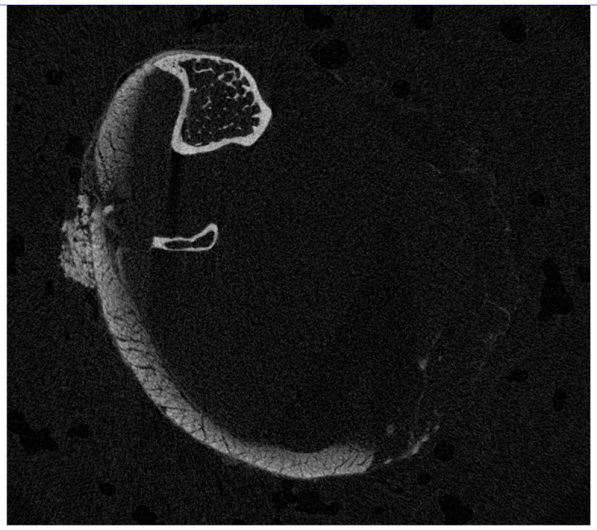
Trial 4	Sodium Tungstate ($Na_2WO_{4)}$	25% w/v in DiH2O	48hours	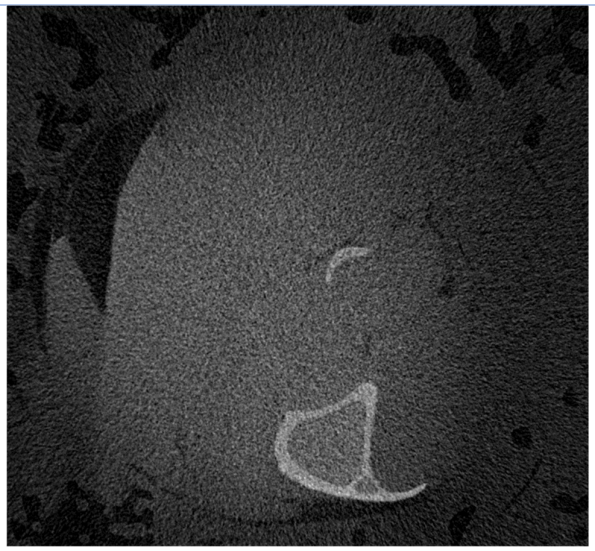

Trial 5	Sodium Tungstate ($Na_2WO_{4)}$	25% w/v in DiH2O	72hours	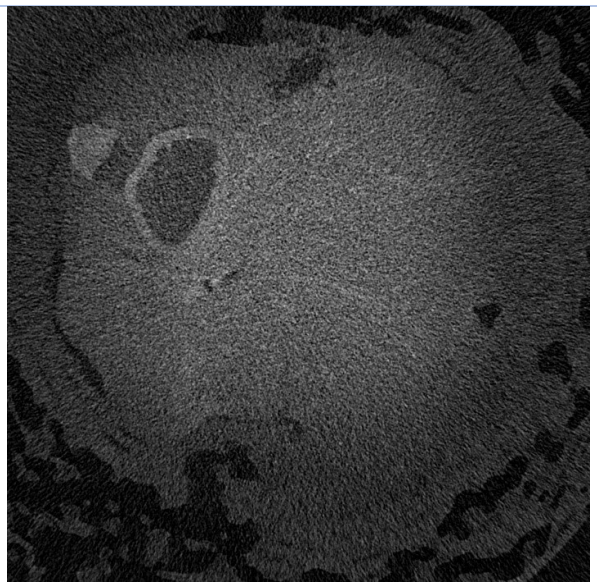
Trial 6	Sodium Tungstate ($Na_2WO_{4)}$	50% w/v in DiH2O	48 hours	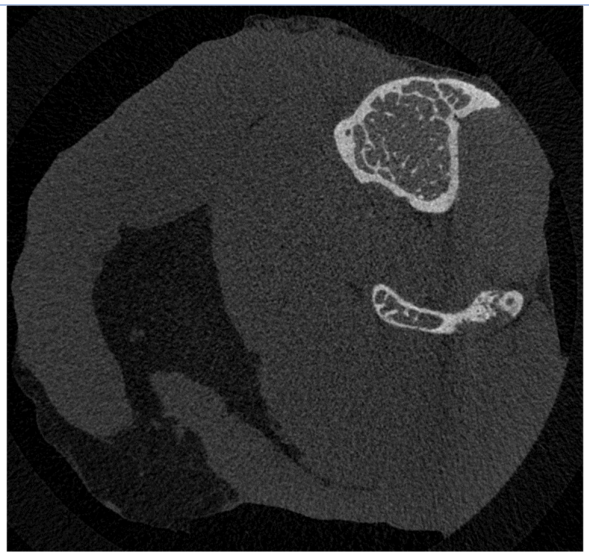
Main Study	Sodium Tungstate ($Na_2WO_{4)}$	50% w/v in DiH2O	48 hours	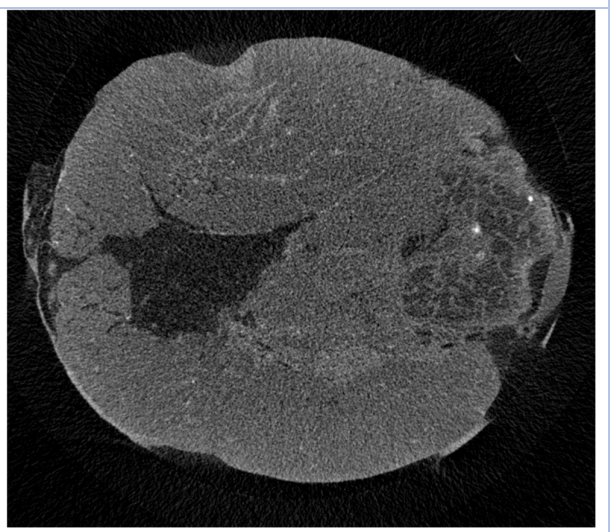

4.2.2.4 Histological analysis

The TA muscles were excised from mice whilst under general anaesthesia as described in *Chapter 3, S3.2.3.1*. Immediately after excision, muscles were coated in optimal cutting temperature (OCT) compound, snap frozen in liquid nitrogen-chilled isopentane (Sigma Aldrich, Australia) and stored at -80^{oC} for future analysis. Frozen OCT compound embedded TA muscles were cryo-sectioned mid-belly (10µm). Haematoxylin and eosin (H&E) staining was completed as previously described by us [159] to measure muscle fibre area and fibre size distribution. This was done using a standard H&E staining protocol (30s incubation in haematoxylin and 1m 45s incubation with eosin) and mounted with Dibutylphthalate Polystyrene Xylene (DPX, Sigma Aldrich, Australia). Images of all sections were taken using a Zeiss Axio Imager Z2 microscope (Carl Zeiss MicroImaging GmbG, Germany) at 10x and 200x. Images of the TA were taken from the most anterior, middle and most posterior areas of each histological section (due to localisation of differing fibre types in different areas of the muscle [528,529]).

Fibre size frequency distribution analysis was completed by manually outlining fibres (at least 200 fibres or all fibres on the image) using an imaging computer, stylus and ImageJ software (v1.52k, National Institute of Health, USA).

As the EDL and SOL muscles were used in the contractile functional analysis, the EDL and SOL muscles from the contralateral limb would have been preferred for histological analysis over the TA muscle. However, due to the contralateral limb being excised in whole for µCT analysis, another muscle for histological analysis was needed. The TA was chosen for H&E analysis as the greatest effects induced by the chemotherapy regimens were seen in the fast twitch EDL muscles (see *Chapter 3, S3.3.3 and S4.3.7* below). Moreover, the TA is

commonly used for histological analysis due to its size, enabling a large number of fibres to be analyses for fibre size distribution. As such, the TA muscle from the same leg as the EDL and SOL muscles used in the contractile analysis was selected as the TA muscle contains predominantly fast-twitch fibres, which is similar to that of the EDL muscle.

4.2.2.5 Assessment of mitochondrial function

4.2.2.5.1 Flexor digitorum brevis excision

Following confirmed anesthesia, a small incision was made down the lateral side of both feet through which the skin of the plantar section of the foot could be removed, exposing the *flexor digitorum brevis m.* (FDB), which was then removed. FDB muscles were placed in warmed dissociation media (DSM, refer Table 4.4 for details) and incubated for 95min at 5.0% CO_2 at 37^{oC}.

Table 4.4: Solutions used in the isolation of FDB fibres, their abbreviations and their components.

Solution	Component	Amount
***Dissociation Media* (DSM)**	DMEM (Gibco, no phenol red)	To total volume required
	Fetal bovine serum (FBS)	2.0% of total volume
	Gentamicin Solution (Gibco, 50µg/mL)	0.1% of total volume
	Collagenase A (Gibco, 4mg/ml)	5.0% of total volume
***Incubation Media* (IM)**	DMEM (Gibco, no phenol red)	To total volume required
	FBS	2.0% of total volume
	Gentamicin Solution (Gibco, 50µg/mL)	0.1% of total volume
***Measurement Buffer* (Total volume 1000ml) pH = 7.4**	NaCl (58.44g/mol)	7.01 g
	KCl (74.55 g/mol)	0.26 g
	$CaCl_2$ (110.98 g/mol)	0.144 g
	KH_2PO_4 (136.08 g/mol)	0.54 g
	$MgCl_2$ (203.3 g/mol)	0.2 g
	HEPES (238.3 g/mol)	1.2 g
	D-Glucose (180.15 g/mol)	0.45 g
	L-Carnitine (161.19 g/mol)	0.081 g

4.2.2.5.2 Isolated fiber preparation of the Flexor Digitorum Brevis muscle

After incubation in DSM, the muscles were washed in incubation media (IM, refer Table 4.4 for details) and triturated with pipettes of decreasing size (no greater than 10 passes per muscle) to dissociate fibres from connective tissue. All tissue other than muscle fibres were manually removed under a light microscope (refer Figure 4.4). After fibre isolation, a volume not exceeding 160µL of the remaining solution was added to 3 separate Matrigel coated wells of a 24 well cell culture plate (Seahorse Bioscience, XF24 cell culture plate, refer Table 4.6 for layout used) for Seahorse analysis of mitochondrial function. Fibres were plated

to ~60% confluency and allowed to adhere for 30min. After adherence had occurred, well volume was increased to a total of 180µL/well and returned to the incubator (37^{oC}, 5.0% CO_2). Once isolated FDB fibres of all animals from each treatment group (where no group exceeded n=5) were plated and fibre adherence to the plate was achieved, the plate was incubated overnight to allow cellular equilibration and stabilisation.

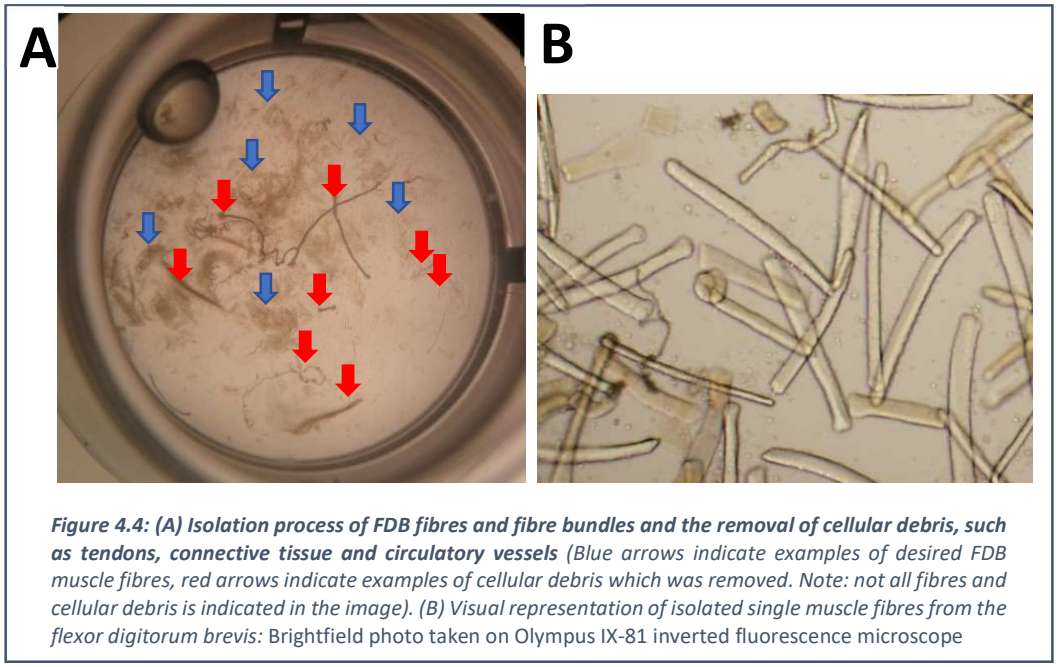

Figure 4.4: (A) Isolation process of FDB fibres and fibre bundles and the removal of cellular debris, such as tendons, connective tissue and circulatory vessels *(Blue arrows indicate examples of desired FDB muscle fibres, red arrows indicate examples of cellular debris which was removed. Note: not all fibres and cellular debris is indicated in the image). (B) Visual representation of isolated single muscle fibres from the flexor digitorum brevis:* Brightfield photo taken on Olympus IX-81 inverted fluorescence microscope

4.2.2.5.3 Seahorse mitochondrial performance analysis of isolated FDB fibres

After overnight adherence, fibres were washed using protocol previously described by us [112] (and as described in Table 4.5) with care taken not to disturb or remove any fibres and then re-incubated for 2 hours (37^{oC}, 0% CO_2). During the incubation period the sensor

cartridge (Seahorse Bioscience, XF24 Sensor Cartridge) was prepared as per Table 4.6 and the XF24 analyser was calibrated using the standard calibration procedure described by Seahorse Bioscience [530]. After the incubation period the fibres were analysed using the XF24 analyser with the protocol outlined in Table 4.7.

Through the coordinated addition of partial and complete mitochondrial inhibitor and stimulant compounds, a metabolic profile of the muscle fibres within each well can be produced (see Figure 4.5 for visual representation). First, measurement of basal oxygen consumption rate (OCR) is measured after the wells (and fibres) equilibrate to the environment and the solution mixed. Through repeated mixing and measurement cycles, the rate of O_2 consumption and CO_2 production in the microchamber created between the fibres and the probe sensors is determined. Oligomycin, once injected, inhibits ATP synthase (complex V) within the mitochondria, therefore inhibiting oxidative ATP synthesis, causing a rapid decline in O_2 consumption and corresponding increase in anaerobic glycolytic ATP production as measured through extracellular acidification. Next, carbonyl cyanide 4-(trifluoromethoxy)phenylhydrazone, or FCCP, is injected which disrupts the mitochondrial membrane potential ($\Delta\Psi$) driving maximal O_2 consumption (maximal respiration). Finally, Antimycin A is injected into the wells which acts as a potent inhibitor of complex III to inhibit electron transport and all mitochondrial associated respiration (O_2 consumption), allowing non-mitochondrial respiration driven by other cellular organelles and processes to be measured.

Table 4.5: Washing procedure used prior to Seahorse analysis for isolated fibres.

Procedure	Total volume remaining in well
1. Remove 105µL of solution from wells	75µL
2. Add 1000µL of pre-warmed measurement buffer to wells	1075µL
3. Remove 1000µL of pre-warmed measurement buffer to well	75µL
4. Add 600µL of pre-warmed measurement buffer to wells	675µL

Table 4.6: XF24 Sensor cartridge layout and corresponding stimulant/inhibitor solutions used for FDB isolated fibre metabolism performance analysis.

Port	**Solution**	**Volume per port**
A	2µg/mL Oligomycin (Seahorse Bioscience) in measurement buffer	75µL
B	400nM FCCP (Seahorse Bioscience) in 10mM Sodium Pyruvate (Gibco)	83µL
C	1µM Antimycin A (Seahorse Bioscience) in MB	92µL
D	Nil	Nil

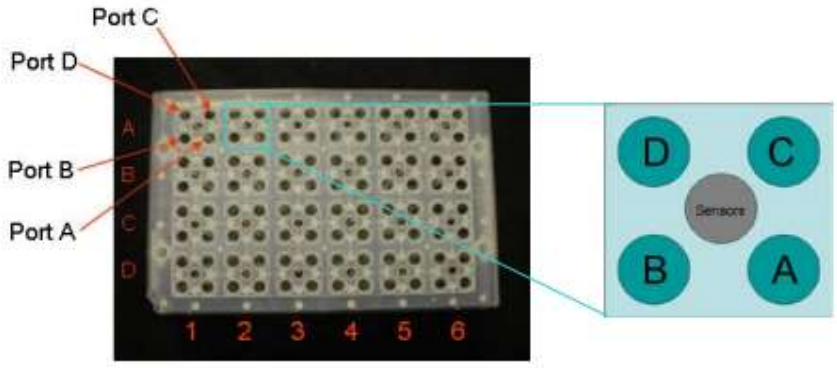

***Table 4.7: Outline of the protocol used for analysis of FDB isolated fibres using the XF24 Analyser**. Where S= standard operating time. 'Loop Start 3x' indicates procedures between loop start and loop end are to be completed in sequential order before being repeated an additional two times.*

Command	Time (min)	Port
Calibrate	S	
Equilibrate	S	
Loop Start	3X	
Mix	3	
Wait	2	
Measure	3	
Loop End	NA	
Inject	NA	A
Loop Start	3X	
Mix	3	
Wait	2	
Measure	3	
Loop End	NA	
Inject	NA	B
Loop Start	3X	
Mix	3	
Wait	2	
Measure	3	
Loop End	NA	
Inject	NA	C
Loop Start	3X	
Mix	3	
Wait	2	
Measure	3	
End	NA	

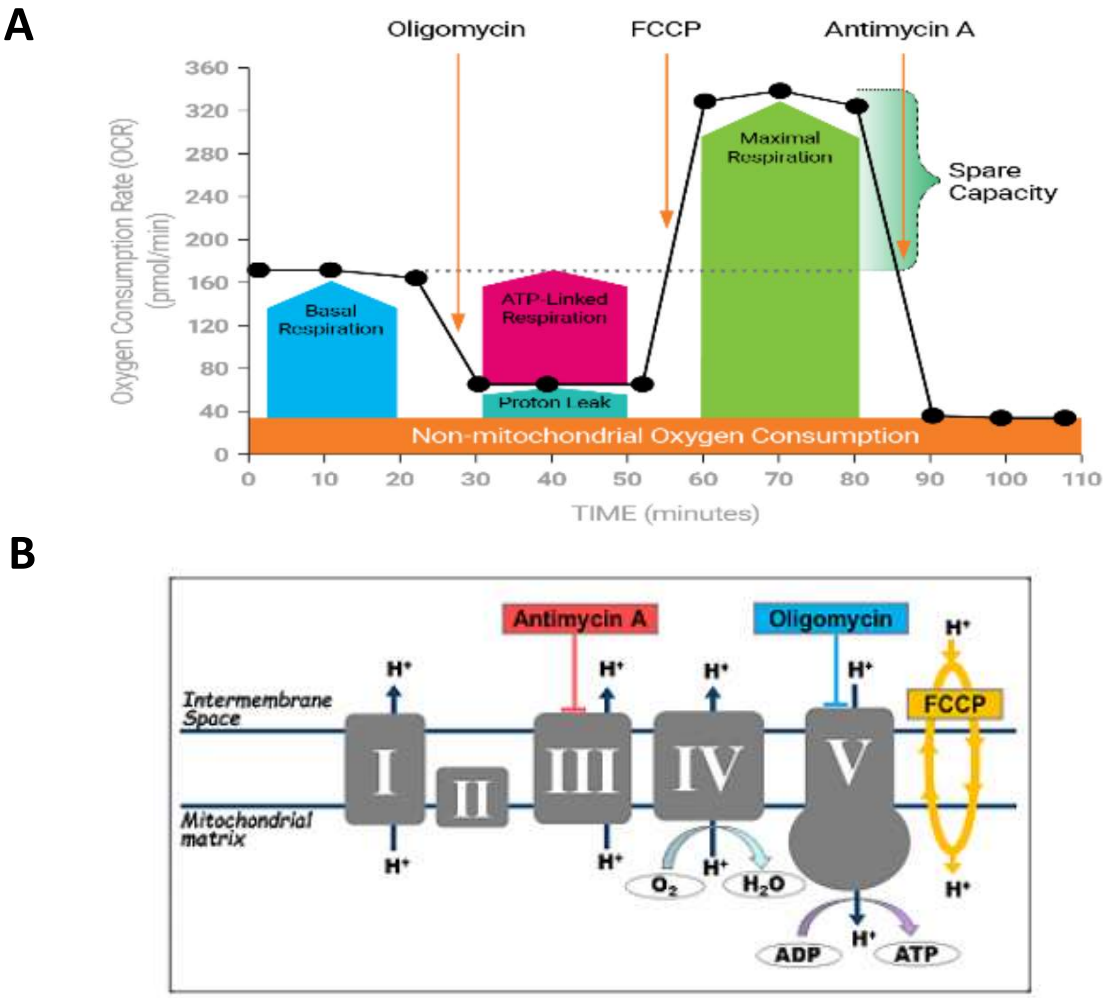

Figure 4.5: (A) Visual representation of the sequence of injection and effect of stimulants and inhibitors on mitochondrial respiration *(oxygen consumption rate). Image modified from Agilent Technologies Seahorse User Guide [498]. (B) Visual representation of the Electron Transport Chain within the mitochondria and targets of the mitochondrial stimulants/inhibitors used in the Seahorse mitochondrial function assay. Image modified from Agilent Technologies [498].*

4.2.2.6 Statistical analysis

Statistical analysis was performed on Graphpad Prism 7 software. One-way analysis of variance (ANOVA) with Tukey's post hoc test was used to assess statistical differences at specific time-point measures; such as grip strength, muscle contractile and mitochondrial parameters. Repeated measures ANOVA with Tukey's post hoc test was used to assess statistical differences in longitudinal data sets; such as changes in day-by-day body weight and food intake, muscle fatigue and recovery data sets and longitudinal μ-CT analysis of muscle volume. An α value of 0.05 was considered statistically significant. Data is presented as mean ± standard deviation (unless otherwise stated). IPGTT and survival rate measures were analysed using a two-way ANOVA. Geisser-Greenhouse correction and Sidak's multiple comparison test were used post-hoc for IPGTT analysis, and the Log-rank (Mantel-Cox) test and Gehan-Breslow-Wilcoxon tests were used post-hoc for survival rate analysis. All tests were performed using GraphPad Prism (V8.4.3).

4.3 Results

4.3.1 MB-LCV therapy has no adverse effects on survival

Survival and 5-year event-free-survival rates are often used as key indicators of a chemotherapy regimens success against a cancer [338-341,532,533]. Here, survival rates were determined as a measure of toxicity and lethality which can be solely attributed to the chemotherapy. Of the 34 mice that received the MB-LCV regimen, 100% survived the duration of the regimen and all survived through to 30-weeks of life (Figure 4.6). One lethal idiopathic incident was recorded in the VEH treated group. Blinded necropsies (Cerberus Laboratory Animal Diagnostics, Melbourne, Australia) returned no significant histopathological or clinical findings in the 12-week MB-LCV treated mice. Interestingly, three of the five 30-week-old MB-LCV treated mice, presented with moderate-high neutrophil counts and two of the five presented with mild multifocal interstitial lymphoplasmacytic infiltrate and scattered cortical basophilic tubules within the kidneys (suggestive of regenerative change; see Table 4.8). A well-circumscribed, subcutaneous haemorrhage in the right axilla and lateral flank adipose tissue of one of the 30-week mice was also described; however, this was thought to be acute in nature and idiopathic. No other remarkable findings were described for this group.

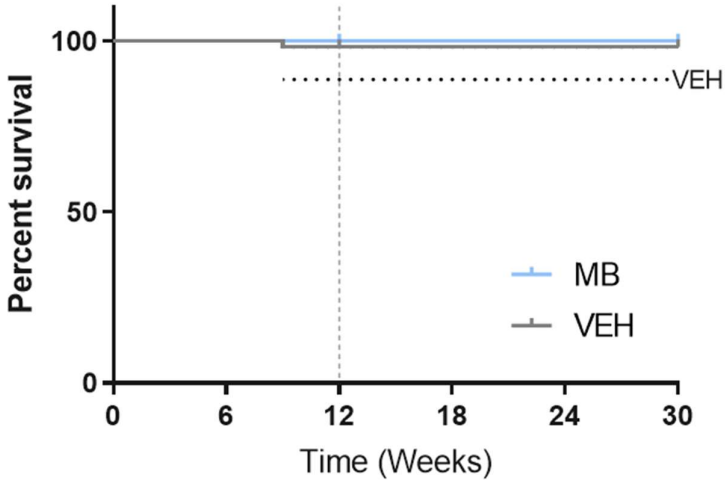

Figure 4.6: MB-LCV therapy survival over 30-week chemotherapy administration was unchanged from VEH. *VEH n = 60 <12 weeks, n = 25 >12weeks with one death in week 9 (and resultant error line denoted by VEH). MB-LCV n = 34 <12 weeks, n = 20 >12 weeks with no recorded deaths. Non-survival event recorded as either ethical euthanasia or natural death.*

Table 4.8: Pathological observations of VEH (V), MB-LCV (MB), treated mice during necropsy at 12 and 30 weeks of age. *Abbreviations: RV: Right ventricle, S: Intraventricular septum, LV: Left ventricle, GIT: gastrointestinal tract, +: pathology observed.*

Treatment group	Mouse	Pathology observed												
		Cachectic appearance	Perianal faecal staining	Ascites	Multifocal interstitial lymphoplasmacy	RV:S:LV	Thinning & dilation of RV myocardium	RV Myocardial inflammation	Cholangitis	Hepatosteatosis	Hepatocellular swelling	Renal hydronephrosis	Basophilic renal tubules	GIT inflammation
V12	1					1:6:6	+				+			
	2					1:6:5	+				+			
	3					1:4:4			+		+			
	4					1:4:4					+			
	5					1:5:5					+			
MB12	1					1:6:4			+		+		+	
	2					1:4:4					+		+	
	3				+	1:6:6			+		+			
	4					1:5:5					+			
V30	1					1:5:5					+			
	2					1:4:5			+					
	3					1:3:4								
	4					1:3:4								
MB30	1					1:3:4								
	2				+	1:3:4		+					+	
	3					1:4:3								
	4					1:3:3								
	5				+	1:3:2.5							+	

4.3.2 MB-LCV therapy induces acute but not chronic weight loss

Weight loss occurred immediately upon commencement of treatment with MB-LCV therapy with a significant difference in weight gain from day two through day 20, likely as a result of CCNU and/or CDDP therapy-induced weight loss (see Figure 4.7). MB-LCV treated mice were 6-18% lighter during this period when compared to VEH highlighting a failure to thrive even though weight-gain was noted (p<0.05). Although mice recovered by D21, weight-loss was again observed after the second administration of CCNU and CCP on days 29 and 30 which was not recovered until day 42 (MB-LCV mice were 8-17% lighter on average through this period). From then on, there was no discernible difference between the MB-LCV and the VEH treated groups.

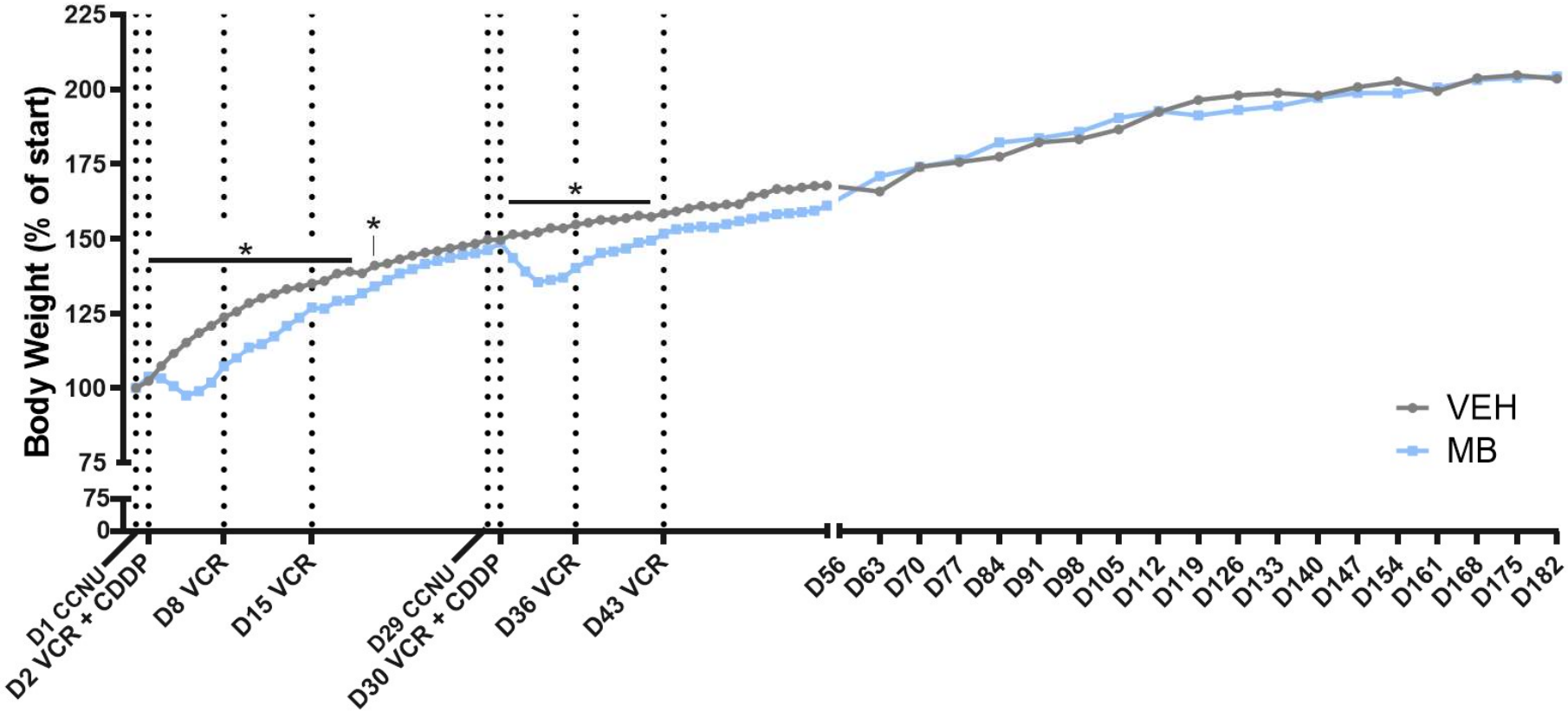

Figure 4.7: Weight measurements of VEH and MB-LCV treated mice over 8 weeks of regimen administration: *CDDP and or CNNU therapy induced acute weight-loss over 3-4 days post treatment (D2) which took 20 days to recover. A similar 3-4-day weight loss occurred at D30. VEH n = 60 <12 weeks, n = 25 >12weeks. MB-LCV n = 34 <12 weeks, n = 20 >12 weeks (n excludes deaths), Error not shown for ease of viewing. Significance symbols: *:p<0.05*

MB-LCV treated mice tended to consume less food during the first 9 days of treatment (~20%; Figure 4.8), and then again during the first few days following administration of the second chemotherapy cycle (~10%; Figure 4.8) when compared to VEH, suggesting that mice experienced nausea which was induced by either CCNU and/or CDDP. Interestingly, MB-LCV treated mice tended to increase food intake for close to 7 days after the second decline in food intake by approximately 20%, essentially negating the preceding decline in intake. Overall, total food consumption over the lifespan was comparable between VEH and MB-LCV groups, with MB-LCV treated mice consuming less food during periods and more food immediately after periods of active chemotherapy.

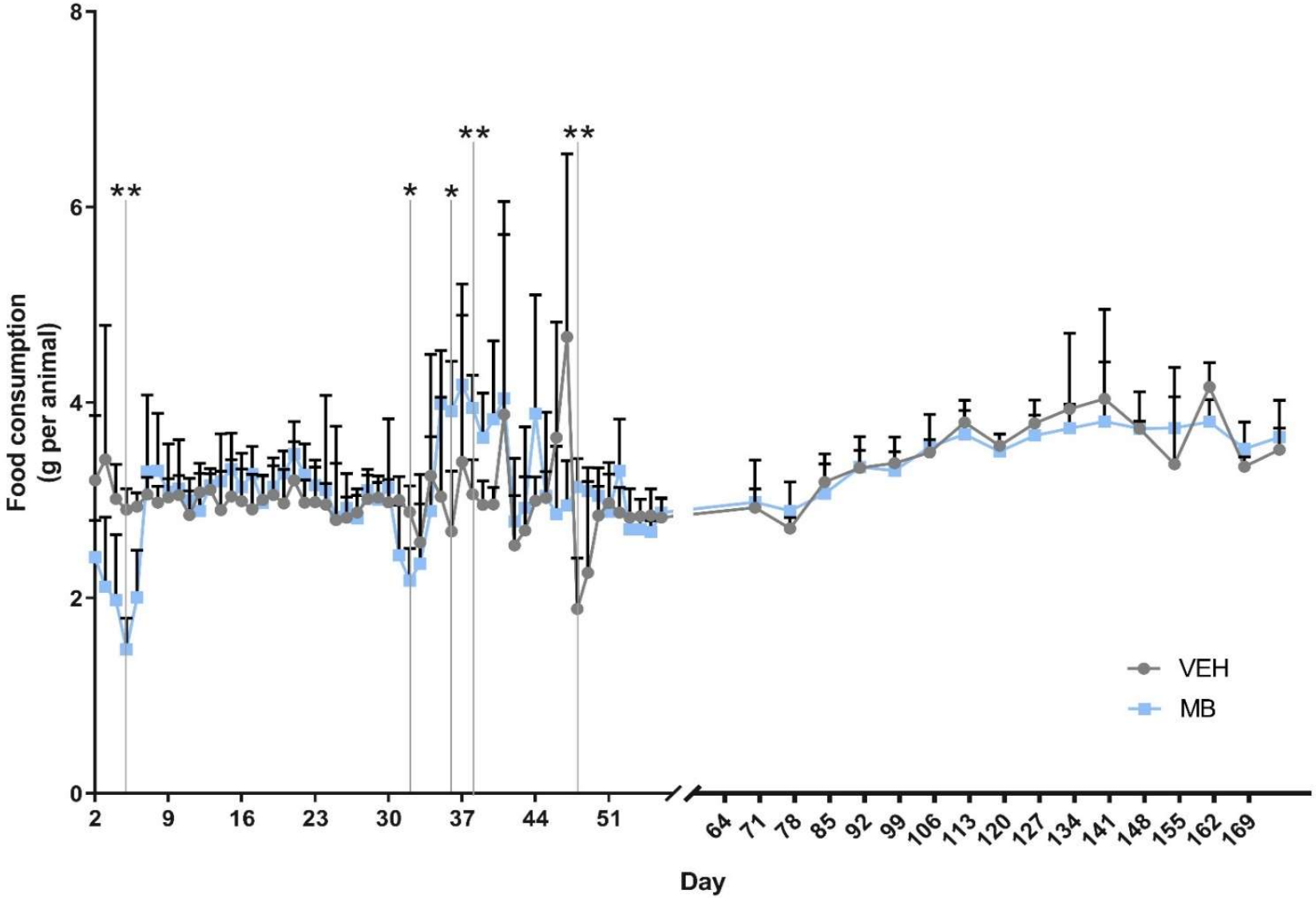

Figure 4.8: Food consumption of VEH vs MB-LCV treated mice over the life span shows no discernible difference: *Total food consumption per cage was normalised for animal number thus values are derived approximates per animal only. Food consumption dropped in MB-LCV treated mice post CDDP and CCNU treatment (day 1,2, 29, 30). n=7-13 cages. Significance symbols: *:p<0.05, **p<0.005, ***p<0.001, ****:p<0.0001.*

4.3.3 Effect of MB-LCV therapy on muscle and organ weight

Body weight and absolute organ weights at the two sampling time points are shown in Table 4.9. As there were no significant differences in body weight between the MB-LCV treated and VEH groups at 12 or 30 weeks, relative organ weights are displayed in Figure 4.9. After correcting for bodyweight, the SOL muscle was observed to increase by 42.5% at 12 weeks of age before returning to VEH levels (p<0.0001, Figure 4.9). MB-LCV therapy tended to suppress mean cardiac weight at 8-weeks by 7.5% (p=0.0629). Splenomegaly was observed in MB-LCV treated mice at 30 weeks of age (an increase in spleen weight of 19%, p<0.05) however this manifestation was not observed at the 12-week timepoint. Aside from a trend for MB-LCV therapy to reduce heart/bodyweight ratio at 12-weeks (-7%, p<0.0629), no other significant changes in organ weights were observed in bodyweight corrected changes in mass.

Table 4.9: Absolute average bodyweight and muscle weight values from VEH (V) and MB-LCV (MB) treated mice at both 12 and 30 weeks of age. Data expressed in grams.

			EDL		SOL		TA		PLA		QUAD	
	Av. BW	*SD*	*Mean*	*SD*	*Mean*	*SD*	*Mean*	*SD*	*Mean*	*SD*	*Mean*	*SD*
V12	26.80	1.43	0.010	0.002	0.012	0.002	0.043	0.004	0.016	0.002	0.130	0.042
MB12	27.19	1.26	0.012	0.001	0.016	0.002	0.048	0.003	0.015	0.003	0.158	0.014
V30	32.95	1.52	0.013	0.002	0.014	0.003	0.054	0.004	0.020	0.004	0.223	0.039
MB30	33.09	1.52	0.014	0.003	0.014	0.004	0.055	0.007	0.023	0.003	0.221	0.023

			HEART		KIDNEY		SPLEEN		LIVER	
	Av. BW	*SD*	*Mean*	*SD*	*Mean*	*SD*	*Mean*	*SD*	*Mean*	*SD*
V12	26.80	1.43	0.125	0.011	0.154	0.020	0.101	0.006	1.147	0.153
MB12	27.19	1.26	0.124	0.006	0.175	0.016	0.119	0.025	1.352	0.127
V30	32.95	1.52	0.174	0.011	0.259	0.019	0.123	0.023	1.489	0.171
MB30	33.09	1.52	0.179	0.012	0.258	0.042	0.146	0.017	1.603	0.168

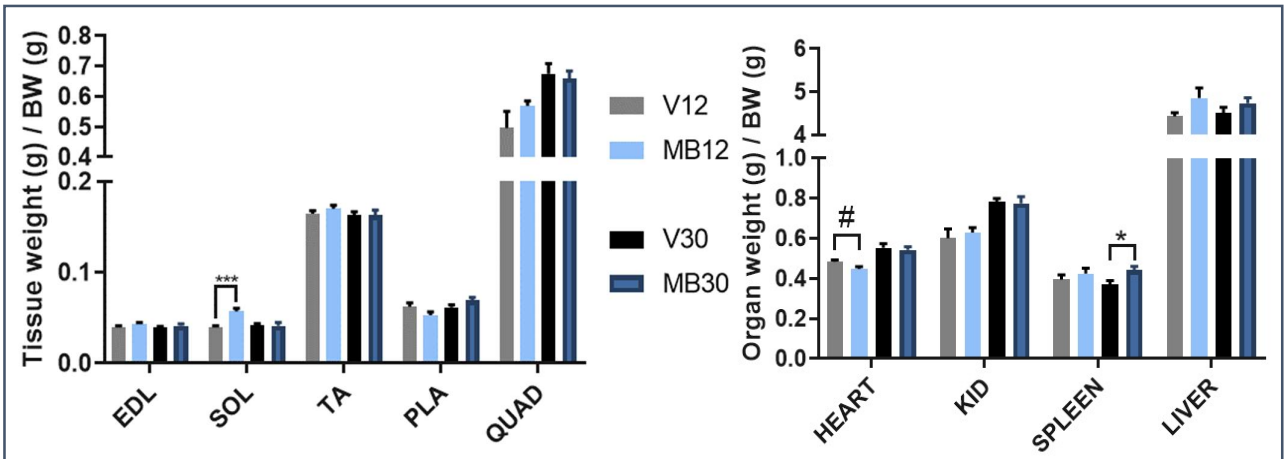

Figure 4.9: Organ and tissue wet weight changes (corrected for animal body weight in g/g) in Vehicle (V) and MB-LCV (MB) treated mice as of 12 and 30 weeks of age *Muscle and organ wet weight post excision during necropsy shows acute cardiac myopathy but chronic splenomegaly. Data corrected for bodyweight of mouse at time of necropsy and is expressed as wet weight of tissue over the mouse's body weight (g/g). n= 4-11. Abbreviations: EDL: Extensor digitorum longus m., SOL: Soleus m., TA: Tibialis Anterior m., PLA: Plantaris m., QUAD: Quadriceps complex. Significance via ANOVA with Tukey's post hoc, where #: p=0.0629 and *:p<0.05, **p<0.005, ***p<0.001,*

4.3.4 Micro-computed tomography analysis of the effect of MB-LCV therapy on hind-limb muscle mass

A hallmark of cancer and chemotherapy is the cachectic phenotype where loss of weight is characteristic. By investigating skeletal muscle mass in chemotherapy treated mice without cancer, an understanding of the underlying cause – whether it be cancer, chemotherapy or both – can be achieved. Using micro-computed tomography, we calculated the volume of cross-sections at the proximal 1/3 of the right lower hind limb. There was no effect of the MB-LCV chemotherapy regimen at either 12 or 30 weeks of age (Figure 4.10). This was not all together surprising considering no overall weight-loss was measured in MB-LCV treated mice as compared to VEH.

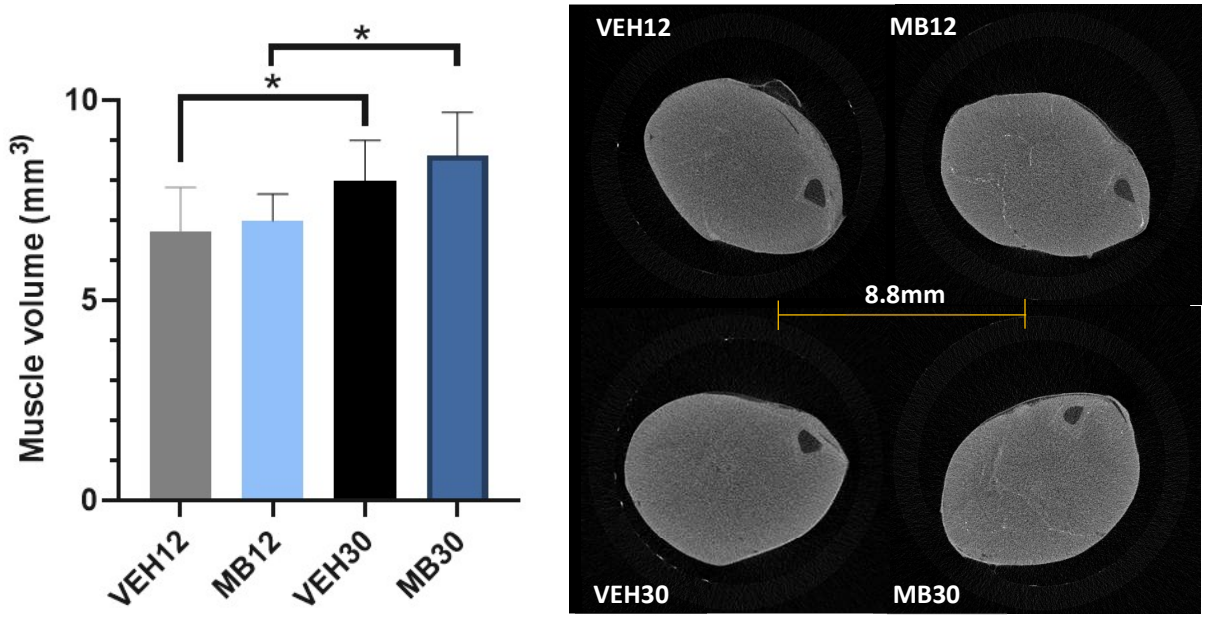

Figure 4.10: Hind-limb volume as measured by µ-CT imaging of at the proximal 1/3 of the tibia in VEH (V) and MB-LCV (MB) treated mice at 12 and 30 weeks of age. *MB-LCV therapy did not impact hind limb volume in the lower limb at either 12 or 30-weeks of age. Representative images supplied. n=6-9 assessed by 2-way ANOVA with Tukey's post-hoc test with error expressed as SD. Significance symbols: *:p<0.05*

4.3.5 The effect of MB-LCV therapy on haematological parameters

Thrombophilia was evident at the 12-week (post therapy) time point (VEH: 1167 ±112.99, MB: 1497.33 ±44.24, $p<0.05$) together with monocytophilia (VEH 0.02 ±0.045, MB-LCV 0.11 ±0.02, $p<0.05$). However, no change in circulating neutrophils (either segmented or lobular) or lymphocytes were noted, suggesting a state of acute inflammation. All other measures were unchanged from VEH. At 18 weeks post therapy (30 weeks of age), platelet and monocyte levels had normalised (compared to VEH), however, elevated levels of circulating segmented neutrophils (and thus an elevated total circulating white cell count as well as elevated total protein level) were observed. It should be noted that total elevated protein may be due to other proteins which were not able to be measured due to low sample volume.

Table 4.10: Haematological (count and smear) and biochemical investigations for the effect of MB-LCV therapy on mice. *Data expressed as difference between MB-LCV mean and VEH mean (with treatment group SD). Significance values >0.1 apply where values not reported. UA: Unavailable due to low sample blood levels. $: often expressed together with globulin levels, globulin level measurement was UA. n=3-5.*

Measure	ΔM12	±SD	*p value*	ΔMB30	±SD	Sig (*p*)
Red cell count ***(x10^{12}/L)***	+0.697	1.142		+0.743	1.894	
Haematocrit ***(L/L)***	+4.450	5.852		-2.000	5.252	
Haemoglobin ***(g/L)***	+10.050	19.856		-3.500	23.274	
Mean corpuscular volume ***(fl)***	+1.550	0.500		-5.000	3.000	<0.05
Mean corpuscular haemoglobin (MCH) ***(pg)***	-0.200	0.000		-1.500	0.577	
MCH concentration ***(g/L)***	-8.050	4.573		+4.250	14.900	
*Platelet count****(x10^{9}/L)***	+330.333	44.242	<0.005	-20.417	73.786	
Total white cell count ***(x10^{9}/L)***	+0.935	1.729		+2.750	1.587	<0.1
Segmented neutrophils ***(x10^{9}/L)***	-0.075	0.222		+0.650	0.512	<0.1
*Total lymphocyte count****(x10^{9}/L)***	+1.030	1.515		+2.025	1.493	
Monocyte count ***(x10^{9}/L)***	+0.09	0.02	<0.05	+0	0.05	
Total Protein ***(g/L)***	+2.917	4.933		-3.000	2.363	<0.1
Albumin ***(g/L) ($ see figure note)***	+2.867	3.512		-2.500	1.708	
Urea ***(mmol/L)***	+1.808	2.831		-0.342	0.714	
ALT	+0.083	27.154		UA	UA	UA
AST ***(mmol/L)***	+34.750	138.667		+25.750	29.848	
Creatine Kinase ***(mmol/L)***	+73.533	154.940		+130.000	166.649	

4.3.6 The effect of MB-LCV therapy on *in vivo* grip strength analysis

Mice were assessed for grip strength at 8, 12 and 30 weeks of age (which aligns with the end of course 1, course 2 and the treatment regimen, respectively; Figure 4.11). Surprisingly, no changes in grip strength at 8- or 12-weeks was noted, however, a decline of close to 40% in grip strength was observed at 30 weeks of age (Figure 4.11, $p<0.05$). As no change in grip-strength was observed during active chemotherapy (from 4-12 weeks of age), this data suggests that, despite an increase in muscle volume observed with µCT, the detrimental effect induced by MB-LCV therapy requires time to manifest, resulting in larger but dysfunctional muscle.

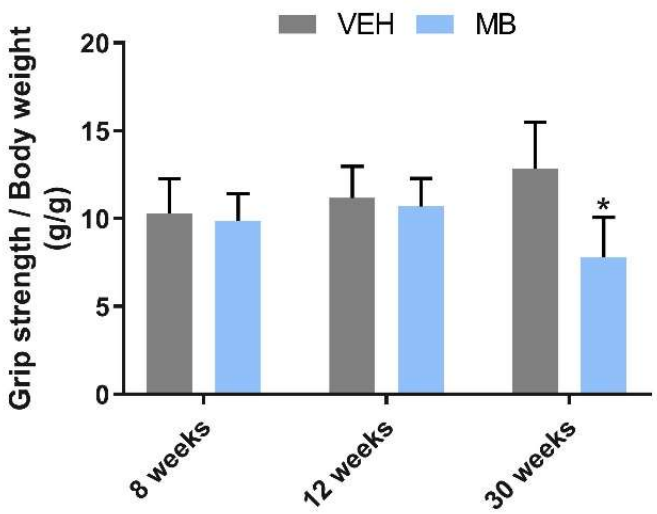

Figure 4.11: Maximal grip strength reduced by MB-LCV at 30-weeks of age but not during active chemotherapy. *No significant changes were noted at 8 and 12 weeks of life, or, at the end of course 1 or course 2 of the MB-LCV regimen. After 18 weeks of no treatment, grip strength was suppressed by 39.8% in previously MB-LCV treated mice as compared to VEH (p<0.05). n=15-20 Significance in assessed by student's t-test with error expressed as SD. Significance symbols: *:p<0.05*

4.3.7 Analysis of MB-LCV treatment effect on contractile function

4.3.7.1 Contractile properties

Muscle functional parameters were assessed in EDL and SOL muscle fibres which were harvested from tendon to tendon from 12- and 30-week mice. These muscles were selected due to their predominant expression of fast-twitch Type II and slow-twitch Type I fibres, respectively. Although 12-week MB-LCV treated EDL m. and SOL m. were ~14% and ~20% larger in CSA, respectively (p<0.05, Figure 4.12A-D) than vehicle, no other remarkable changes in CSA or L_o were noted. Interestingly, the peak twitch contractional force (P_t) relative to maximal tetanic force (P_o) ratio, or P_t/P_o, was lowered by almost 40% in the EDL of 30-week old MB-LCV treated mice (p<0.005, Figure 4.12E). At this point, and after establishing a force-frequency relationship, the maximal absolute (or raw) force and specific force (force corrected for muscle CSA) was established during force-frequency analysis (Figure 4.13). Both the absolute and specific forces of EDL and SOL muscles were significantly reduced at 30-weeks of age following MB-LCV therapy in both EDL and SOL muscle (Figure 4.13). These data suggest MB-LCV-induced changes (structural, functional or both) to the contractile apparatus itself, since similar declines were observed between absolute and CSA-corrected force values.

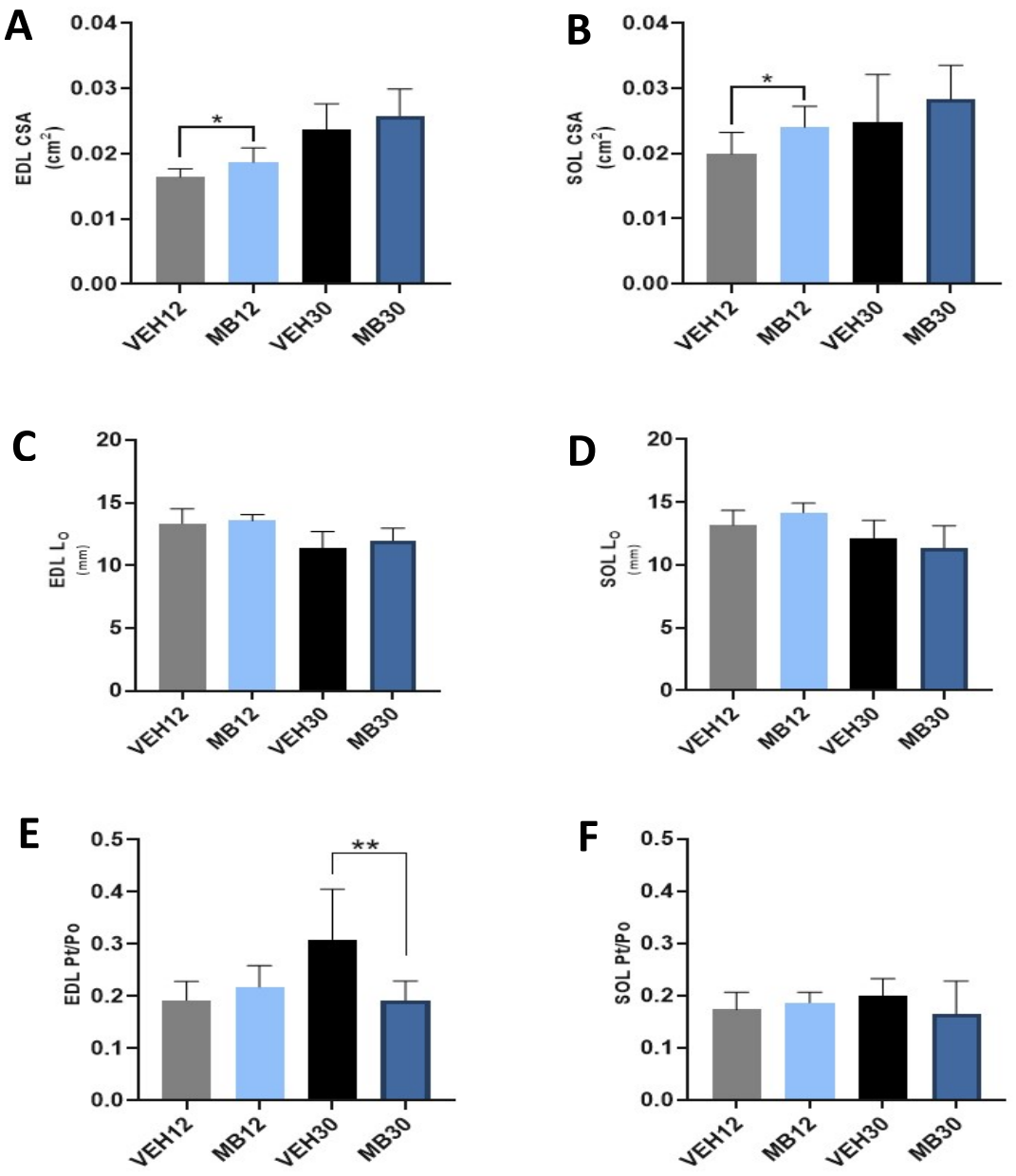

Figure 4.12: Cross-sectional area (CSA), optimal length (L_o) and peak twitch to tetanic ratio (P_t/P_o) of the fast-twitch extensor digitorum longus (EDL) and slow-twitch soleus (SOL) muscles of vehicle (VEH) and MB-LCV (MB) treated mice at 12 and 30 weeks of age. *MB-LCV therapy increased CSA at 12 weeks by 13.8% and 20.6% in EDL m. and SOL m. respectively ($p<0.05$) but showed no effect at 30 weeks or on the SOL muscle (A & B). No effect of treatment on L_o measures were noted in either muscle or time group (C & D). P_t/P_o was supressed by 38% at 30-weeks in MB-LCV treated mice, though treatment elicited no changes at 12 weeks in EDL or any changes in SOL muscle (E & F). n=4-10 assessed by ANOVA with Tukey's post-hoc test with error expressed as SD. Significance symbols: *:$p<0.05$, **$p<0.005$*

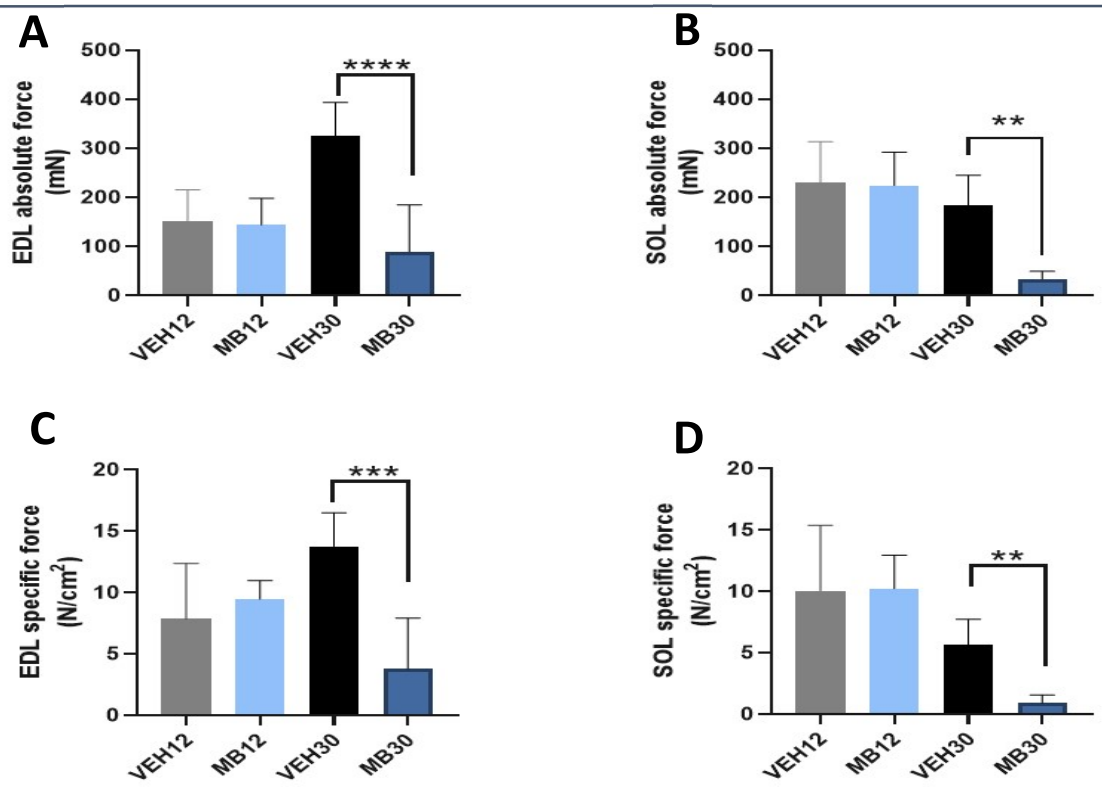

Figure 4.13: Absolute and specific force production of the fast-twitch extensor digitorum longus (EDL) and slow-twitch soleus (SOL) muscles from vehicle (VEH) and MB-LCV (MB) treated mice at 12- and 30-weeks of age. *No changes to absolute force were seen with MB-LCV treatment at 12 weeks of age in either EDL or SOL muscle, however marked reductions of 82.5% (p<0.0001) and 81.2% (p<0.005) at 30-weeks in EDL and SOL muscle respectively (A & B). A similar decline was seen in specific force with MB-LCV treatment causing a 72.5% (p<0.001) and an 83.8% (p<0.005) reduction in EDL and SOL muscle respectively (C & D). n=4-10 assessed by ANOVA with Tukey's post-hoc test with error expressed as SD. Significance symbols: *:p<0.05, **p<0.005, ***p<0.001, ****:p<0.0001.*

4.3.7.2 Force-frequency relationship

To establish the force-frequency relationship, muscles were stimulated at increasing frequencies and peak force was measured at each frequency. Data are presented as absolute force vs frequency, and, as the percentage of maximum force vs frequency in Figure 4.14. At 12 weeks of age, there was no effect of treatment on either the force produced or the force-frequency relationship in either the EDL or SOL muscle (Figure 4.14, A-D). At 30 weeks of age, however, EDL muscle treated with the MB-LCV regimen produced ~75% less force at all frequencies (p<0.001 10-30Hz, p<0.0001 50-100Hz, p<0.001 120Hz, p=0.063 150Hz, Figure 4.14E). A similar result was observed in 30 week SOL muscle which consistently produced ~80% less force than VEH treated muscle (Figure 4.14D). The force-frequency relationship shifted to the right in 30 week old MB-LCV treated EDL muscle (significant differences were noted at 30Hz, 50Hz, and 80Hz, Figure 4.14E). Interestingly, these findings were not seen in SOL muscle which maintained a comparable force-frequency relationship to VEH treated SOL muscle (Figure 4.14F). These data highlight specific effects on fast-twitch type II skeletal muscle fibres which may indicate an even faster muscle phenotype (due to less summation at lower frequencies), or a reduced sensitivity to calcium (as less force was observed at submaximal levels).

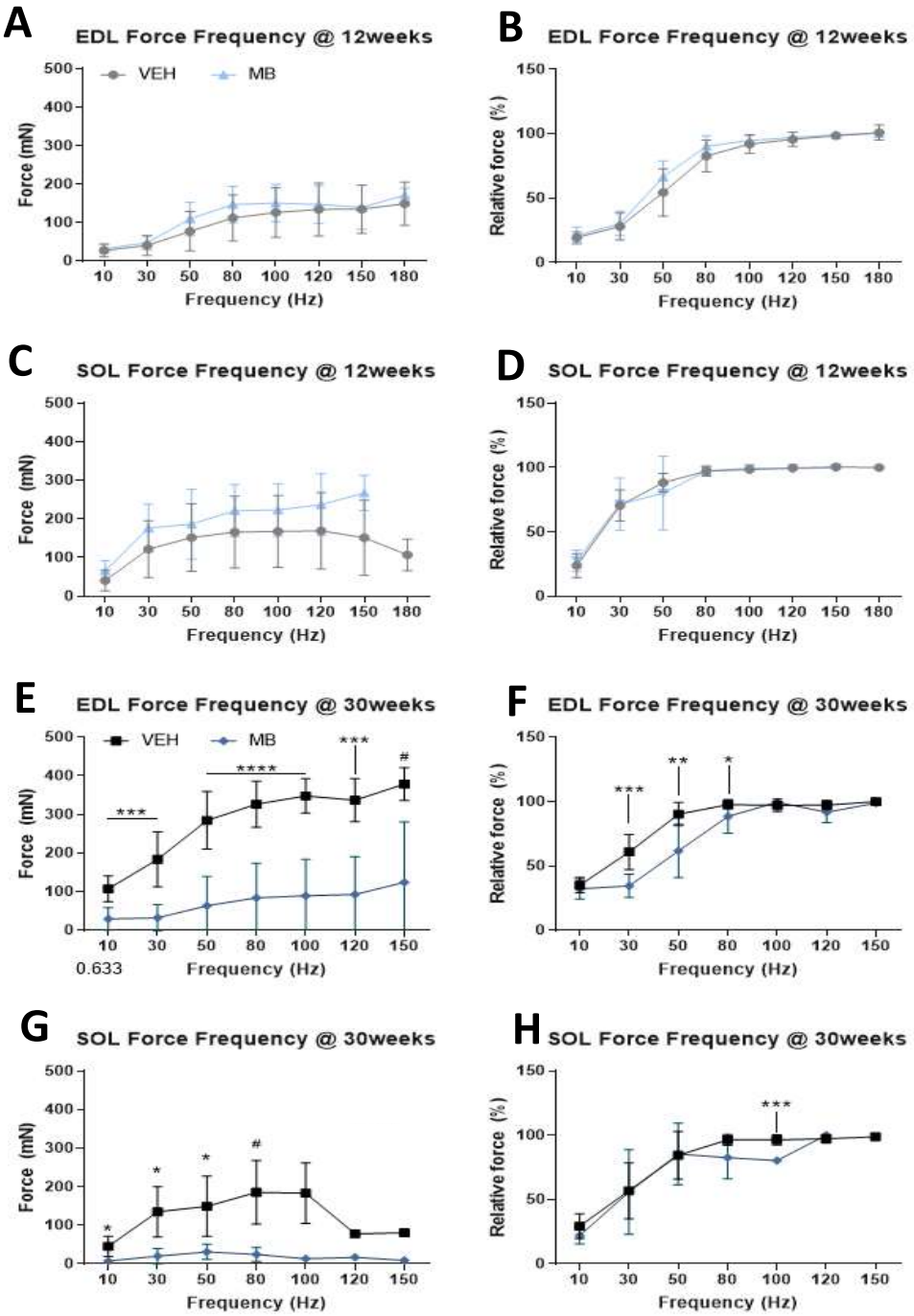

Figure 4.14: Effect of MB-LCV therapy on absolute and relative force frequency relationship in fast-twitch extensor digitorum longus (EDL) and slow-twitch soleus (SOL) muscles from vehicle (V) and MB-LCV (MB) treated mice at 12- and 30-weeks of age. *Muscle stimulation was of 500ms in tetanic length with consecutive 0.2ms pulses at 10, 30, 50, 80, 100, 120 and 150 Hz. There was no statistically significant treatment effect on EDL and SOL muscles at 12 weeks of age (VEH n=13 & 10 and MB-LCV n=9 & 10 for EDL and SOL respectively, A through D). However, the effect of treatment was pronounced after 30 weeks of age, with raw forces at all frequencies considerably supressed by over 4-fold (p<0.0001- #: p=0.063, Figure E). The force-frequency relationship was also significantly suppressed between 30-80Hz in treated EDL muscle (F). MB-LCV treated SOL muscle at this time point produced considerably less absolute force at all levels although the force-frequency relationship was not altered aside from at the 100Hz level (#: p=0.061, G & H).*

*n=10 & 15 for V30 EDL and SOL muscles respectively and n=7 & 4 for M30 EDL and SOL muscles respectively. Of note only one MB-LCV sample and one VEH treated SOL produced forces above 80Hz and 100Hz respectively at 30 weeks. Relative forces presented were normalised to the greatest force produced for that muscle and data presented as mean ± STD. Significance assessed by ANOVA with Tukey's post-hoc test with error expressed as SD. Significance symbols: *:p<0.05, **p<0.005, ***p<0.001, ****:p<0.0001.*

4.3.7.3 Fatigue properties

To conclude analysis of muscle contractile function, fatiguability was assessed by continuously stimulating EDL and SOL muscles for three minutes. Muscles were then allowed to recover, whilst intermittently being stimulated to assess recovery capacity. No changes in fatiguability or recovery parameters were observed at the 12-week time point in either EDL or SOL muscle. Fatigability was not affected by treatment at 30 weeks of age in EDL muscle, albeit the absolute forces were very low throughout due to lower tetanic force produced in this group. Interestingly, after initial typical recovery, a marked decline in function occurred after 5min of recovery. EDL muscle force production steeply declined by 47% at 10min ($p<0.05$) and continued to decline until almost no force was produced (5.5% of initial force was produced by MB-LCV treated EDL muscle at 60min of recovery, which was only 6.6% of VEH at the same time point; $p<0.001$). Remarkably, the 30w old MB-LCV-treated SOL muscles could not withstand the fatigue/recovery protocol – all either tore or failed to respond at some point during the fatigue-induction protocol.

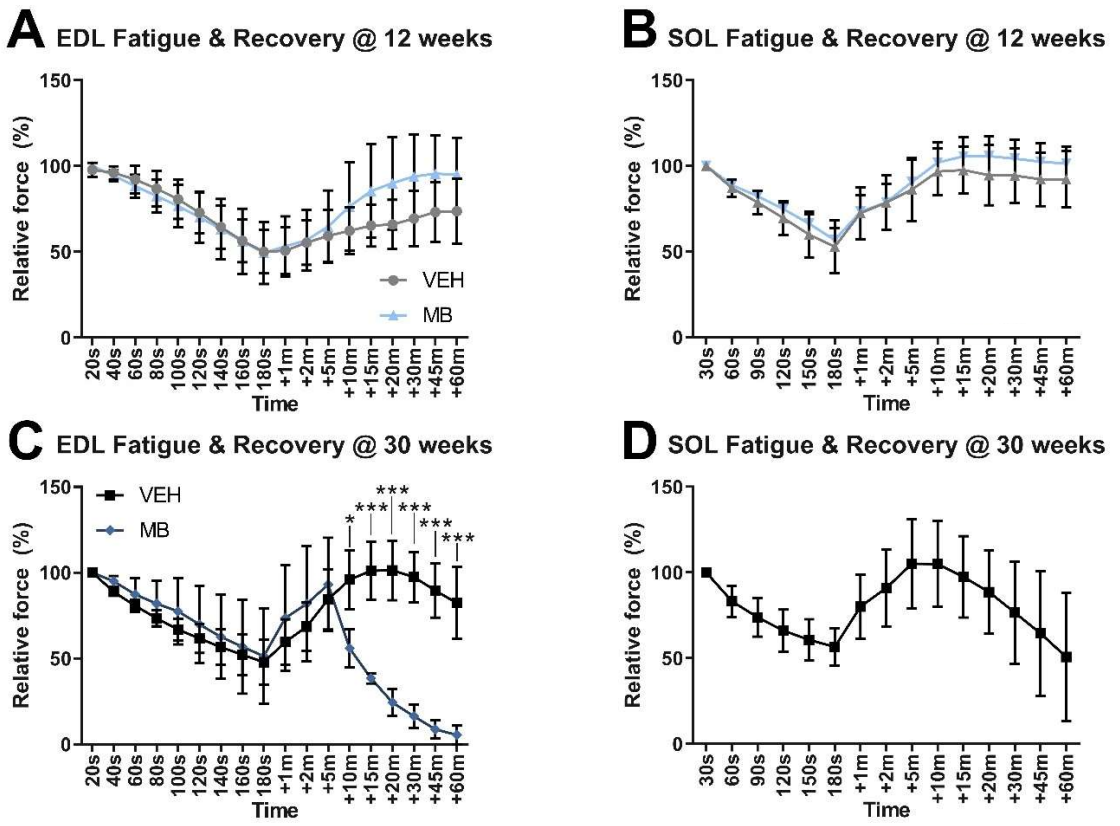

Figure 4.15: Effect of childhood MB-LCV therapy on young and aged EDL and SOL muscle endurance and recovery: No significant differences were noted in endurance (fatiguability) performance in any group. **A+B:** Recovery was improved in MB-LCV treated 12 week old mice in both EDL and SOL (EDL: p=0.0006 n=(VEH=6, MB=5), SOL: p=0.0157 n=(VEH=11, MB=7)). **C**: EDL muscle from 30 Week-old mice failed to recover from the endurance bout (total force produced during recovery: p<0.0001 n=(VEH=7, MB=3, significant difference between time points shown, significance via unpaired t-test). No SOL muscle assessed was able to complete the fatigue protocol (n=(VEH=7). Data points are of the average force produced between time points and expressed as the relative force as compared to the first time point ±SD, significance of area under curve and individual points via unpaired t-test. *Significance symbols: *:p<0.05, **p<0.005, ***p<0.001*

4.3.8 Histological effects of MB-LCV therapy on *Tibialis Anterior* muscle.

With chemotherapy-induced muscle dysfunction established as a clear characteristic of MB-LCV therapy, investigations into the underlying histopathology were performed. Using a standard H&E stain, TA muscle fibres from each treatment and age group were assessed for mean fibre area and a frequency distribution of fibre size was created. No significant difference in the average fibre size or distribution were observed between 12-week VEH and MB-LCV or 30-week VEH and MB-LCV treatment groups.

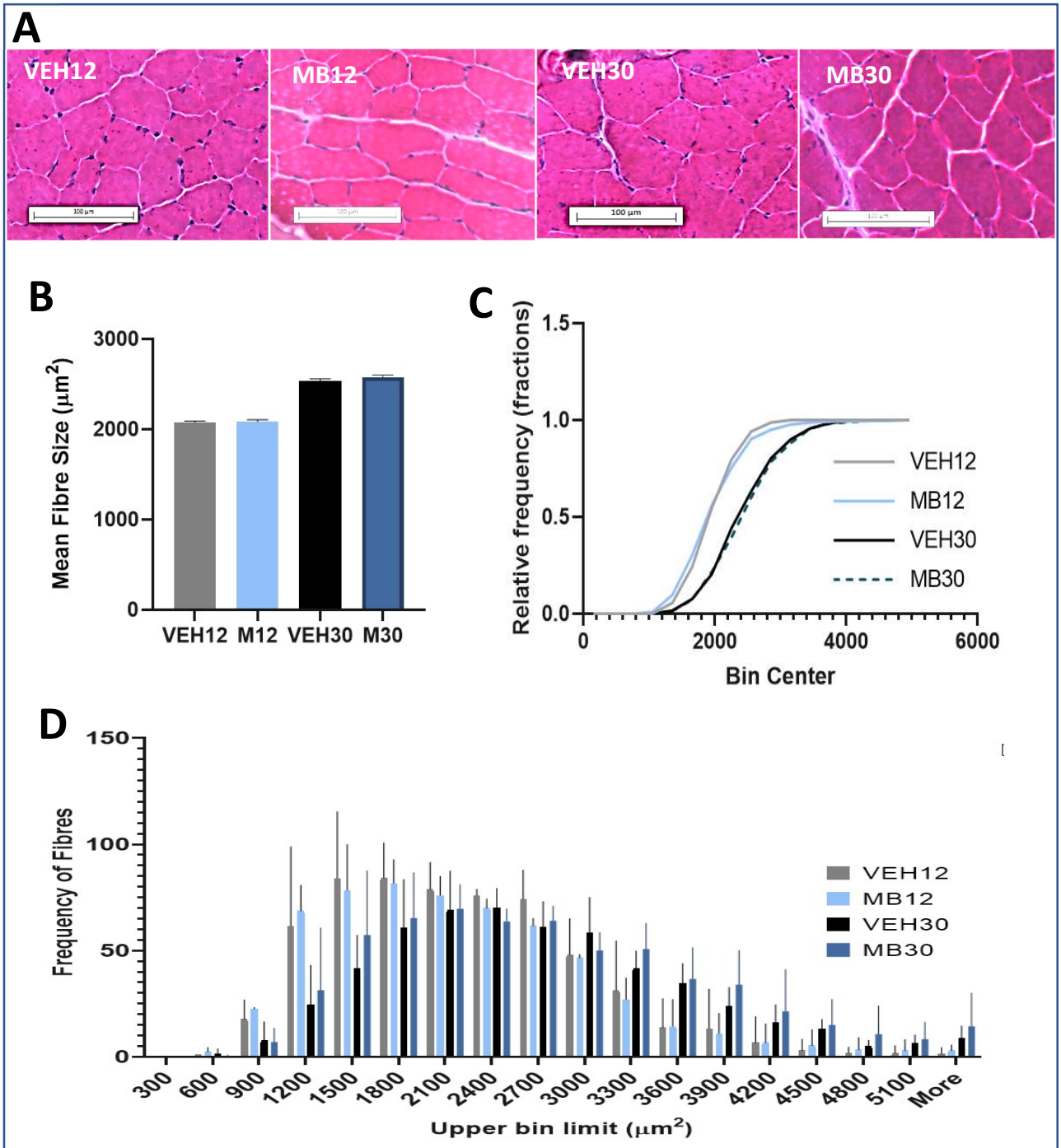

Figure 4.16: Mean fibre size and fibre size frequency in Tibialis Anterior (TA) muscles of vehicle (VEH) and MB-LCV (MB) treated mice at 12 and 30 weeks of age. A) *Representative images of H&E stained TA muscle B) Mean fibre size of VEH and MB-LCV treated TA muscle showed no change in response to treatment (n=~2400 fibres per group, data presented as mean±SD)* ***C)*** *Data presented as the cumulative fraction of fibre distribution with error removed for ease of viewing.* ***D)*** *Relative fibre size frequency histogram showing MB-LCV treatment having no significant effect on fibre size frequency. n=4-5 with ~600 fibres per n with data presented as mean±SD. Significance via ANOVA Tukey's post-hoc for panels B and C and 2-way ANOVA with Tukey's post-hoc for panel D. No statistical differences between V12 and MB12 or V30 and MB30 were found.*

4.3.9 MB-LCV chemotherapy improves long-term glucose handling

Baseline glucose levels after fasting is universally accepted as a measure of endogenous glucose production as no glucose has been consumed during fasting (6 hours of fasting was used here).[534-538] After an initial glucose bolus is adminsitered, how quickly the organism takes up the glucose from the blood stream is indicative of glucose handling (or, cellular uptake).[536,537,539] These measures are important here as we hypothesise that chemotherapy inadvertantly targets the mitochondria, thus altering cellular energy homeostasis and consequently glucose handling.

Glucose tolerance testing as performed at 8 (during treatment), 12 (at the end of treatment) and 30 weeks (18 weeks post treatment) of age was conducted, here, on VEH and MB-LCV treated mice (Figure 4.17). As expected, blood glucose levels in all mice spiked within 15 minutes of initial glucose injection before declining over the next 1 hour and 45 minutes. Endogenous glucose production and usage rates were well regulated (t0) and there was no difference between the groups at any other time point. An exception to this observation was at 5 minutes for the 8 week old animals (Figure 4.17). At this point, plasma glucose levels in MB-LCV treated mice were 17% lower, however, this decrease was short lived and glucose levels returned to VEH by the next time point with no other changes noted (VEH = 12.0, MB-LCV = 10.2; *p<0.005).* At 30 weeks of age, MB-LCV mice showed significantly improved glucose handling at 15 and 30 minute time points (15min: VEH=14.1, MB-LCV=12.4, 30min: VEH= 10.5, MB-LCV = 8.9) but this normalised by 45 minutes and was comparable to VEH for the remainder of the assay. Collectively, these data suggest that MB-LCV therapy alters early

glucose handling, especially by 30-weeks of age, by increasing the rate of cellular glucose uptake.

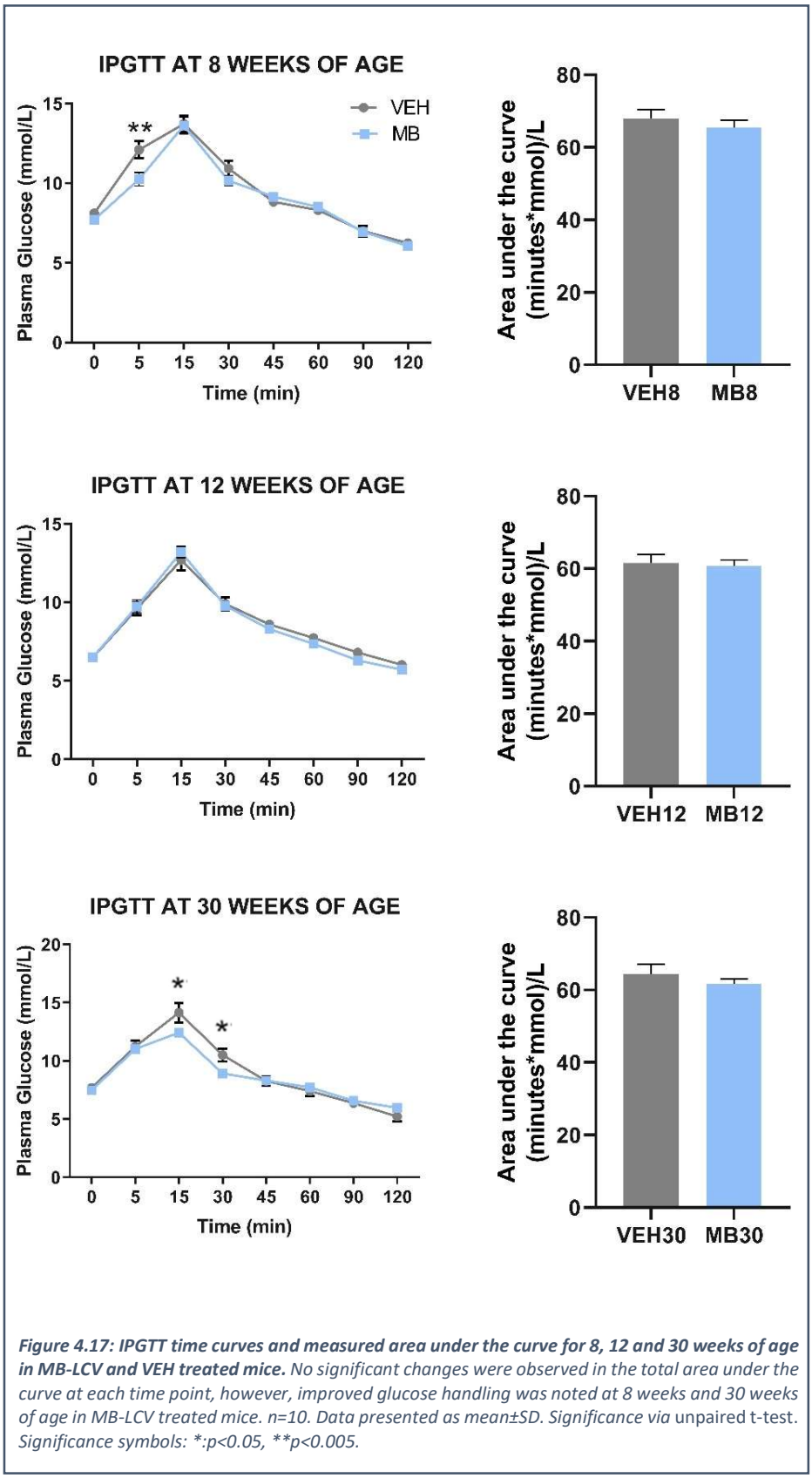

Figure 4.17: IPGTT time curves and measured area under the curve for 8, 12 and 30 weeks of age in MB-LCV and VEH treated mice. *No significant changes were observed in the total area under the curve at each time point, however, improved glucose handling was noted at 8 weeks and 30 weeks of age in MB-LCV treated mice. n=10. Data presented as mean±SD. Significance via* unpaired t-test. *Significance symbols: *:p<0.05, **p<0.005.*

4.3.10 *Ex vitro* analysis of mitochondrial function using the Seahorse XF24 Flux analyser

One major contributor to skeletal muscle fatiguability/endurance is the capacity of the mitochondria to meet ATP demand. As such, mitochondrial function was a logical next-step investigation to perform. Consistent with our theory that chemotherapy induces mitochondrial function [1], here we have shown that by 12-weeks of age, immediately post MB-LCV therapy, all measures of mitochondrial function aside from coupling efficiency and glycolytic-dependent (anaerobic) metabolic capacity were suppressed. Specifically, basal respiration was reduced by 49% (p=0.09, Figure 4.18A), phosphorylating respiration by 63% (O_2 consumption linked to ATP-production, p<0.05, Figure 4.18B), spare respiratory capacity by 74% (p<0.001, Figure 4.18C) and the aerobic metabolic potential by 57% (p<0.005, Figure 4.18E). In contrast to VEH-treated mice, which saw spare respiratory capacity halve and coupling efficiency decline by 25% with age, there were no age-related changes observed in MB-LCV-treated mice when compared to VEH. While mitochondrial function in VEH treated FDB fibres showed an age-related decline in aerobic metabolic potential, a concomitant increase in anerobic metabolic potential was surprisingly observed (-33%, p<0.005 and +438%, *p<0.005 respectively,* Figure 4.18E & F); a shift that was inhibited by MB-LCV treatment. Collectively, these data suggests that MB-LCV treatment initially truncates the mitochondrial response to uncoupling stress (i.e. induced by FCCP) resulting in reduced oxidative phosphorylation during times of heightened demand. By 30-weeks of age, treatment caused a significant increase in basal respiration and ATP production at rest, suggesting raised metabolic demand at rest. Although, spare respiratory capacity was unchanged from 12-weeks, maximal oxygen consumption (as induced by oligomycin) was

unchanged from VEH – indicating that although the mitochondria were respiring at a significantly greater level at rest, the maximal respiratory capacity remains functional and comparable to VEH (Figure 4.19). This is in stark contrast to the mitochondria at 12-weeks of age where a significant reduction in both basal respiration and maximal oxygen consumption (-90%, $p<0.001$) was observed.

These data suggest that the mitochondria at 12-weeks of age, and after 8 weeks of MB-LCV therapy, show a reduced basal rate of activity together with a considerably reduced ability to increase phosphorylation to meet metabolic demand. Contrastingly, at 30-weeks, basal mitochondrial activity was significantly raised and, due to this there was a reduced margin to increase phosphorylation. However, the mitochondria from 30-week old mice produced maximal phosphorylation rates similar to VEH suggesting that the dysfunction seen at 12-weeks of age had been repaired by 30-weeks of age.

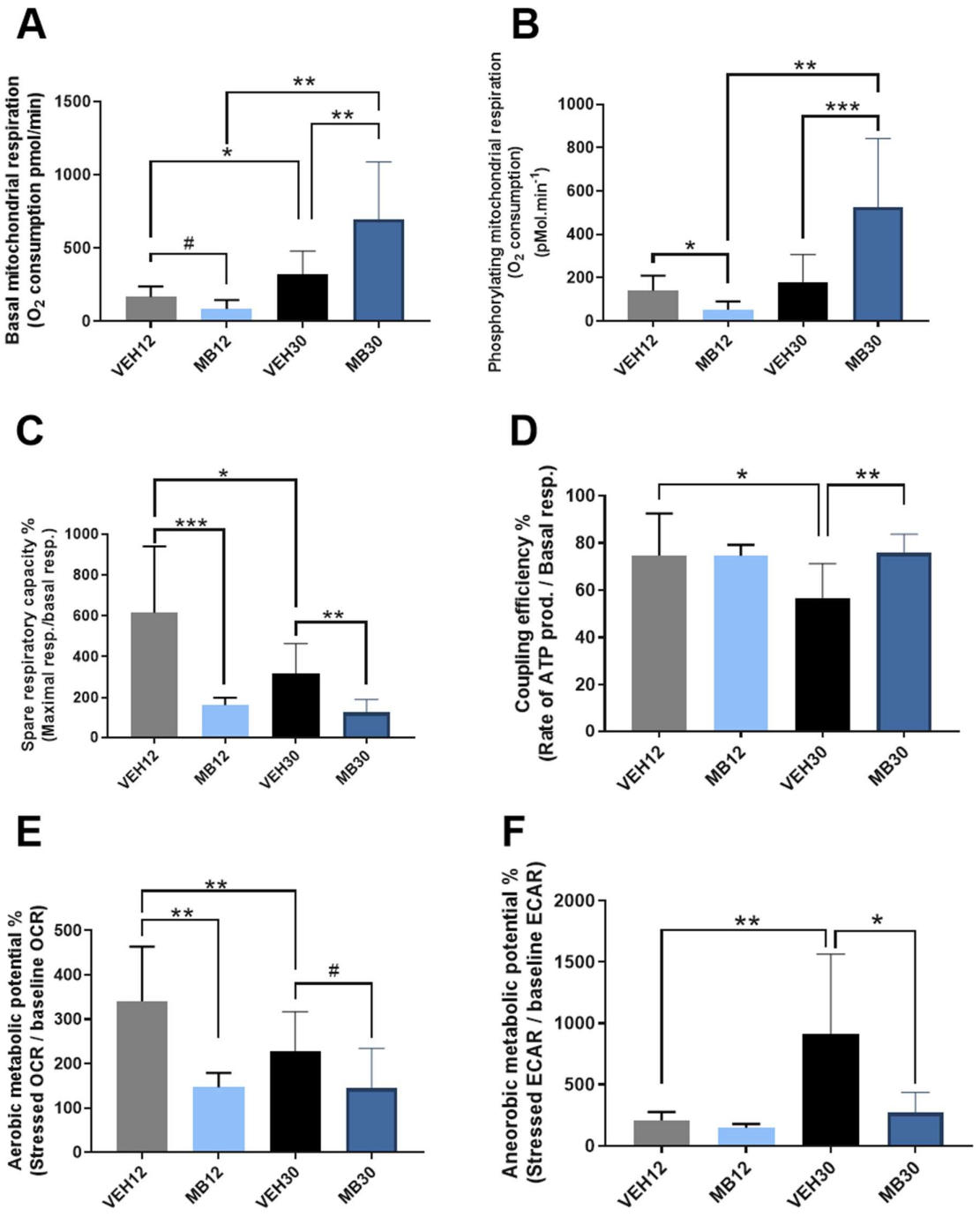

***Figure 4.18*: Mitochondrial respiratory function of VEH and MB-LCV treated 12- and 30-week old mice.** *Isolated muscle fibres from bi-lateral flexor digitorum brevis. m were assessed for basal (A), ATP-associated phosphorylating (B) and uncoupling-associated spare (C) respiration. Mitochondrial coupling efficiency (D), aerobic (E) and anaerobic (F) metabolic potentials were calculated using these measures. MB-LCV therapy reduced basal mitochondrial respiration in 12-week-old mice (#: p=0.090, n=VEH:7. MB:4) but exacerbated the age-related increase in basal respiration by 30-weeks by 128% (p<0.005, n=VEH:8. MB:11, A). A similar trend was observed with ATP production, however the increase seen in MB-LCV treated mice was not observed in VEH (B). Although spare respiratory capacity was reduced 75% with MB-LCV treatment in 12-week old mice ([<0.001), age-related decline was not observed (C). No effect was seen on coupling efficiency at 12 weeks, however age-related decline was not seen with this measure either with 30-week old mice showing elevated coupling efficiency with MB-LCV treatment (p<0.005). Although aerobic metabolic potential was greatly reduced by MB-LCV treatment at 12-weeks (p<0.005), aerobic and anaerobic metabolic potentials did not change between 12- and 30-week time points. Anaerobic metabolic potential was unchanged by treatment at 12-weeks. Data presented as mean±SD. Significance via* ANOVA with Tukey's post hoc. V12 n=8, V30 n=9, MB12 n=6, MB30 n=10. *Significance symbols: *:p<0.05, **p<0.005, ***p<0.001.*

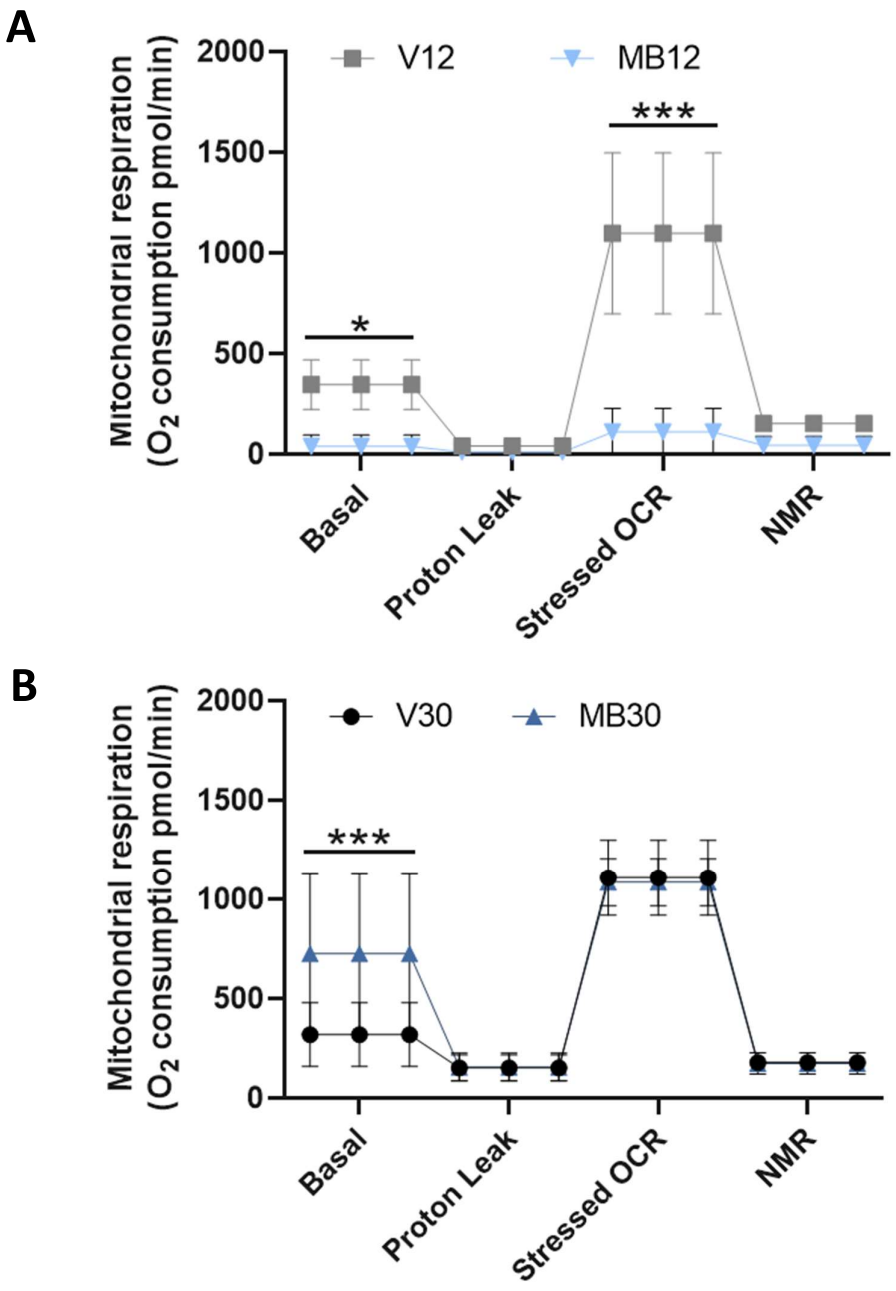

Figure 4.19: Changes to cellular oxygen consumption in response to mitochondrial inhibitors and stimulants induced by early-life MB-LCV therapy at 12- and 30-weeks of age. *MB-LCV therapy administered from 4-12 weeks of age reduced basal respiration by almost 90% (p=0.09) and significantly decreased maximal respiration by 90% (p<0.001) in 12-week mice. By 30-weeks of age, maximal respiration had significantly increased relative to VEH by 128% (p<0.001) with maximal respiration levels returning to that of VEH. No significant changes to proton leak or non-mitochondrial respiration (NMR) was observed. Error expressed as SD where n=9-10. Significance symbols: #:p=0.09, ***: p<0.001.*

4.4 Discussion

Within this study, mice treated with the IAMDF modified Children's Cancer Group (CCG) medulloblastoma chemotherapy regimen [124,331] were monitored from the time of treatment at 4 weeks of age, throughout the subsequent 8 weeks of chemotherapeutic treatment, and through to 30 weeks of age, to assess for short-term and long-term sequalae of the MB-LCV chemotherapy regimen (which contains CCNU, CDDP and VCR). In doing so, we've demonstrated that MB-LCV treatment in young mice caused: 1) significant reductions in skeletal muscle contractile function which was endured throughout the lifespan, even in the absence of observable systemic toxicity, chemotherapy-induced muscle atrophy, or mortality. These functional reductions were accompanied by; 2) mitochondrial dysfunction characterised by a reduced ability to adapt to metabolic demand. This confirmatory IMADF study partially supports our original hypothesis and results from our pilot study in Chapter 3, that common paediatric chemotherapy regimens induce skeletal muscle dysfunction and wasting through mitochondrial dysfunction, however in this instance, we saw no evidence of muscle wasting in mice.

4.4.1 MB-LCV therapy does not affect survival or overall life-time growth in young mice

MB-LCV treated mice survived both rounds of chemotherapy with no impact on survival. Although this study administered only 2 of the 8 courses prescribed within the CCG study [124], the time frame of treatment in mice was like that which is experienced in human patients; allowing for reasonable comparison. In the CCG study, progression-free survival was

reported as 86%±4% and 70%±7% at 3 years and 5 years post therapy, respectively [331]. Other studies with this and modified versions of the regimen, have returned similar survival rates (5-year event free survival (EFS) with the same regimen 82%±2.8% vs cyclophosphamide substituted for VCR, 5-year EFS 80%±3.1% [331]). Importantly, these studies indicated that the deaths were not directly due to treatment toxicity but rather from complications of metastatic disease, infection or cancer progression [124,331]. Aside from cancer recurrence, long-term survival is often reported together with a myriad of treatment-induced side-effects. These side-effects persevere long after treatment has ceased and the cancer survived, and greatly contribute to the overall disease burden associated with cancer survival. Weight-loss, for example, is generally associated with lean mass loss with or without the loss of fat mass [147,152,279] which is often solely attributed to cancer-induced cachexia. Here, mice undergoing treatment sustained a ~5% drop in bodyweight following the commencement of chemotherapy (D2, Figure 4.7). After 3 days post CDDP therapy, weight gain was observed and occurred at a greater velocity than VEH, resulting in MB-LCV treated mice recovering to VEH levels within 2 weeks. Body weight loss was again evident after commencement of the second course of chemotherapy at D29 with a ~14% drop in weight observed, which, again, was normalised due to an increase in weight gain velocity over the next two weeks. It is likely that the observed weight-loss was caused by CDDP, since it was observed in the immediate days following CDDP administration. Not surprisingly, drops of up to 50% in food consumption matched the periods of weight-loss (Figure 4.8), likely due to the intense nauseating effects of CDDP [540]. Presumably to correct for the caloric deficit, mice increase their food consumption by ~28% for the 7 days thereafter.

Our collaborators have previously shown that platinum-based chemotherapeutic agents induce gastrointestinal dysfunction [421,422,541,542]. Specifically, they have shown that

platinum-based alkylating agents decrease gut motility and enteric neuron number which could explain how, here, food consumption is reduced after administration of CDDP. If indeed this is occurring here, if food flow through the gut is slowed, this could be misinterpreted as an appropriate level of satiety resulting in elevated inhibitory feeding signals to the brain [543]. Although not investigated here, it is feasible to suggest that the gastrointestinal dysfunction seen previously, and associated malabsorption, may be the missing underlying variable which resulted in the rapid weight-loss seen here. Importantly, mice undergoing MB-LCV therapy were observed to show diarrhoea-like symptoms which support this hypothesis. However, Hyltander *et al* [455] showed parenteral nutrition delivery offered little protection against body weight loss in cancer patients (refer to Step 7: Application in Chapter 2 for more) highlighting that nutritional intake and utilisation is far more complex than purely the intestinal-venous interaction. If gastrointestinal dysfunction was induced by CDDP (or any of the other agents administered in the MB-LCV regimen), it was transient since body weight could be later restored. Since early life is characterised by rapid growth, even small deficits or modifications in nutrient intake and absorption can have catastrophic effects on overall weight gain and weight-gain velocity. Maintenance of a positive nutritional status in patients undergoing chemotherapy has been a well-known prognostic factor for decades [544]. A study in 1981, highlighted that a higher serum albumin content and absence of weight-loss (defined as <5%) at the time of diagnosis resulted in median survival times more than doubling (5 months to 12 months, p=0.008) [545]. More recently it has been established that cancer-induced malnutrition negatively effects survival outcomes if not rectified before chemotherapy commences [546,547]. Prior to treatment with MB-LCV therapy, mice were of sound nutritional status and no impact on survival or long-term weight gain was noted. The failure to normalise body weight following anti-cancer treatment and the consequential impact on survival rate

thus seems likely to represent a complex interplay between cancer-induced cachexia and chemotherapy-induced toxicity, rather than caused by chemotherapy alone. Ness *et al* (2007) showed that long-term chemotherapy survivors exhibited greater body fat and lower lean muscle mass percentages compared to their untreated counterparts without change in body-mass-index [18]. While treated mice did not exhibit a decline in overall excised wet muscle weight (Figure 4.9), it is important to note that this measure is a rudimentary assessment of muscle mass and thus does not definitively rule out the possibility that chemotherapy-induced alterations in body composition were present in our mice. In an attempt to elucidate whether chemotherapy was impacting the quality of the muscle tissue, micro-computed tomography was undertaken on the hind limbs of all mice within this study. Unfortunately, after promising trials, the hind-limbs were over-stained requiring alternative methods for analysis (see *S4.2.2.3.1)*. This compromised our ability to differentiate different soft tissue types from each other, in the hind-limb. Still, through volumetric analysis we were able to estimate muscle volume and showed that hind-limb volume increased with age, but was not effected by MB-LCV therapy (see Figure 4.10).

4.4.2 Immediate and long-term chemotherapy-induced skeletal muscle dysfunction: A sequalae of MB-LCV therapy

Skeletal muscle dysfunction is a multi-faceted pathology resulting in a decline in endurance capacity (i.e. enhanced fatiguability), strength, or both. CI-SMDW has been a well identified yet poorly defined phenotype of chemotherapy survivorship [13,18-20,22,93,95,145,509]. Within clinical settings, one of the most widely used measures of skeletal muscle strength is

grip strength, which assesses maximal isometric strength of the forearm. As hand grip strength has been widely used for decades in the clinical setting, the available pool of data enables comparisons to healthy populations possible [548-550]. With numerous studies assessing grip strength in patients undergoing chemotherapy [379,551], survivors of chemotherapy [151,380,552,553], and patients both before and immediately after treatment [554], it is well identified that chemotherapy survivors develop muscle weakness observable as a decline in grip strength. Long-term investigations of CI-SMDW in survivors of medulloblastoma though are only just emerging [555]. However, due to the complex nature of skeletal muscle contraction, the underlying problem resulting in muscle dysfunction may lay anywhere from nerve impulse initiation in the brain, through to the transfer of this impulse to muscle fibre via the neuromuscular junction, down to the physiological and mechanical mechanisms that regulate and enact contraction. Peripheral neuropathy has been indicated as a significant sequalae in MB-LCV therapy [496,542,556-560], although where along the brain-muscle axis the damage is occurring is currently unclear. In Medulloblastoma patients, an obvious limitation of grip strength studies is the uncertainty as to whether the cerebellar cancer is impairing efferent nervous communication to the muscle, or, whether the chemotherapy is causing the dysfunction somewhere along the axis. The grip strength studies performed in mice in this study, are independent of brain cancer, and showed no effect of chemotherapy either after 4 weeks or 8 weeks of treatment. However, grip strength was significantly reduced in treated mice at 30 weeks of age (18 weeks after chemotherapy had ceased, Figure 4.11). As a clinical comparison, this is the equivalent of a 5-8 year old child receiving recurrent chemotherapy without a loss in grip strength, but, after chemotherapy ceases in their early teens, exhibiting a loss of strength upon assessment in their thirties [436]. The underlying mechanisms behind this delay is thought to be a two-pronged insult. One, on the physiological front, where

chemotherapy is thought to damage the support cells of the child's skeletal muscle, namely satellite cells, mitochondria and motor neurons, impeding physical and motor skill development [11]. The other, on the physical capacity front, as once development has been hindered and physical ability diminished, the child is unable to engage in the same levels of physical activity with their peers, further compounding the deficit in physical function which manifests more and more as they age [18,509].

To further investigate whether MB-LCV therapy induces skeletal muscle dysfunction, *ex vivo* contractile analysis of *EDL* (predominantly fast twitch fibres) and *SOL* (mixed fast and slow) muscles was performed. This type of functional testing removes neurological variables such as nerve impulse creation and transmission from brain to muscle, and solely measures the physiological capacity of the muscle – something that is obviously not possible in humans. A similar phenotype to that seen in our grip strength studies was observed in our *ex vivo* muscles in that absolute force production (raw strength, Figure 4.13A,B), specific force production (force corrected for muscle size, Figure 4.13C,D) and fatiguability and recovery capacity (Figure 4.15) were normal for both fast-twitch EDL and slow-twitch SOL at 12 weeks of age. However, at 30 weeks of age, a significant decrease in absolute and specific force was observed in both EDL and SOL muscle. These data suggest chemotherapy administration induced effects at the molecular cross-bridge level rather than as a function of muscle wasting, since specific force is corrected for muscle cross-sectional area and no changes in muscle weights or fibre cross-sectional area were observed. Declines in grip strength at 30-, but not 12-weeks of age, serves to corroborate the theory that MB-LCV therapy has reduced overall muscle quality which has required time to manifest. Although chemotherapy had no effect on the fatiguability of the EDL at the 30-week time point – likely due to the very low forces being produced by the muscles – a decline of functional recovery capacity was seen in

EDL muscle, a potential indication that fast twitch fibres are targeted by chemotherapy leaving slow-twitch fibres to produce force in response to the stimulus. Following fatigue-inducing contractions, 30-week MB-LCV EDL muscles failed to recover force relative to VEH muscles, and then ultimately, failed to respond to stimuli at all (Figure 4.15C). Further, we were unable to complete the fatigue protocol with any MB-LCV-treated SOL muscles as all samples either tore or ceased responding to stimuli. Although suggestive of perfuse muscular damage or insufficient or irregular structural architecture (such as abnormal dystrophin, collagen, fibrin, etc.). Our group has recently demonstrated that chemotherapeutic agents alter the structural composition of the extracellular matrix (unpublished findings, D.Campelj) highlighting this as a possible mechanism.

4.4.3 Chemotherapy-induced mitochondrial dysfunction likely underpins SMDW

As similar dysfunctions were noted between grip strength and contractile experiments, these data suggest that the underlying aetiology is not chemotherapy-induced neuropathy but rather inextricably linked to muscle structure and/or function. Although histological assessment of the EDL or SOL muscle were, regrettably, not undertaken, histological assessment of the TA showed no signs of structural damage or fibre atrophy (albeit these muscles were not subjected to a maximal fatigue protocol). Aside from the structural capacity of a muscle, skeletal muscle bioenergetics are an important component of cross-bridge cycling and the overall contractile process. Considering the large ATP requirement of muscle tissue, any reductions in ATP production capacity could be vastly

detrimental to its aerobic (and anerobic) capacity; and thus performance. Firstly, glucose uptake capacity was assessed; (S4.3.9, Figure 4.17) an indirect measure of the mouse's ability to remove glucose from the circulation and into metabolically-demanding tissue, including the musculature. MB-LCV induced no change in this ability at 12-weeks when mice were delivered a weight-corrected injection of glucose to the peritoneum. In contrast, at 30 weeks of age, MB-LCV treated mice showed a significantly improved ability to remove glucose from the blood. Specifically, increased rates of glucose uptake were noted at both the 15- and 30-minute time points. In hindsight, accompanying these data with circulating insulin analyses would have provided a better understanding of glucose regulation – but, nevertheless, glucose handling was clearly altered after the cessation of chemotherapy administration. Considered with the marked suppression of muscle performance, it is possible that if the mitochondria were in fact dysfunctional, cellular energy production would depend more so upon anerobic glycolysis, elevating endogenous glucose requirements.

The mitochondria are largely responsible for the glucose-energy conversion within the cell and, as such, they were functionally assessed using the Seahorse live-cell extra cellular flux system as described in S4.3.8. 30-week old VEH mice exhibited an elevated basal respiratory rate than their 12 week old counterparts, with treatment elevating these levels further (Figure 4.18A). This increase in basal cellular respiration at rest in healthy mice can be explained by the natural increase in mitochondrial density with age [561,562] and thus increased oxygen consumption. We have shown previously that treatment with a single platinum-based chemotherapeutic agent (OXA) in mice significantly increases mitochondrial density and reactive oxygen species production, but reduces the number of viable mitochondria within the cell [159]. In this study, spare respiratory capacity was significantly reduced at both 12- and 30-weeks of age (Figure 4.18C), without any observed changes in coupling efficiency. This

decline of metabolic flexibility highlights a reduced capacity for the mitochondria to meet the elevated metabolic demand in times of stress. It is this process that the skeletal muscle relies on for repletion of ATP during times of stress. With two of the three agents used in LCV acting as DNA alkylating agents (lomustine and cisplatin), it stands to reason that both of these agents have a capacity to damage the mitochondria, particularly due to the single stranded nature of the organelle's DNA.

As MB-LCV treatment greatly impacted the capacity of this process, significant ramifications on skeletal muscle performance is an obvious downstream effect as mitochondrial function cannot escalate to meet the demands of exercise, which was clearly observed in the fatigue protocol of both the EDL and SOL muscles (Figure 4.14). The underlying reasons for this are curious, as we noted no increase in skeletal muscle fibre size (Figure 4.16) or overall muscle volume (Figure 4.10) which could have explained the elevated metabolic demand. Importantly, the mitochondria at 12-weeks of age showed significant dysfunction which was highlighted by a reduction in spare respiratory capacity (Figure 4.18). Moreover, fibres which did not receive appropriate amounts of ATP to sustain cross-bridge cycling would essentially cease to work, entering a state of rigor and ultimately sustaining damage if used thereafter. There is a potential that this has caused irreparable damage to the muscle at 12-weeks of age, which has manifested into the state of muscular dysfunction seen at 30-weeks. Juvenile muscle is still undergoing hyperplastic growth in the early years of life, which is mediated by the highly mitotic muscle satellite cell population.[188,563] Any anti-mitotic insult to these cells would both greatly reduce their capacity to repair and, worse still, deplete the satellite cell population all together, impeding the muscles capacity to repair. The phenotype presented here, although without signs of atrophy, is in fact consistent with that of early onset sarcopenia; which is characterised by an elevated state of systemic

inflammation, reduced muscular strength, increased muscle fatigue, a muscle fibre type switch to a predominantly slow-twitch fibre, increased propensity for the muscle to sustain damage, and musculature with smaller, fewer and less adaptive mitochondria. [314,315,564] Although further investigations are required to substantiate these hypotheses, particularly histological investigations to elucidate fibre-type switching and fibrotic changes, MB-LCV therapy undeniably induces a decline of muscle function at the ultra-structural level which is potentially underpinned by mitochondrial dysfunction. Although the exact mechanisms remain to be elucidated here, even though muscular atrophy was not observed here by the 30-week time point, it is likely that MB-LCV therapy has induced a pre-sarcopenic-like state and that muscular atrophy is likely to follow.

4.5 Chapter summary

We present here a clinically relevant animal model for investigating the effects of the CCG developed MB-LCV chemotherapeutic regimen. We have shown that a clinically relevant, modified version of the CCG MB-LCV therapy induces a somewhat pre-sarcopenic state; where skeletal muscle dysfunction, elevated levels of systemic inflammation and dysfunctional mitochondria are present without signs of muscular atrophy. Of note, skeletal muscle recovery was greatly impacted by chemotherapy, demonstrating a greatly reduced – if not removed – ability to recover from a maximal 'exercise' bout. With the mitochondria unable to escalate to meet metabolic demand in times of stress in early life, the skeletal muscle dysfunction presented here at 12-weeks of age appears underpinned, if not at least

exacerbated, by mitochondrial dysfunction. With some capacity returning to the mitochondria later in life, but muscle dysfunction worsening, we hypothesis that the damage induced by a detrimental triad of inflexible mitochondria, systemic inflammation and skeletal muscle dysfunction in the early years of life has manifested into an early-onset sarcopenic state – all of which is instigated by childhood administration of MB-LCV therapy.

Chapter 5

Investigation of CI-SMDW Induced by NHBL-Indicated CHOP Therapy in Juvenile Mice

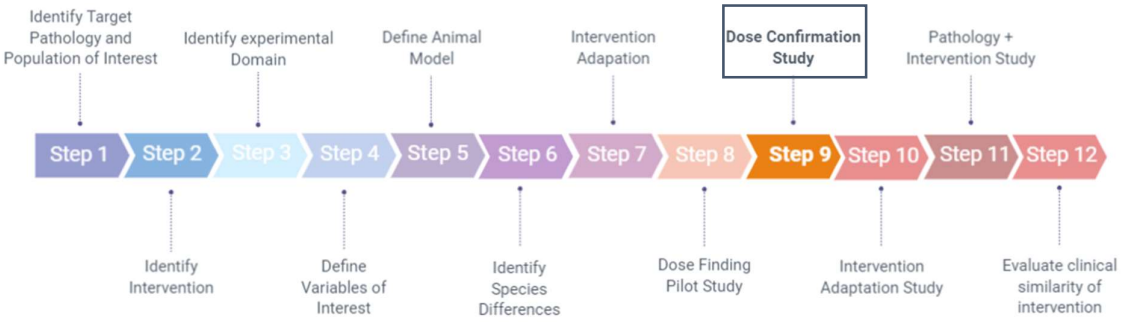

5.1 Introduction

Prior to 1998, the 5 year event free survival (EFS) estimate for children and adolescents with newly diagnosed NHBL was below 78% [565]. Fortunately, these patients have been afforded remarkable improvements in prognosis since then. The *FAB/LMB* 96 trial highlights the importance of on-going scrutiny of current 'gold-standard' regimens. During the trial, survival rates for children suffering from NHBL were improved to near 100% when treated with a modified CHOP therapy regimen (5 year EFS for children with limited disease was reported as 97 ± 0·5% [566]). Other studies using CHOP regimens report similar improvement in survival rates [338]. These survival improvements can be largely attributed to advancements in the application of chemotherapeutics and supportive therapies. However, these statistics fail to include the children who succumb to treatment toxicity. Within the *FAB/LMB* 96 study [566], of the 217 patients who were eligible to commence treatment, 49 experienced a treatment failure event which resulted in them being removed from the study, with only seven of those children surviving. It should be recognised that, although close to 100% of patients of whom did not experience a treatment failure event went on to enjoy a 5 year EFS period, close to 20% did not. A further 81% of patients undergoing treatment experienced stomatitis, 95% experienced infection, and over 25% were reported to experience Grade III/IV haemorrhage, transaminase, diarrhea, and electrolyte toxicities [341,566]. These acute treatment sequalae are then amplified by long-term side-effects which manifest well after treatment cessation and well after the patients are discharged from the hospital setting. Weakness, fatigue, skeletal muscle dysfunction and wasting, failure to thrive, and reduced life-span and quality of life are just a few of the long list of chemotherapy-associated sequalae [161,567-569]. Furthermore, chemotherapy toxicity, which is commonly identified as a treatment failure event whereby

the therapy induces unacceptable risk or toxicity to the patient, often results in the patient being removed from the study and the subsequent statistical analysis. Thus, caution should be taken when interpreting treatment success rates. Regardless, that many patients experience severe treatment toxicity both during and after treatment, highlights an area where vast improvement to treatment tolerability and patient quality of life can be made.

In the previous chapters we have rudimentarily established that the ALL-POMP and BL-CHOP regimens induce skeletal muscle dysfunction in EDL muscle and, although this was substantiated in the MB-LCV regimen, we are yet to conclusively show that the BL-CHOP regimen induces skeletal muscle dysfunction. Mitochondrial dysfunction was shown to be a likely contributor to the skeletal muscle dysfunction seen in the MB-LCV regimen, however, we have yet to establish whether chemotherapy can induce the full skeletal muscle dysfunction and wasting sequalae when administered without the cancer that the regimens aim to treat. This chapter aims to build on the completed NHBL pilot study presented in Chapter 3, by expanding animal numbers, post-therapy observation periods and investigative techniques to 1) ensure the IAMDF-modified BL-CHOP therapy is clinically relevant and appropriately replicates the clinical picture induced by the chemotherapy regimen; 2) investigate the CI-SMDW phenotype and the mechanisms which underpin it; and in contrast to human studies which are based on the combined effects of cancer and anti-cancer treatment, this study will 3) determine the magnitude of impact of BL-CHOP therapy alone. We hypothesise that the BL-CHOP regimen, which is centralised around anthracycline therapy which is known to induce skeletal muscle atrophy and mitochondrial dysfunction on its own, will induce the CI-SMDW sequalae and that this dysfunction and wasting will be observed in conjunction with mitochondrial dysfunction.

5.2 Method

Methods are as per Chapter 3: Pilot and Chapter 4: MB-LCV confirmation study, unless otherwise stated below. Methods below were performed in addition to methods outlined in previous chapters.

5.2.1 Animals

All animal conditions are as previously described except for animal numbers. Here, 49 mice began treatment housed in cages of five (with one group of four). 19 mice were allocated to the 12-week group and were culled for analysis on the last day of the regimen (D56 of treatment/D84 of life), while the remainder were culled at week 30 of life (D120 of life). The VEH group used in this chapter is the same as that presented in Chapter 4.

5.2.1.1 Chemotherapy treatment summary

Following from the success of the NHBL pilot study, the 80% IAMDF derived dose was selected for use in this confirmatory study as outlined below. Treatments herein were adapted from the *French American-British Lymphome Malins de Burkitt* (FAB LMB) 96 study [338,339] which was a collaboration between the *Française d'Oncologie Pédiatrique* (SFOP), the CCG, and the *United Kingdom Childhood Cancer Study Group* (ULCCSG).

Table 5.1: Drug names, delivery modes and doses for selected BL-CHOP regimen

Drug	*Mode of delivery*	*Delivery times*	*Dose per delivery*	*Total daily dose*	*Days of course delivered*
Cyclophosphamide (CPM)	Oral gavage	7-9am + 1-3pm	180.00 mg/kg	360.00 mg/kg	1-6
Vincristine (VCR)	Intraperitoneal injection	7-9am + 1-3pm	0.39 mg/kg	0.78 mg/kg	1,6
Prednisone (PRED)	Oral Gavage	7-9am + 1-3pm	11.81 mg/kg	23.62 mg/kg	1-6
Doxorubicin (DOX)	Intraperitoneal injection	7-9am + 1-3pm	2.60 mg/kg	5.20 mg/kg	1

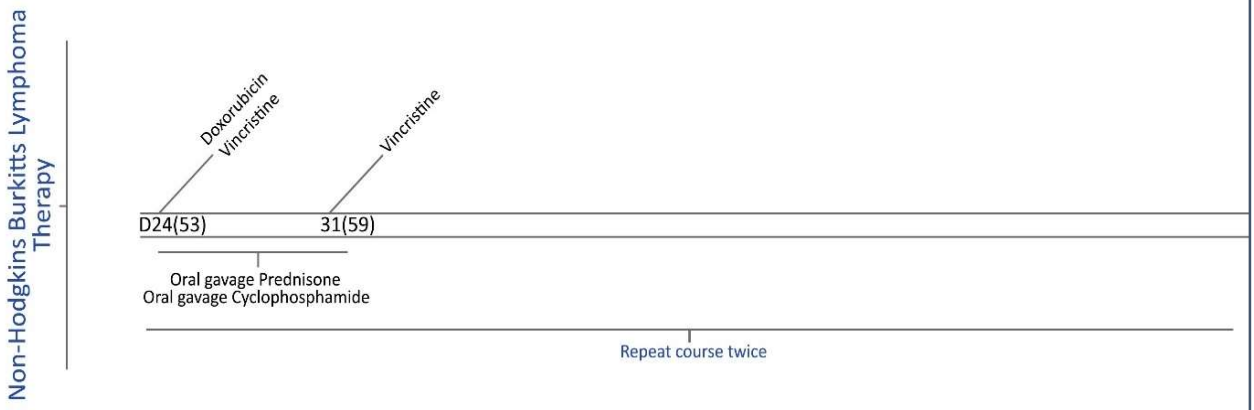

Figure 5.1: BL-CHOP regimen outline. *Days indicate age of life of mice with bracketed numbers indicating day of treatment for the second course.*

5.3 Results

5.3.1 Low percent survival and systemic pathology in modified BL-CHOP therapy in mice

Although survival was achieved in the IMADF pilot study in Chapter 3, toxicity and lethality levels of the regimen were, in fact, far more significant than originally projected. 85.7% of mice completed the 12-week regimen successfully with 7 deaths (from the 49 mice which commenced treatment) recorded over the course of therapy. Of the remaining mice, 33% survived through to the 30-week time point. Necropsy of 4 mice from the 12-week time point (as performed and reported by veterinary pathologists at Cerberus Sciences, Melbourne, Australia; reported observational data) consistently showed ascites, eccentric hypertrophy of the right ventricle of the heart (3/4) and gross hepatocellular swelling and scattered lipid vacuolation (steatosis) of liver hepatocytes (4/4). As reported in Chapter 3, necrosis throughout the intestinal tract was also observed (3/4) with 2/4 mice presenting with enlarged, full caecum's with significant fluid containment within the colon (see Table 5.2). Interestingly, mice which died from treatment were consistently observed to suffer gross enlargement of the large intestines (potentially toxic megacolon, Figure 5.3). Unfortunately, due to limited time and resources, this data is only observational in nature with GIT sections being frozen for future analysis by our lab and collaborators.

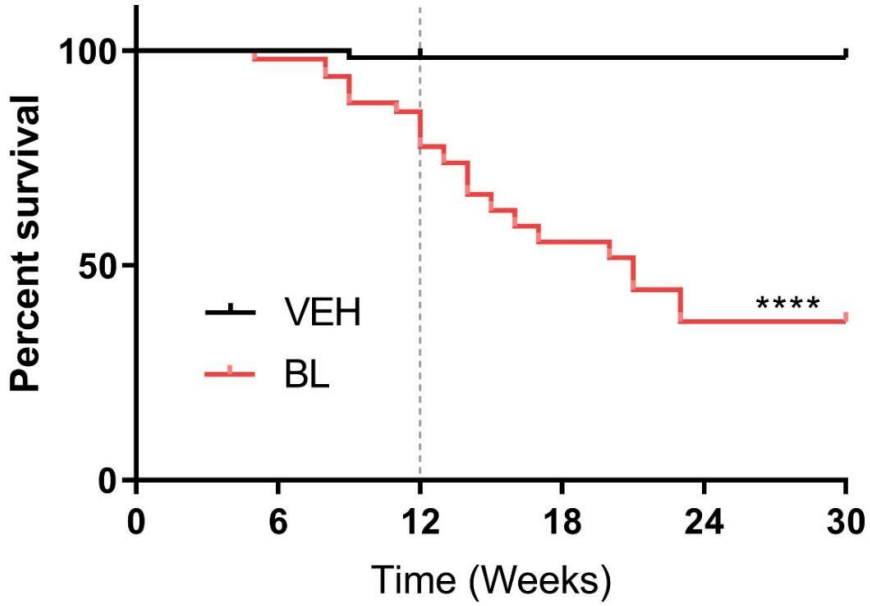

Figure 5.2: Survival rates of VEH (V) and BL-CHOP (BL) treated mice at 12 and 30 weeks of age. *Survival was significantly reduced during and post BL-CHOP therapy administration (p<0.0001). Non-survival was recorded as either euthanasia or natural death. The vertical dotted line indicates the 12-week cull point where 17 mice were culled for time point analysis with the surviving mice culled at 30 weeks (cull events not represented in this graph). VEH n = 60 <12 weeks, n = 25 >12weeks with one death in week 9. BL-CHOP n = 49 <12 weeks, n = 30 >12 weeks. Significance symbols: ****:p<0.0001.*

***Table 5.2: Pathological observations of VEH (V) and BL-CHOP (BL) treated mice during necropsy at 12 and 30 weeks of age**. Abbreviations: RV: Right ventricle, S: Intraventricular septum, LV: Left ventricle, GIT: gastrointestinal tract, +: pathology observed.*

		Pathology observed												
Treatment group	**Mouse**	Cachectic appearance	Perianal faecal staining	Ascites	Interstitial lymphoplasmic infiltration	RV:S:LV	Thinning & dilation of RV myocardium	RV Myocardial inflammation	Cholangitis	Hepatosteatosis	Hepatocellular swelling	Renal hydronephrosis	Basophilic renal tubules	GIT inflammation
V12	1					1:6:6	+				+			
	2					1:6:5	+				+			
	3					1:4:4			+		+			
	4					1:4:4					+			
	5					1:5:5					+			
BL12	1					1:4:3	+		+		+			+
	2					1:4:3	+		+		+			+
	3	+	+			1:4:4	+		+		+	+		+
	4	+	+			1:5:5	+		+		+			+
V30	1					1:5:5					+			
	2					1:4:5			+					
	3					1:3:4								
	4					1:3:4								
BL30	1	+	+	+		1:2:2								
	2	+	+	+		1:2:3		+		+		+	+	
	3			+		1:4:5		+		+		+	+	
	4					1:4:3				+				
	5			+		1:4:3				+				

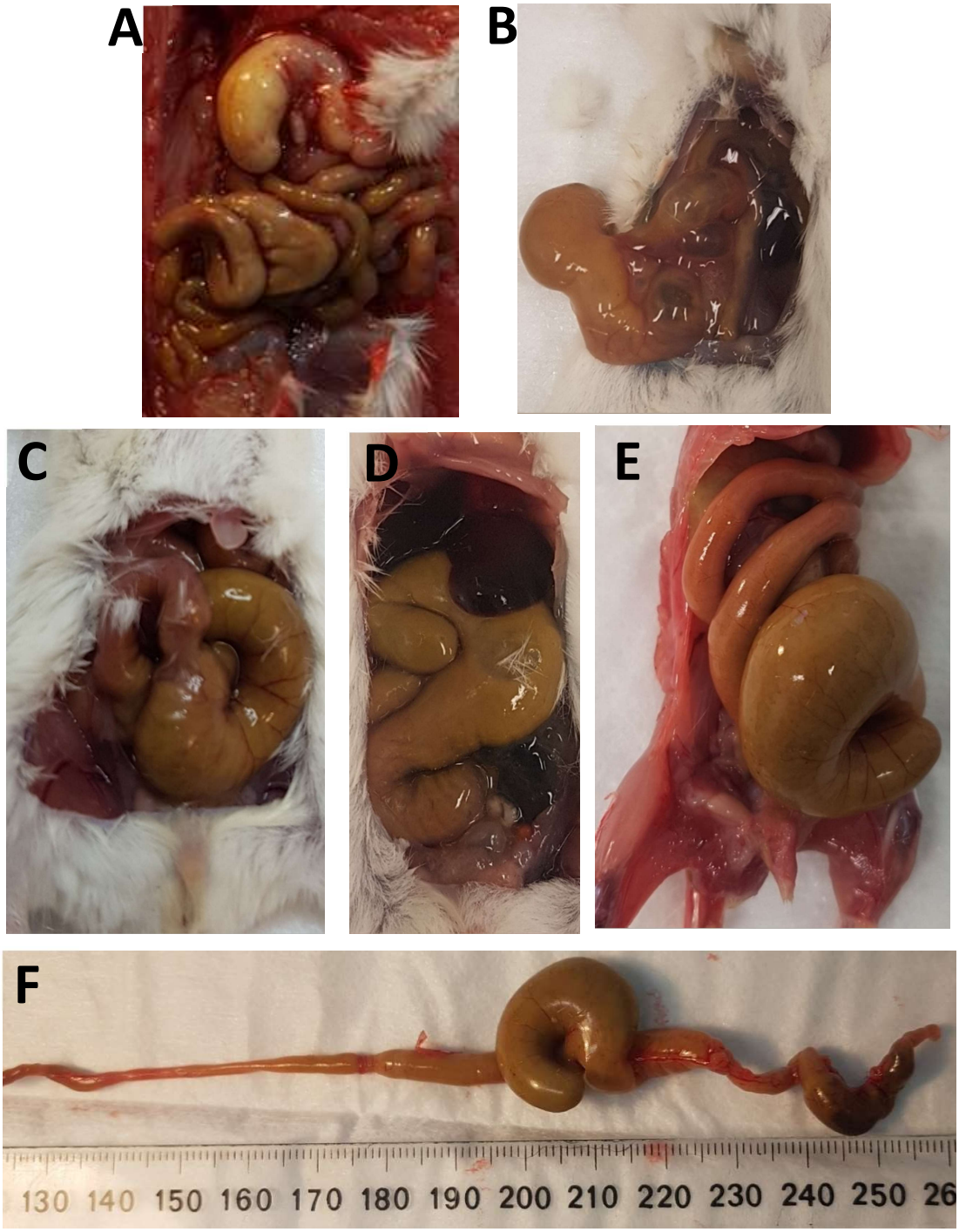

Figure 5.3: Images of gastrointestinal pathology induced by NHBL therapy. *A) Necropsy of healthy, VEH treated mouse. B-E) NHBL treated mice which died at varying ages all showing signs of gastrointestinal pathology and suspected toxic megacolon. F) NHBL treated gastrointestinal tract removed and measured on a centimetre ruler for reference (prevalence reported as ~90% of mice which died as a result of treatment toxicity).*

5.3.2 A failure to thrive: BL-CHOP therapy induces acute weight-loss followed by catch-up growth

From day 1 of treatment (DOX and VCR with the commencement of bi-daily PRED and CPM, Figure 5.4) mice sustained critical weight-loss (-21.5% from VEH and -10% from starting weight, percent of starting weight at day 4: VEH 112% BL-CHOP 90 which was exacerbated during periods of active treatment (Day 1-6 and D29-34 of therapy). During the first round of BL-CHOP therapy, mice began to regain weight 3 days after Day 1 DOX+VCR treatment, however, weight-gain velocity was still below that of VEH treated mice (VEH=3.50g per day average, BL=2.25g per day average from D4-D9). BL-CHOP weight-gain velocity correctively increased thereafter, with a rate which superseded the VEH growth rate (VEH=1.62g per day average, BL=3.52g per day average from D10-D15), indicating catch-up rebound growth [570]. Therapy-induced weight-loss was exacerbated during the second round of therapy which, at its most extreme, resulted in a 18% loss in body weight over an eight-day period (BL-CHOP D29: 142%, D37: 124%). When compared to VEH, mice treated with two rounds of therapy were, on average, 31% lighter than their untreated counterparts (VEH D29: 150%, D37: 155.5%). This loss in weight remained uncorrected until some 100 days after cessation of treatment.

Food consumption (Figure 5.5), for the most part, was consistently similar between treatment groups with differences seen only during the first three days of each treatment round. At times, due to welfare concerns, standard chow mash (ground standard chow mixed with water) was added to cages to supplement food consumption where weight loss was considered too great (refer to *S3.2.1* for details) and that cage's food data was removed from

analysis. Food consumption data was limited in its value from D50 as all BL-CHOP treated mice were supplemented with chow mash. Every attempt was made to approximate food consumption using the dry weight of food added to each cage before it was combined with water. However, true food consumption from this point was ultimately inaccurate and excluded as the animals would track through the mash and intersperse the food through the cage bedding.

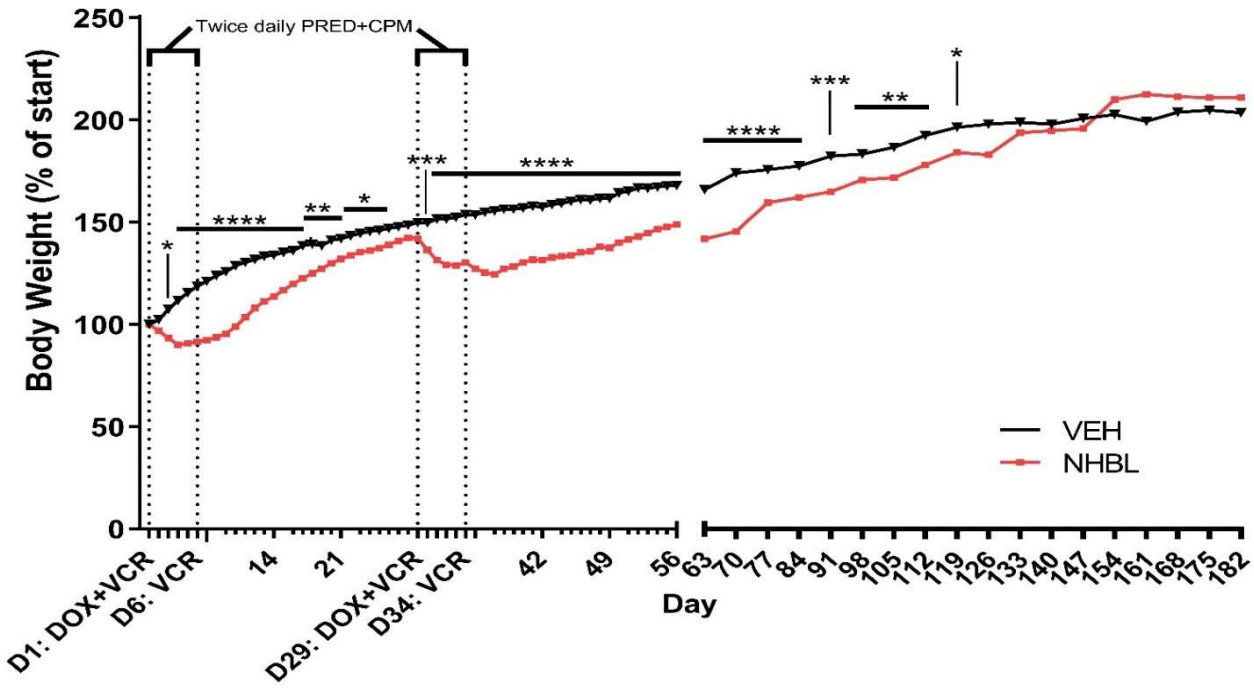

Figure 5.4: Body weight as measured by percent change from starting weight in VEH (V) and BL-CHOP (BL) treated mice at 12- and 30- weeks of age. *Significant weight loss induced immediately after commencement of treatment which, after an initial recovery 3 weeks later, was exacerbated by the second round of chemotherapy. This loss was recovered from 90 days later. VEH n = 60 <12 weeks, n = 25 >12weeks. BL-CHOP n = 49 <12 weeks, n = 30 >12 weeks (n excludes deaths, refer to Figure 5.2 for accurate numbers), error not shown for ease of viewing. Significance symbols: *:p<0.05, **p<0.005, ***p<0.001, ****:p<0.0001.*

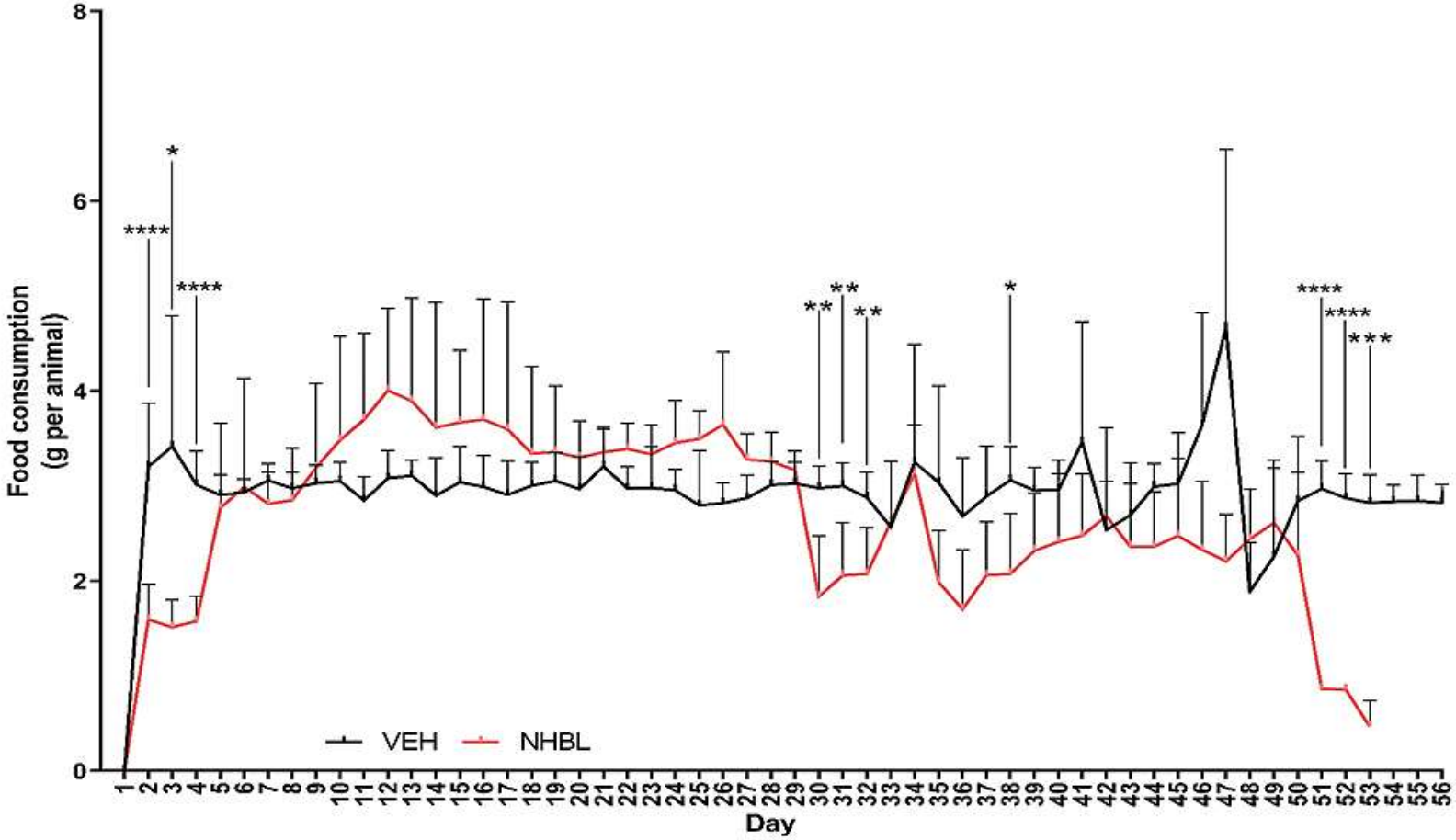

Figure 5.5: Food consumption as measured by daily food average food intake per animal in VEH (V) and BL-CHOP (BL) treated mice at 12 and 30 weeks of age. *Food consumption of VEH vs BL-CHOP treated mice over the life span shows no discernible difference outside of active treatment periods. Mice showed significantly decreased food consumption for 3 days post DOX administration. Consumption returned to VEH levels thereafter. At Day 50, BL-CHOP cages were supplemented with chow mash and an expected decline in dry food weight consumption was seen, as mice almost exclusively consumed the diet alternative. n=7-13 cages. Error presented as SD. Significance symbols: *:p<0.05, **p<0.005, ***p<0.001, ****:p<0.0001.*

5.3.3 Micro-computed tomography (µCT) analysis of the effect of BL-CHOP therapy on hind-limb muscle volume

Considerable weight loss was observed with treatment which was normalised by 30-weeks of age (as seen in *section 5.3.2*). Importantly, µCT analysis was used to assess the impact of the regimen on skeletal muscle mass. Imaging investigations showed clear signs of muscular wasting at both 12- (-15% from VEH, $p<0.05$) and 30-weeks (-16% from VEH, $p<0.05$) in BL-CHOP therapy when compared to VEH (Figure 5.6). After treatment had ceased, muscle mass in the hind-limb of BL-CHOP treated mice increased by the same proportion as VEH treated mice over 18-weeks between time-points (~18% growth over the age).

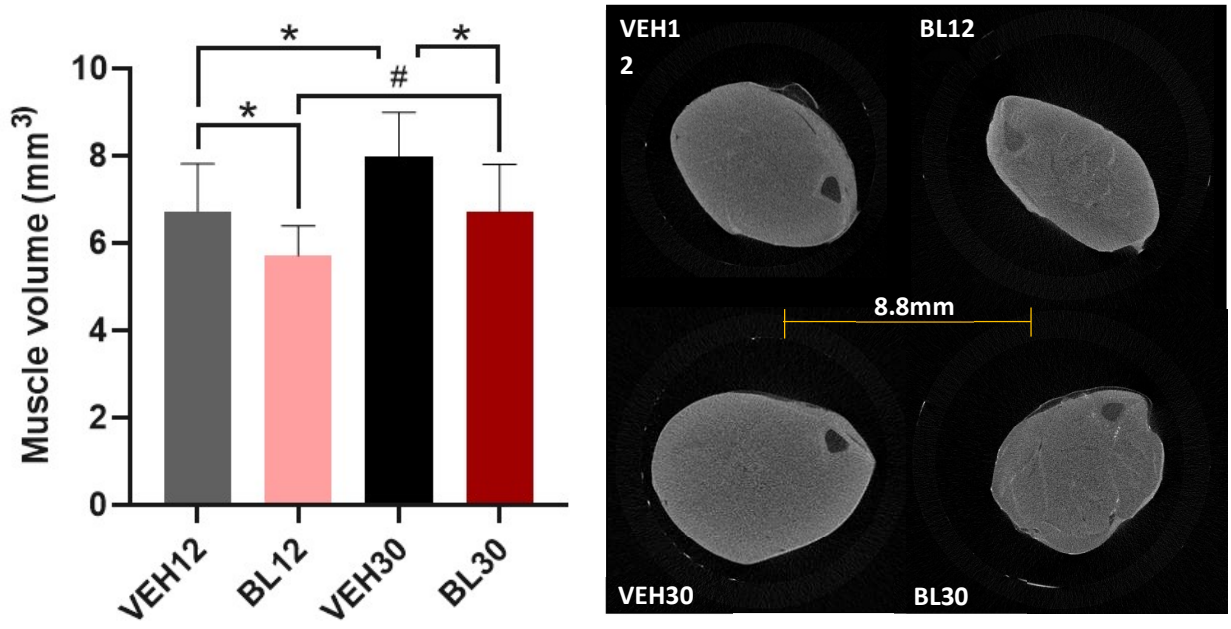

Figure 5.6: Muscle volume as measured by µ-CT imaging of at the proximal 1/3 of the tibia in VEH (V) and BL-CHOP (BL) treated mice at 12 and 30 weeks of age. *BL-CHOP therapy significantly reduced muscle volume in the lower limb at both 12 and 30-weeks of age by 15% and 16% respectively (p<0.05). BL-CHOP treated muscle increased by 18% between 12- and 30-weeks (p=0.064) which was the same increase seen in VEH (18%, p<0.05). Representative images supplied. n=7-10 assessed by ANOVA with Tukey's post-hoc test with error expressed as SD. Significance symbols: #:p=0.064, *:p<0.05.*

5.3.4 BL-CHOP therapy shows minimal long-term change in wet muscle and organ weights

Body weight and absolute organ weights at the two sampling time points are shown in Table 5.3. As a rudimentary measure of atrophy/hypertrophy, excised muscles were weighed. No change was noted between treatment groups with BL-CHOP therapy showing only a propensity to acutely increase TA (+18% from VEH, $p<0.05$) and QUAD (+41% from VEH, $p<0.05$) wet muscle weight. These changes were normalised by 30w of age with all muscle weights returning to VEH levels, except for the PLA muscle which was elevated (+25% from VEH, $p<0.05$). Organ weights remained unchanged, though kidney weight was acutely increased by 20% ($p=0.079$) with BL-CHOP treatment.

Table 5.3: Absolute average bodyweight and weight muscle weight values from VEH (V) and BL-CHOP (BL) treated mice at both 12 and 30 weeks of age

			EDL		SOL		TA		PLA		QUAD	
	Av. BW	*SD*	*Mean*	*SD*	*Mean*	*SD*	*Mean*	*SD*	*Mean*	*SD*	*Mean*	*SD*
V12	26.80	1.43	0.010	0.002	0.012	0.002	0.043	0.004	0.016	0.002	0.130	0.042
BL12	21.76	1.60	0.009	0.001	0.010	0.003	0.039	0.007	0.014	0.002	0.143	0.034
V30	32.95	1.52	0.013	0.002	0.014	0.003	0.054	0.004	0.020	0.004	0.223	0.039
BL30	22.12	2.46	0.015	0.001	0.016	0.006	0.049	0.004	0.025	0.004	0.226	0.026

			HEART		KIDNEY		SPLEEN		LIVER	
	Av. BW	*SD*	*Mean*	*SD*	*Mean*	*SD*	*Mean*	*SD*	*Mean*	*SD*
V12	26.80	1.43	0.125	0.011	0.154	0.020	0.101	0.006	1.147	0.153
BL12	21.76	1.60	0.102	0.013	0.150	0.024	0.066	0.024	0.902	0.199
V30	32.95	1.52	0.174	0.011	0.259	0.019	0.123	0.023	1.489	0.171
BL30	22.12	2.46	0.165	0.018	0.258	0.042	0.146	0.017	1.294	0.148

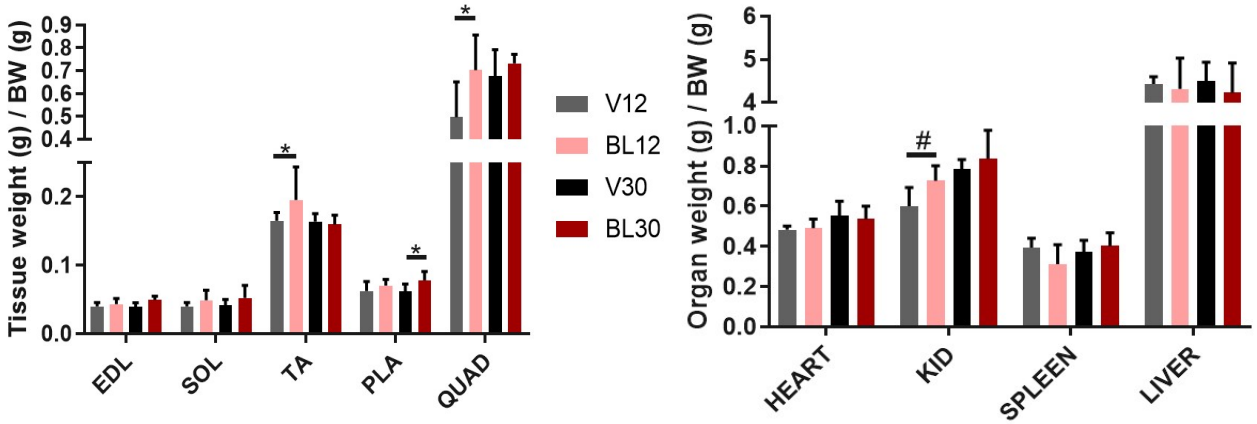

Figure 5.7: Organ and tissue wet weight (g) in VEH (V) and BL-CHOP (BL) treated mice at 12 and 30 weeks of age. *Muscle and organ wet weight post excision during necropsy shows acute increases in TA and QUAD weight:BW ratio ($p<0.05$) and increases in KID size ($p=0.079$) at 12 weeks, all of which was corrected by 30-weeks of age (+18%, 41% and 20% respectively). PLA muscle size alone increased by 30weeks by 12.5% ($p<0.05$). Data corrected for bodyweight of mouse at time of necropsy and is expressed as wet weight of tissue over the mouse's body weight (g/g). n= 4-11. Abbreviations: EDL: Extensor digitorum longus m., SOL: Soleus m., TA: Tibialis Anterior m., PLA: Plantaris m., QUAD: Quadriceps complex. Significance symbols: #:$p=0.079$, *:$p<0.05$*

5.3.5 Haematological investigations in BL-CHOP-therapy treated mice

Full blood examination (FBE) of blood sampled from 12 weeks old animals revealed BL-CHOP therapy induced no change when compared to VEH, aside from a reduction in MCH levels (as calculated by MCH= Hb (in g/L)/RCC (in millions/µL)). All other haematological measures at 12 weeks were unremarkable following BL-CHOP treatment when compared to VEH. By 30 weeks, all measures of red cell and Hb content were depressed, indicative of microcytic microchromic anaemia which is commonly observed in patients receiving chemotherapy due to high erythroid progenitor sensitivity to antineoplastic agents. Significantly, however, this sequalae was maintained 18 weeks after chemotherapy has ceased. [8] This hypothesis of chemotherapy-induced anaemia is supported by normal levels of total protein and albumin (suggestive of normal liver function in the absence of liver function tests (LFT)). Due to low sample volumes and technical error, LFT's and iron studies were unable to be completed, which is unfortunate as a finding of low iron could explain this form of anaemia.

Table 5.4: Haematological (count and smear) and biochemical investigations in VEH (V) and BL-CHOP (BL) treated mice at 12 and 30 weeks of age. for the effect of BL-CHOP therapy on mice. *Data expressed as difference between BL-CHOP mean and VEH mean (with treatment group SD). Significance values >0.1 apply where values not reported. UA: Unavailable due to low sample blood levels. $: often expressed together with globulin levels, globulin level measurement was UA. n.c: not calculatable due to values being identical in each group; VEH30 (16, 16, 16, 16), BL30 (15, 15). n=2-5.*

Measure	**ΔBL12**	**±SD**	**Sig (*p*)**	**ΔBL30**	**±SD**	**Sig (*p*)**
Red cell count (RCC) (x10^{12}/L)	0.119	0.181		-0.225	0.304	
Haematocrit (HC) (L/L)	-2.13	3.51		-6.25	1.41	<0.05
Haemoglobin (Hb) (g/L)	-1.86	9.71		-11.0	2.83	<0.05
Mean corpuscular volume (MCV) (fl)	-2.20	2.00		-5.00	0.707	<0.05
Mean corpuscular haemoglobin (MCH) (pg)	-0.867	0.577	<0.1	-1.00	0.00	
MCH concentration (MCHC) (g/L)	7.530	10.07		17.75	4.950	<0.005
Platelet count(x10^{9}/L)	255.0	47.57		77.25	57.98	
Total white cell count (x10^{9}/L)	-0.94	0.95		-1.40	1.34	
Segmented neutrophils (x10^{9}/L)	0.10	0.17		-0.17	0.35	
Total lymphocyte count(x10^{9}/L)	-1.12	0.87		-1.20	0.92	
Monocyte count (x10^{9}/L)	0.013	0.058		-0.025	0.00	
Total Protein (g/L)	UA	UA		1.75	11.3	
Albumin (g/L) ***($: see note in figure legend)***	UA	UA		0.25	6.36	
Urea (mmol/L)	-0.525	0.79		-2.72	0.21	<0.05
ALT (mmol/L)	UA	UA		UA	UA	
AST (mmol/L)	UA	UA		UA	UA	
AST:ALT	UA	UA		UA	UA	
Creatine Kinase (mmol/L)	UA	UA		UA	UA	

5.3.6 BL-CHOP chemotherapy reduces endogenous basal glucose levels but not handling

After 4 weeks of BL-CHOP therapy, mice exhibited greater rates of glucose uptake after the bolus challenge (10.5% lower total area under the curve (AUC)) which was highlighted by a tendency for plasma glucose levels to peak at lower concentrations from 5-30min (p<0.05 at 5min, p<0.01 at 15, and 30min). By 30 weeks, BL-CHOP therapy had suppressed basal serum glucose levels (through suppression of endogenous glucose production) by 18.4% at t0 at 12 weeks of age, and 25.8% at t0 at 30 weeks of age. BL-CHOP therapy-induced reductions in serum glucose levels (first seen at baseline) were preserved throughout both glucose challenges, with similar differences seen in total area under the curve as compared to VEH (-18.3% and -19.8% post BL-CHOP treatment at 12 and 30 weeks, respectively). Suppression of basal glucose levels aside, the shape of the curve and overall difference from VEH remained consistent throughout the challenge.

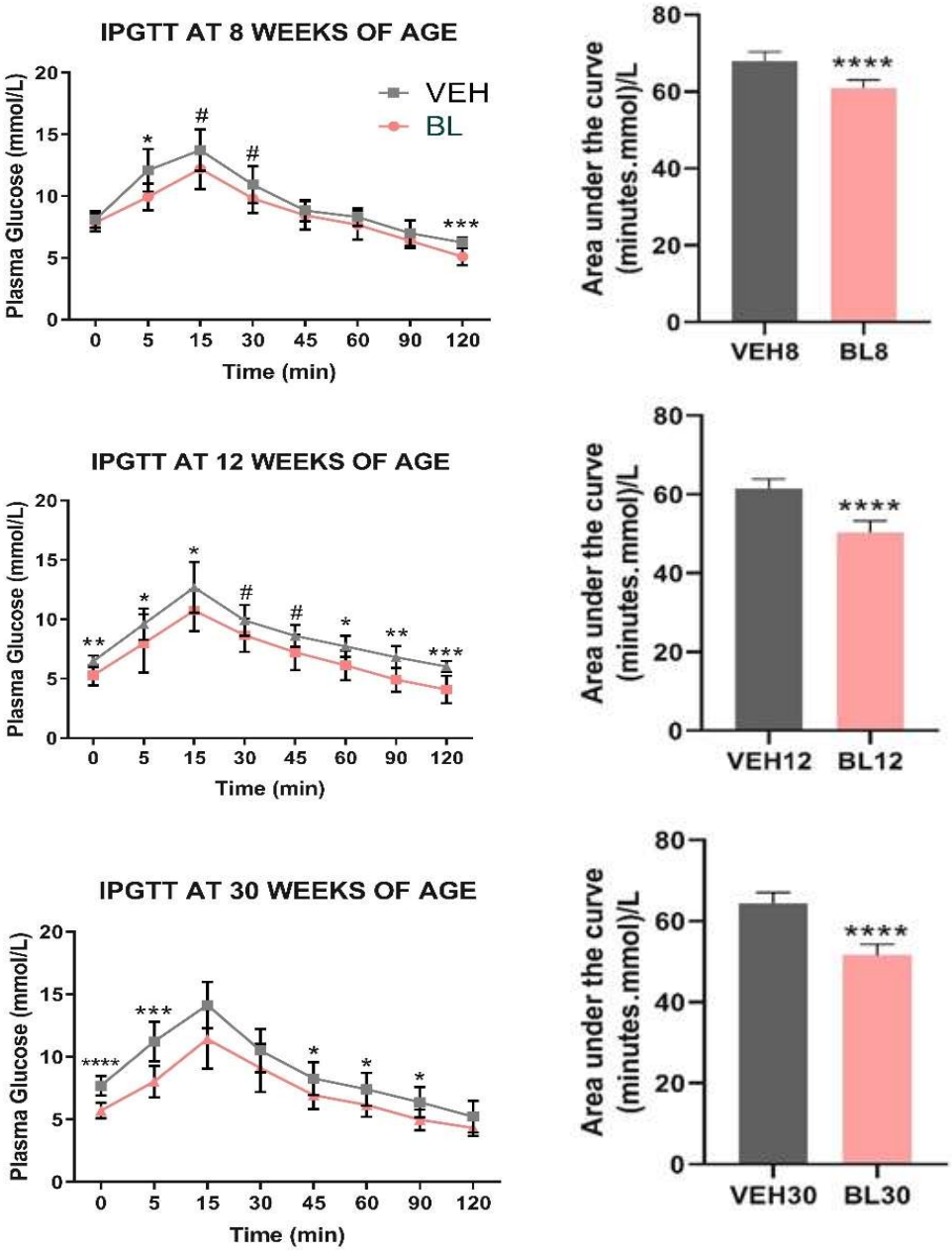

***Figure 5.8*: Changes in blood glucose levels (mmol/L) as in response to weight standardised glucose injection in VEH (V) and BL-CHOP (BL) treated mice at 12 and 30 weeks of age.** *Intraperitoneal glucose tolerance test shows progressive suppression of basal glucose levels over the lifespan after BL-CHOP therapy. The 8-week challenge shows improved glucose uptake from blood serum with no change to basal glucose levels however, at both 12 week and 30 weeks, basal glucose levels are greatly suppressed and no change to glucose handling post injection were noted. n=10. Data presented as mean±SD. Significance symbols: *:p<0.05, **p<0.005, ***p<0.001, ****:p<0.0001.*

5.3.7 Chronic muscle weakness induced by BL-CHOP therapy as measured by grip strength

Grip strength, performed as previously described in *Chapter 4; S4.2.2.2*, was severely impaired in BL-CHOP treated mice and was notable from 4 weeks of treatment (8 weeks of age). Remarkably, this strength impairment was sustained (i.e. at 30w), with grip strength comparable in 8-, 12- and 30-week old BL-CHOP treated mice (when corrected for body weight, refer Figure 5.9, $p>0.3$), illustrating no strength gain up to 30 weeks of age. In contrast, VEH treated mice increased grip strength by 20% between the 8- to 30-week sampling ages, such that BL-CHOP treated mice trailed their age-matched counterparts by 20% and 24% at 12 and 30 weeks, respectively.

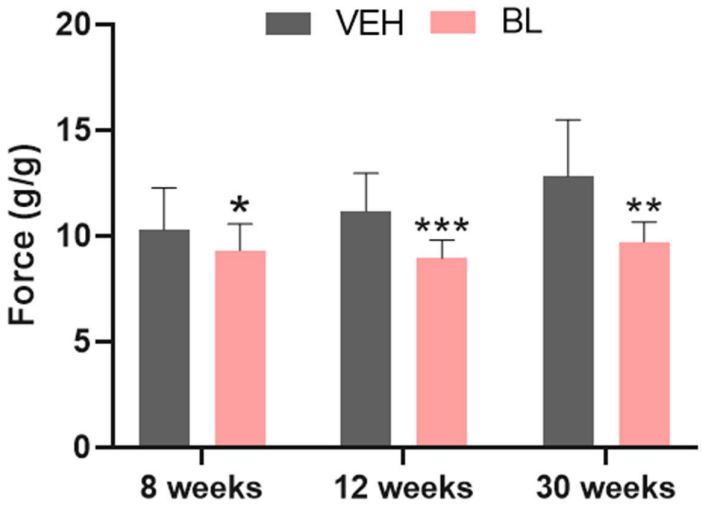

Figure 5.9: Animal grip strength corrected for bodyweight in VEH (V) and BL-CHOP (BL) treated mice at 12 and 30 weeks of age. *Bodyweight corrected strength suppressed by initial chemotherapy regimen which was not recovered from throughout the lifespan. Grip strength was suppressed in treatment group in all age groups when compared to VEH (VEH8 10.3±1.9, BL8 9.9±1.5; VEH12 11.2±1.8, BL12 8.9±0.9; VEH30 12.8±2.6 BL30 9.7±0.9). 12- and 30-week BL-CHOP force production did not statistically differ from BL8-week recordings (p>0.3). No significant differences in rate of fatigue between the groups was observed (measured by comparison of average force at each attempt compared between groups). n=15-20 with error expressed as SD. Significance symbols: *p=0.05, **p<0.005, ***p<0.001.*

5.3.8 Effects of BL-CHOP therapy on muscle contractile function

5.3.8.1 Muscle contractile properties

Structural analyses of the fast-twitch EDL and slow-twitch SOL highlighted that BL-CHOP therapy almost exclusively effected the EDL. An increase in CSA of 21% ($p<0.05$, Figure 5.10A) from VEH as a result of BL-CHOP therapy was observed, however 30-week EDL muscle returned to VEH levels. No changes to the CSA of SOL muscle was observed. An important measure which can be used to infer (albeit rudimentarily) whether structural changes have occurred is through the measurement of muscle optimal length (L_o). L_o describes the length at which optimal overlap of myosin and actin filaments within the sarcolemma occurs, resulting in maximal force production. Here, BL-CHOP induced a decline in L_o by 30% at 12-weeks of age ($p<0.005$, Figure 5.10B), was observed which was reversed by 30-weeks where L_o was increased by 23% in comparison to VEH ($p<0.001$, Figure 5.10C). The L_o of BL-CHOP treated SOL muscle was also observed to increase from 12 to 30-weeks of age (~5%, $p<0.05$, Figure 5.10D), however neither measure was statistically different from VEH.

BL-CHOP therapy caused an increase in Pt/Po ratio in both EDL (23%, $p=0.061$, Figure 5.10E) and SOL (32%, $p=0.058$, Figure 5.10F) muscle at 12-weeks of age when compared to VEH. This is in contrast to VEH where Pt/Po increased between the 12w and 30w muscles by 61% for EDL ($p<0.05$) and 15% for SOL ($p<0.05$), whereas the Pt/Po of EDL from BL-CHOP treated mice did not increase with age in either muscle (Figure 5.10E,F)

In VEH muscle, P_o (absolute force) and SP_o (specific force) production increased with age by almost 2 -fold in EDL muscle ($p<0.0001$ Figure 5.11A and $p<0.005$ Figure 5.11C respectively), with specific force falling by close to half in SOL muscle ($p<0.05$, Figure 5.11D).

In EDL muscle, BL-CHOP therapy did not affect either P_o or SP_o at 12 weeks of age, but decreased both measures by 30 weeks (P_o: -84%, $p<0.0001$; SP_o:-58%, $p<0.05$, Figure 5.11AC). In SOL muscle, there was no significant change to either P_o or SP_o at 12-weeks as a result of BL-CHOP therapy either, however, by 30-weeks, treatment had reduced P_o by 58% ($p<0.05$) and showed a tendency to reduce SP_o by 57% ($p=0.07$, Figure 5.11B,D).

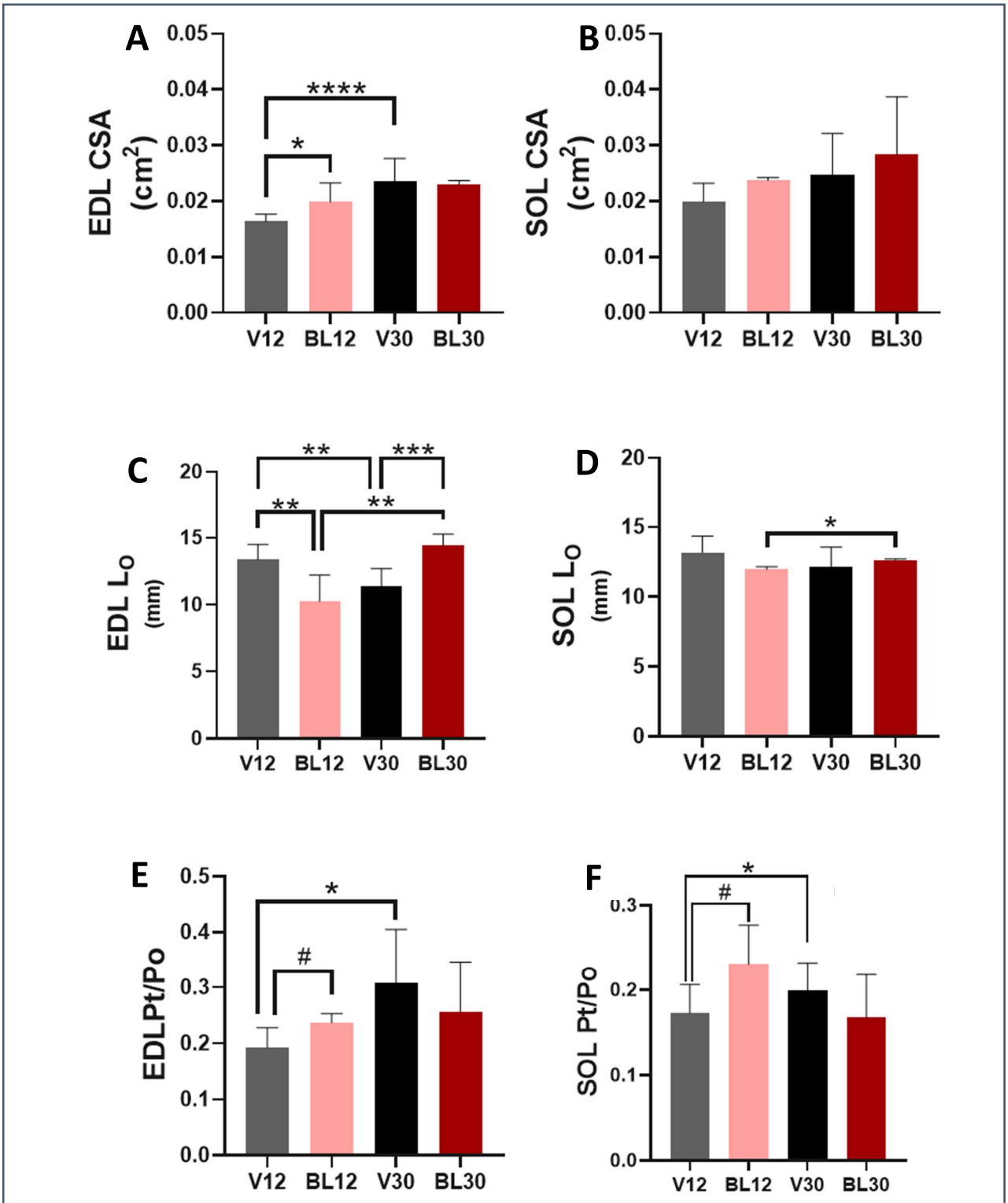

Figure 5.10: Cross-sectional area (CSA), optimal length (L_o) and peak twitch to tetanic ratio (P_t/P_o) of the fast-twitch extensor digitorum longus (EDL) and slow-twitch soleus (SOL) muscles of vehicle (VEH) and BL-CHOP (BL) treated mice at 12 and 30 weeks of age. *BL-CHOP therapy induced an EDL specific increase in CSA by 20% ($p<0.05$) however no change from 12-30 weeks in BL-CHOP treated EDL was observed (A). Treatment had no effect on SOL CSA (B). EDL L_o was decreased by 26% at 12 weeks and, interestingly, increased by 26% at 30 weeks when compared to time-controlled VEH samples. SOL L_o followed a similar trend, increasing by 5.5% between 12- and 30-weeks with BL-CHOP treatment ($p<0.05$). An increase in both EDL ($p=0.061$) and SOL ($p=0.058$) Pt/Po was observed in response to BL-CHOP when compared to VEH. n=3-10. With error expressed as SD. Significance symbols: (E) #:p=0.061, (F)#:p=0.058, *:p<0.05, **p<0.005, ***p<0.001, ****p<0.0001*

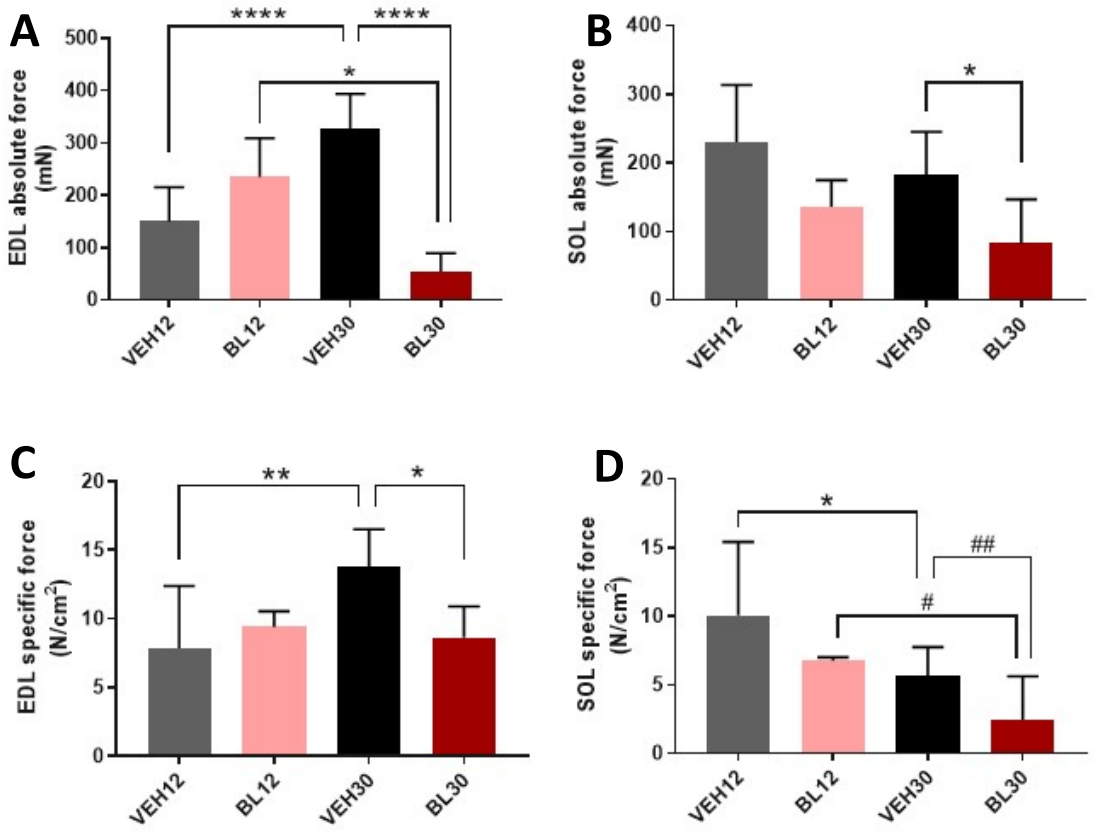

Figure 5.11 Absolute and specific force production of the fast-twitch extensor digitorum longus (EDL) and slow-twitch soleus (SOL) muscles from vehicle (VEH) and BL-CHOP (BL) treated mice at 12- and 30-weeks of age. *Treatment had no effect on absolute or specific force production in EDL or SOL at 12 weeks of age, however both measures were negatively affected by 30 weeks when compared to VEH with EDL and SOL absolute force reduced by 85% and 55% respectively. Specific force at 30-weeks was reduced by 38% and 57% for EDL and SOL respectively. n=2-10 (BL12 n=2-3 for EDL and SOL). Error expressed as SD where #:p=0.070 and ##:p=0.055 and *:p<0.05, **p<0.005, ****p<0.0001*

5.3.8.2 Force-frequency relationship

Development of force-frequency relationships are as described in previous chapters and are presented together with raw force values in Figure 5.12. In response to BL-CHOP chemotherapy, the force-frequency relationship in 12-week EDL muscle was shifted to the left, indicating elevated force-output at lower stimuli (significant changes of 230% at 10Hz, 240% at 30Hz and 159% 50Hz with BL-CHOP treatment compared to VEH, Figure 5.12B) . A similar shift was seen in 12-week SOL muscle (significant percent increases of 136% at 30Hz and 114% at 30Hz from VEH, Figure 5.12D). SOL force production, however, began to fail at 80Hz and testing ceased thereafter from concerns of muscle resilience (which is the standard protocol used for all muscles tested). Contrastingly, and consistent with reductions seen in absolute and specific forces in the previous section, at 30-weeks of age BL-CHOP treated EDL muscle decreased when compared to VEH in raw force output at all frequency levels (Figure 5.12E). Together with lowered force output, chemotherapy induced a rightward shift in the EDL muscle force-frequency relationship (significant percent decreases of 45% at 30Hz, 52% at 50Hz, 20% at 80Hz and 8% at 100Hz from VEH Figure 5.12F), a complete reversal of the phenotype seen at 12-weeks. This effect was fibre-type dependent as the force output of SOL muscle returned to VEH levels by 30-weeks.

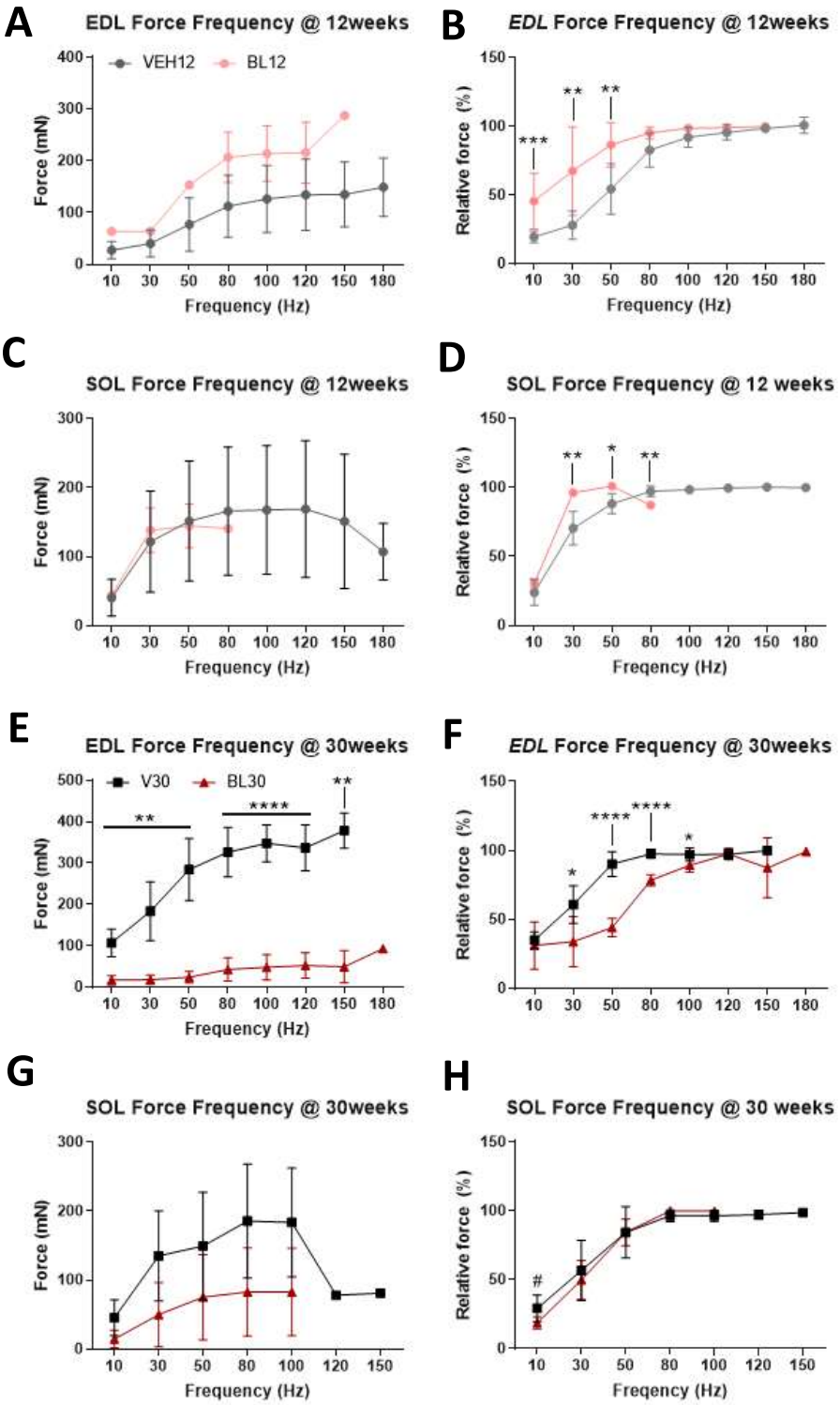

Figure 5.12: ***Effect of BL-CHOP therapy on absolute and relative force frequency relationship in fast-twitch extensor digitorum longus (EDL) and slow-twitch soleus (SOL) muscles from vehicle (V) and BL-CHOP (MB) treated mice at 12- and 30-weeks of age.*** *Muscle stimulation was of 500ms in tetanic length with consecutive 0.2ms pulses at 10, 30, 50, 80, 100, 120 and 150 Hz. There was no statistically significant treatment effect on raw force production at 12 weeks in either muscle, however SOL contraction was not viable after 80Hz or EDL after 180Hz. A leftward shift in relative force was seen in both muscles (VEH n=13 & 10 and BL-CHOP n=3 & 3 EDL and SOL respectively, A through D). The effect of treatment was pronounced after 30 weeks of age, with EDL raw forces at all frequencies considerably supressed (p<0.005, E). The force-frequency relationship was shifted to the right in treated EDL muscle (*p<0.05, *F). BL-CHOP treated SOL muscle at 30weeks did not show any statically significant changes in raw or relative forces aside from a strong trend at 10Hz (#: p=0.051, G & H).*

*n=10 & 15 for V30 EDL and SOL muscles respectively and n=4 for BL30 EDL and SOL muscles. Of note only one VEH sample at 30 weeks produced forces above 100Hz. Relative forces presented were normalised to the greatest force produced for that muscle and data presented as mean ± STD. n=3-10 assessed by two-way ANOVA with Tukey's post-hoc test with error expressed as SD. Significance symbols: *:p<0.05, **p<0.005, ***p<0.001, ****p<0.0001*

5.3.8.3 Fatigue properties

Next, the fatigue and recovery profile of the muscles was assessed, in both the EDL and SOL muscles. EDL muscle fatigue occurred almost immediately with lower force production in BL-CHOP compared to VEH, which was observed after 20s in 12-week (p<0.05) and 30-week (p=0.0507) animals (Figure 5.13). No recovery was observed in BL-CHOP treated 12- and 30-week EDL or 12-week SOL muscle, with contractional force not improving beyond the final force recorded in the fatigue protocol (p<0.05, Figure 5.13A-C). Although BL-CHOP treated SOL muscle was able to withstand the force-frequency protocol in the previous section, no SOL muscle was able to withstand the fatigue protocol, with all muscles either tearing or failing to respond to stimuli (Figure 5.13D).

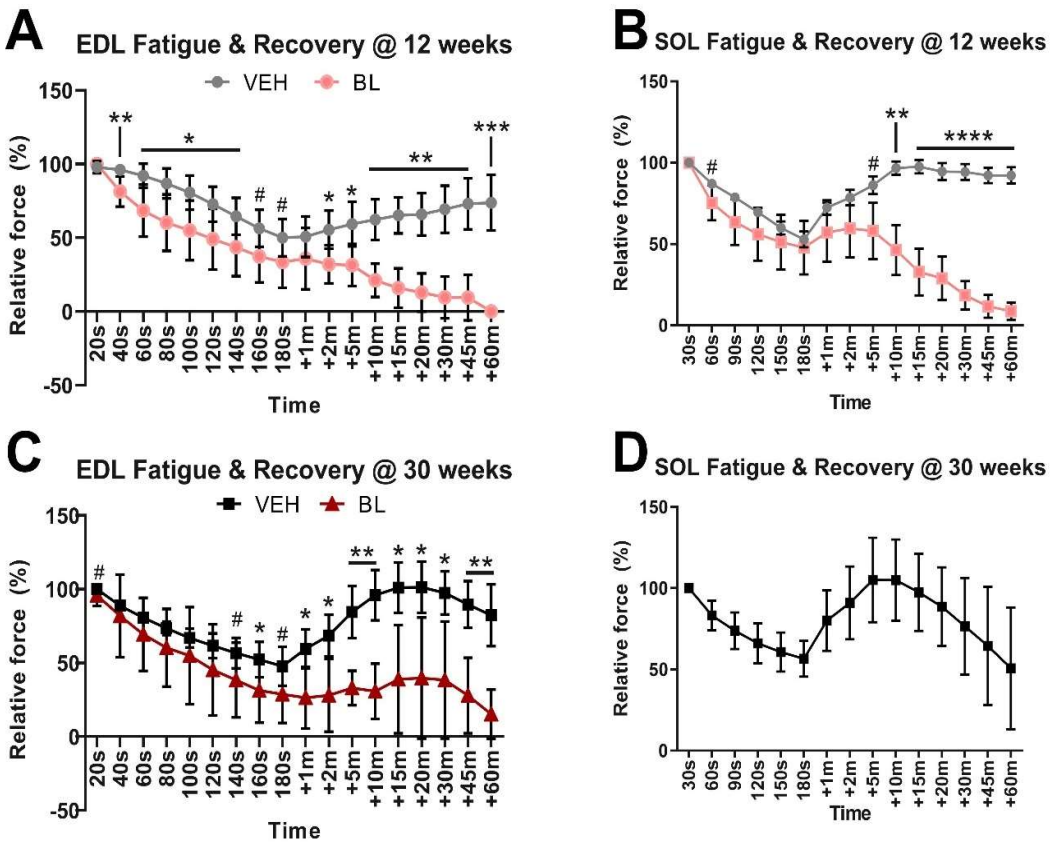

Figure 5.13: Effect of BL-CHOP therapy in juvenile mice on muscle endurance and recovery over the lifespan: *A+C) Endurance capacity was suppressed in NHBL treated EDL muscle at both 12 and 30 week time points where relative force was reduced, on average, by 24-28% at 12 weeks and 7-14% at 30 weeks. Recovery capacity was also greatly decreased in both groups which was consistently evident at 12 weeks, and inconsistently so (although significant) at 30 weeks. B) Endurance was largely unaffected in 12-week NHBL treated SOL muscle although recovery capacity was greatly hindered with muscles failing to recover between contractions resulting in a consistent decline in force output (rather than the expected increase). D) No NHBL SOL muscle could withstand the fatigue protocol with all excised SOL muscles failing to contract or tearing at some point throughout the 180s bout.* Data presented as mean ± STD. Significance symbols #:p=0.0507, **:p<0.05, **p<0.005, ***p<0.001, ****p<0.0001*

5.3.9 BL-CHOP therapy induces enduring skeletal muscle fibre atrophy

Histological analysis of H&E-stained TA fibres revealed a BL-CHOP-induced reduction of 19% and 5.5% in mean fibre cross-sectional area for 12- and 30-week old mice, respectively (refer Figure 5.14A). With such reductions in overall mean fibre size, the resultant leftward skew in 12-week old TA muscles was as expected due to a significant increase in smaller fibres (as compared to VEH, Figure 5.14C). A similar phenotype was seen in 30-week old TA fibres, with an increase (although non-significant) in smaller fibres (see Figure 5.14C and D).

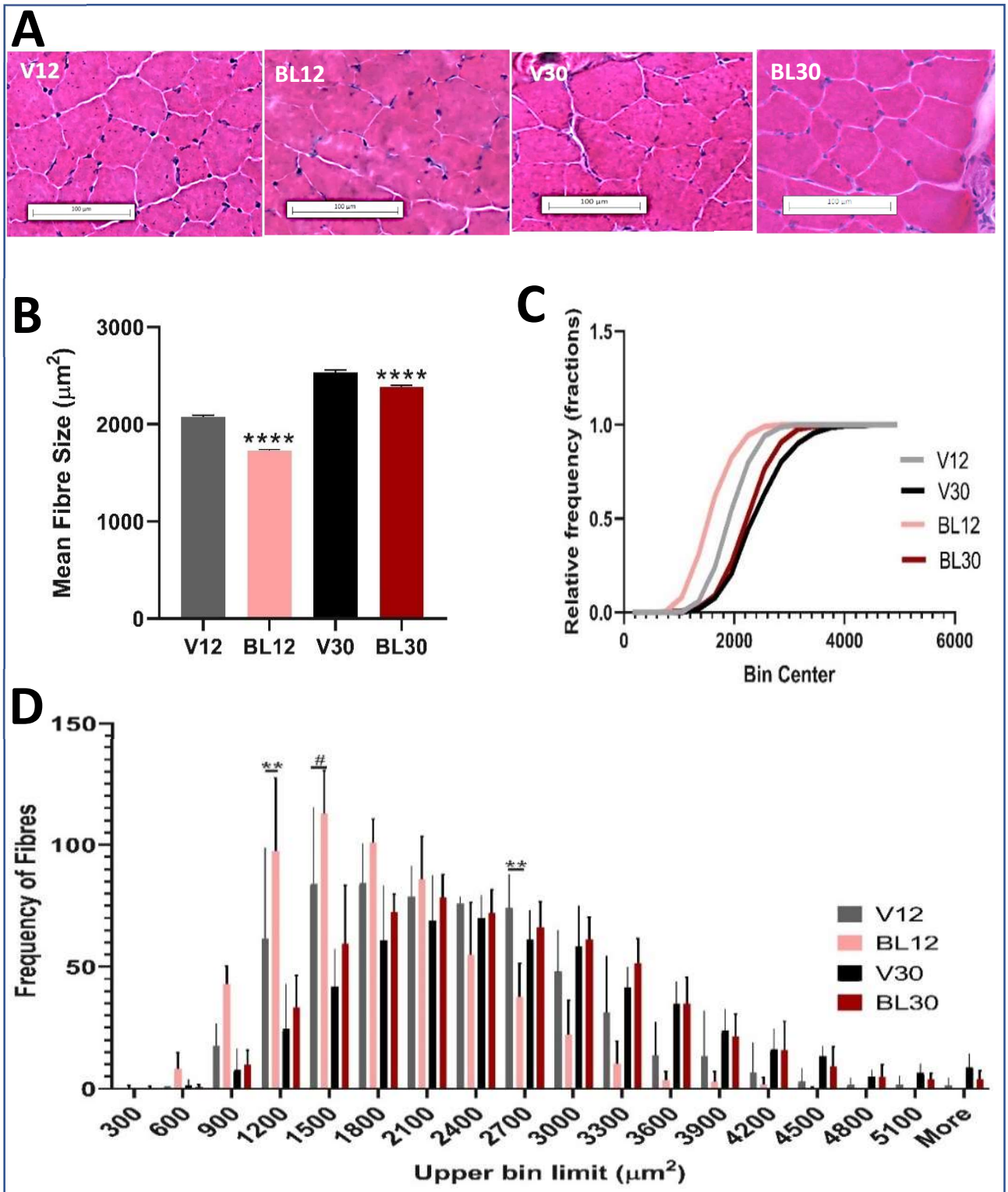

Figure 5.14: TA muscle fibre cross sectional area and fibre size frequency as measured in VEH (V) and BL-CHOP (BL) treated mice at 12 and 30 weeks of age. *A) Representative images of H&E stained TA muscle.* ***B)*** *Mean fibre size of VEH and BL-CHOP treated TA muscle fires showed significant reduction in average fibre size between VEH and treatment (n=~2400 fibres per group, data presented as mean±SEM)* ***C & D)*** *Fibre size frequency histogram showing treatment at 12 weeks skewed to the right with markedly increased BL12 fibre numbers in bins <2100 but less thereafter. BL30 treatment improved spread symmetry by increasing fibres in the middle bins alone. n=4-5 with ~600 fibres per n with data presented as mean±SD). Significance figures #=0.0523. Significance symbols: *:p<0.05, **p<0.005, ****p<0.0001. D) Data presented as the cumulative fraction of fibre distribution with error removed for ease of viewing.*

5.3.10 Mitochondrial function analysis

As discussed previously (*Chapter 1, S1.4.1 and Chapter 4, S4.3.8*), mitochondrial capacity is inextricably linked to skeletal muscle performance. As such, a decline in mitochondrial function will lead to a resultant decline in muscle performance. It should be noted prior to the presentation of these results that due to equipment failure, 30-week old BL-CHOP treated mice were unable to be assessed for mitochondrial function. Never-the-less, at the 12-week timepoint, there was no observable difference in basal mitochondrial oxygen consumption, ATP production or coupling efficiency were observed (Figure 5.15A, B and D respectively) indicating that mitochondrial coupling is unaffected by BL-CHOP treatment. No significant difference here serves to suggest that mitochondrial performance at baseline was unaffected by BL-CHOP therapy. These findings are in stark contrast to our previous findings which showed considerable mitochondrial dysfunction, which was expected here considering that anthracyclines are reduced at Complex 1 of (and thus remove electrons from) the electron transport chain.[1] However, although no effect was seen at baseline, BL-CHOP chemotherapy truncated mitochondrial ability to respond to metabolic stress by almost half (as measured by metabolic spare respiratory capacity, $p<0.05$, Figure 5.15C) which was characterised by a significantly reduced maximal respiration rate by 50% ($p<0.05$, Figure 5.16)

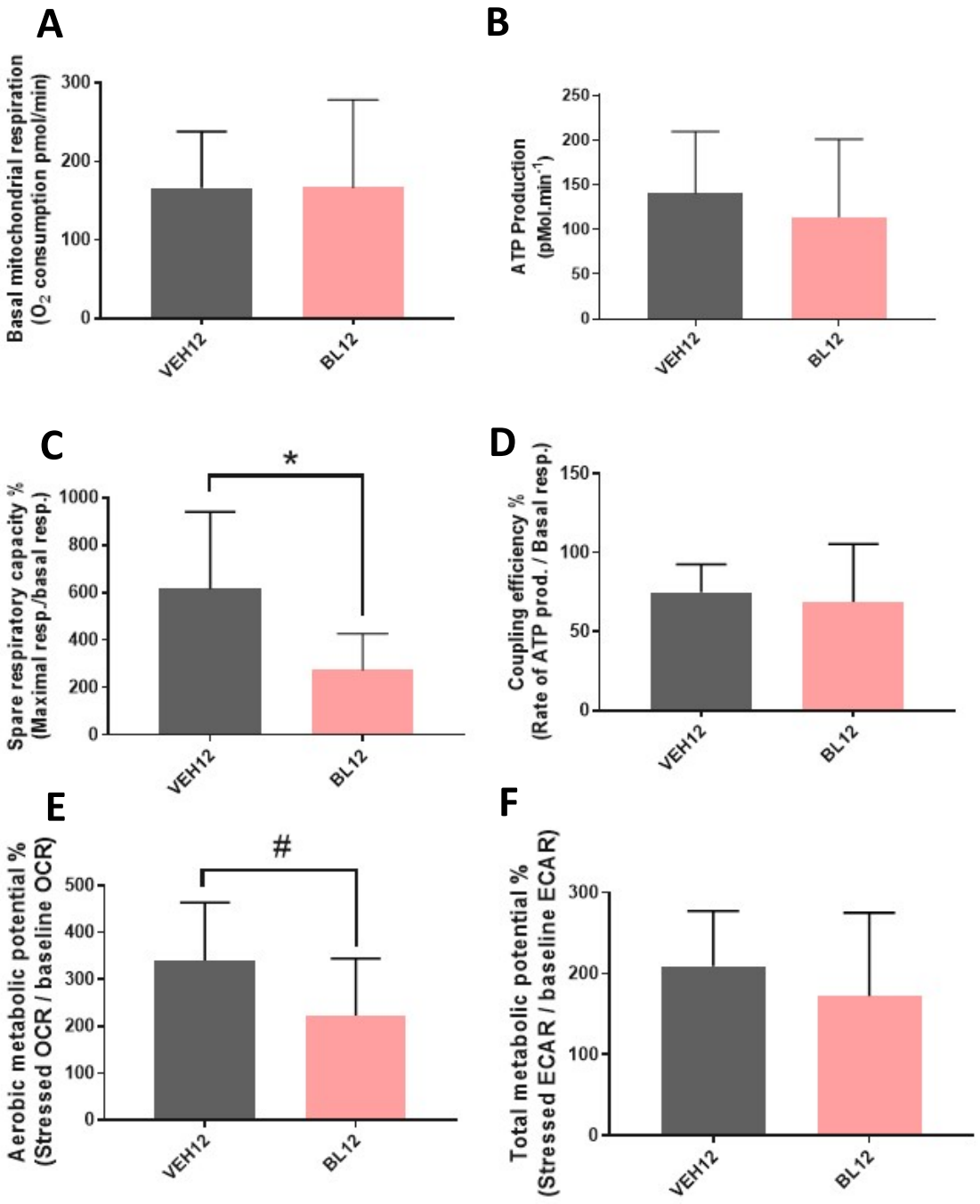

Figure 5.15 Mitochondrial respiratory function of VEH and BL-CHOP treated 12 week old mice *No changes in basal mitochondrial respiration (A), ATP production (B) or mitochondrial coupling efficiency (D) were measured in FDB fibres as a result of BL-CHOP therapy*. Spare respiratory capacity was reduced at 12-weeks after 2 rounds of BL-CHOP therapy by 56% (*$p<0.05$, C) which was coupled with a similar decrease in aerobic metabolic potential (-45% from VEH, $p=0.0858$, E). No change in anaerobic metabolic potential was observed (F). Data presented as mean±STD. Significance via student's t-test. VEH12 n=8, BL12 n=7*

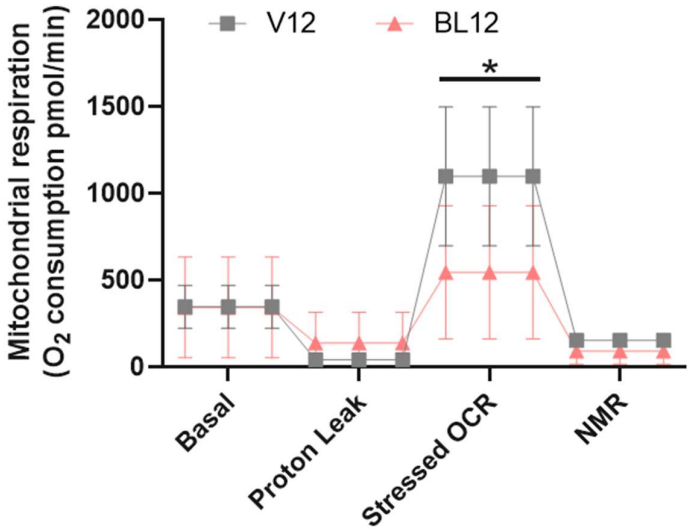

Figure 5.16 Changes to cellular oxygen consumption in response to mitochondrial inhibitors and stimulants induced by early-life BL-CHOP therapy at 12-weeks of age. *BL-CHOP therapy administered from 4-12 weeks of age significantly reduced significantly decreased maximal respiration by 50% ($p<0.001$) in 12-week mice. No significant changes to proton leak or non-mitochondrial respiration (NMR) was observed. Error expressed as SD where n=9-10. Significance symbols: *:p=0.05*

5.4 Discussion

CHOP therapy continues to be accepted as the gold standard therapy against paediatric NHBL [571]. However, and as with all chemotherapeutic regimens, patients undergoing therapy often develop severe, acute and chronic sequalae. Here, we investigated the effects of two rounds of IAMDF-modified CHOP therapy on juvenile mice. Importantly, these effects were measured both at the cessation of treatment at 12 weeks and well into adulthood at 30-weeks of age. These time points were selected to maximise clinical relevancy by matching sampling points in mice to the age of paediatric patients undergoing therapy between 5-12 years of age, with follow ups after chemotherapy has ceased (refer to *Chapter 2, Step 7* for further details). In doing so, we demonstrated that the IAMDF modified CHOP therapy used here in mice, adequately replicates the clinical picture induced by CHOP therapy in humans. Here, we show that IAMDF-modified CHOP therapy in mice 1) greatly impaired growth rates and overall survival; 2) induced severe organ toxicity inclusive of cardiomyopathy and renal-, liver- and gastrointestinal-opathies; 3) induced lifelong skeletal muscle dysfunction and wasting which was characterised by reduced grip strength, mean muscle fibre size, *ex vivo* muscle endurance and recovery capacity; and 4) truncated mitochondrial metabolic flexibility at 12-weeks. This study presents a mouse model which adequately replicates the clinical sequalae induced by CHOP therapy and emphasises that CI-SMDW is a critical and enduring side-effect of juvenile chemotherapy. Further, this study also supports our hypothesis that BL-CHOP chemotherapy induces mitochondrial dysfunction (at least at 12-weeks of age) which is characterised by an inability to increase metabolic output in times of demand.

5.4.1 CHOP therapy induces severe lethality and systemic toxicity in mice

The IAMDF modified CHOP therapy used herein, produced similar adverse events as previously described by others in humans [338,340,341,566], with 14% (7/49) of mice succumbing to treatment toxicity before completion of the regimen (refer *S5.3.1*). Of those that were observed for 30 weeks post treatment cessation, 33% (10/30) survived the regimen – producing a survival rate far worse than that described in the literature for humans. Upon necropsy, mice showed signs of severe systemic toxicity including right ventricular dilatation and hepatocellular swelling (although not confirmed in wet-weight analysis, Figure 5.7). These gross anatomical observations indicate a state of congestive heart failure which is a well described sequalae of CHOP therapy, or, more specifically; that doxorubicin with concomitant cyclophosphamide increases risk of developing congestive heart failure due to an elevated state of oxidative stress within the cardiomyocytes [369,572-574]. Also consistent with clinical findings, mice were found to present with diffuse gastrointestinal inflammation and, though mostly in necropsy cases, skipping (non-continuous) necrotic lesions throughout the intestines. When considered with the a high incidence rate of toxic megacolon in BL-CHOP treated mice, chemotherapy-induced mucositis underpinned by an elevated oxidative state within the mucosae is the likely cause, as indicated by others [575,576]. Although not histologically confirmed by us here, mucositis is also a well described finding in patients undergoing CHOP therapy with some studies reporting incidence rates of up to 85% [370,577].

Concordant with a diagnosis of CHOP-induced mucositis, food consumption was reduced during active treatment periods and consistently after the second round of therapy

– indicating a state of gastrointestinal distress (Figure 5.5). Observationally, mice who were observed to consistently lose body weight over a 3- day period (15% cumulative), continued to lose body weight and ultimately died. In response to initial deaths, mice who matched this pattern of weight-loss were isolated and fed a watered and mashed food substitute which improved survival in some cases. With all CHOP treated groups consistently consuming less food for 10 days post second round of therapy, the mash food substitute replaced hard foods which, again, improved survival outcomes. Nutritional deficit due to reduced food intake is a common hurdle of chemotherapy, which is often combated by supplemental food alternatives [578,579]. As could be expected with a reduction in food consumption, a concomitant drop in body weight was recorded during active periods of chemotherapy. Body weight was significantly reduced in CHOP treated mice with a loss of 9.95% from pre-therapy weight (a difference of 21.64% to VEH, $p<0.0001$). Interestingly, after each chemotherapeutic insult had ceased, mice exhibited "catch-up growth" which has been described as a restoration of original growth patterns after an insult has been alleviated [580]. After 30-weeks, however, the surviving mice (33% of mice that commenced therapy) returned to VEH weight.

μ-CT analysis highlights that the early loss of mass could be attributed to a loss of lean muscle mass, with BL-CHOP treated mice losing ~15% of hind leg volume compared to aged-matched, VEH treated mice. Although mice which received chemotherapy returned to VEH body weight by 30 weeks, survivors of childhood chemotherapy are observed to have increased body and intramuscular fat and less lean mass than the healthy population in their adult years[18,581]. This is likely the case here as BL-CHOP treated mice did not replenish muscle mass, but rather, had 16% less volume in their hind-limbs than VEH counterparts at 30w of age. Interestingly, there was no change in the hind-limb muscle weight from the contra-lateral limb, indicating these changes are not as straight forward as a loss of total mass. Although

our μ-CT analysis measured for volume and not lean mass, when considered with the reduction in specific force (SP_o) as measured during contractile function analyses and reduced fibre size as measured by histology, these data collectively suggest a decline in skeletal muscle size and quality and thus contractile strength; where lean mass has likely been replaced with non-contractile tissue, like that seen in survivors of childhood chemotherapy.

Together with altered body composition (high fat mass to muscle mass ratio), aberrant glucose handling has also been linked to malnutrition during childhood. A study into malnourished children (sans chemotherapy or cancer aetiology) showed that a weight deficit which exceeded 25% when compared to healthy controls was a prognostic factor for life-long hypoglycaemia [582]. CHOP-treated mice were also commonly observed to suffer from hepatic steatosis which is indicative of malnourishment when found in juveniles [583]. Glucose handling here, however was not found to be dysfunctional *per se* in that BL-CHOP mice receiving a glucose bolus challenge responded with similar rises and falls (both in rate and total amount) in blood glucose levels (Figure 5.8). What was significant, however, was that from 12-weeks of age, BL-CHOP mice presented with a significant reduction in endogenous glucose levels which was exacerbated with age (18.4%, $p<0.005$ and 25.8%, $p<0.0001$ at 12- and 30-weeks respectively). This reduction in endogenous glucose level is likely a further manifestation of malnourishment, however, mice only experienced periods of malnourishment and went on to experience catch-up, rebound growth. Although further *in vivo* insulin resistance studies would be required to definitively catergorise the underlying aetiology, it could be reasoned that elevated insulin levels could underpin the endured hypoglycaemia seen throughout the lifespan (due to insulin-mediated cellular glucose uptake). A study by Mittelman *et al* suggests

this is due to insulin suppression of adipocyte breakdown, resulting in decreased free fatty acids and gluconeogenisis [584]. This theory has been supported by a large epideimilogical study which longditundinally followed children whom exhibited catch-up growth in their formative years. The study highlights that these children were more likely to develop hyperinsulinaemia, hypoglycaemia and elevated fat storage – likely to protect them against further bouts of malnutrition [570].

5.4.2 CI-SMDW in CHOP treated mice is characterised by skeletal muscle atrophy, weakness, fatigue and poor post-exercise recovery

Mice treated with the BL-CHOP regimen did not improve grip strength (when corrected for bodyweight) over the life span, with force produced at 12- and 30- weeks comparable to 8-week force production (p>0.3), suggestive of mass-independent dysfunction. These findings in mice are similar to those seen in chemotherapy survivors, with Ness *et al* reporting survivors experience chronic reductions in strength and endurance capacity over the lifespan [18,555]. Out of the CHOP therapy constituents, doxorubicin has been indicated by many to cause severe and enduring damage to the skeletal muscle [143,585]. Doxorubicin-induced increases in intra-cellular ROS has been linked to the activation of muscle catabolism pathways [239,263,586]. Thus, the doxorubicin constituent of BL-CHOP therapy could be recognised as a potential, yet major, contributing factor to the muscle atrophy and weakness seen within this study. This mechanism, combined with the caloric reduction we observed here, suggests that muscle weakness and atrophy (together with body-weight loss) is likely a result of a two-pronged insult: one which induces skeletal muscle atrophy due to

increases in skeletal muscle ROS, and one that inadvertently activates muscle catabolism by activating starvation-induced muscle autophagy.

Further impeding a survivor's quality of life, is the characteristic reduction in skeletal muscle endurance and recovery capacity which is endured long-after chemotherapy has ceased [93,144,587]. Muscle fatiguability and recovery capacity in BL-CHOP treated mice showed fast-twitch muscles (as seen in EDL) sustained significant reductions in endurance capacity, which was characterised by a faster, more sustained reduction in force output during exercise (Figure 5.13). Strikingly, EDL at 12- and 30-weeks, and SOL muscle at 12 weeks failed to recover after the exercise bout, with BL-CHOP-treated muscle failing completely after an hour of rest (interspersed with maximal contractions). Moreover, the force-frequency relationship in 12-week EDL muscle was shifted to the left, indicating an elevated force-output at lower stimuli treatment compared to VEH. Alternatively, these data could indicate an increase in muscle Ca^{2+} sensitivity as an adaption to accommodate an improvement in force production. Although further investigations would be needed to substantiate the mechanisms of this, we hypothesise that this is indicative of a muscle fibre change towards a slower, weaker phenotype. These data which show a state of chemotherapy-induced skeletal muscle dysfunction, weakness and fatigue are consistent with the sequalae observed in childhood chemotherapy survivors. Further, our findings here serve to suggest that the skeletal muscle dysfunction experienced by survivors is more likely underpinned by structural contractile dysfunction rather than a sole loss of muscle mass.

5.4.3 Chemotherapy-induced mitochondrial dysfunction: An underlying pathology of SMDW?

Doxorubicin, an anthracycline class chemotherapy and key agent in BL-CHOP therapy, is directly metabolised within the mitochondria into its active form, removing electrons from the electron transport chain and producing ROS in the process (refer to *Chapter 1, S1.4.1* for review). As mentioned previously, and above, it is these ROS that are believed to activate catabolic pathways within the skeletal muscle. Moreover, vincristine has also been implicated in elevated ROS production[588]. High levels of ROS have been shown to induce structural damage to mitochondrial enzymes, ultimately hindering their oxidative performance. [159,220,589-592] Reductions in mitochondrial performance precedes reductions in skeletal muscle performance, particularly endurance and recovery capacity; as the powerhouse organelle of the cell cannot meet the energy requirements of the contractile tissue. With doxorubicin administration, together with clearly described deficits in skeletal muscle performance, mitochondrial dysfunction was expected. Skeletal muscle mitochondria from 12-week old BL-CHOP treated mice exhibited a 44% decrease (p<0.05) in spare respiratory capacity – an indication that the mitochondria's ability to meet energy demands during times of stress was impeded. In conjunction with the observed decrease in oxidative metabolic potential (-35% when compared to VEH, p=0.085), we suggest that BL-CHOP therapy (likely due to doxorubicin metabolism) inhibits the oxidative capacity of the mitochondria, and the ability of the muscle to defend metabolic stress. Although no clear link has been made here, a study investigating the effects of hepatic steatosis (which is indeed what was found here in CHOP treated mice) clearly linked the condition to defective mitochondrial respiration [593], further supporting our

hypothesis that CHOP therapy is acting to disrupt metabolic homeostasis and mitochondrial stress response capacity.

5.5 Chapter summary

In summary, these results demonstrate that the IMADF-modified CHOP therapy produces a clinically similar side-effect profile to that experienced in human patients. This highlights the BL-CHOP mouse model as an appropriate pre-clinical investigative tool upon which further investigations into how both the BL-CHOP sequalae can be induced, and how the regimen can be improved, can be conducted. This study also highlighted that nutritional deficit and long-term irregular glucose handling, likely driven by chemotherapy-induced gastrointestinal pathology, was an important and under-recognised driver of CI-SMDW. We also showed that characteristic CHOP therapy toxicity, underscored by cardiomyopathy, skeletal muscle dysfunction and atrophy, was concomitant with and likely underpinned by mitochondrial dysfunction.

With these results, for the most part, replicating what was observed in Chapter 4 as a result of MB-LCV therapy, similarities between the two side-effect profiles can be drawn. Mitochondrial dysfunction is a clear mechanism which underpins the skeletal muscle dysfunction seen, which was present regardless of regimen or the involved chemotherapeutic constituents (as seen in *Chapters 3-5,* with ALL-POMP, MB-LCV and BL-CHOP regimens) . Thus,

targeting the mitochondria to afford protection to the organelles respiratory function may indeed prove therapeutic against CI-SMDW.

Chapter 6

Therapeutic efficacy of Idebenone against chemotherapy-induced skeletal muscle dysfunction and wasting in Juvenile Mice

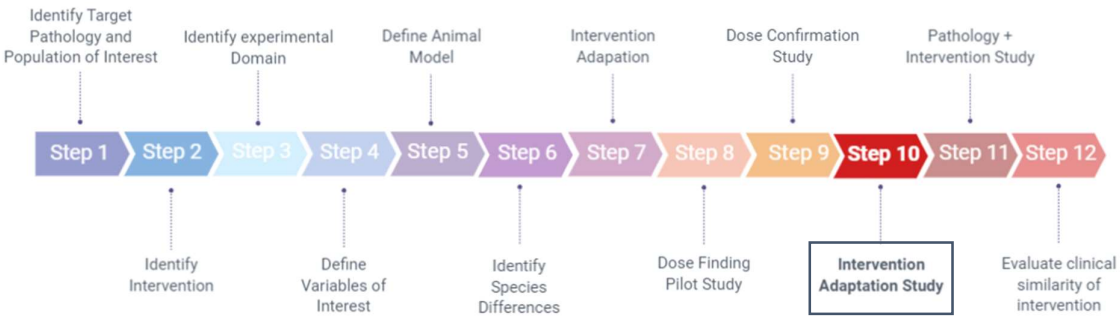

6.1 Introduction

In *Chapter 4* and *5*, we have established that chemotherapy induces skeletal muscle dysfunction and wasting in both the Intervention Animal Model Development Framework (IAMDF) modified MB-LCV and BL-CHOP regimens *in vivo*. With the side-effect profile of these chemotherapy regimens mostly matching the reported side-effect profile of patients in the clinical setting, it is likely that the underlying molecular mechanisms of CI-SMDW are comparable. As highlighted earlier in this thesis, it is important to recognise that side-effects induced by the chemotherapy regimens can be both independent of and cumulative upon the sequalae induced by cancer. This is an important step in characterising the modes of action upon which they induce their debilitating side effects. With mitochondrial dysfunction seeming to underpin the skeletal muscle pathology seen in both the MB-LCV and BL-CHOP regimens, as well as the mitochondria being identified by us (and others) previously as a potential therapeutic target (as outlined in Chapter 1 and 2) using a targeted mitochondrial therapy to afford protection against chemotherapy-induced toxicity was decided upon. Further, by observing the effect of a pharmacological agent with a known mechanism of action which targets the mitochondria, the chemotherapy-induced mitochondrial dysfunction seen here could be better characterised.

We have previously investigated the effects of a two-week, metronomic oxaliplatin (OXA) (a platinum based chemotherapeutic agent of similar molecular structure and mode of action as CDDP included in the LCV regimen) administration, on adult mice. We showed that two weeks (nine individual doses) of OXA administration induced a 15% (p<0.05) muscle mass

loss and increased mtROS production which was likely linked to the observed OXA-induced platinum accumulation within the mitochondria [159,160]. These findings suggest that OXA can enter the mitochondria and induce dysfunction through platinum adduction of the mtDNA. We also established that Idebenone (IDEB), a synthetic Coenzyme Q10 (CoQ10) analogue [291,292] (discussed in length in *Chapter 1 S1.6.1*), was an effective co-therapeutic which directly targeted the mitochondria and protected the organelle during the two-week chemotherapy regimen. When administered during OXA treatment, IDEB co-therapy not only protected against the observed OXA-induced mitochondrial dysfunction, but also protected against OXA-induced lean muscle loss in mice [272]. Ultimately, however, the model used chemotherapy regimens which were not representative of clinically utilised treatments (i.e. single agents delivered in nine doses over two weeks), thus the results merely established IDEB as a potential candidate for future, more clinically relevant, pre-clinical animal studies. Moreover, OXA, in some instances, is no longer used as the gold standard treatment of paediatric cancers and is situationally replaced with CDDP, further highlighting the need for a modified, updated trial. As discussed in *Chapter 1. S1.6.1*, targeting the mitochondria to afford protection against chemotherapeutic insult, particularly by mediating ROS, could also theoretically provide downstream protection to the skeletal muscle. Although other co-therapeutics were identified in the literature review component of this thesis, IDEB was selected based on its mechanism of action and its potential to rectify the mitochondrial linked pathology as seen with both MB-LCV and BL-CHOP therapy by reducing mtROS and driving mitochondrial function. As both regimens induced mitochondrial dysfunction which was characterised by a reduced mitochondrial spare respiratory capacity, it was theorised co-treatment with a synthetic CoQ10 analogue would improve mitochondrial respiration by chaperoning electrons directly to the ETC (IDEB and its mechanism of action is discussed at greater lengths in *Chapter*

1, S1.4). Moreover, as IDEB is primarily thought to scavenge these electrons from ROS and other free radicals, concomitant therapy with IDEB should serve to increase both mitochondrial respiration and protect the mitochondria from elevated ROS which is characteristic of chemotherapy [1,159,160,239,272,588,590]. As elevated ROS has also been inextricably linked to muscle atrophy pathways [1,162,186,217,248,275,590,594-596], we hypothesise that concomitant treatment of IDEB with MB-LCV and BL-CHOP therapy will protect against the CI-SMDW phenotype associated with both these regimens by improving mitochondrial function and protecting against CI-SMDW. Thus, in this chapter we aim to evaluate the efficacy of IDEB co-therapy as a therapeutic against CI-SMDW as induced by BL-CHOP and MB-LCV therapy. To do this, we will measure markers of skeletal muscle mass and function, mitochondrial function, as well as an assessment of overall toxicity of the regimens when delivered in concert with IDEB.

6.2 Method

Methods are as per Chapter 3, 4 and 5, unless otherwise stated below. All investigations as outlined in *Chapter 4, S4.2.2* were performed here with no additions. Statistical analysis methods are as previously described in *Chapter 4, S4.2.2.5*.

6.2.1 Animals

All animal housing conditions are as previously described. Additionally, 40 balb/c mice were randomly allocated into either MB-LCV+IDEB or NHBL-CHOP+IDEB treatment groups

and housed in cages of 5 (henceforth referred to as MBi-LCV or BLi-CHOP groups). Originally, all mice were allocated to the 12-week time point with the aim of being culled for analysis on the last day of the regimen (D56 of treatment/D84 of life). Due to the lifelong sequalae associated with BL-CHOP treatment and the 100% survival rate to the 11-week time point in BLi-CHOP treated mice (BL-CHOP therapy alone resulted in an 87.5% survival rate to 12 weeks), it was decided that 10 mice be continued up to 30 weeks of life. All MBi-LCV mice were culled at 12 weeks of age and analysed. Additional food mash was given to IDEB co-therapy groups on the days corresponding with chemotherapy-only treated counterparts. As MBi-LCV induced greater toxicity than MB-LCV alone, mice which were considered unwell and required supplemental mash were isolated in a separate cage for feeding. Both MBi-LCV and BLi-CHOP groups are compared to MB-LCV and BL-CHOP data presented in *Chapters 4* and *5* respectively. VEH groups shown are the same as previous chapters.

6.2.1.1 Treatment summary

Following on from *Chapter 4 and 5*, this chapter includes the MB-LCV and BL-CHOP therapies with the addition of daily IDEB (100mg/kg/day) delivered in saline solution (0.9% sodium chloride in sterile water) via oral gavage for 56 days (the length of two chemotherapy courses). As DOX is reduced into its active semiquinone state within the mitochondria (refer to Chapter 1), we hypothesise that IDEB co-therapy would increase the rate of DOX metabolism into its active form due to IDEB's highly reducing (antioxidant) nature. Since DOX exhibits rapid tissue uptake and an initial distribution half-life of 5 minutes [597], IDEB was

administered 24 hours after DOX, on days 2-28 of the BL-CHOP course only (as described in *Chapter 5*, and Table 6.1 below).

Table 6.1: Drug names, delivery modes and doses for selected BLi-CHOP and MBi-LCV regimens.

	Drug	*Mode of delivery*	*Delivery times*	*Dose per delivery*	*Total daily dose*	*Days delivered per regimen*
BLi-CHOP	Cyclophosphamide (CPM)	Oral gavage	7-9am + 1-3pm	180.00 mg/kg	360.00 mg/kg	1-6
	Vincristine (VCR)	Intraperitoneal injection	7-9am + 1-3pm	0.39 mg/kg	0.78 mg/kg	1,6
	Prednisone (PRED)	Oral Gavage	7-9am + 1-3pm	11.81 mg/kg	23.62 mg/kg	1-6
	Doxorubicin (DOX)	Intraperitoneal injection	7-9am + 1-3pm	2.60 mg/kg	5.20 mg/kg	1
	Idebenone (IDEB)	**Oral Gavage**	**7-9am**	**100mg/kg**	**100mg/kg**	**2-28***
MB-LCV	Lomustine (CCNU)	Oral gavage	7-9am + 1-3pm	11.07 mg/kg	22.14 mg/kg	1
	Cisplatin (CDDP)	Intraperitoneal injection	7-9am + 1-3pm	11.07 mg/kg	22.14 mg/kg	2
	Vincristine (VCR)	Intraperitoneal injection	7-9am + 1-3pm	0.22 mg/kg	0.44 mg/kg	2, 7,14
	Idebenone (IDEB)	**Oral Gavage**	**7-9am**	**100mg/kg**	**100mg/kg**	**1-28**

*Idebenone not administered on days where Doxorubicin is administered due to drug interactions (refer Chapter 1 and [1])

6.2.2 Adaptions to mitochondrial analysis with the Seahorse XF24

As Idebenone seemed to reduce the ability for Antimycin A (a mitochondrial complex III inhibitor) to shut down the respiratory chain, we were unable to use the non-mitochondrial respiration (NMR) measure usually attributed to oxygen consumption after Antimycin A injection. To correct for this, the NMR measure was added to the measures of basal mitochondrial respiration, ATP-production associated oxygen consumption and proton leak associated oxygen consumption, as the Seahorse XF24 software automatically subtracts NMR from these measures. Although NMR was negligible in both the MB-LCV and BL-CHOP regimens alone, although unlikely, there is the potential that NMR was elevated with IDEB and that this was masked with our amendment. This is a notable limitation with our

mitochondrial investigations and one that has been discussed in the thesis limitations in *Chapter 7*.

6.3 Results

6.3.1 Effects of IDEB on survival rates in MBi-LCV and BLi-CHOP combination regimens

Co-administration with BL-CHOP therapy mitigated chemotherapy associated mortality. Specifically, BL-CHOP 12-week survival was improved from 85.7% (42/49) to 100% (20/20) with adjuvant IDEB therapy, while 30-week survival was improved from 33% (10/30) to 100% (7/7) (p<0.05, RR=0.446, Figure 6.1). In contrast, adjuvant IDEB treatment with MB-LCV increased mortality during the regimen, with two deaths occurring at week 1 and 3 during the first course of treatment (week 4 and 7 of life respectively, p=0.078, RR=1.1). Mice were visibly unwell, anaemic, and exhibited rapid weight loss in the days preceding death (mouse 1: 12.5% loss of BW over 6 days; mouse 2: 5.7% loss of BW over 4 days, discussed previously in S4.3.2). The efficacy of adjuvant therapeutics when co-administered with chemotherapy regimens are often measured on whether they improve mortality rates. As such, co-administration of IDEB with MB-LCV therapy was ceased at 12 weeks, with no mice proceeding to the 30-week endpoint.

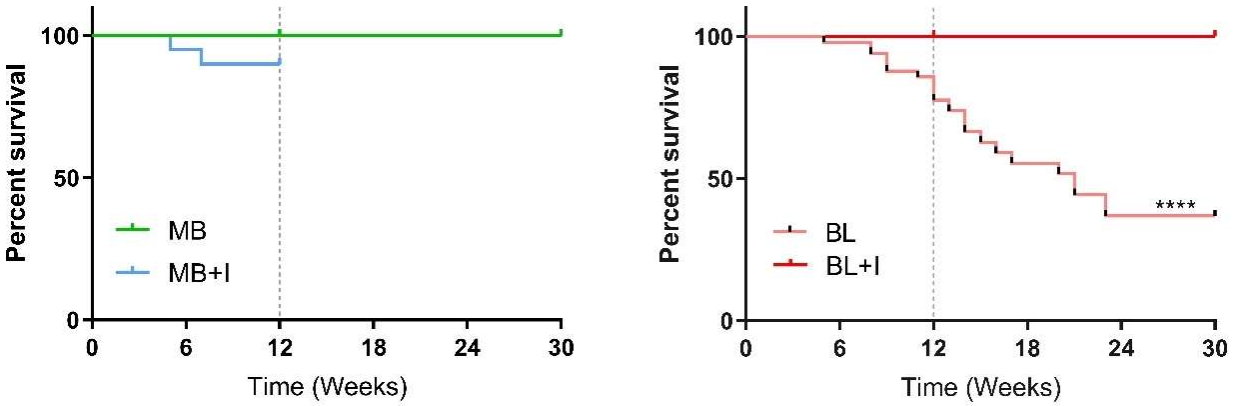

Figure 6.1: Animal survival in response to (left) MB-LCV (MB) and MBi-LCV (MBi) therapy and, (right) BL-CHOP (BL) and BLi-CHOP (BLi) treated mice at 12 and 30 weeks of age. *Co-administration of IDEB exacerbated mortality in MB-LCV therapy but alleviates BL-CHOP associated mortality. A) MB-LCV n = 0/35 <12 weeks, n = 0/20 >12 weeks. MBi--LCV n = 2/20 < 12 weeks. RR=1.1* ***B)*** *BL-CHOP n = 7/49 <12 weeks, n = 20/30 >12 weeks. BLi-CHOP n = 0/20 <12 weeks, n = 0/7 > 12 weeks, RR=0.445. Non-survival event recorded as either ethical euthanasia or natural death. Data presented herein as deaths/total alive at end point. Significance via Log-rank (Mantel-Cox) test.*

6.3.2 Effects of adjunct IDEB therapy on MB-LCV and BL-CHOP growth rates and food consumption

Co-administration with IDEB increased the overall growth rates of mice throughout the treatment regimen particularly over the first 12 weeks as compared to base chemotherapy regimens (MBi-LCV +20%, $p<0.0001$ Figure 6.2; and BLi-CHOP 54%, $p<0.0001$ Figure 6.3). Together with an elevated growth rate, IDEB administration with MB-LCV resulted in a greater loss of weight during the second round of therapy, with mice losing up to 29.9% of their body weight (MBi-LCV rate of weight loss during days 29-35 was 17%, where MB-LCV rate of weight loss was 5% over the same period, $p<0.001$, Figure 6.2). This effect was unique to the MBi-LCV treatment and was not replicated when IDEB was co-administered with the BL-CHOP regimen. Overall, IDEB co-therapy promoted greater growth when administered with mice ending the observation period with weights equal to or greater than VEH mice. Specifically, VEH mice at 12 weeks weighed +168% and MBi-LCV mice weighed +181% from their starting weight (VEH to MBi-LCV at D56 $p>0.05$, Figure 6.2). VEH mice at 30 weeks weighed +203% and BLi-CHOP mice weighed +252% from their starting weight (VEH to BLi-CHOP at D182 $p<0.007$, Figure 6.3).

Curiously, total food consumption was decreased in MBi-LCV treated groups (in comparison to MB-LCV alone, ~-23%, $p<0.0001$) even though weight-gain was greater. Of note, MB-LCV mouse food consumption was significantly reduced by the second round of chemotherapy with a mean of 0.2g of food per animal consumed on day 35 (compared to

4.0g per animal in MB-LCV treatment alone, $p<0.0001$, Figure 6.4A). This reduction in food consumption followed CCNU then VCR+CDDP administration on days 29 and 30, respectively.

A similar effect of IDEB co-therapy was seen when combined with BL-CHOP therapy. Total food consumption decreased with adjunct IDEB therapy when compared to BL-CHOP therapy alone (BLi-CHOP ~-12% total food consumption when compared to BL-CHOP therapy by day 47, $p<0.05$ Figure 6.4B).

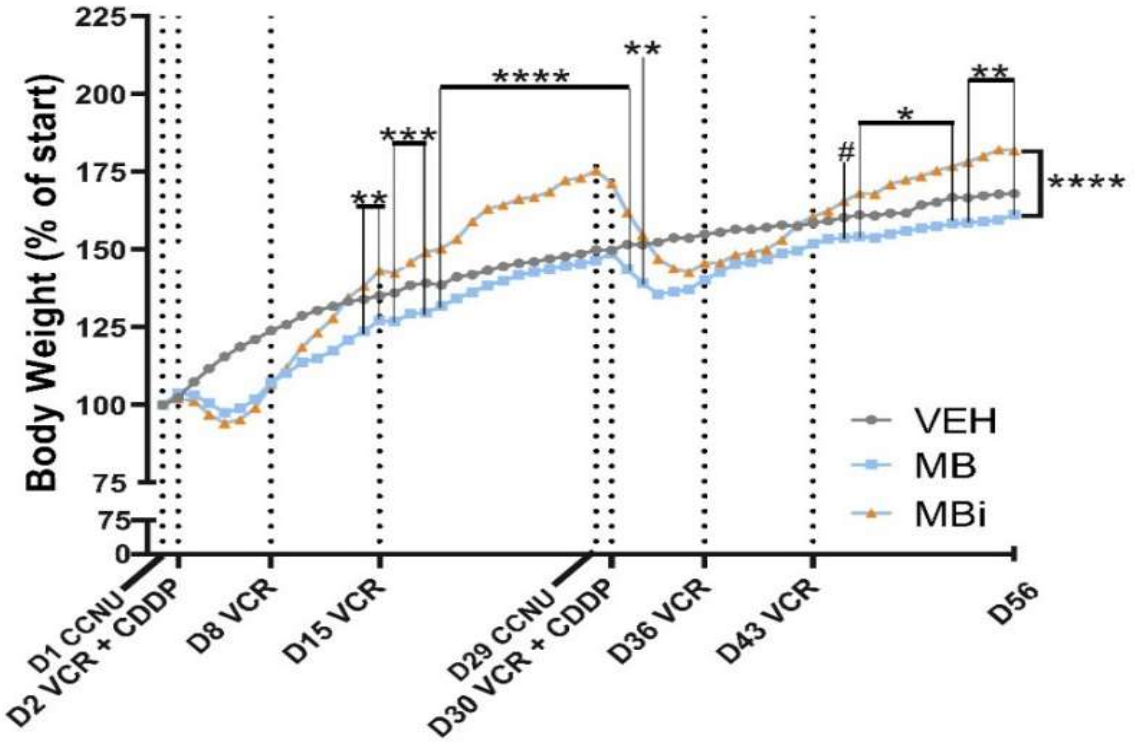

Figure 6.2: Body weight as measured by percent change from starting weight in VEH (V), MB-LCV (MB) and MBi-LCV (MBi) treated mice. *IDEB co-administration with MB-LCV therapy greatly improves weight-gain overall and during inter-treatment phases of therapy but elevates rate of weight-loss during active treatment. MB-LCV: n=39, MBi--LCV: n=18-20. Significance via RMANOVA with Tukey's post-hoc, where #=0.066.*

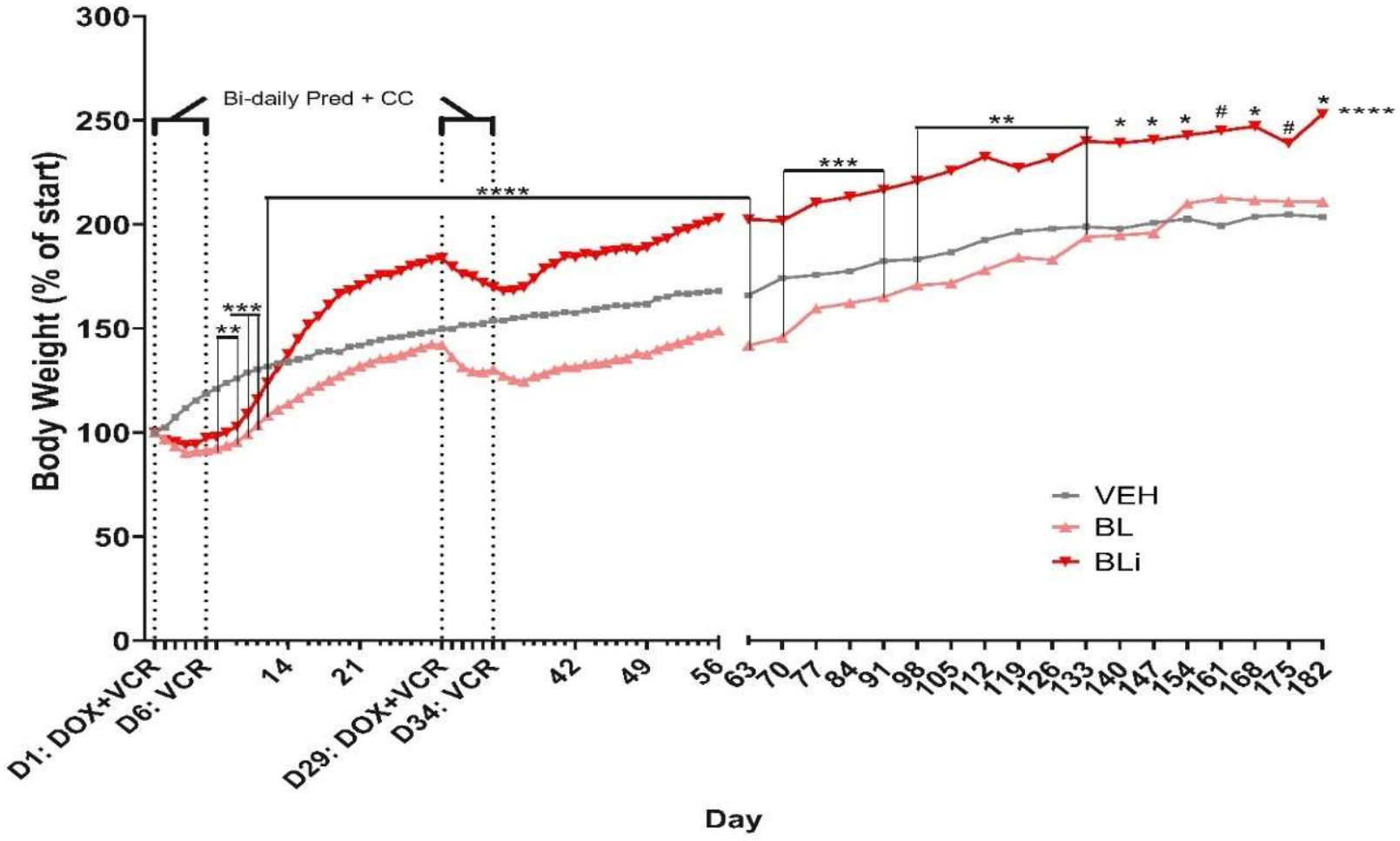

Figure 6.3: Body weight as measured by percent change from starting weight in VEH (V), BL-CHOP (BL) and BLi-CHOP (BLi) treated mice. *Daily IDEB co-administration with BL-CHOP therapy greatly increases weight gain and weight maintenance over the lifespan.* Mice co-treated with IDEB at the cessation of treatment (D56) were, on average, 36% heavier than their chemotherapy counterparts (p<0.0001) with this increase being maintained over the lifespan. Animals: <12 weeks BL-CHOP n=42-49, BLi: n=20, >12weeks BL-CHOP n=10-30, BLi-7. Significance via RMANOVA with Tukey's post-hoc.

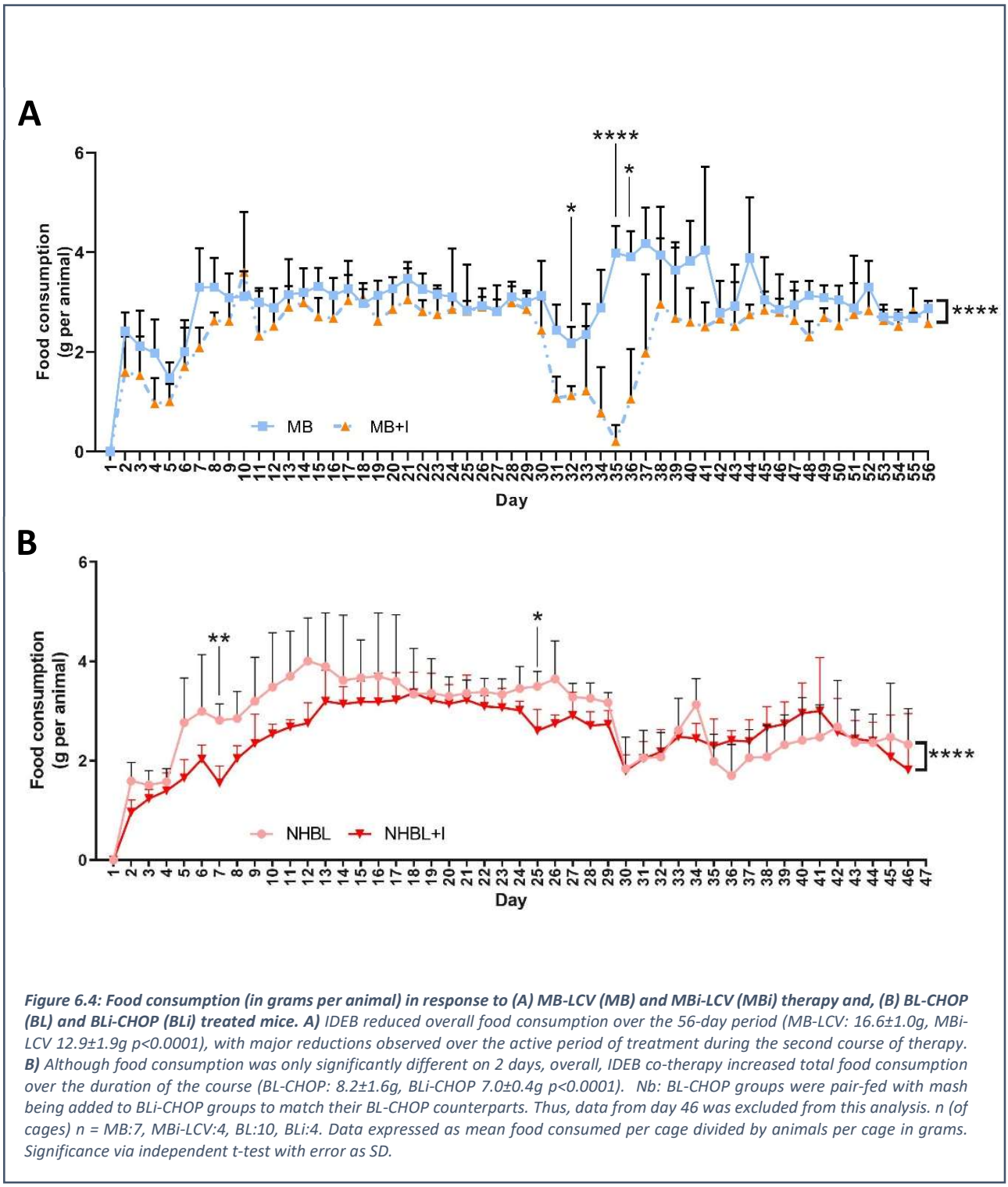

Figure 6.4: Food consumption (in grams per animal) in response to (A) MB-LCV (MB) and MBi-LCV (MBi) therapy and, (B) BL-CHOP (BL) and BLi-CHOP (BLi) treated mice. A) *IDEB reduced overall food consumption over the 56-day period (MB-LCV: 16.6±1.0g, MBi-LCV 12.9±1.9g p<0.0001), with major reductions observed over the active period of treatment during the second course of therapy.* ***B)*** *Although food consumption was only significantly different on 2 days, overall, IDEB co-therapy increased total food consumption over the duration of the course (BL-CHOP: 8.2±1.6g, BLi-CHOP 7.0±0.4g p<0.0001). Nb: BL-CHOP groups were pair-fed with mash being added to BLi-CHOP groups to match their BL-CHOP counterparts. Thus, data from day 46 was excluded from this analysis. n (of cages) n = MB:7, MBi-LCV:4, BL:10, BLi:4. Data expressed as mean food consumed per cage divided by animals per cage in grams. Significance via independent t-test with error as SD.*

6.3.3 Micro-computed tomography analysis of hind-limb muscle mass in adjunct IDEB adjunct therapy with MB-LCV and BL-CHOP regimens

Anti-neoplastic chemotherapeutic treatment options are often greatly limited, or contra-indicated, in patients with low lean mass. Moreover, anti-neoplastic treatment may well be withdrawn from patients who lose lean mass due to concerns of elevated treatment toxicity and reduced overall survival in these patients. The capacity for adjunct IDEB therapy to protect the skeletal musculature from atrophy is thus a key measure of its efficacy in this setting. In combination IDEB and MB-LCV therapy (MBi-LCV), tibial muscle mass was reduced by 23% ($p<0.005$, Figure 6.) when compared to MB-LCV therapy alone.

Daily IDEB adjunct therapy in combination with BL-CHOP therapy (BLi-CHOP) showed far greater therapeutic promise. Adjunct IDEB therapy completely protected against BL-CHOP-induced lean mass loss at both 12- and 30-week time points (Figure 6.). Specifically, the 15% and 16% reductions in tibial lean mass seen at 12- and 30-week time points in BL-CHOP treated mice were completely abolished ($p<0.05$). Adjunct IDEB protected against lean mass loss induced by BL-CHOP therapy, maintaining lean mass values to that of age matched VEH treated animals.

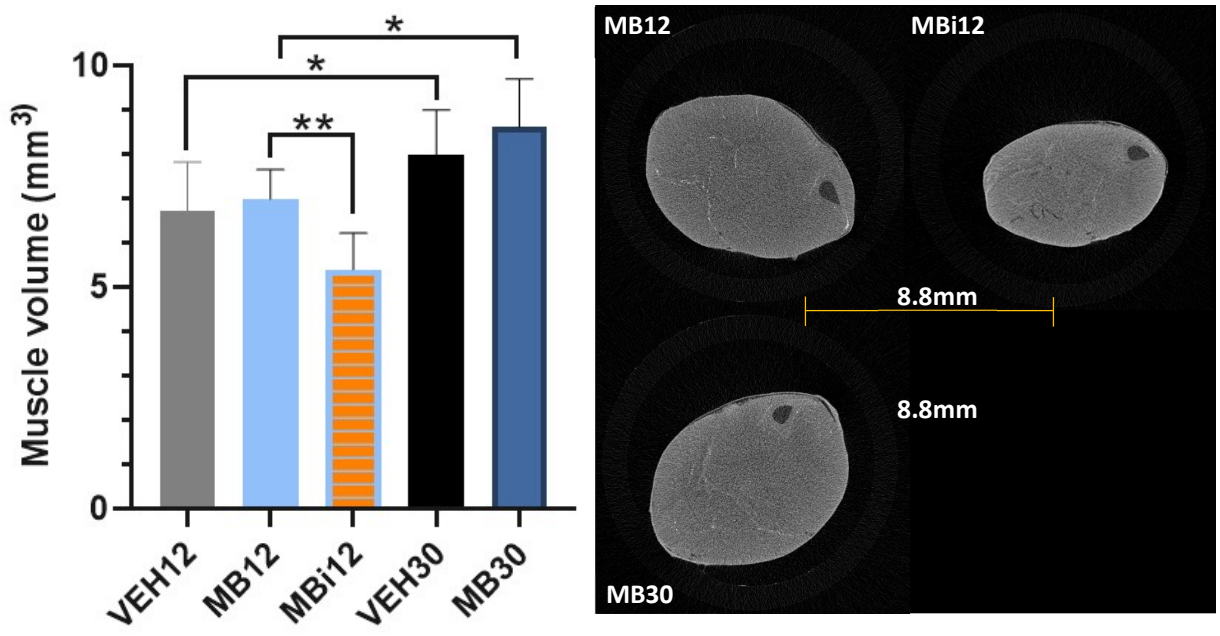

***Figure 6.5:** Muscle volume as measured by µ-CT imaging of at the proximal 1/3 of the tibia in VEH (V), MB-LCV (MB)and MBi-LCV (MBi) treated mice at 12 and 30 weeks of age. MB-LCV therapy alone did not impact muscular volume in the lower limb at either 12 or 30-weeks of age. IDEB co-therapy with the MB-LCV regimen (MBi) induced a considerable loss in muscle mass of 23% (p<0.005) when compared to 12-week MB-LCV treatment alone. Representative images supplied. n=6-9 assessed by ANOVA with Tukey's post-hoc test with error expressed as SD.*

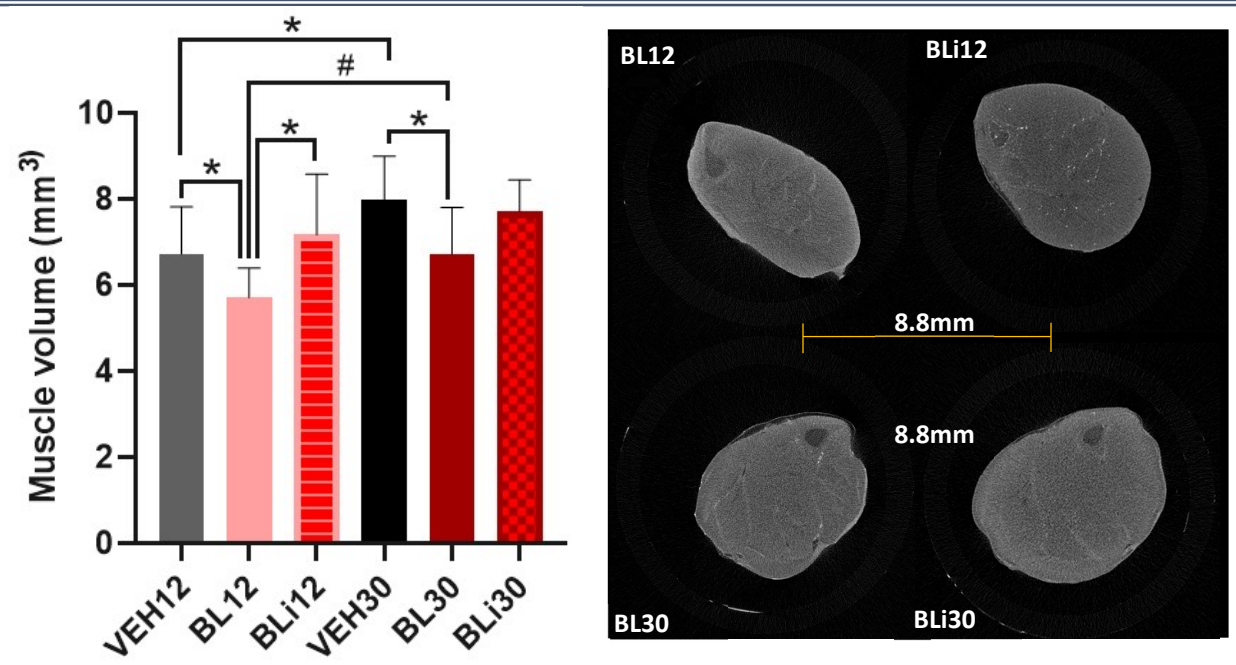

***Figure 6.6:** Muscle volume as measured by µ-CT imaging of at the proximal 1/3 of the tibia in VEH (V), BL-CHOP (BL) and BLi-CHOP (BLi) treated mice at 12 and 30 weeks of age. BL-CHOP therapy significantly reduced muscle volume in the lower limb at both 12 and 30-weeks of age by 15% and 16% respectively (p<0.05). BL-CHOP treated muscle increased by 18% by 30-weeks of age (p=0.064) which was the same increase seen in VEH (18%, p<0.05). IDEB in combination with BL-CHOP therapy (BLi) protected against lean mass loss at 12 and 30 weeks, maintaining lean mass values to that of age matched VEH treated animals. Representative images supplied. n=7-10 assessed by ANOVA with Tukey's post-hoc test with error expressed as SD.*

6.3.4 Effects of adjunct IDEB therapy on haematological and gross pathology induced by MB-LCV and BL-CHOP regimens

In blinded gross pathology assessments of a sub-set of treated mice performed by veterinary pathologists (Cerberus Laboratory Animal Diagnostics, Melbourne, Australia), no significant pathology was observed in BLi-CHOP treated mice – suggesting IDEB protected against the mechanisms which induced the cardiomyopathy and hepatopathy seen in BL-CHOP treated mice (namely right ventricular dilation, hepatosteatosis, hepatocellular swelling, oedema indicative of congestive heart failure when presenting in combination, see Table 6.2, refer *Chapter 5, S5.3.1* for more details). The visible absence of gastrointestinal, renal and hepatic pathology in BLi-CHOP treated mice, suggests IDEB has a significant protective effect on these systems (see Table 6.2). However, chemotherapy-induced increases to the kidney in BL-CHOP treated 12-week old mice was not alleviated by IDEB.

At an organ and muscular level, MB-LCV chemotherapy-induced changes to SOL were not affected by IDEB adjunct therapy, however, IDEB did increase PLA and QUAD tissue to body weight ratios (~30% and 18% respectively when compared to MB-LCV therapy alone, $p<0.05$ Figure 6.7). Moreover, IDEB co-therapy increased liver:body weight ratio at 12-weeks (12% from MB-LCV, $p<0.05$, Figure 6.7) but protected against MB-LCV-induced 8% decrease in heart:body weight ratio ($p<0.05$, Figure 6.7). IDEB adjunct therapy had little effect when combined with the BL-CHOP regimen, aside from affording protection against the regimen's propensity to increase TA size ($p<0.05$, Figure 6.8).

Haematologically, MBi-LCV treated mice showed an increased propensity to develop hypochromic (--22.85g/L compared to MB-LCV, $p<0.05$) microcytic (-2.75fl compared to MB-LCV, $p<0.005$) anaemia with thrombocytopenia (-394.33x10^9/L compared to MB-LCV, $p<0.05$) which was not found at 12-weeks of age in MB-LCV therapy alone (refer Table 6.3). Interestingly, thrombophilia was evident at the 12-week (post therapy) time point (+330.33 x10^9/L compared to VEH, $p<0.05$) also. As reported in *Chapter 4 S4.3.3*, MB-LCV therapy tended to decrease heart wet weight (p=0.0629) which IDEB therapy protected against. Unfortunately, haematological investigations of BLi groups were not completed due to experimental error.

Overall, IDEB co-administration was not associated with any significant unmanageable organ-pathology and, most importantly, alleviated gross pathology in both 12- and 30-week BL treated mice.

Table 6.2: Pathological observations of VEH (V), MB-LCV (MB), MBi-LCV (MBi), BL-CHOP (BL) and BLi-CHOP (BLi) treated mice during necropsy at 12 and 30 weeks of age. *Abbreviations: RV: Right ventricle, S: Intraventricular septum, LV: Left ventricle, GIT: gastrointestinal tract, +: pathology observed.*

Treatment group	Mouse	Pathology observed												
		Cachectic appearance	Perianal faecal staining	Ascites	interstitial lymphoblastic infiltration	RV:S:LV	Thinning & dilation of RV myocardium	RV Myocardial inflammation	Cholangitis	Hepatosteatosis	Hepatocellular swelling	Renal hydronephrosis	Basophilic renal tubules	GIT inflammation
V12	1					1:6:6	+				+			
	2					1:6:5	+				+			
	3					1:4:4			+		+			
	4					1:4:4					+			
	5					1:5:5					+			
M12	1					1:6:4			+		+		+	
	2					1:4:4					+		+	
	3				+	1:6:6			+		+			
	4					1:5:5					+			
Mi12	1					1:2.5 :2								
	2					1:5:5							+	
	3					1:5:5							+	
	4					1:3:3							+	
	5					1:5:4								
BL12	1					1:4:3	+		+		+			+
	2					1:4:3	+		+		+			+
	3	+	+			1:4:4	+		+		+	+		+
	4	+	+			1:5:5	+		+		+			+
BLi12	1					1:3:2 .5								
	2					1:5:5		+						
	3					1:3:3								
V30	1					1:5:5					+			
	2					1:4:5			+					
	3					1:3:4								
	4					1:3:4								
BL30	1	+	+	+		1:2:2								
	2	+	+	+		1:2:3		+		+		+	+	
	3			+		1:4:5		+		+		+	+	
	4					1:4:3				+				
	5			+		1:4:3				+				
BLi30	1					1:5:6								
	2					1:4:6		+						
	3					1:5:5								

Table 6.3: Haematological (count and smear) and biochemical investigations in MB-LCV (BL) and MBi-LCV treated mice at 12. *Data expressed as difference between MBi-LCV mean and MB-LCV mean (with MBi group SD). UA: Unavailable due to low sample blood levels. $: often expressed together with globulin levels, globulin level measurement was UA. n=2-5. NC: not calculatable due to values being identical in each group*

Measure	**ΔMBi12**	**±SD**	**Sig (*p*)**
Red cell count (RCC) (x10¹².L⁻¹)	-1.75	0.13	<0.05
Haematocrit (HC) (L.L⁻¹)	-10.85	1.67	<0.05
Haemoglobin (Hb) (g.L⁻¹)	-22.85	3.85	<0.05
Mean corpuscular volume (MCV) (fl)	-2.75	1.22	<0.005
Mean corpuscular haemoglobin (MCH) (pg)	0	0	n.c
MCH concentration (MCHC) (g.L⁻¹)	22.45	5.36	<0.001
Platelet count(x10⁹.L⁻¹)	-394.33	127.19	<0.005
Total white cell count (x10⁹.L⁻¹)	1.82	2.64	
Segmented neutrophils (x10⁹.L⁻¹)	0.43	0.67	
Total lymphocyte count(x10⁹.L⁻¹)	0.83	2.2	
Monocyte count (x10⁹.L⁻¹)	0.14	0.28	
Total Protein (g.L⁻¹)	-2.87	6.53	
Albumin (g.L⁻¹) ***($: see note in figure legend)***	UA	UA	-
Urea (mmol.L⁻¹)	-2.01	1.05	
ALT (mmol.L⁻¹)	94.4	302.6	
AST (mmol.L⁻¹)	UA	UA	-
AST:ALT	UA	UA	-
Creatine Kinase (mmol/.L⁻¹)	182.42	372.00	

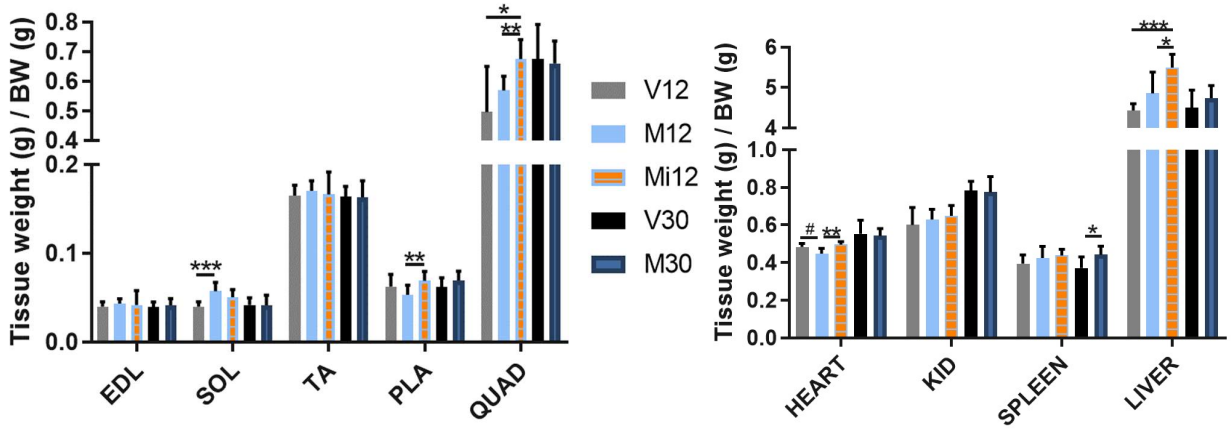

Figure 6.7: Organ and tissue wet weight changes (corrected for animal body weight in g/g) in VEH (V) and MB-LCV (MB) and MBi-LCV (MBi) treated mice as of 12 and 30 weeks of age. *IDEB adjunct therapy increased PLA and QUAD muscle:body weight by ~30% and 18% respectively when compared to MB-LCV therapy alone. IDEB also protected against MB-LCV-mediated reductions in heart:BW weight (an initial reduction of 8%), and induced hepatomegaly at 30-weeks of age (12% from MB-LCV, 24% from VEH). Adjunct IDEB therapy corrected cardiac atrophy at 12 weeks(p<0.005). Abbreviations: EDL: Extensor digitorum longus m., SOL: Soleus m., TA: Tibialis Anterior m., PLA: Plantaris m., QUAD: Quadriceps complex. Significance via ANOVA with Tukey's post hoc, where # p=0.062 and ## p=0.082.*

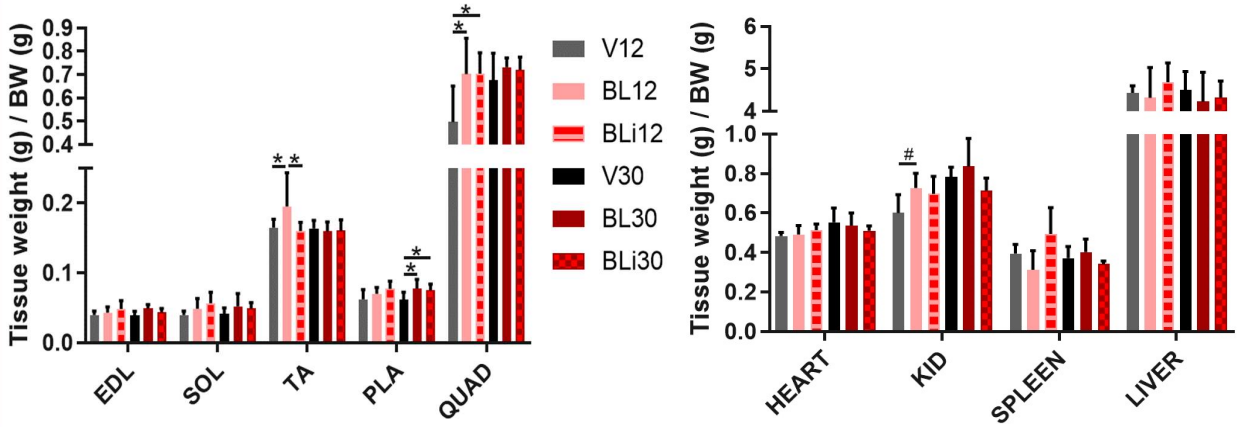

Figure 6.8 Organ and tissue wet weight changes (corrected for animal body weight in g/g) in VEH (V) and VEH (V), BL-CHOP (BL) and BLi-CHOP (BLi) treated mice at 12 and 30 weeks of age. *Muscle and organ wet weight post excision during necropsy shows acute increases in TA and QUAD weight:BW ratio ($p<0.05$) and increases in KID size ($p=0.079$) at 12 weeks, all of which was corrected by 30-weeks of age (+18%, 41% and 20% respectively). PLA muscle size alone increased by 30weeks by 12.5% ($p<0.05$). IDEB adjunct therapy attenuated chemotherapy-induced TA changes ($p<0.05$) but failed to attenuate changes in PLA, QUAD or KID. Data corrected for bodyweight of mouse at time of necropsy and is expressed as wet weight of tissue over the mouse's body weight (g/g). n= 4-11. Abbreviations: EDL: Extensor digitorum longus m., SOL: Soleus m., TA: Tibialis Anterior m., PLA: Plantaris m., QUAD: Quadriceps complex.*

6.3.5 Effects of adjunct IDEB therapy on glucose handling when delivered with MB-LCV and BL-CHOP regimens

In normal physiological states, blood glucose levels are tightly regulated by a raft of measures; including the mitochondria. In states of mitochondrial dysfunction, particularly in those that are charactersised by a diminshed ability to effectively utilise glucose substrates (such as a reduced metablic flexibility seen in *Chapter 4* and *5*), a decline in mitochondrial energy output will often result in an insulin-mediated increase in cellular glucose uptake [598]. Over time, this can manifest into a state of insulin resistance, increasing endogenous blood glucose levels and reducing gluocse uptake rates [599]. MB-LCV therapy on its own was not found to cause any major abnormalities in glucose handling, though co-administration with IDEB increased glucose uptake rates in 8-week old mice by an average of 11% over the time course (Figure 6.9A, $p<0.0001$). In contrast, the co-administration of IDEB with BL-CHOP therapy reduced endogenous glucose production by 2.7mmol/L (-34%, Figure 6.10C, $p<0.0001$) as well as . No other significant effects of IDEB co-therapy on glucose handling was observed at any other time point for the other treatment groups.

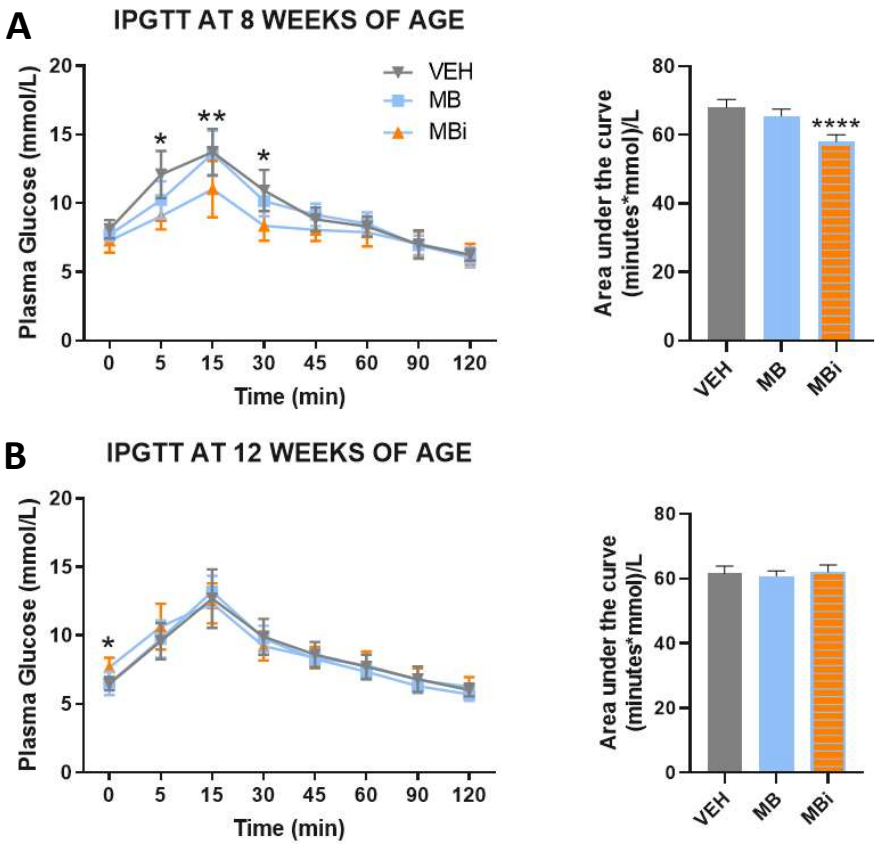

Figure 6.9: Changes in blood glucose levels (mmol/L) as in response to weight standardised glucose injection in VEH (V), MB-LCV (MB) and MBi-LCV (MBi) treated mice at 8 and 12 weeks of age. *A) glucose uptake at 8-weeks was significantly increased in MBi-LCV mice when compared to MB-LCV treated mice which was resolved by 12 weeks of age (B). n=10 for all groups. Significance for time course (A,C) assessed by RMANOVA with Tukey's post-hoc with error expressed as SD. Significance shown on time course graphs denotes difference between MB-LCV and MBi-LCV (A,C).*

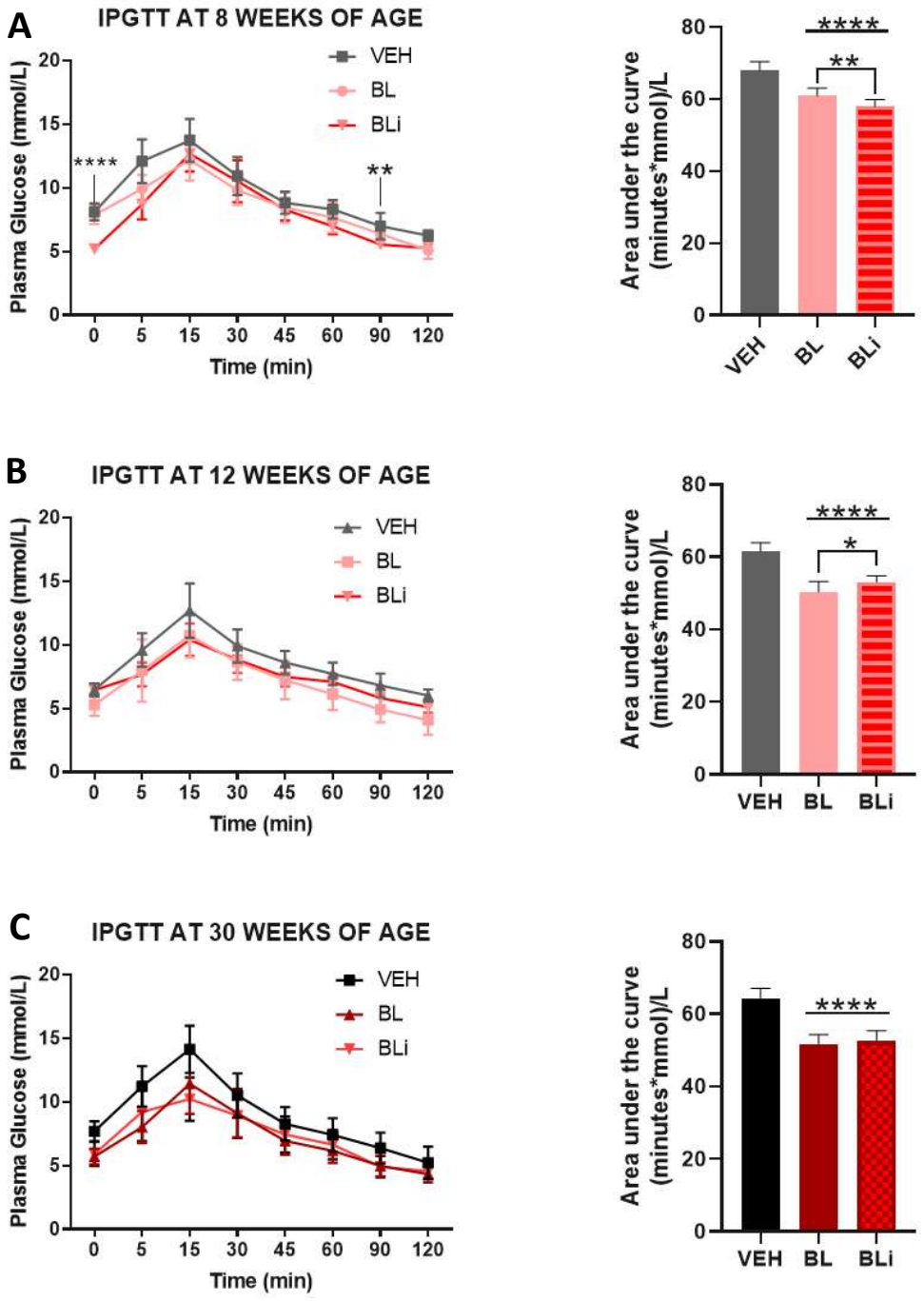

Figure 6.10 Changes in blood glucose levels (mmol/L) as in response to weight standardised glucose injection in VEH (V), MB-LCV (MB) and MBi-LCV (MBi) treated mice at 8 and 12 weeks of age. *A) IDEB caused an acute decrease in endogenous glucose production in BL-CHOP treated 8-week old mice which was resolved by D) 12 weeks of age with no differences between BL-CHOP and BLi-CHOP groups throughout the lifespan there after. Error expressed as SD. Significance shown on time course graphs denotes difference between BL and BLi (A,B,C).*

6.3.6 Effects of adjunct IDEB therapy on grip strength when delivered with MB-LCV and BL-CHOP regimens

As both chemotherapy regimens used in the previous chapters showed clear signs of CI-SMDW, whether IDEB could protect against the reduction in muscle strength and lean mass is an important step in determining its therapeutic value in this setting. Using a purpose built grip strength platform, we measured the effect of both the MB-LCV and BL-CHOP chemotherapy regimens on mouse grip strength at 8, 12 and 30-weeks of age with and without IDEB adjunct therapy.

MB-LCV therapy with or without IDEB did not induce changes in strength at 8 or 12 weeks of age when compared to VEH (Figure 6.11, left, refer to Chapter 4, S4.3.5 for more on MB-LCV effects). IDEB therapy in co-administration with the BL-CHOP regimen (Figure 6.11, right) improved strength in 12-week-old BL-CHOP treated mice (+16.5%, $p<0.005$), and returned grip strength to VEH levels at 12- and 30- weeks. Surprisingly, IDEB co-therapy exacerbated the loss of force output seen at 8-weeks (-11.4%, $p<0.05$) suggesting a higher cumulative dose of IDEB is required for therapeutic action than what was received by 8 weeks, or, the mechanisms by which IDEB aids strength recovery, takes time to reach a therapeutic threshold.

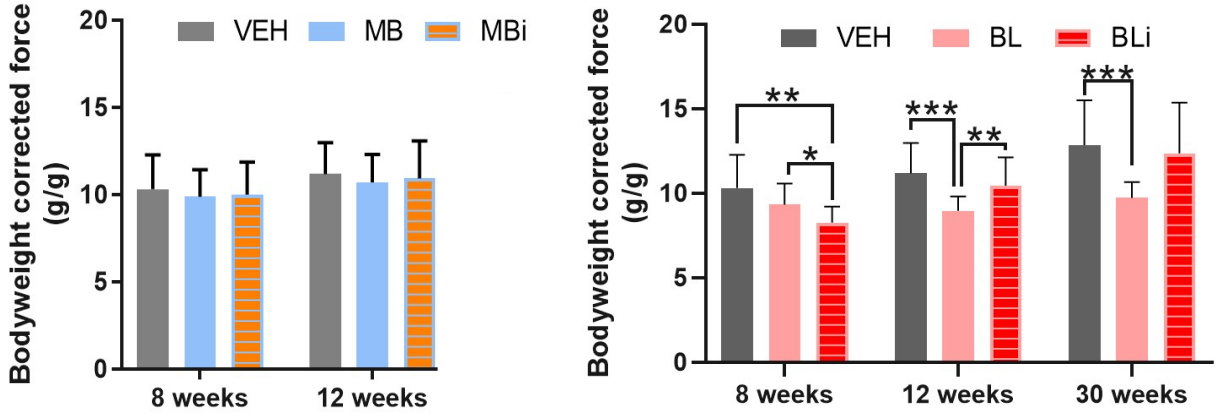

Figure 6.11: Changes in bodyweight corrected grip strength in response VEH (V), MB-LCV (MB) and MBi-LCV (MBi) treatment (left) and BL-CHOP (BL) and BLi-CHOP) treatment (tight) in mice at 8, 12 and 30-weeks of age. (left) *IDEB therapy afforded no improvements in strength when co-administered with the MB-LCV regimen.* ***(right)*** *no change to 8 week strength was observed, however significant improvements to grip strength was noted thereafter. Group n = 20 (where BL-CHOP at 30 weeks = 10, and BLi=7). Significance via RMANOVA (mixed-effects analysis) with Tukey's post hoc.*

6.3.7 Effect of IDEB on muscle contractile function with IDEB when co-administered with MB-LCV and BL-CHOP therapies

In the previous chapters we have shown that both the MB-LCV and BL-CHOP regimens induce skeletal muscle dysfunction; which was characterised by significant reductions in force output and recovery capacity which largely manifested later in life, long after chemotherapy had ceased (as measured in EDL and SOL muscles, refer *Chapter 4: S4.3.7.1* and *Chapter 5: S5.3.8.1*). To assess IDEB's therapeutic efficacy against chemotherapy-induced skeletal muscle dysfunction (by targeting the underlying mitochondrial dysfunction induced by both regimens), *ex vivo* evaluation of muscle contractile properties and function in chemotherapy-treated mice (MB-LCV and BL-CHOP) with and without IDEB was performed.

6.3.7.1 Contractile properties in MBi-LCV treated EDL and SOL muscle

Functional parameters of the EDL and SOL were assessed after they were harvested from mice treated with either MB-LCV or BL-CHOP chemotherapy with and without IDEB adjunct administration. MB-LCV chemotherapy induced no effect on muscle parameters aside from elevated muscle cross-sectional area (CSA) (refer *Chapter 4, S4.3.7.1* for results). IDEB co-therapy did not affect CSA, however, the adjunct did act to reduce the L_o of both the EDL and SOL by 21% and 19% ,respectively (p<0.001, Figure 6.12C, D). Optimal length is determined as the length at which the muscle produces its maximal force. As IDEB reduced this measure in a non-fibre type specific manner, it is likely that the contractile apparatus itself undertook structural change. Specifically, a shorter apparatus length was needed in IDEB

treated muscle to achieve optimal actin/myosin overlapping and thus peak force output. IDEB co-therapy also significantly increased the twitch to tetanic contractional force ratio (Pt/Po) by 29.4% (p<0.05*)* and 103.1% (p<0.0001) for EDL and SOL, respectively (Figure 6.12E, F). As discussed in previous chapters (*Chapter 4, S4.3.7.1* and *Chapter 5, S5.3.8.1*), this suggests a decrease in sarcoplasmic $Ca2^{+}$ releasing and re-uptaking capacity between subsequent contractions of a tetanic contraction, resulting in a lowered overall tetanic force [600]. If this is indeed the case, the observed reductions in absolute (EDL -68%, p<0.05 and SOL -78%, p<0.001, Figure 6.13 A & B) and specific force (69%, p<0.005 and 74% p<0.001 Figure 6.13 C & D) in both the EDL and SOL muscle serve to support this. These data further support our theory that the functioning of contractile apparatus itself in IDEB treated MB-LCV mice was compromised.

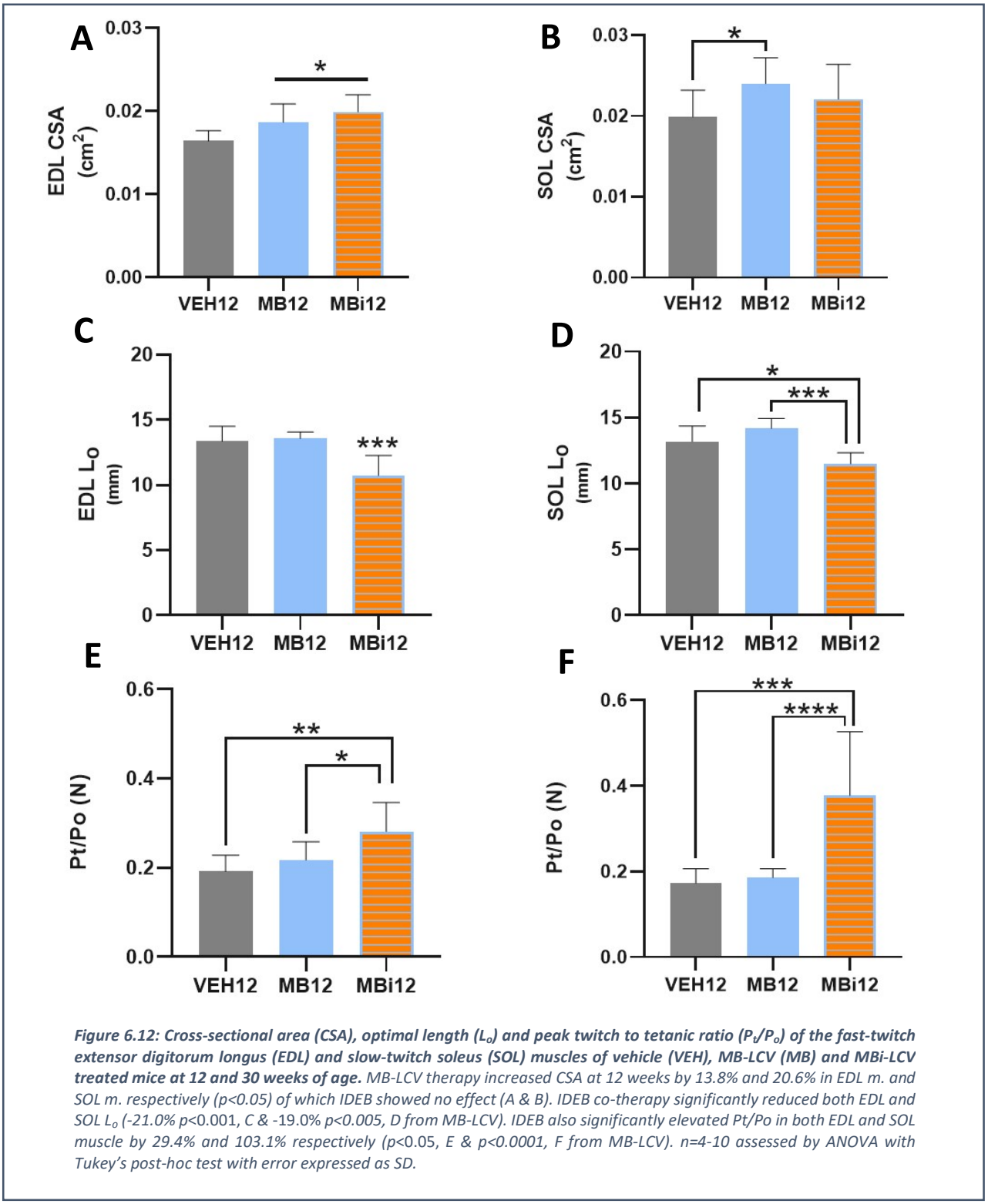

Figure 6.12: Cross-sectional area (CSA), optimal length (L_o) and peak twitch to tetanic ratio (P_t/P_o) of the fast-twitch extensor digitorum longus (EDL) and slow-twitch soleus (SOL) muscles of vehicle (VEH), MB-LCV (MB) and MBi-LCV treated mice at 12 and 30 weeks of age. *MB-LCV therapy increased CSA at 12 weeks by 13.8% and 20.6% in EDL m. and SOL m. respectively ($p<0.05$) of which IDEB showed no effect (A & B). IDEB co-therapy significantly reduced both EDL and SOL L_o (-21.0% $p<0.001$, C & -19.0% $p<0.005$, D from MB-LCV). IDEB also significantly elevated Pt/Po in both EDL and SOL muscle by 29.4% and 103.1% respectively ($p<0.05$, E & $p<0.0001$, F from MB-LCV). n=4-10 assessed by ANOVA with Tukey's post-hoc test with error expressed as SD.*

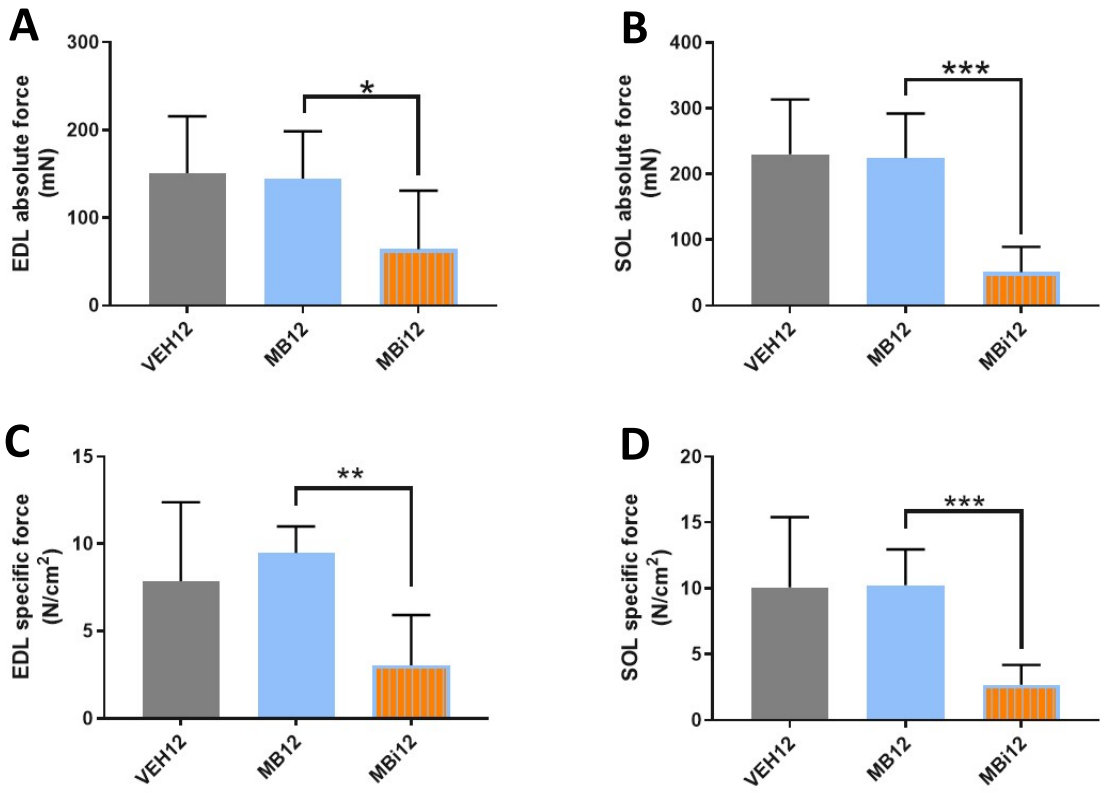

Figure 6.13: Absolute and specific force production of the fast-twitch extensor digitorum longus (EDL) and slow-twitch soleus (SOL) muscles from vehicle (VEH), MB-LCV (MB) and MBi-LCV treated mice at 12-weeks of age. *MB-LCV therapy on its own did not change measures of absolute or specific force when compared to VEH. IDEB co-therapy significantly reduced absolute force in both EDL and SOL muscle by 68% ($p<0.05$) and 78% ($p<0.001$) respectively (A & B). A similar decline was seen in specific force with MBi-LCV treatment causing a 69% ($p<0.005$) and 74% ($p<0.001$) reduction in EDL and SOL muscle respectively (C & D). n=4-10 assessed by ANOVA with Tukey's post-hoc test with error expressed as SD.*

6.3.7.2 Force-frequency relationship in MBi-LCV treated EDL and SOL muscle

To investigate the relationship between force produced and strength of the stimuli delivered, muscles were stimulated at increasing frequencies and the force produced from the tetanic contraction measured. No effect was seen in MB-LCV therapy alone, however, IDEB co-therapy significantly reduced raw force produced by both the EDL and SOL. at all frequencies (refer Figure 6.14A,D with significance tabulated in C & F) levels . Although this did not affect the force-frequency relationship when corrected for maximal force, suggesting muscle force production increased in similar proportions to the increases in stimuli frequency. IDEB co-therapy did, however, considerably truncate both EDL and SOL ability to response to increasing stimuli, with no EDL capable of withstanding stimuli above 120hz, or the SOL m. above 80Hz. A decrease of 60hz and 100hz respectively from MB-LCV treatment alone.

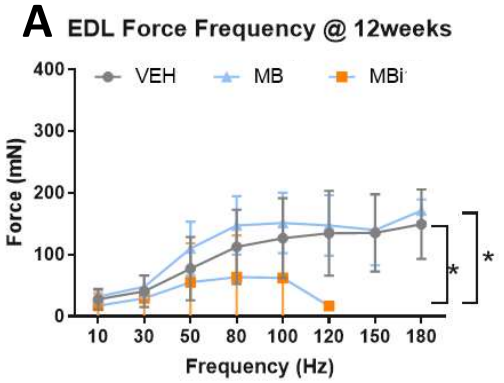

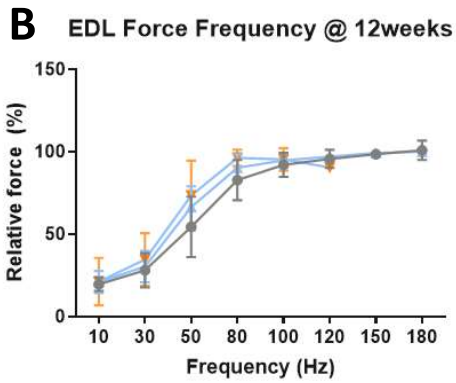

C

Frequency	VEH vs MB	VEH vs MBi	MB vs MBi
10 Hz	n.s	n.s	*p=0.*088
30 Hz	n.s	n.s	n.s
50 Hz	n.s	n.s	*p*=0.077
80 Hz	n.s	n.s	*p*<0.05
100 Hz	n.s	n.s	*p*<0.05
120 Hz	n.s	*p*<0.05	*p*<0.05
150 Hz	n.s	u.a	u.a
180 Hz	n.s	u.a	u.a

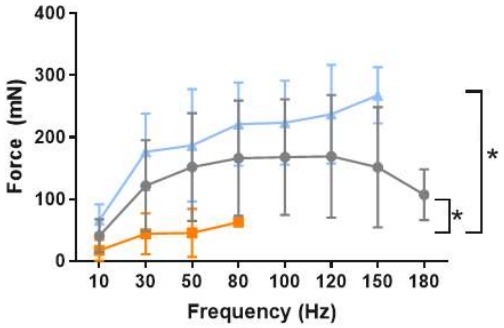

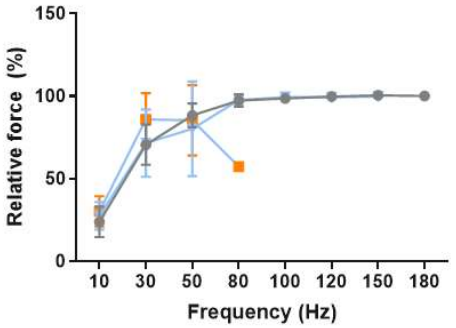

F

Frequency	VEH vs MB	VEH vs MBi	MB vs MBi
10 Hz	*p*=0.055	*p*=0.055	*p*<0.001
30 Hz	*p*=0.098	*p*<0.05	*p*<0.001
50 Hz	n.s	*p*<0.05	*p*<0.005
80 Hz	n.s	n.c	n.c
100 Hz	n.s	n.c	n.c
120 Hz	n.s	n.c	n.c
150 Hz	n.s	n.c	n.c
180 Hz	n.c	n.c	n.c

Figure 6.14: The force-frequency relationship of the fast-twitch extensor digitorum longus (EDL) and slow-twitch soleus (SOL) muscles from vehicle (VEH), MB-LCV (MB) and MBi-LCV treated mice at 12-weeks of age. *Muscle stimulation was of 500ms in tetanic length with consecutive 0.2ms pulses at 10, 30, 50, 80, 100, 120 and 150 Hz. MB-LCV therapy alone did not elicit an effect on the relative force frequency relationship in either muscle when corrected to maximal force produced (relative force, B & E). IDEB co-therapy induced a leftward shift in the raw force to frequency relationship in both EDL and SOL, with the muscle producing significantly less force at 80, 100 and 120Hz in the EDL muscle (C) and at all registered forces in the SOL muscle (F). N=3-10. Relationship significance assessed by two-way ANOVA with Tukey's post-hoc test with error expressed as SD. n.s.= not significant. n.c = statistics not calculatable due to small n.*

6.3.7.3 Fatigue properties in MBi-LCV treated EDL and SOL muscle

An important yet debilitating sequalae of CI-SMDW is the considerable decline in endurance and recovery capacity, which causes significant impact on patient quality of life [144,587]. In *Chapter 4*; *S4.3.7.3* we showed MB-LCV therapy alone did not induce any considerable changes to the fatiguability or recovery capacity of 12-week mice. IDEB co-therapy significantly increased the rate of fatigue in EDL which was observable from 40s and produced forces at levels of only 20% of VEH and MB-LCV alone (refer Figure 6.15C for significance). MBi-LCV treated EDL was seen to recover at a normal capacity in the first 10 min, but force production fell to 50% after 30min recovery, with no force produced by 60min ($p<0.005$). Considering IDEB treatment in combination with the MB-LCV regimen acts to reduce absolute force, likely through aberrant Ca^{2+} handling (as discussed in S6.3.6.1), an extended exercise bout (by way of repeated contractions) would only amplify the dysfunction seen in singular contractions (EDL and SOL Pt/Po, Figure 6.15E, F). As Ca^{2+} release and reuptake are imperative to initiate, maintain and relax contractions, dysfunction here is likely the reason for increased rates of fatiguability and poor recovery in both the EDL and SOL muscle.

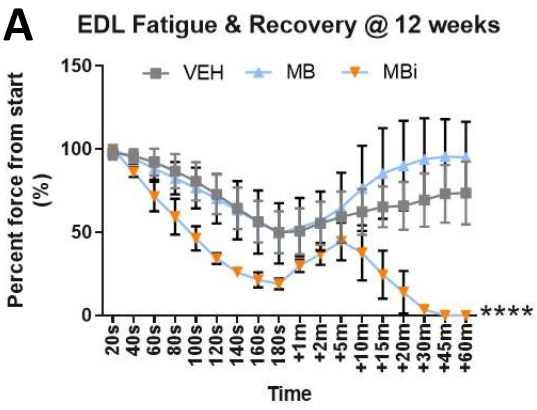

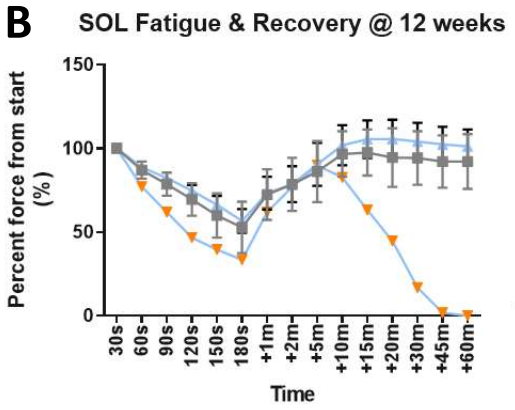

C

		Fatigue (s)								
EDL		20	40	60	80	100	120	140	160	180
	VEH v MB	*n.s*	n.s	n.s	n.s	n.s	n.s	n.s	n.s	n.s
	VEH v MBi	*n.s*	*p*<0.005	*p*<0.05	*p*<0.05	*p*<0.001	*p*<0.0001	*p*<0.0001	*p*<0.001	*p*<0.001
	MB v MBi	*u.a*	*p*<0.005	ns	*p*<0.05	*p*<0.005	*p*<0.05	*p*<0.05	*p*<0.05	*p*<0.05
		Recovery (minutes from end of fatigue protocol)								
		1	2	5	10	15	20	30	45	60
	VEH v MB	*n.s*	*n.s*	*n.s*	*n.s*	*n.s*	*n.s*	*n.s*	*n.s*	*n.s*
	VEH v MBi	*p*<0.05	*p*<0.05	*n.s*	*n.s*	*p*<0.005	*p*<0.005	*p*<0.001	*p*<0.001	*p*<0.001
	MB v MBi	*n.s*	*n.s*	*n.s*	*n.s*	*p*<0.05	*p*<0.005	*p*<0.005	*p*<0.005	*p*<0.005

Figure 6.15: Effect of MB-LCV therapy on fatiguability and recovery capacity in fast-twitch extensor digitorum longus (EDL) and slow-twitch soleus (SOL) muscles from vehicle (VEH), MB-LCV (MB) and MBi-LCV (MBI) treated mice at 12-weeks of age. *IDEB co-therapy with MB-LCV increased rate of fatigue in EDL muscle from 40s and, although rate recovery of recovery was normal in the first 5-10m, thereafter no increases in force was observed until no force production was detected (A, p<0.0001, refer C for significance). Only n=1 MBi-LCV treated SOL muscle completed the fatigue/recovery protocol thus significance is unavailable. However, recovery was notably poor from 10m onwards (similar to EDL) with force progressively lost thereafter until no force production was detected (B). Statistics pertaining to A) seen in C). n.s.= not significant. u.a. = statistics incalculable. n=4-10 where MBi SOL =1.*

6.3.7.4 Contractile properties in BLi-CHOP treated EDL and SOL muscle

In a similar manner to MBi-LCV co-therapy, there was no influence of BLi-CHOP co-therapy on CSA (Figure 6.16A-B). Unlike IDEB's actions with MB-LCV, when co-administered with BL-CHOP, no change beyond what was elicited by the chemotherapy alone was noted at 12-weeks in either Lo or Pt/Po measures (Figure 6.16C-F). However, by 30-weeks, IDEB tended to truncate the BL-CHOP mediated increase in Lo (-9.5% from BL-CHOP, p=0.0508) albeit not back to VEH levels. This suggests that the structural changes induced by the regimen persisted (namely an initial decrease followed by an increase in Lo). This is interesting, since Lo in VEH treated EDL reduced between 12- and 30-weeks of age by close to 15% (Figure 6.16C, p<0.005), a process reversed by and likely linked to, the damaging effects of anthracycline activity on the skeletal muscle (refer *Chapter 1: S1.3* and *Chapter 5: S5.4.2*). Functionally, IDEB co-therapy was uninfluential on the Pt/Po relationship. However, by 30-weeks of age IDEB treatment caused a significant decline in Pt/Po ratio in both EDL (by 39.5%; Figure 6.16E, p<0.001) and SOL (by 30.0%; Figure 6.16F, p<0.005) suggestive of improved Ca^{2+} handling within 30-week co-treated muscle.

Further assessment of muscle function post IDEB co-therapy showed IDEB consistently caused a fibre-type specific reduction in absolute force at 12-weeks in EDL (-59% from BL-CHOP, p<0.05; Figure 6.17A). This was concomitant with a fall of 54% in specific force (p<0.0001; Figure 6.17C) suggesting the fall in force was due to physiological dysfunction and not due to a loss of muscle (corroborated by CSA measures where no change with IDEB co-therapy was observed in EDL at 12 weeks, Figure 6.16A). At 30-weeks, IDEB rescued force

production by 50% ($p<0.05$, Figure 6.17C) which was independent of changes in muscle size (refer Figure 6.17A and Figure 6.17C). Beyond the effect of BL-CHOP therapy on its own, IDEB showed minimal effect on the SOL at either time point, suggesting its mechanism of action largely effects the fast-twitch and largely glycolytic EDL.

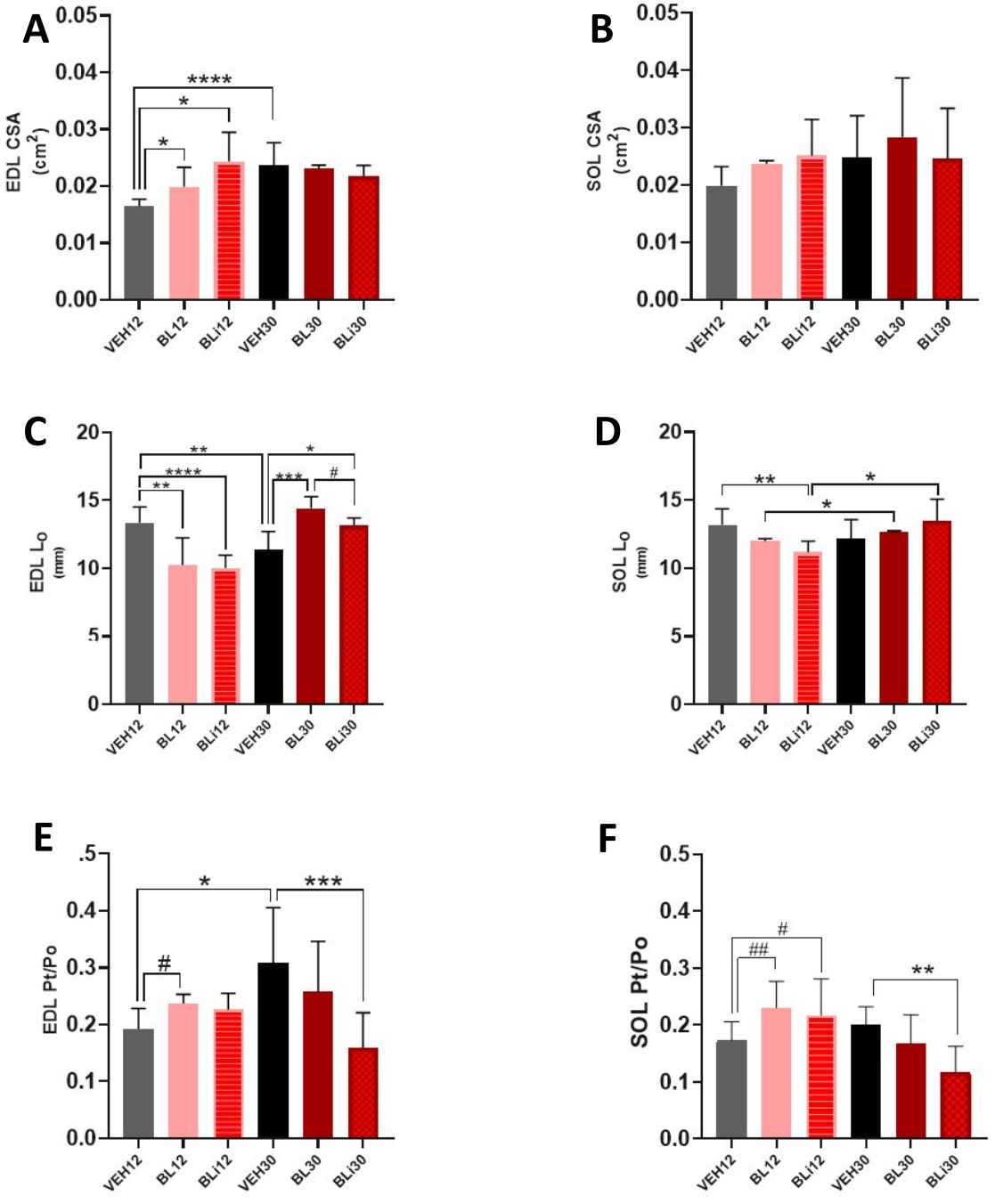

Figure 6.16 Cross-sectional area (CSA), optimal length (L_o) and peak twitch to tetanic ratio (P_t/P_o) of the fast-twitch extensor digitorum longus (EDL) and slow-twitch soleus (SOL) muscles of vehicle (VEH), BL-CHOP (BL) and BLi-CHOP (BLi) treated mice at 12 and 30 weeks of age. *BL-CHOP therapy induced an EDL specific increase in CSA by 20% ($p<0.05$) (A) with IDEB showing no significant effect on this increase in EDL (A). Neither treatment influenced SOL CSA (B). EDL L_o was decreased by 26% at 12 weeks and, interestingly, increased by 26% at 30 weeks when compared to time-controlled VEH samples. IDEB showed a propensity to truncate this change by 30-weeks (C, -9.5% from BL-CHOP, $p=0.0508$). SOL L_o followed a similar trend, increasing by 5.5% between 12- and 30-weeks ($p<0.05$) which was increased by 20% in IDEB co-treated mice (D, $p<0.05$). EDL m. ($p=0.061$) and SOL m. ($p=0.058$) Pt/Po tended to increase in response to BL-CHOP when compared to VEH at 12-weeks with IDEB having no effect on this parameter. At 30-weeks, IDEB co-therapy significantly reduced Pt/Po when compared to VEH by 39.5% in EDL and 30.0% in SOL m. (EDL $p<0.001$, SOL $p<0.005$). n=3-10. Significance assessed by ANOVA with Tukey's post-hoc test with error expressed as SD where (C)#:$p=0.0508$, (E)#:$p=0.061$, (F)#:$p=0.058$, ##:$p=0.068$.*

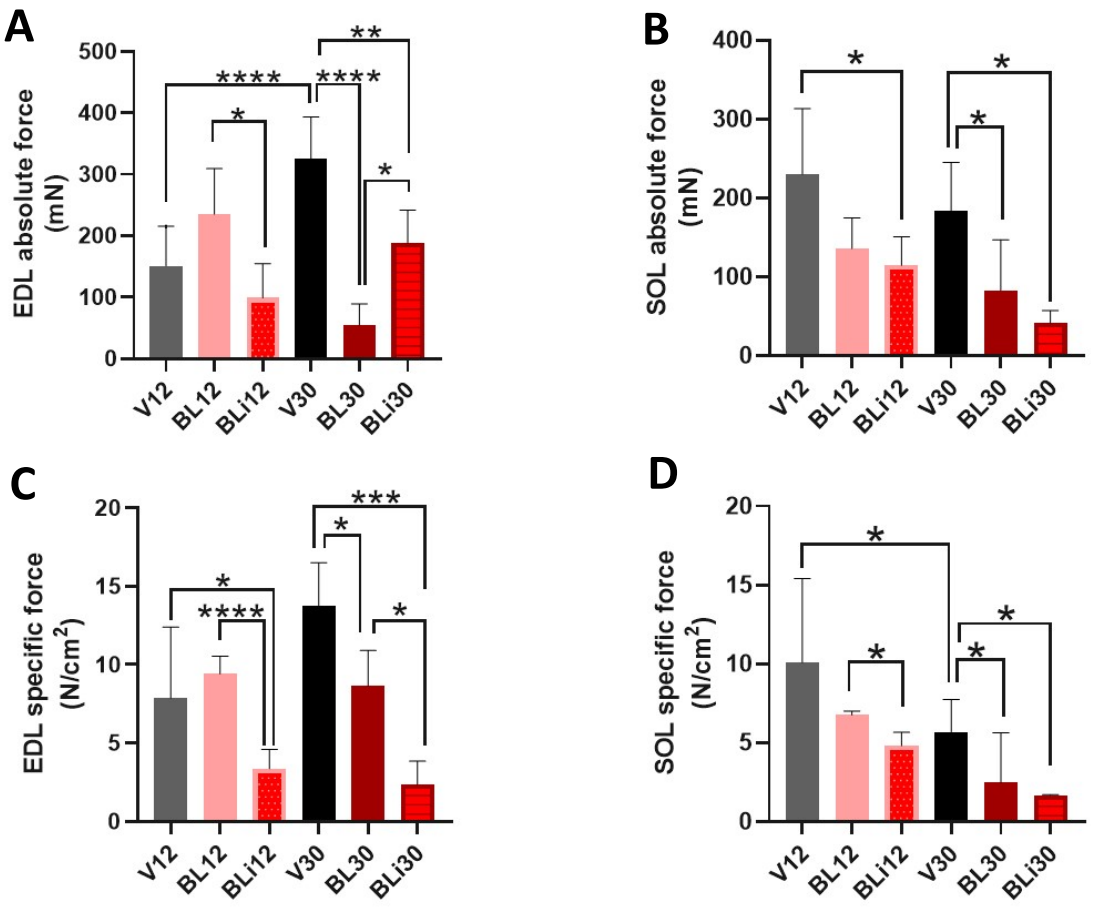

Figure 6.17: Absolute and specific force production of the fast-twitch extensor digitorum longus (EDL) and slow-twitch soleus (SOL) muscles from vehicle (VEH), BL-CHOP (BL) and BLi-CHOP treated mice at 12- and 30-weeks of age. *BL-CHOP treatment alone had no statistically significant effect on absolute or specific force production in EDL or SOL at 12 weeks of age, however, IDEB significantly reduced absolute force by 59% in EDL m. ($p<0.05$ compared to BL-CHOP). A similar effect on specific force was seen in both muscles with a -29% ($p<0.05$) and -54% ($p<0.0001$) reduction in SOL and EDL respectively.*

Both measures were negatively affected by chemotherapy at 30-weeks when compared to VEH with EDL and SOL absolute force reduced by 85% ($p<0.0001$) and 55% ($p<0.05$) respectively. IDEB co-therapy truncated this reduction in EDL m. by 50% ($p<0.05$) with a concomitant 73% reduction in specific force ($p<0.05$). Co-therapy did not affect SOL absolute or specific force. n=3-10. Significance assessed by ANOVA with Tukey's post-hoc test with error expressed as SD where #:p=0.088and ##:p=0.054.

6.3.7.5 Force-frequency relationship in BLi-CHOP treated EDL and SOL muscle

Briefly, BL-CHOP therapy alone elicited a largely glycolytic (fast) fibre type dependent pathology, with a leftward shift in the force-frequency curve (significant changes of 230% at 10Hz, 240% at 30Hz and 159% 50Hz compared to VEH, Figure 6.18A,B,C) which manifested as a significant reduction in force output at all stimuli by 30-weeks, with poorer performance at lower stimuli levels (significant percent decreases of 45% at 30Hz, 52% at 50Hz, 20% at 80Hz and 8% at 100Hz from VEH, Figure 6.18G,H,I). In SOL, on the other hand, there was a significant decrease in the muscles ability to withstand the protocol at 12-weeks, as BL-CHOP treated SOL muscles were unable to withstand stimuli above 80Hz (Figure 6.18, refer to C*hapter 5; S5.3.8.2* for further discussion) but no significant differences were seen in this muscle at 30-weeks in BL-CHOP therapy alone.

At 12-weeks, IDEB co-therapy protected against BL-CHOP-induced changes in absolute force, normalising values to VEH levels (Figure 6.18A,B,C). IDEB, however, failed to improve SOL contractile apparatus resilience at this time point (Figure 6.18D,E,F), as a large number of muscles still failed to complete the fatigue-recovery protocol. At 30-weeks, IDEB afforded some protective capacity against the significant fall in absolute force production at most frequency levels induced by BL-CHOP therapy, improving force output by 4 to 6-fold (at frequencies 50-150Hz, Figure 6.18G,I). However, no effect on the EDL m. relative force-frequency curve was seen at 30-weeks (Figure 6.18H), suggesting that treatment did not affect how the muscle responds to stimuli. Overall, IDEB provided some protection against the largely fast-twitch fibre dependent pathology induced by BL-CHOP therapy. Consistent

with improved absolute force observed in the previous section (*S6.3.5,* Figure 6.17A), force production at most frequency levels was improved by IDEB.

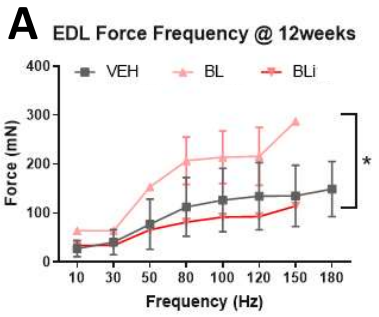

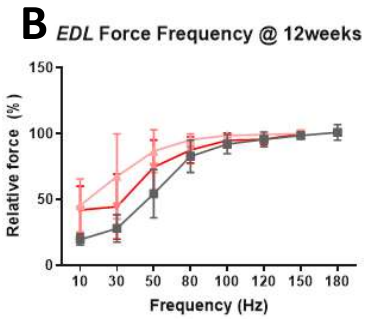

C

(Hz)	VEH vs BL	VEH vs BLi	BL vs BLi
10	*n.s*	*n.s*	*p*<0.05
30	*n.s*	*n.s*	*p*<0.05
50	*p*<0.05	*n.s*	*p*<0.005
80	*p*<0.05	*n.s*	*p*<0.05
100	*p*=0.062	*n.s*	*p*<0.05
120	*p*=0.097	*n.s*	*p*=0.060
150	*n.s*	*n.s*	*n.c*
180	*n.s*	*n.c*	*n.c*

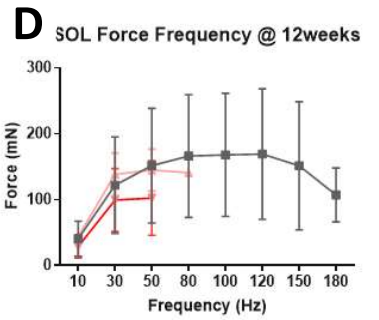

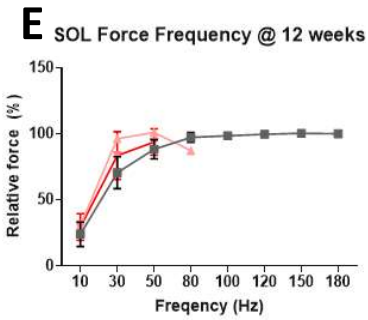

F

(Hz)	VEH vs BL	VEH vs BLi	BL vs BLi
10	*n.s*	*n.s*	*n.s*
30	*n.s*	*n.s*	*n.s*
50	*n.s*	*n.s*	*n.s*
80	*n.s*	*n.c*	*n.c*
100	*n.c*	*n.c*	*n.c*
120	*n.c*	*n.c*	*n.c*
150	*n.c*	*n.c*	*n.c*
180	*n.c*	*n.c*	*n.c*

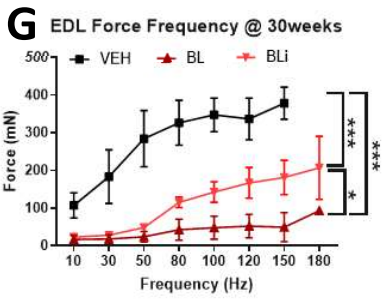

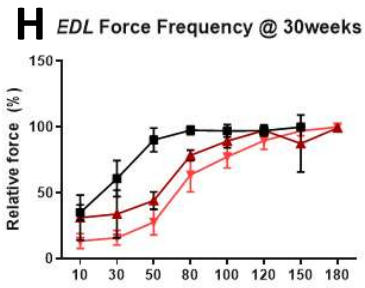

I

(Hz)	VEH vs BL	VEH vs BLi	BL vs BLi
10	*p*<0.001	*p*<0.001	*n.c*
30	*p*<0.005	*p*<0.005	*n.c*
50	*p*<0.001	*p*<0.0001	*p*<0.05
80	*p*<0.0001	*p*<0.0001	*p*<0.05
100	*p*<0.0001	*p*<0.0001	*p*<0.05
120	*p*<0.0001	*p*<0.001	*p*<0.05
150	*p*<0.001	*p*<0.005	*p*<0.05
180	*n.c*	*n.c*	*n.c*

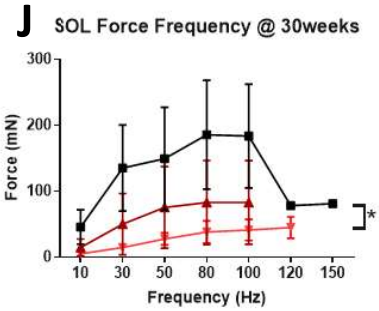

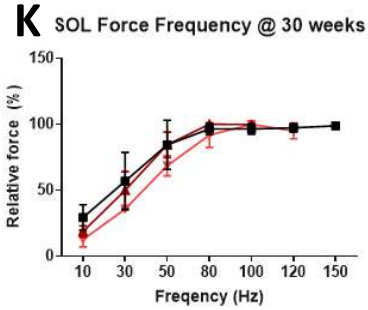

L

(Hz)	VEH vs BL	VEH vs BLi	BL vs BLi
10	*p*=0.080	*p*<0.05	*n.s*
30	*p*=0.067	*p*<0.05	*n.s*
50	*n.s*	*p*<0.05	*n.s*
80	*n.s*	*p*<0.05	*n.s*
100	*n.s*	*p*<0.05	*n.s*
120	*n.c*	*n.c*	*n.c*
150	*n.c*	*n.c*	*n.c*
180	*n.c*	*n.c*	*n.c*

Figure 6.18: Effect of BL-CHOP therapy on absolute and relative force frequency relationship in fast-twitch extensor digitorum longus (EDL) and slow-twitch soleus (SOL) muscles from vehicle (VEH), BL-CHOP (MB) treated mice at 12- and 30-weeks of age. *Chemotherapy induced a 2-fold increase in force production at 50Hz and 80Hz in 12-week EDL m. (A, statistical significance for absolute force-frequency in C) but did not change the relative force curve. IDEB corrected this and returned values to VEH levels. Neither BL-CHOP chemotherapy or IDEB co-therapy afforded an effect on SOL m. at 12-weeks (D-F). Changes induced by BL-CHOP therapy by 12-weeks, manifested by 30-weeks, with absolute force values ~10-fold lower than VEH at all stimuli frequencies (p<0.001, G) with a considerable shift in the relative force-frequency curve to the right (H). IDEB served some protection against a drop in absolute force, with force production significantly improved from 50-150Hz by 4 to 6-fold.(G, I) though did not correct the rightward shift in the relative force-frequency curve (H). Adjunct IDEB therapy provoked no further changes in SOL muscle compared to BL-CHOP alone (J-K). Of note only one VEH sample at 30 weeks produced forces above 100Hz. Significance tables based on absolute forces (C,F,I,L). Relative forces presented were normalised to the greatest force produced for that muscle and data presented as mean ± SD. n=3-10. Significance assessed by two-way ANOVA with Tukey's post-hoc test with error expressed as SD. n.s.= not significant. n.c = stastics not calculatable due to small n.*

6.3.7.6 Fatigue properties in BLi-CHOP treated EDL and SOL muscle

BL-CHOP therapy significantly affected skeletal muscle recovery in EDL and SOL when administered alone. Specifically, EDL and SOL at 12-weeks of age failed to recover after the fatigue protocol (with recovery defined as an improvement in force output from previous contraction after a rest period). We have already established that BLi-CHOP therapy increases skeletal muscle size but does not proportionally increase force production (Figure 6., Figure 6.17A-D). With increased size of the musculature being of clinical importance for treatment options, whether IDEB improved fatigue and/or recovery capacity in the muscle would have a direct positive, and profound, impact on patient quality of life. IDEB showed no ability to reduce the rate of fatigue or improve recovery in EDL at either time point (Figure 6.19A, C) but did, however, vastly improve mechanical resilience of SOL at 30 weeks – greatly improving the muscles ability to withstand the fatigue protocol as well as returning fatigue and recovery values to that of VEH (Figure 6.19D).

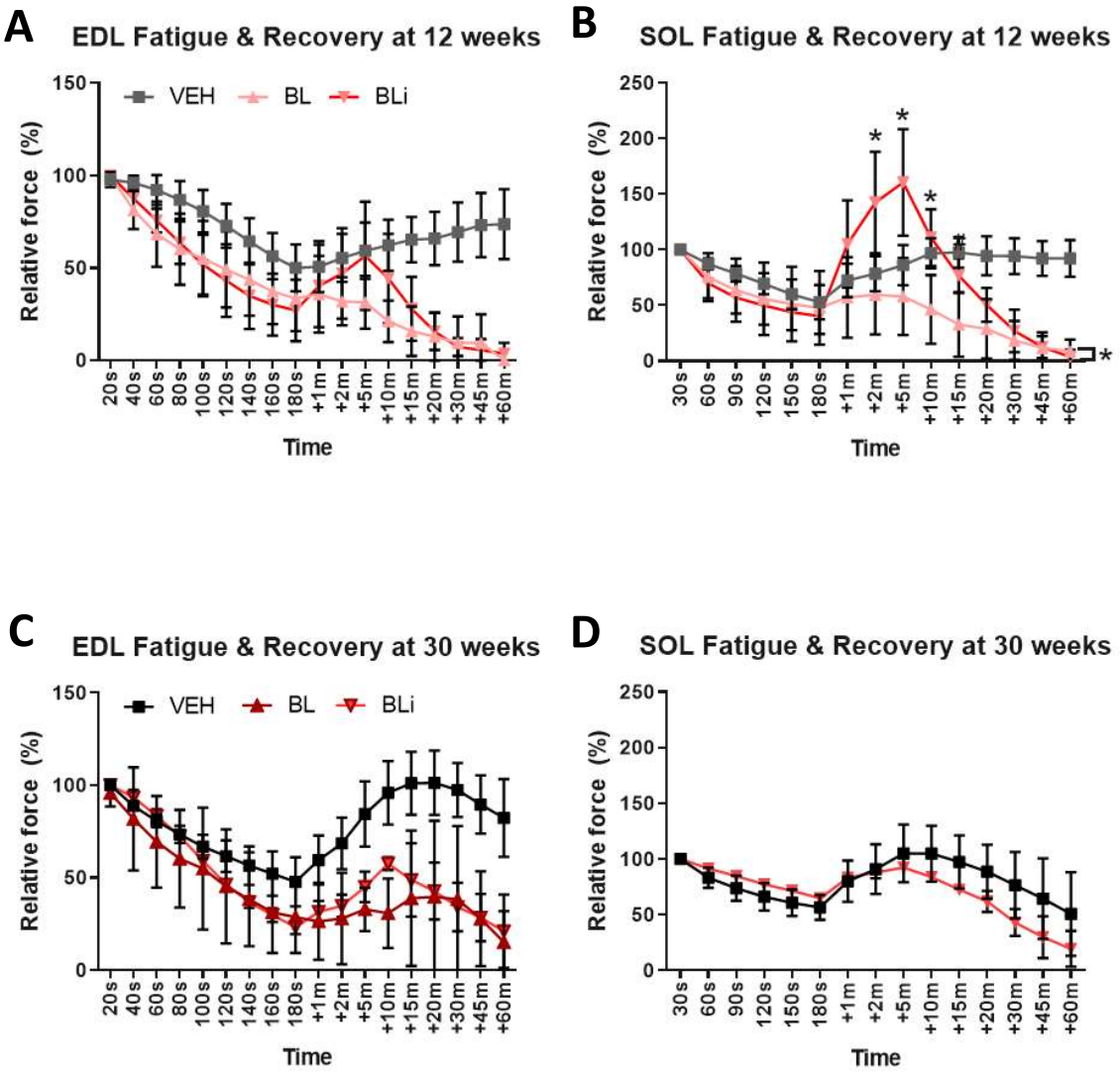

Figure 6.19: Effect of BL-CHOP therapy on fatiguability and recovery capacity in fast-twitch extensor digitorum longus (EDL) and slow-twitch soleus (SOL) muscles from vehicle (VEH), BL-CHOP (BL) and BLi-CHOP treated mice at 12- and 30-weeks of age. *IDEB co-therapy afforded no protection against BL-CHOP therapy-induced muscular dysfunction at 12-weeks of age, with both EDL and SOL muscle showing a considerable decline in recovery capacity, ultimately failing to respond to any stimuli (like BL-CHOP treated muscle). At 30-weeks, IDEB co-therapy showed no change to muscle fatigue and recovery parameters in EDL BL-CHOP treated muscle. Remarkably, however, co-treatment with IDEB completely reversed BL-CHOP therapy-induced dysfunction in SOL m. No BL-CHOP treated SOL m. could withstand the protocol, however, IDEB co-therapy protected SOL m. against this sequalae and returned fatigue and recovery measures to VEH levels. Significance in B between BL-CHOP (BL) and BLi-CHOP (BLi). For VEH to BL data refer to Chapter 5, s5.3.8.3, Figure 5.13.*

6.3.8 Effect of IDEB co-therapy BL-CHOP regimen on fibre size and distribution in Tibialis Anterior muscle.

In previous sections we have shown that IDEB co-therapy significantly effects muscle size, whether that be a reduction with MBi-LCV or an increase with BLi-CHOP therapy. To quantify whether this is attributed to muscle-fibre hypertrophy, or increases in intermuscular tissue (such as fat, connective tissue, fibrosis), histological assessment of Tibialis Anterior muscles harvested from treated mice was performed using a standard H&E stain (refer *Chapter 4, S4.2.2.3* for method).

MB-LCV therapy alone induced no change to Tibialis Anterior (TA) muscle fibre size, or fibre distribution, with co-administration of IDEB also failing to induce an effect (Figure 6.20). BL-CHOP therapy, on the other hand, significantly reduced muscle fibre size by ~17% at 12-weeks and 6% at 30-weeks of age (p<0.0001, Figure 6.21B). IDEB co-therapy truncated the reduction of fibre size seen at 12-weeks by abrogating the loss to 9.8% (p<0.0001). IDEB co-therapy, however, exacerbated BL-CHOP-induced reductions in fibre size at 30-weeks by a further ~4% (*p<0.005* from BL-CHOP, Figure 6.21B). These reductions in mean fibre size at both 12- and 30-weeks were reflected in the fibre size distribution with BL-CHOP treated TA muscle, both with and without IDEB, showing a propensity to house a greater number of smaller muscle fibres with statistically significant reductions in the 1200 μm^2 (p<0.005), 1500 μm^2 (p<0.05), 2700 μm^2 (p<0.001)and 3000 μm^2 (p<0.01) bins (Figure 6.21C-E).

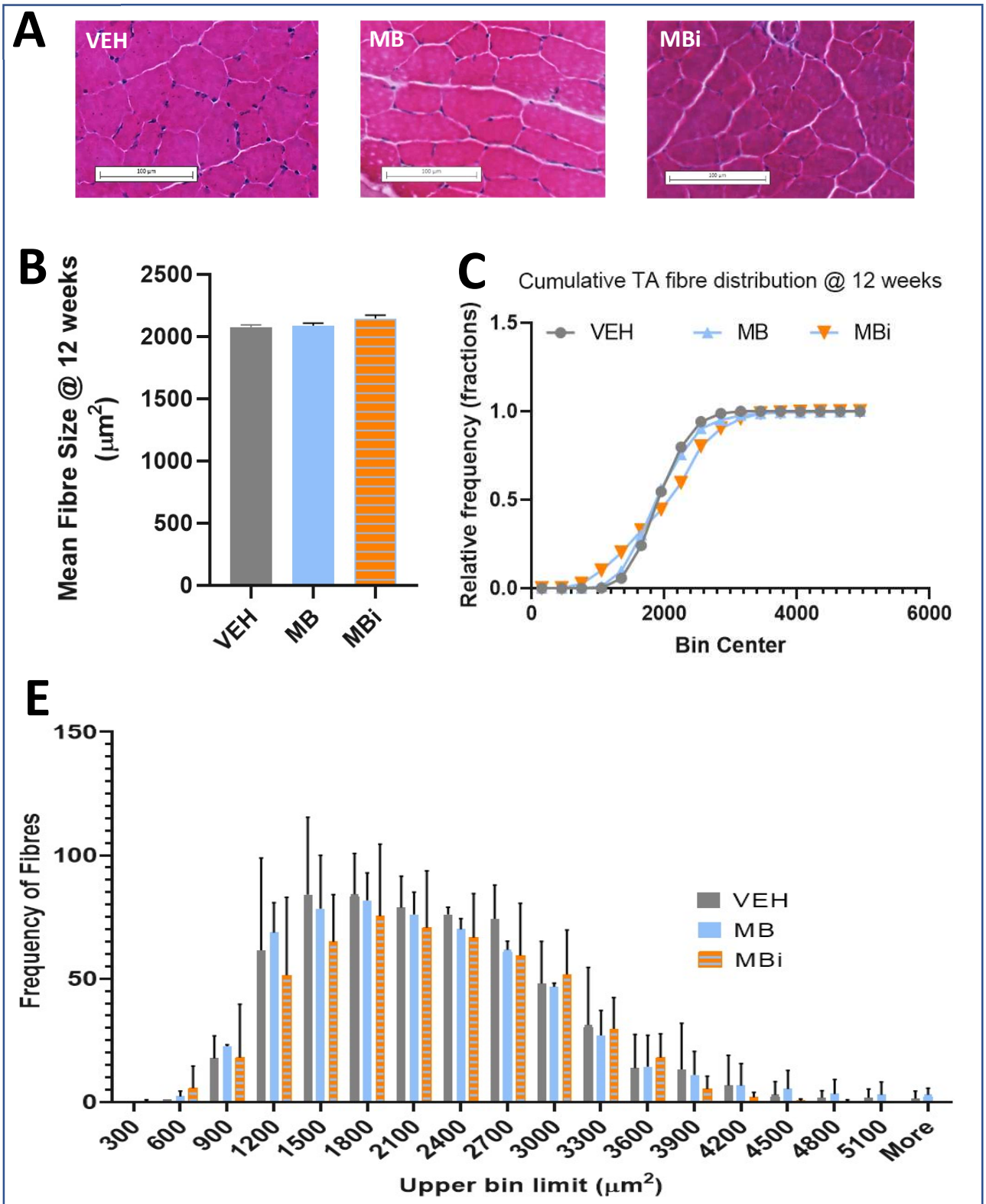

Figure 6.20: Effect of MB-LCV therapy on muscle fibre cross-sectional area (CSA) in tibialis anterior (TA) muscles from vehicle (VEH), MB-LCV (MB) and MBi-LCV (MBI) treated mice at 12-weeks of age. *A) representative images of H&E stained TA muscle B) IDEB co-therapy showed no effect on TA muscle CSA C+D) IDEB did not induce any significant changes in TA CSA from MB-LCV or VEH levels Significance via 2-way ANOVA with Tukey's post-hoc test with data in C) presented as the cumulative fraction of fibre distribution with error removed for ease of viewing.*

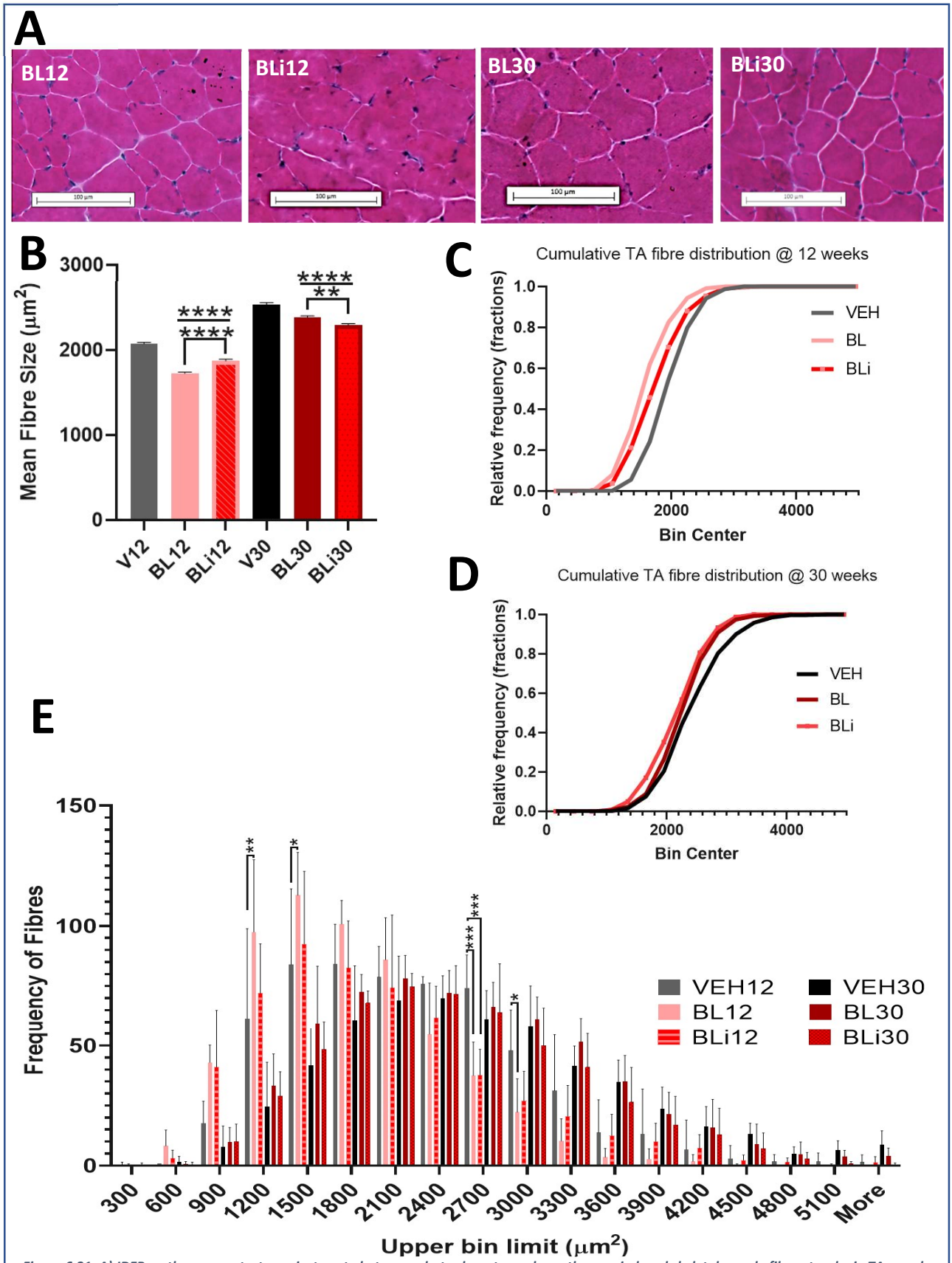

Figure 6.21: A) IDEB co-therapy protects against acute but exacerbates long-term chemotherapy-induced skeletal muscle fibre atrophy in TA muscle. *B) representative images of H&E stained TA muscle.* ***C+D)*** *IDEB co-administration shifts fibre frequency to the right at 12-weeks with an increased number of larger fibres (rightward skew) with BLi30 less larger fibres but a similar curve of distribution. n=4-5 (with ~600 fibres per n for segment A). Significance via 2-way ANOVA with Tukey's post-hoc test where #=0.0523. D) Data presented as the cumulative fraction of fibre distribution with error removed for ease of viewing.*

6.3.9 The effect of IDEB co-therapy with MB-LCV and BL-CHOP therapy on mitochondrial function

IDEB co-therapy was selected due to its ability to scavenge cellular electrons and deliver them to the mitochondria. As previously discussed, IDEB has been reported to oxidise cytosolic ROS and deliver those electrons directly to the succinate dehydrogenase enzyme of the electron transport chain of the mitochondria [298]. Importantly, chemotherapy regimens, regardless of class, have been shown to elevate cellular ROS levels [1,111,254,277] and, although ROS induces many effects within the cell, these molecules have a profound effect on skeletal muscle growth and atrophy pathways and, when in high enough concentrations, induces a net loss of lean mass [589,601,602] (refer to *Chapter 1, S1.2.3* for more detail). As previously mentioned in the *S6.2.2*, as IDEB seemed to bypass the competitive inhibition of antimycin A on complex III, non-mitochondrial respiration (NMR) was measured by the Seahorse XF24 as exceedingly high in the BL-CHOP regimen (refer to Figure 6.24). To correct for this, the NMR measure was added to the measures of basal mitochondrial respiration, ATP-production associated oxygen consumption and proton leak associated oxygen consumption, as the Seahorse XF24 software automatically subtracts NMR from these measures. Although NMR was negligible in both the MB-LCV and BL-CHOP regimens alone, there is the potential that NMR is elevated with IDEB.

IDEB, when delivered with both MB-LCV and BL-CHOP therapy, significantly increased basal respiration rate by 8- and 5-fold respectively (p<0.0001, Figure 6.23A, Figure 6.25A respectively). This increase was associated with an increase in ATP production only when co-administered with MB-LCV (7-fold increase, p<0.0001, Figure 6.23B), but not with

BL-CHOP therapy (Figure 6.25B). With a significantly increased baseline cellular respiration rate without a concomitant increase in ATP production, it is of no surprise that proton leak was significantly increased in both combination therapies (a 4-fold increase with BLi-CHOP, $p<0.0001$, Figure 6.25C), with IDEB and MB-LCV co-therapy also increasing proton leak also by 13-fold from MB-LCV levels ($p<0.0001$, Figure 6.23C).

With IDEB co-therapy, both treatment groups (MBi-LCV and BLi-CHOP) were observed to significantly increase their baseline ceullular activity. An important measure of mitochondrial function is the organelles ability to increase respiratory function to meet metabolic demand. Concomitant with the increase in baseline levels was an almost proportional increase in maximal respiratory capacity in both combination therapies (a 9 fold increase in MBi-LCV when compared to MB-LCV alone, $p<0.0001$; and a 2 fold increase in BLi-CHOP when compared to BL-CHOP alone, $p<0.005$) resulting in no change to spare respiratory capacity (Figure 6.22, Figure 6.23D, Figure 6.24 and Figure 6.25D). Coupling efficiency, however, was significantly reduced in both regimens when IDEB was co-administered, suggestive of a greater electron flux through the mitochondria without a proportional increase in ATP production (an 85% decrease in MBi-LCV, $p<0.0001$ Figure 6.23E, and a 70% reduction in BLi-CHOP, $p<0.0001$, Figure 6.25E). Although ATP production was elevated with MBi-LCV co-therapy, this suggests that the modest increase in ATP production was still accompanied by significant proton leak. Curiously, when given in combination with the BL-CHOP regimen, IDEB thwarted the action of Antimycin A (a potent inhibitor of cytochrome b [603]), masking the non-mitochondrial respiration measure as the mitochondria continued to respire after the inhibitor was administered (Figure 6.24). Although not investigated here, this suggests IDEB has the capacity to overcome the competitive inhibitor and drive electron flow through the electron transport chain even in its presence.

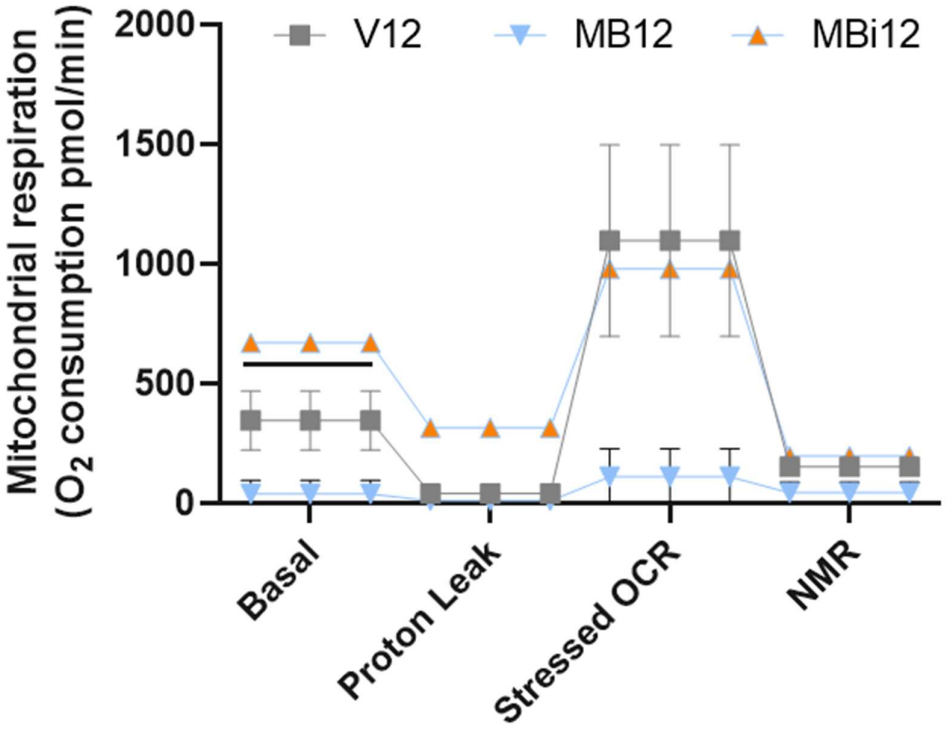

	V12 vs MB12	MB12 vs MBi12	MBi12 vs V12
Basal	<0.05	<0.0001	<0.0001
Proton leak	n.s	<0.0001	<0.0001
Stressed OCR	<0.001	<0.0001	n.s
NMR	<0.001	<0.0001	n.s

Figure 6.22 Changes to cellular oxygen consumption in response to mitochondrial inhibitors and stimulants induced by early-life MB-LCV and IDEB co-therapy at 12-weeks of age. *MB-LCV therapy administered from 4-12 weeks of age to reduced basal respiration by almost 90% and significantly decreased maximal respiration by 90% (p<0.001) as well. IDEB co-therapy rescued maximal respiration returning the value to VEH levels, however basal respiration and proton leak were also elevated above VEH levels by 94% and by over 10-fold respectively. B) Significance values for A) expressed in table format for ease of reference. Error expressed as SD where n=9-10. Significance symbols. These measures are have been corrected for NMR.*

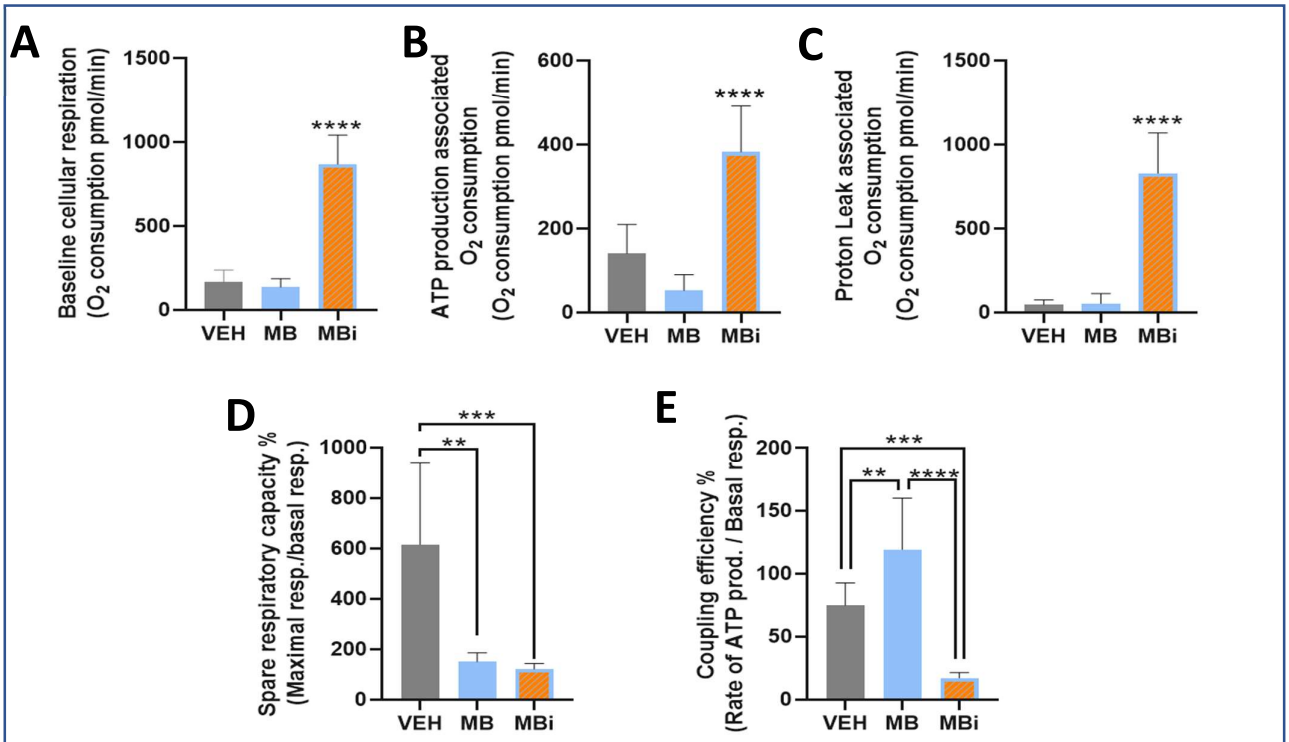

Figure 6.23: Mitochondrial respiratory function of vehicle (VEH), MB-LCV (MB) and MBi-LCV (MBi) treated 12-week old mice: *Isolated muscle fibres from bi-lateral flexor digitorum brevis. m was assessed for baseline cellular respiration (A), ATP-associated oxygen consumption (B) and O_2 consumption linked to proton leak (C). Mitochondrial spare respiratory capacity and coupling efficiency (D & E) were calculated using these measures. IDEB greatly elevated baseline cellular respiration by almost 8-fold (A, p<0.0001), ATP production by 7-fold (B, p<0.0001) and proton leak by 13-fold (C, p<0.0001). Spare respiratory capacity did not change from MB levels remaining at ~130% (D). Coupling efficiency, however, fell with IDEB co-therapy by ~85% when compared to MB-LCV treatment alone (E, p<0.0001). n=6-10 with data presented as mean±SD. Significance via ANOVA with Tukey's post-hoc test. These measures are not corrected for NMR.*

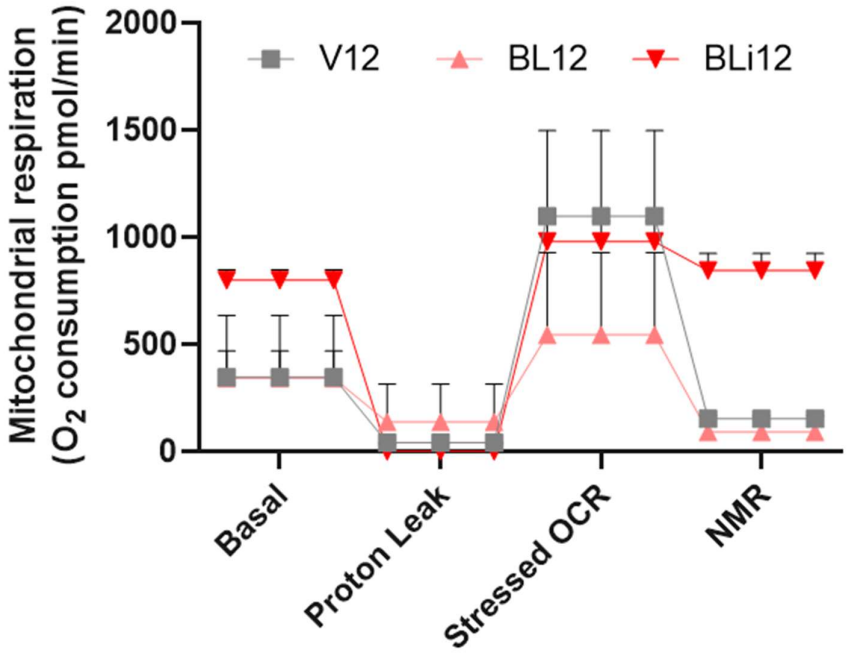

	V12 vs BL12	BL12 vs BLi12	BLi12 vs V12
Basal	n.s	<0.0001	<0.0001
Proton leak	n.s	<0.0001	<0.0001
Stressed OCR	<0.05	<0.005	<0.0001
NMR	<0.05	<0.0001	<0.0001

Figure 6.24 Changes to cellular oxygen consumption in response to mitochondrial inhibitors and stimulants induced by early-life BL-CHOP and IDEB co-therapy at 12-weeks of age*. A) BL-CHOP therapy administered from 4-12 weeks of age significantly reduced significantly decreased maximal respiration by 50% (p<0.001) in 12-week mice. IDEB co-therapy corrected this loss, returning OCR within ~10% of VEH levels, with basal respiration significantly elevated by IDEB co-therapy as well by 133% compared to VEH. Antimycin A response was abrogated by IDEB co-therapy, with little inhibition of complex III being observed after its injection (as measured by NMR) B) Significance values for A) expressed in table format for ease of reference. Error expressed as SD where n=7-10. These measures are corrected for NMR (non-mitochondrial respiration).*

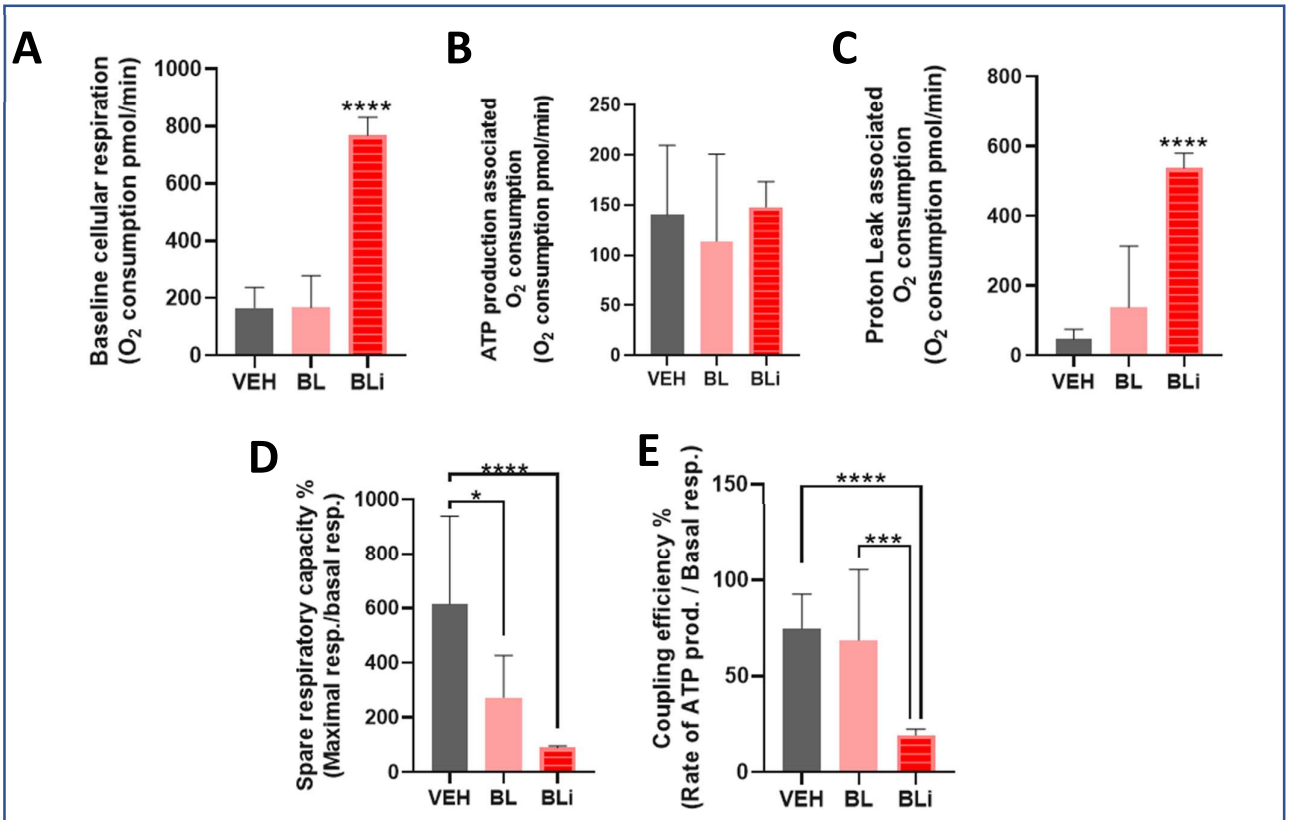

Figure 6.25: Mitochondrial respiratory function of vehicle (VEH), BL-CHOP (BL) and BLi-CHOP treated mice at 12- weeks of age: *Isolated muscle fibres from bi-lateral flexor digitorum brevis. m was assessed for basal (A), ATP-associated oxygen consumption (B) O_2 consumption linked to proton leak (C). Mitochondrial spare respiratory capacity and coupling efficiency (D & E) were calculated using these measures. IDEB greatly elevated basal mitochondrial respiration by almost 5-fold (A, $p<0.0001$) and proton leak by 4-fold (C, $p<0.0001$) with no change to ATP production (b). Spare respiratory capacity did not change from BL levels (D). IDEB co-therapy significantly reduced coupling efficiency from BL levels by 70% (D, $p<0.001$). n=6-10 with data presented as mean±SD. Significance via ANOVA with Tukey's post-hoc test. These measures are not corrected for NMR (non-mitochondrial respiration).*

6.4 Discussion

Although associated with considerable acute and long-term toxicity, chemotherapy is considered as the leading non-surgical treatment against cancer. Reductions of toxicity and side-effects induced by these chemotherapy regimens is an important and effective way to improve efficacy and, thus, the quality of life for those which are treated with it. In the previous chapters we describe two animal models which, to date, most accurately replicate the side-effect profile of gold-standard chemotherapy regimens, MB-LCV and BL-CHOP, used against paediatric medulloblastoma and NHBL respectively. To protect against the cytotoxic damage induced by these regimens to the skeletal muscular system, we have investigated the therapeutic efficacy of IDEB to ameliorate regimen-associated toxicity when co-administered daily in young mice. In doing so, we showed that IDEB co-therapy with BL-CHOP-therapy: (1) completely protected against BL-CHOP lethality and reduced CHOP-associated organ pathologies in the kidney, liver and gastrointestinal system as well as anthracycline-mediated cardiotoxicity; (2) protected against chemotherapy-induced skeletal muscle atrophy which promoted weight gain during and after each active chemotherapy cycle; and (3) protected against life-long skeletal muscle weakness as measured by grip-strength induced by CHOP therapy. In contrast, IDEB co-therapy with LCV-therapy promoted chemotherapy-induced toxicity as evidenced by increased mortality and afforded no protection to the skeletal muscular system (as assessed by grip strength), but rather decreased muscle mass (as per volumetric analysis of tibial cross-section) and muscle endurance and recovery capacity (as per *ex vivo* analysis).

6.4.1 Therapeutic efficacy of IDEB co-therapy against MB-LCV-induced toxicity

In *Chapter 4*, we showed that MB-LCV therapy induced a pre-sarcopenic state, which was characterised by weakened and dysfunctional skeletal muscle, mitochondria which were unable to increase metabolic activity to meet demand, and a state of elevated systemic inflammation, however, skeletal muscle atrophy was yet to be observed. The primary goal of delivering IDEB in concert with chemotherapy was to alleviate, or completely abrogate, the toxic effects of the regimen. IDEB co-therapy with MB-LCV therapy was shown to increase the mortality rate by 10% (p=0.078, RR=1.1, Figure 6.1). Although only a small increase in mortality, and one where statistical significance was considered a trend at best, any increase in mortality is an unacceptable one. It is, however, entirely reasonable to suggest that had appropriate supportive care been available, these deaths could have been avoided, but due to the limitations in resources this wasn't available here. Nevertheless, IDEB co-therapy was ceased at 12-weeks and investigations into the long-term effects of IDEB and MB-LCV combination therapy (from 12-30 weeks of age) was not commenced. IDEB co-therapy, however, showed promise in other areas, including the co-therapy's ability to significantly increase weight gain during the period of chemotherapy administration. IDEB caused an increase in body weight by 20% when compared to chemotherapy without IDEB (p<0.0001) in the 12 weeks treatment which was characterised by a significant increase in catch-up growth after the initial insult of anti-neoplastic treatment. As weight-loss is often linked to a poor prognosis in chemotherapy patients, an ability to improve patient weight-gain – or at least maintain weight during treatment – could prove to be highly beneficial in the clinic [483]. Perplexingly, however, the observed weight gain was concomitant with an overall decrease

in food consumption (Figure 6.4). Calorie restriction has numerous benefits to skeletal muscle through rerouting energy metabolism and inducing autophagy [604,605]. We theorise that this may be a result of improved energy utilisation afforded by IDEB, resulting in an improved respiratory performance and utilisation of energy substrates such as glucose and lipids (effect of IDEB on mitochondrial respiration discussed in more depth below). In instances where the mitochondria produce ATP which exceeds energy demand, fatty acid oxidation is switched off (through AMPK-mediated inactivation of fatty-acid oxidation via CPT1 inhibition) resulting in elevated fat storage and induction of growth signals, together with a reduction of feeding via leptin signalling to the hypothalamus [606].

Although molecular investigations of this weight gain were outside the scope of this thesis, to investigate the nature of this weight gain, μCT analysis was used to quantify hind limb mass at the proximal portion of the tibia; which is typically nearly homogenous in lean mass tissue aside from bone [527]. These investigations showed that MB-LCV and IDEB co-therapy induced a reduction in hind-limb volume at 12-weeks, however wet-weights of the TA, SOL, EDL and PLA (major muscles in this area) remained unchanged. Fibre size of the TA muscle (as measured by histological analysis, Figure 6.20) also remained unchanged. This is intriguing as these data suggest a decline in overall muscle size without a matched reduction in muscle weight or fibre cross sectional area. Contractile function investigations showed the optimal length required to produce maximal force of both EDL and SOL muscles were also both significantly reduced by 21% (p<0.001) and 19% (p<0.001), respectively (Figure 6.12). Taken together with reductions in specific force (force corrected for muscle mass, EDL -69%, p<0.005; SOL -74%, p<0.001), these data show that, although muscle weight or cross-sectional

area has not changed, muscle fibres are shorter in nature and their functional capacity to produce force is impaired. Moreover, IDEB co-therapy further exacerbated fatiguability and hindered recovery all together in both the EDL and SOL muscles (Figure 6.15). As eluded to in *Chapter 4*, there is the potential that MB-LCV therapy alone may induce a pre-sarcopenic state which is categorised by skeletal muscle dysfunction but without muscular atrophy. However, when MB-LCV is administered with IDEB, atrophy, as measured by a loss of total muscular volume, is evident which may be indicative that IDEB has accelerated the chemotherapy-induced progression into a true sarcopenic state.

It is interesting to speculate how IDEB co-therapy promotes the pathological processes underpinned by MB-LCV therapy. Although the mechanism of action of IDEB is currently under speculation, it is primarily thought that IDEB scavenges electrons from the cellular environment and delivers them to directly to Complex III, in sorts mimicking co-enzyme Q10 [296,298,607]. More recent, mechanistic studies of IDEB have also postulated that IDEB increases insulin sensitivity, increasing glucose uptake into the cell [608-610]. In our mitochondrial investigations of IDEB with MB-LCV, we show that IDEB markedly increased basal and ATP associated oxygen consumption (p<0.0001, Figure 6.23) and returned maximal oxidative capacity to VEH levels (an improvement of 90% from MB-LCV therapy alone p<0.0001), supporting the theory that the CoQ10 analogue drives scavenged electrons through the oxidative phosphorylation machinery of the mitochondria. As discussed in *Chapter 4*, the primary constituents of LCV therapy are lomustine (CCNU, an alkylating nitrourea) and cisplatin (CDDP, a platinum-based alkylating agent), and vincristine (VCR, a mitotic inhibitor) with cisplatin shown to greatly impair mitochondrial function through adduction of the

organelles single-stranded DNA. Previously, we were the first to show that the platinum-based alkylating agent oxaliplatin directly penetrates the mitochondria and accumulates within the organelle, causing significant increases in mtROS and signs of mitochondrial dysfunction [159]. When considered in the current context, it may well be that the potentially CDDP-damaged mitochondria were unable to cope with the heightened IDEB-mediated electron flux during times of amplified metabolic demand. This could explain the elevated rates of muscular fatigue during extended bouts of exercise as seen in our contractile function experiments.

6.4.2 Therapeutic efficacy of IDEB co-therapy against BL-CHOP-induced toxicity

In the previous chapter we showed that BL-CHOP therapy clearly induced the CI-SMDW phenotype; causing chronic skeletal muscle dysfunction characterised by decreased muscle mass, strength and endurance and recovery capacity. Moreover, at the 12-week timepoint, BL-CHOP treated mitochondria showed a supressed spare respiratory capacity which was underpinned by an inability to match oxidative phosphorylation to demand at increased rates during times of metabolic demand. All of this, in combination with multi-organ pathologies of the liver, heart and kidney resulted in a significantly elevated mortality rate of 77% in the first 30-weeks of life. IDEB co-therapy, remarkably, completely protected mice from BL-CHOP lethality, with no mice which underwent combination IDEB+BL-CHOP therapy succumbing to treatment. This drastic improvement in survivability is likely underpinned by the significant improvement in weight-gain during the treatment course, with mice being 36%

heavier than their chemotherapy-treated counterparts which did not receive IDEB. Although a similar improvement in weight was seen in the MB-LCV with IDEB combination therapy, here, weight gain was associated with an 18% increase in muscle mass as a result of IDEB co-therapy (Figure 6.). IDEB co-therapy also alleviated cardiac-, hepatic-, renal- and gastrointestinal-associated pathologies (Table 6.2). Although the mechanisms of pathology induction by the BL-CHOP regimen was not investigated, elevated levels of ROS has been indicated in the aetiology of all organ-pathologies observed here [593,611,612]. Moreover, cardiomyopathies are a well-described sequalae mediated by anthracycline-induced oxidative stress within cardiomyocytes. [114,235,236,613-615]. If indeed IDEB is acting as a power antioxidant as the literature suggests, this would explain how the molecule remedies the organ-pathologies seen whilst simultaneously driving mitochondrial function. Moreover, doxorubicin-mediated skeletal muscle atrophy has also been linked with elevated states of oxidative stress [263,590]. As IDEB co-therapy ameliorated the observed chemotherapy-induced wasting in the BL-CHOP regimen, this further reinforces our hypothesis that IDEB is acting as a powerful antioxidant, scavenging electrons and delivering them to the mitochondria. Conversely, adjuvant IDEB therapy instigated skeletal muscle wasting when given in combination with the MB-LCV regimen, highlighting that antioxidant therapy may be efficacious in a U-like relationship (Figure 6.). MtROS, and oxidative stress in general, has been shown to contribute to a delicate balance of growth and atrophy through various intracellular pathways – such as exercise mediated oxidative stress which at certain levels promotes anabolic effects through the NF-κB, MAPK/ERK and PI3K/Akt pathways [616,617]. As IDEB protected against skeletal muscle wasting in the BL-CHOP regimen, but initiated wasting (or more likely inhibited growth pathways) in the MB-LCV regimen, this serves to suggest that completely resolving oxidative stress can also be detrimental. The concept of hormesis is

important here, whereby certain levels of a substance promote a favourable response, however, any levels outside this biphasic, hormetic zone induces an adverse reaction [618]. In this instance, skeletal muscle growth and cytoprotective adaption appears to requires a certain level of ROS to initiate change, however, without any level at all, the important "cross-talk" to develop cytoprotective capacity and adaptive growth to stress within the cells has ceased to exist.

Adjunctive IDEB treatment with BL-CHOP therapy, at the mitochondrial level, resulted in both an increase in baseline and maximal respiration by 133% and 50% respectively, indicative of higher mitochondrial flux (p<0.0001 from VEH, Figure 6.24 and Figure 6.25). Interestingly, when IDEB was given together with antimycin A, a complex III inhibitor, IDEB mitigated the inhibition. The mechanism of mitochondrial inhibition afforded by antimycin A is through competitive inhibition of the quinone reduction site on the cytochrome bc_1 complex [603]. As this was overcome in the BL-CHOP regimen, but not the MB-LCV regimens, we propose that, due to the anthracycline redox reaction occurring at complex I, a greater number of available electrons are present within the mitochondria (associated with the reduced doxorubicin analogue). As IDEB is thought to act as a semi-quinone and electron scavenger, we hypothesise that IDEB is able to chaperone these electrons directly to the quinone reduction site in a high enough concentration to overcome the competitive inhibition of antimycin A. Alternatively, it is possible that IDEB delivers its electrons to an alternative site, either elsewhere on the cytochrome bc_1 or further down the respiratory chain. Although it is interesting to speculate, the exact mechanisms of how IDEB overcame antimycin A inhibition of the mitochondria requires further targeted investigations to elucidate.

The ability for IDEB to completely protect against chemotherapy-induced skeletal muscle wasting and mortality in the BL-CHOP regimen is an exciting property, however, more work to elucidate its therapeutic mechanisms are needed to enable benchtop to bedside translation. Long-term survivors of chemotherapy still, however, suffer from a decline in skeletal muscle function by way of weakness and fatigue. Our investigations into the protective nature of IDEB against skeletal muscle dysfunction show promising results. After 8 weeks of daily IDEB treatment, grip strength returned to VEH levels, an improvement of 16.5% from BL-CHOP levels (Figure 6.11). In *ex vivo* analysis of contractile function, IDEB co-therapy significantly improved SOL endurance and recovery capacity and, although no improvements were noted in these parameters in the EDL muscle, importantly, no decline was observed either.

6.5 Chapter Summary

In summary, IDEB co-therapy afforded mixed protection, dependent on the chemotherapy regimen it was delivered with. On the one hand, when delivered in concert with the MB-LCV regimen, IDEB exacerbated the MB-LCV sequalae, increasing mortality, skeletal muscle dysfunction and wasting and mitochondria dysfunction. We hypothesise that this was underpinned by the adducting nature of cisplatin; whereby the platinum-based alkylating agent induces damage to the mitochondria. As IDEB was shown here to drive baseline cellular respiration and stressed mitochondrial function, increased flux through these damaged mitochondria may very well have resulted in aberrant metabolic flux and ROS production, driving the already present MB-LCV-created pathologies. Moreover, IDEB co-

therapy with the MB-LCV regimen was shown to have a detrimental effect on skeletal muscle growth suggesting that too much antioxidant defence could in fact be detrimental. On the other hand, IDEB co-therapy successfully mediated the CI-SMDW sequalae induced by the anthracycline-based BL-CHOP regimen in a healthy animal model. Importantly, IDEB co-therapy completely protected against BL-CHOP-induced mortality and skeletal muscle atrophy, as well as affording protection against multiple-organ pathologies; such as right ventricular cardiomyopathy and gastrointestinal mucositis. Here we have shown in a clinically relevant, pre-clinical healthy mouse model, that the co-Q10 analogue, IDEB, is a viable therapeutic to combat anthracycline-based regimen toxicity and lethality. Although further investigations are required to assess the molecules therapeutic efficacy with other regimens, and in the setting of the treatment with its associated pathology, the addition of continuous IDEB treatment in concert with the CHOP regimen may very well afford complete protection against CI-SMDW and mortality during childhood chemotherapy administration.

Chapter 7

Conclusions & Future Directions

7.1 Summary of the thesis

The broad aim of this thesis was to determine whether mitochondrial targeting therapies, specifically IDEB, can prevent acute and/or long-term skeletal muscle dysfunction and wasting induced by juvenile gold-standard chemotherapy treatment in clinically relevant mouse models. In particular, this thesis has successfully developed clinically relevant juvenile mouse models for the investigation of gold-standard chemotherapy regimens used against paediatric ALL-POMP, MB-LCV and BL-CHOP. Further, this thesis investigated the efficacy of IDEB to alleviate the CI-SMDW sequalae by targeting the mitochondria to afford protection to both the organelle and the skeletal muscle.

7.1.1 Summary of the major findings

Although paediatric cancer comprises 1% of all cancer cases [3], the disease state is responsible for the loss of over 150,000 years of potential life each year in the United States alone [90]. Moreover, Australian children diagnosed with cancer are 2000 times more likely to die within 5 years of diagnosis than other healthy children [6]. The front-line anti-neoplastic treatments used to combat paediatric cancer – namely chemotherapy and radiotherapy – base their efficacy around attenuating the ability of neoplastic cells to replicate and grow. Unfortunately for the children that receive these therapies, they too are undergoing rapid and concerted growth. Due to the non-specific and systemic mode of action, chemotherapy elicits effects on healthy and neoplastic cells alike inducing a plethora of side-effects which significantly increase morbidity and mortality experienced by these children. Growing

evidence also suggests that normal skeletal muscle growth and repair processes are compromised by chemotherapeutic treatment, which can manifest into chronic chemotherapy-induced skeletal muscle dysfunction and wasting (CI-SMDW) throughout the lifespan, culminating in reduced strength, endurance and mobility which is exacerbated when treatment is administered during childhood [18,19,21,22]. Due to the complexity of the chemotherapy regimens used to treat childhood cancer, the multitude of chemotherapeutic agents used, and duration of administration, appropriate investigatory animal models to elucidate the exact pathological mechanisms which underpin CI-SMDW have yet to be developed. In light of this, the broad aim of *Chapter 2* was to develop a framework which could be used to create clinically relevant animal models which could investigate interventions against chemotherapy-induced sequalae. This framework, titled the '*Intervention Animal Model Development Framework' (*IAMDF) was then used to create clinically relevant animal models upon which the CI-SMDW pathology could be investigated.

Through review of the literature in *Chapter 1*, and the application of the IAMDF described in *Chapter 2,* the gold-standard chemotherapy regimens 'POMP' (using primarily 6-mercaptopurine (Purinethol), vincristine (Oncovin), methotrexate and prednisone, developed by the *Children's Cancer Group* [322]), 'LCV' (using Lomustine, Cisplatin and Vincristine developed by the *Children's Cancer Group* [124,331-334]) and 'CHOP' (using Cyclophosphamide, doxorubicin (Hydroxydaunorubicin), vincristine (oncovin) and prednisone, developed by collaboration between *Française d'Oncologie Pédiatrique* and the *United Kingdom Childhood Cancer Study Group* [338]) which are used to combat ALL, medulloblastoma and NHBL were adapted for use in juvenile mice. The viability of these models were then assessed in in juvenile mice in *Chapter 3,* where pilot studies were used to refine the human modified ALL-

POMP, MB-LCV and BL-CHOP regimens to be both tolerable and as close to clinically relevant doses as possible.

The major accomplishments of *Chapters 2* and *3* were that, through the application of the IAMDF, juvenile mouse models which accurately depict the clinical sequalae experienced by children undertaking ALL-POMP, MB-LCV or BL-CHOP therapy were developed. Specifically, after dose and regimen modifications were made, all three regimens induced similar levels of weight loss, skeletal muscle dysfunction, and generalised pathology as described in the clinic setting. Moreover, the modified ALL-POMP regimen accurately replicated clinically appropriate levels of immune suppression which is a pivotal characteristic of chemotherapy intervention against ALL. Although we present here validated, clinically relevant juvenile mouse models capable of investigating the ALL-POMP, MB-LCV and BL-CHOP regimens, due to the extensive amount of time taken to develop the ALL-POMP model, only the MB-LCV and BL-CHOP models were investigated further in this thesis.

Considering the accomplishments of *Chapters 2* and 3*, Chapter 4* and *5* used the developed MB-LCV and BL-CHOP models to investigate the CI-SMDW phenotype further. The major findings in *Chapter 4* was that MB-LCV administration in juvenile mice caused: 1) significant reductions in skeletal muscle contractile function which was endured throughout the lifespan, even in the absence of observable systemic toxicity, chemotherapy-induced muscle atrophy, or mortality. These functional reductions were accompanied by; 2) a state of elevated systemic inflammation; and 3) mitochondrial dysfunction characterised by a reduced ability to adapt to metabolic demand. When these are considered together, MB-LCV therapy appears to induce an early onset pre-sarcopenic state; where skeletal muscle dysfunction was present without signs of muscle atrophy. Specifically, we showed that MB-LCV therapy

induced moderate levels of skeletal muscle dysfunction at 12 weeks of age which worsened by 30-weeks of age (characterised by a 40% loss in grip strength, and significant declines in post-exercise/contractile recovery capacity which was not present at 12 weeks). We also showed that singular twitch *ex vivo* muscle contractions produced significantly less force which was independent of atrophy, suggesting that chemotherapy was inducing some form of at the molecular or structural level. Although not directly investigated here, damage at the molecular cross-bridge level, ROS induced structural damage or Ca^{2+} dysregulation could all be implicated in the dysfunction seen here [1,112,619-622]. These dysfunctions were concomitant with significant declines in mitochondrial function, with mitochondria from chemotherapy-treated muscle showing reduced responsiveness to chemical uncoupling, i.e. metabolic stress. These findings in *Chapter* 4 suggest that the decline in skeletal muscle endurance and recovery induced by MB-LCV therapy are likely underpinned by chemotherapy-damaged mitochondria; which are unable to escalate oxidative phosphorylation to meet the metabolic demands of exercise. We have shown in previous studies that the platinum-adducting alkylating agent oxaliplatin (the same class of drug as cisplatin used in MB-LCV therapy) are capable of penetrating and damaging the mitochondria [159]. This is likely the case here, as the mitochondria play a cardinal role in the replenishment of ATP which is required for on-going skeletal muscle contraction and performance. Any abrogation in muscle energy homeostasis demonstrably results in poor muscle performance and damage as ATP is required for continuous and effective cross-bridge cycling [623].

Where *Chapter 4* presented the implementation of the modified MB-LCV therapy and its consequent induction of the SMDW phenotype; *Chapter 5* presented the implementation

of the modified BL-CHOP regimen and the investigation of its effects on juvenile mice. The major findings of this study was that BL-CHOP therapy in juvenile mice 1) induced a reduction in muscle volume by 15% and reduced overall survival by 77% by 30-weeks of age; 2) induced severe organ toxicity inclusive of cardiomyopathy and renal-, liver- and gastrointestinal-opathies; 3) induced lifelong skeletal muscle dysfunction and wasting which was characterised by significant reductions in grip strength, muscle fibre size , *ex vivo* muscle endurance and recovery capacity; and 4) truncated mitochondrial metabolic flexibility at 12-weeks, which was categorised by a 44% reduction in spare respiratory capacity. Importantly, mice treated with BL-CHOP therapy were as strong at 12-weeks as they were at 30-weeks (as determined by grip strength) and showed no improvement in muscular endurance and recovery over the same time period. Although BL-CHOP-treated mice recovered bodyweight back to VEH levels, skeletal muscle volume of the hind limb was 16% less than VEH-treated counterparts. These findings show that skeletal muscle wasting was induced by CHOP therapy during the juvenile years of the animals and that, ultimately, the underlying mechanisms were irreparable. Although not directly measured here, us, and others, have previously shown that chemotherapeutic agents, irrespective of class and mechanism of action (in particular the anthracycline and alkylating classes used here in the BL-CHOP and MB-LCV regimens), increase mitochondrial reactive oxygen species (mtROS) production. This increase in mtROS levels is thought to be due to chemotherapy-induced damage to the mitochondrial respiratory enzymes, subsequently causing electron leak from the respiratory chain which ultimately reduces oxygen, forming ROS. These highly reactive molecules have been shown to further damage both the skeletal muscle and mitochondria, as well as cause activation of various intra-cellular pathways, such as atrophy, resulting in the cessation or abrogation of growth [624]. When taking this into consideration with the fact that both the MB-LCV and BL-

CHOP regimens induced significant declines in mitochondrial and skeletal muscle function, it seems unequivocal that the mitochondria, at the very least, exacerbates the CI-SMDW phenotype. Thus, we hypothesised that by using an electron scavenging antioxidant which could simultaneously protect the mitochondria and the skeletal muscle from elevated ROS, whilst improving mitochondrial function could prove to be therapeutic against CI-SMDW.

Therefore, the overall aim of the study presented in *Chapter 6* was to determine whether co-delivery with the mitochondrial Co-Q10 analogue; IDEB, could protect the mitochondria, and thus the skeletal muscle, against the dysfunctions induced by the BL-CHOP and MB-LCV regimens. In doing so, we showed that IDEB co-therapy with BL-CHOP-therapy: (1) completely protected against BL-CHOP lethality and reduced CHOP-associated organ pathologies in the kidney, liver and gastrointestinal system as well as anthracycline-mediated cardiotoxicity; (2) protected against chemotherapy-induced skeletal muscle atrophy which promoted weight gain during and after each active chemotherapy cycle; and (3) protected against life-long skeletal muscle weakness as measured by grip-strength induced by CHOP therapy. In contrast, IDEB co-therapy with the LCV-therapy promoted chemotherapy-induced toxicity as evidenced by increased mortality and afforded no protection to the skeletal muscular system (as assessed by grip strength), but rather decreased muscle mass (as per volumetric analysis of tibial cross-section) and muscle endurance and recovery capacity (as per *ex vivo* analysis). Although further investigations are required to assess IDEB's therapeutic efficacy with other regimens, the addition of continuous IDEB treatment in concert with the CHOP regimen afforded near-complete protection against CI-SMDW and mortality during childhood chemotherapy administration.

7.1.2 Discussion of the major findings

The collective studies presented in this thesis have investigated CI-SMDW in clinically relevant mouse models which have highlighted that, regardless of regimen, skeletal muscle dysfunction is accompanied by aberrant mitochondria. Work done by Talvensaari *et al* [22,259,625] and Ness *et al*. collectively show that survivors of childhood cancer and chemotherapy (of various chemotherapeutic regimens) display increased body fat metabolic abnormalities, as well as reduced skeletal muscle strength, mass and endurance capacity – the very phenotype that we have displayed here with chemotherapy administration independent of cancer [16,18,509,626]. These studies, together with the ones presented within this thesis, serve to highlight that chemotherapy may in fact bring about early sarcopenia of within the musculoskeletal system. Although further research into the molecular profile of the pathology is needed, the sequalae described here clinically mirrors the sequalae described in sarcopenia; namely "progressive and generalized loss of skeletal muscle mass and strength [which] strictly correlate[s] with physical disability, poor quality of life and death" [627]. Moreover, the similarities between our animal investigations here and what is experienced in the clinic, further highlights that chemotherapy-induced damage sustained in childhood is not fully reversible and that impairment of growing muscle, and mitochondria could, either singularly or together, lead to the emergence of delayed or persistent skeletal muscle dysfunction many years after chemotherapy administration has ceased.

By using the antioxidant and Co-Q10 analogue, IDEB, we have shown that by improving mitochondrial function we could, to some degree, ameliorate the CI-SMDW. Importantly, co-administration with the notoriously lethal and aggressive BL-CHOP therapy regimen, completed protected juvenile mice against death and life-long morbidity. The

therapeutic efficacy of IDEB in this setting is promising, however, it also provides a significant insight into the CI-SMDW pathology, suggesting that mitochondrial dysfunction likely underpins, to some level, the severe toxicity induced by chemotherapy administration; at least by the BL-CHOP regimen.

7.2 Study Limitations

Although several significant and positive findings were made and presented in this thesis in relationship to CI-SMDW and the efficacy of IDEB adjuvant therapy, there are several limitations of these studies worthy of discussion:

1. As outline in *Chapter 4: S4.2.1.2,* the VEH group used for comparison within this thesis was based off the most aggressive regimen: namely, ALL-POMP. This was done to reduce the total number of animals used and the human resources required to complete the VEH studies. In doing so, this VEH regimen induced the greatest level of handling, injections and gavages that the animals would have experienced in the ALL-POMP regimen and was used as the VEH group for the less aggressive MB-LCV and BL-CHOP regimens. This is a clear limitation of this thesis as the effects of each regimen would have been more scientifically sound if they were compared to a matching VEH regimen. By comparing the MB-LCV and BL-CHOP effects to a VEH regimen based on the ALL-POMP regimen, the increased aggressiveness of this VEH regimen may have masked, or reduced, the effects

of seen due to chemotherapy administration. This study would have benefited by including VEH regimens based on the regimens that they were designed to be compared to.

2. Although clinical relevancy of the animal models were maximised to the best of our ability within the limits of available resources, it would have been beneficial to deliver some of the chemotherapeutics via intravenous feed; as is done in the clinical setting. Murine osmotic pumps are available which can effectively replicate the intravenous administration of chemotherapeutics, however, due to their high cost per unit and the high number of animals used in these studies, there use were not viable. Thus, it is possible that the acute nature of delivery of some of the chemotherapies used in our studies, such as doxorubicin and methotrexate, could have exacerbated their toxicity profile beyond what is experienced in the clinical setting.

3. Bodyweight and micro-computed tomography imaging were employed to measure general loss of weight and lean mass, respectively. Due to the shortcomings of our contrasting method for the hind-limb – which, if successful, would have allowed for accurate volume and density measures of muscle, fat, connective and bone tissue – accurate measurements of skeletal muscle volume and density together with the ability to differentiate from other tissue types within the hind-limb were lost. Although volumetric analysis was possible, this method did not definitively measure the skeletal muscle and thus the loss of volume measured by us could have been due to loss (or infiltration) of other tissue types, such as fat or connective tissue. Further, it is possible that, by using this method of volumetric analysis, lean mass loss may have been masked by or underestimated due to fat infiltration or fibrosis. It would have been beneficial here

for our contrast method to have been successful. However, whole body computed tomography imaging of the mouse would have provided far greater detail of body composition changes, and more accurately been able to define the changes seen in response to chemotherapy administration.

4. Further to the prior limitation, the exact mechanisms of skeletal muscle loss were not quantitated in this study. Similarities were drawn from previous studies by us, and others, to our studies presented here – specifically, that chemotherapy administration, regardless of class, increased mtROS levels. The studies, and conclusions presented within this thesis would have been strengthened by measurements of mtROS levels and downstream effects on atrophy, extracellular matrix remodelling, satellite cell turnover, mitophagy and mitochondrial fusion and fibre type changes to mention a few. Moreover, investigations elucidating the underlying changes in molecular structure and signalling pathways of the skeletal muscle to appropriately characterise the loss of function and mass seen here would have beneficial. Although western-blot analysis of molecular markers of atrophy, protein synthesis, autophagy and mitophagy were commenced (specifically Bax, P70-S6 kinase, the ubiquitin-proteasome pathway via the non-radioactive SUnSET method, ERK1/2 and mTOR), investigations are yet to be completed due to time-constraints.

5. Although nuclear and mitochondrial DNA were isolated from muscle homogenates by us to assess for any chemotherapy-induced gene DNA damage or changes to gene expression, we were unable to complete this side of the study due to time constraints. It was planned to use the high-throughput next generation sequencing MiSeq System (Illumina, USA) to assess for any changes to skeletal muscle or mitochondrial coding nDNA

sequences and the entire mtDNA plasmid. The studies here would have benefited from these investigations as any changes to these coding sequences (and resulting proteins) could provide further insight to the CI-SMDW characterised here.

6. In adjuvant IDEB therapy with the BL-CHOP regimen, IDEB significantly mitigated the action of antimycin A, resulting in exceedingly high levels of non-mitochondrial respiration being measured. To account for this, the NMR value was added back to measures which were normally corrected for NMR. Although the NMR was largely negligible in mitochondria from BL-CHOP and MB-LCV treated muscle with out IDEB, there is the potential that IDEB elevated NMR and that our corrections have masked these changes. These studies would have benefited from the addition of other mitochondrial inhibitors, such as rotenone, to adequately shut down the mitochondria and for true non-mitochondrial respiration to be measured.

7. As the EDL and SOL muscles were used in the contractile function and µCT analysis protocols, histological assessment of these muscles were not performed in this study. As such, the TA was histologically assessed as the muscle is within the same compartment as the EDL and the same anatomical region as the SOL muscle. The TA also provides a relatively homogenous mix of both fast and slow twitch muscle fibres upon which histological investigations could be performed. Moreover, these studies would have benefited from a more comprehensive histological analysis of the musculature, particularly fibre typing to assess for fibre-type switching as the loss of type II fibres being characteristic of the sarcopenic phenotype together with connective tissue and fat infiltration for signs of structural change and fibrosis.

8. The effects of chemotherapy and mitochondrial dysfunction on circulating insulin and glucagon levels was not investigated in concert with glucose tolerance testing. Although the glucose tolerance test is commonly used in the clinic as an assessment of glucose handling, although only some changes to glucose levels were observed, investigations which considered changes to these hormones would have been beneficial.

9. Although the co-administration of IDEB was successful in reducing if not alleviating the various sequalae induced by chemotherapy administration, the studies here would have benefited from investigating other antioxidants (like SS-31 mentioned in Chapter 2), as well as investigating the therapeutic efficacy of IDEB in combination with other therapies (like ALL-POMP) and at different dosages.

10. Any alteration to gold-standard therapies raise concerns that their therapeutic efficacy may be mitigated. Although investigations of the BL-CHOP and MB-LCV regimens with IDEB in a xenograft cancer model were planned, it is unknown whether the addition of IDEB would affect the anti-cancer efficacy of the chemotherapy regimens against the cancer they aim to treat. Moreover, it is unknown whether the side-effect profile of BL-CHOP and MB-LCV would change if they were delivered in a model which expresses the cancer they are aimed to treat. These studies would have been greatly beneficial to this thesis, however, due to the considerable resources and time required to develop these models and complete these studies, they were unable to be included in the timeframe of this PhD candidacy.

~~12.~~11. Treatments and treatment regimens are consistently changing over the course of each year, with considerable improvements to gold standard therapies being made frequently. At the time

of authorship, the regimens used within this thesis were considered the gold standard therapy, however, these treatments have evolved and will continue to evolve after the publication of this thesis. Follow-up research conducted by us, and others, which use the findings within this thesis would benefit from updating the regimens to reflect current gold standards.

7.3 Future directions

The investigations performed in this thesis and their subsequent findings have prompted further questions which warrant further scientific enquiry, these include:

1. Is IDEB therapeutic in combination with other gold-standard chemotherapy regimens? What is the dose-effect relationship with IDEB therapy when delivered in concert with chemotherpay regimens? And, is the therapeutic efficacy of IDEB against the CI-SMDW pathology species dependent? As IDEB showed the greatest promise in combination with the BL-CHOP regimen, the next logical step would be to assess the therapeutic efficacy of IDEB against BL-CHOP therapy in another animal species (as required by the FDA for approval of human trials). Further, as IDEB therapy was not as effective against MB-LCV-induced SMDW and mitochondrial dysfunction, studies which investigate differing doses of IDEB may show that IDEB holds therapeutic promise at alternative dosages, or whether it interacts with a spefic drug within the MB-LCV regimen. Further still, due to the success that IDEB showed here against the CI-SMDW pathology, its therapeutic efficacy should be

further investigated in other clinically relevant animal models of other gold-standard chemotherapy regimens.

2. Does the addition of IDEB alter the anti-cancer efficacy of chemotherapy? The final investigatory step of the IAMDF was to confirm the therapeutic efficacy of IDEB co-treatment with ALL-POMP, MB-LCV and BL-CHOP in animal models which express the cancer that these regimens aimed to treat. Therefore, follow-up studies should investigate the BL-CHOP and MB-LCV regimens, with combination IDEB therapy, in animals which express NHBL and medulloblastoma respectively.

3. Is the CI-SMDW phenotype actually an accelerated musculoskeletal ageing or early-onset sarcopenia model?

4. Is the skeletal muscle dysfunction induced by chemotherapy associated with structural changes at the cross-bridge level? To answer this, single fibre muscle analysis in chemotherapy-treated muscle is needed.

5. Do other antioxidants offer the same, or better, therapeutic effect against the CI-SMDW pathology as IDEB does in combination with poly-agent chemotherapy regimens? Alternatively, could targeting the molecular response to oxidative stress (i.e. nrf2) constitute a better approach?

6. Is the loss of skeletal muscle post-exercise recovery capacity induced by chemotherapy administration linked to mitochondrial dysfunction, structural damage and/or elevations in cellular oxidative stress?

7. Does IDEB afford therapeutic efficacy against the CI-SMDW pathology through an antioxidant mode of action?

7.4 Conclusions

Collectively, the studies presented within this thesis show that chemotherapy regimens, when administered to juvenile mice, induce significant skeletal muscle and mitochondrial dysfunction which endures well into adulthood, and long after chemotherapy administration ceases. This is indicative that chemotherapy, during active treatment, acts to damage the skeletal muscle and mitochondria resulting in significant declines in the functional capacity of both. From these findings, we postulate that chemotherapy damages the mitochondria which ultimately underpins, or at the very least exacerbates, the skeletal muscle dysfunction and wasting seen in survivors of childhood chemotherapy. In addition, this thesis has developed a framework which can be used to develop clinically relevant animal models within which gold-standard interventions can be scrutinised, adapted and improved upon. Through the use of this framework, this thesis developed clinically relevant animal models which are capable of investigating the CI-SMDW pathology induced by the three gold-standard chemotherapy regimens, POMP, LCV and CHOP, which are used against the most common paediatric cancers (ALL, medulloblastoma and NHBL). Moreover, this thesis demonstrated that concomitant treatment with the Co-Q10 analogue, Idebenone, failed to provide therapeutic value when delivered in combination with MB-LCV therapy, we question

whether this could be due to insufficient IDEB dosing or due to the relatively low level of SMDW induced by this regimen in contrast to CHOP therapy. However, Idebenone co-therapy when delivered with the anthracycline based CHOP therapy, completely protected against chemotherapy-induced lean mass loss, cardiomyopathy and, most importantly, mortality. These findings highlight that IDEB could be an invaluable addition to gold-standard anti-cancer chemotherapy regimens used world-wide and, after we confirm that the anti-cancer efficacy of the combined treatment is preserved, could provide unprecedented protection against chemotherapy-induced skeletal muscle dysfunction and wasting, and mortality.

Chapter 8

References

1. Sorensen, J.C.*, et al.* Mitochondria: Inadvertent targets in chemotherapy-induced skeletal muscle toxicity and wasting? *Cancer chemotherapy and pharmacology* **78**, 673-683 (2016).
2. Cancer, I.A.f.R.o. World Cancer Report 2014. (ed. Stewart, B.W., C.) (World Health Organisation, 2014).
3. Welfare, A.I.o.H.a. Cancer in Australia 2017. (Canberra, 2017).
4. Health, A.I.o. *Cancer survival and prevalence in Australia: period estimates from 1982 to 2010*, (AIHW, 2012).
5. Welfare, A.I.o.H.a. GRIM (General Record of Incidence of Mortality books 2014: All causes combined (AIHW, Canberra, 2017).
6. Welfare, A.I.o.H.a. A picture of Australian's Children Vol. Cat. no. PHE 167 (Canberra: AIHW, 2012).
7. Miller, K.D.*, et al.* Cancer treatment and survivorship statistics, 2016. *CA: a cancer journal for clinicians* **66**, 271-289 (2016).
8. Bryer, E. & Henry, D. Chemotherapy-induced anemia: etiology, pathophysiology, and implications for contemporary practice. *International Journal of Clinical Transfusion Medicine* **6**, 21 (2018).
9. Coates, A.*, et al.* On the receiving end—patient perception of the side-effects of cancer chemotherapy. *European Journal of Cancer and Clinical Oncology* **19**, 203-208 (1983).
10. Lind, M.J. Principles of cytotoxic chemotherapy. *Medicine* **36**, 19-23 (2008).
11. Scheede-Bergdahl, C. & Jagoe, R.T. After the chemotherapy: potential mechanisms for chemotherapy-induced delayed skeletal muscle dysfunction in survivors of acute lymphoblastic leukaemia in childhood. *Frontiers in pharmacology* **4**, 49 (2013).
12. Oeffinger, K.C.*, et al.* Chronic health conditions in adult survivors of childhood cancer. *The New England journal of medicine* **355**, 1572-1582 (2006).
13. Mertens, A.C.*, et al.* Late mortality experience in five-year survivors of childhood and adolescent cancer: the Childhood Cancer Survivor Study. *Journal of Clinical Oncology* **19**, 3163-3172 (2001).
14. Diller, L.*, et al.* Chronic disease in the Childhood Cancer Survivor Study cohort: a review of published findings. *Journal of Clinical Oncology* **27**, 2339-2355 (2009).
15. King, A.A.*, et al.* Health and functional status of long term adult medulloblastoma/pnet survivors: A report from the childhood cancer survivor study. in *JOURNAL OF CLINICAL ONCOLOGY*, Vol. 32 (AMER SOC CLINICAL ONCOLOGY 2318 MILL ROAD, STE 800, ALEXANDRIA, VA 22314 USA, 2014).
16. Hudson, M.M.*, et al.* Clinical ascertainment of health outcomes among adults treated for childhood cancer. *Jama* **309**, 2371-2381 (2013).
17. Australia, C. About Children's Cancer. (ed. Australia, C.) (Australian Government, https://childrenscancer.canceraustralia.gov.au, 2016).
18. Ness, K.K.*, et al.* Body composition, muscle strength deficits and mobility limitations in adult survivors of childhood acute lymphoblastic leukemia. *Pediatric Blood & Cancer* **49**, 975-981 (2007).
19. Ness, K.K.*, et al.* Neuromuscular impairments in adult survivors of childhood acute lymphoblastic leukemia. *Cancer* **118**, 828-838 (2012).
20. Phillips, S.M.*, et al.* Survivors of childhood cancer in the United States: prevalence and burden of morbidity. *Cancer Epidemiology and Prevention Biomarkers* **24**, 653-663 (2015).

21. Lexell, J., Sjostrom, M., Nordlund, A.S. & Taylor, C.C. Growth and development of human muscle: a quantitative morphological study of whole vastus lateralis from childhood to adult age. *Muscle & nerve* **15**, 404-409 (1992).
22. Talvensaari, K.K., Lanning, M., Tapanainen, P. & Knip, M. Long-term survivors of childhood cancer have an increased risk of manifesting the metabolic syndrome. *The Journal of Clinical Endocrinology & Metabolism* **81**, 3051-3055 (1996).
23. Pallafacchina, G.*, et al.* An adult tissue-specific stem cell in its niche: a gene profiling analysis of in vivo quiescent and activated muscle satellite cells. *Stem cell research* **4**, 77-91 (2010).
24. Blauwhoff-Buskermolen, S.*, et al.* Loss of Muscle Mass During Chemotherapy Is Predictive for Poor Survival of Patients With Metastatic Colorectal Cancer. *Journal of Clinical Oncology* (2016).
25. Gullett, N.P., Mazurak, V., Hebbar, G. & Ziegler, T.R. Nutritional Interventions for Cancer-induced Cachexia. *Current problems in cancer* **35**, 58-90 (2011).
26. Argilés, J.M., López-Soriano, F.J., Stemmler, B. & Busquets, S. Therapeutic strategies against cancer cachexia. *European journal of translational myology* **29**(2019).
27. Lira, F.S., Neto, J.C.R. & Seelaender, M. Exercise training as treatment in cancer cachexia. *Applied Physiology, Nutrition, and Metabolism* **39**, 679-686 (2014).
28. Lira, F.S., Antunes, B.d.M., Seelaender, M. & Neto, J.C.R. The therapeutic potential of exercise to treat cachexia. *Current opinion in supportive and palliative care* **9**, 317-324 (2015).
29. Pigna, E.*, et al.* Aerobic exercise and pharmacological treatments counteract cachexia by modulating autophagy in colon cancer. *Scientific reports* **6**, 1-14 (2016).
30. Grande, A.J., Silva, V. & Maddocks, M. Exercise for cancer cachexia in adults: executive summary of a Cochrane Collaboration systematic review. *Journal of cachexia, sarcopenia and muscle* **6**, 208-211 (2015).
31. Bayly, J., Higginson, I.J. & Maddocks, M. Early engagement in physical activity and exercise is key in managing cancer cachexia. *Oncology* **31**(2017).
32. Solheim, T.S.*, et al.* Cancer cachexia: rationale for the MENAC (Multimodal—Exercise, Nutrition and Anti-inflammatory medication for Cachexia) trial. *BMJ supportive & palliative care* **8**, 258-265 (2018).
33. Fearon, K.*, et al.* Definition and classification of cancer cachexia: an international consensus. *The lancet oncology* **12**, 489-495 (2011).
34. Deisenroth, A.*, et al.* Muscle strength and quality of life in patients with childhood cancer at early phase of primary treatment. *Pediatric hematology and oncology* **33**, 393-407 (2016).
35. Organisation, W.h. Cancer. Vol. 2015 (WHO, 2015).
36. Mori, H.*, et al.* Chromosome translocations and covert leukemic clones are generated during normal fetal development. *Proceedings of the National Academy of Sciences* **99**, 8242-8247 (2002).
37. Inaba, H., Greaves, M. & Mullighan, C.G. Acute lymphoblastic leukaemia. *The Lancet* **381**, 1943-1955 (2013).
38. Perera, F. & Herbstman, J. Prenatal environmental exposures, epigenetics, and disease. *Reproductive toxicology* **31**, 363-373 (2011).
39. Wang, C.-W. & Hui, E. Ethical, legal and social implications of prenatal and preimplantation genetic testing for cancer susceptibility. *Reproductive biomedicine online* **19**, 23-33 (2009).

40. Lee, E.Y. & Muller, W.J. Oncogenes and tumor suppressor genes. *Cold Spring Harbor perspectives in biology*, a003236 (2010).
41. de Leon, M.P. Oncogenes and tumor suppressor genes. in *Familial and Hereditary Tumors* 35-47 (Springer, 1994).
42. Lobry, C., Oh, P., Mansour, M.R., Look, A.T. & Aifantis, I. Notch signaling: switching an oncogene to a tumor suppressor. *Blood* **123**, 2451-2459 (2014).
43. Chow, A. Cell cycle control by oncogenes and tumor suppressors: driving the transformation of normal cells into cancerous cells. *Nature Education* **3**, 7 (2010).
44. Levine, A.J. & Puzio-Kuter, A.M. The control of the metabolic switch in cancers by oncogenes and tumor suppressor genes. *Science* **330**, 1340-1344 (2010).
45. Esteller, M. Epigenetics provides a new generation of oncogenes and tumour-suppressor genes. *British journal of cancer* **94**, 179 (2006).
46. Lichtenstein, P*., et al.* Environmental and heritable factors in the causation of cancer—analyses of cohorts of twins from Sweden, Denmark, and Finland. *New England journal of medicine* **343**, 78-85 (2000).
47. Verkasalo, P.K., Kaprio, J., Koskenvuo, M. & Pukkala, E. Genetic predisposition, environment and cancer incidence: a nationwide twin study in Finland, 1976–1995. *International Journal of Cancer* **83**, 743-749 (1999).
48. Nawrot, T.S. & Adcock, I. The detrimental health effects of traffic-related air pollution: a role for DNA methylation? (American Thoracic Society, 2009).
49. Esteller, M. Epigenetics in cancer. *New England Journal of Medicine* **358**, 1148-1159 (2008).
50. Sharma, S., Kelly, T.K. & Jones, P.A. Epigenetics in cancer. *Carcinogenesis* **31**, 27-36 (2010).
51. King, M.-C., Marks, J.H. & Mandell, J.B. Breast and ovarian cancer risks due to inherited mutations in BRCA1 and BRCA2. *Science* **302**, 643-646 (2003).
52. Moolgavkar, S.H. & Knudson, A.G. Mutation and cancer: a model for human carcinogenesis. *JNCI: Journal of the National Cancer Institute* **66**, 1037-1052 (1981).
53. Rowland, A*., et al.* Meta-analysis of BRAF mutation as a predictive biomarker of benefit from anti-EGFR monoclonal antibody therapy for RAS wild-type metastatic colorectal cancer. *British journal of cancer* **112**, 1888 (2015).
54. Bignell, G.R*., et al.* Signatures of mutation and selection in the cancer genome. *Nature* **463**, 893 (2010).
55. Ward, E., DeSantis, C., Robbins, A., Kohler, B. & Jemal, A. Childhood and adolescent cancer statistics, 2014. *CA: a cancer journal for clinicians* **64**, 83-103 (2014).
56. Cogliano, V.J*., et al.* Preventable exposures associated with human cancers. *Journal of the National Cancer Institute* **103**, 1827-1839 (2011).
57. Dobson, C.M. The structural basis of protein folding and its links with human disease. *Philosophical Transactions of the Royal Society of London B: Biological Sciences* **356**, 133-145 (2001).
58. Dobson, C.M. Protein folding and misfolding. *Nature* **426**, 884 (2003).
59. Hoeijmakers, J.H. Genome maintenance mechanisms for preventing cancer. *nature* **411**, 366 (2001).
60. Cohen, S.M. & Ellwein, L.B. Genetic errors, cell proliferation, and carcinogenesis. *Cancer research* **51**, 6493-6505 (1991).
61. Ganem, N.J., Storchova, Z. & Pellman, D. Tetraploidy, aneuploidy and cancer. *Current opinion in genetics & development* **17**, 157-162 (2007).

62. Hartwell, L.H. & Kastan, M.B. Cell cycle control and cancer. *Science* **266**, 1821-1828 (1994).
63. Crasta, K.*, et al.* DNA breaks and chromosome pulverization from errors in mitosis. *Nature* **482**, 53 (2012).
64. Itzkowitz, S.H. & Yio, X. Inflammation and cancer IV. Colorectal cancer in inflammatory bowel disease: the role of inflammation. *American Journal of Physiology-Gastrointestinal and Liver Physiology* **287**, G7-G17 (2004).
65. Kundu, J.K. & Surh, Y.-J. Inflammation: gearing the journey to cancer. *Mutation Research/Reviews in Mutation Research* **659**, 15-30 (2008).
66. Elinav, E.*, et al.* Inflammation-induced cancer: crosstalk between tumours, immune cells and microorganisms. *Nature Reviews Cancer* **13**, 759 (2013).
67. Landgren, A.M.*, et al.* Autoimmune disease and subsequent risk of developing alimentary tract cancers among 4.5 million US male veterans. *Cancer* **117**, 1163-1171 (2011).
68. Portela, A. & Esteller, M. Epigenetic modifications and human disease. *Nature biotechnology* **28**, 1057 (2010).
69. Beyer, M. & Schultze, J.L. Regulatory T cells in cancer. *Blood* **108**, 804-811 (2006).
70. John, E.M., Savitz, D.A. & Sandler, D.P. Prenatal exposure to parents' smoking and childhood cancer. *American Journal of Epidemiology* **133**, 123-132 (1991).
71. Hofhuis, W., De Jongste, J. & Merkus, P. Adverse health effects of prenatal and postnatal tobacco smoke exposure on children. *Archives of disease in childhood* **88**, 1086-1090 (2003).
72. Ji, B.-T.*, et al.* Paternal cigarette smoking and the risk of childhood cancer among offspring of nonsmoking mothers. *Journal of the National Cancer Institute* **89**, 238-243 (1997).
73. Sasco, A.J. & Vainio, H. From in utero and childhood exposure to parental smoking to childhood cancer: a possible link and the need for action. *Human & experimental toxicology* **18**, 192-201 (1999).
74. Jensen, C.D.*, et al.* Maternal dietary risk factors in childhood acute lymphoblastic leukemia (United States). *Cancer Causes & Control* **15**, 559-570 (2004).
75. Zack, M., Adami, H.-O. & Ericson, A. Maternal and perinatal risk factors for childhood leukemia. *Cancer research* **51**, 3696-3701 (1991).
76. van Duijn, C.M., van Steensel-Moll, H.A., Coebergh, J. & van Zanen, G.E. Risk factors for childhood acute non-lymphocytic leukemia: an association with maternal alcohol consumption during pregnancy? *Cancer Epidemiology and Prevention Biomarkers* **3**, 457-460 (1994).
77. Preston-Martin, S.*, et al.* Maternal consumption of cured meats and vitamins in relation to pediatric brain tumors. *Cancer Epidemiology and Prevention Biomarkers* **5**, 599-605 (1996).
78. Nielsen, S.S.*, et al.* Childhood brain tumors and maternal cured meat consumption in pregnancy: differential effect by glutathione S-transferases. *Cancer Epidemiology and Prevention Biomarkers* (2011).
79. Linet, M.S., pyo Kim, K. & Rajaraman, P. Children's exposure to diagnostic medical radiation and cancer risk: epidemiologic and dosimetric considerations. *Pediatric radiology* **39**, 4-26 (2009).
80. Wakeford, R. Childhood leukaemia following medical diagnostic exposure to ionizing radiation in utero or after birth. *Radiation protection dosimetry* **132**, 166-174 (2008).

81. Schulze-Rath, R., Hammer, G.P. & Blettner, M. Are pre-or postnatal diagnostic X-rays a risk factor for childhood cancer? A systematic review. *Radiation and environmental biophysics* **47**, 301 (2008).
82. Shu, X.*, et al.* Diagnostic X-ray and ultrasound exposure and risk of childhood cancer. *British journal of cancer* **70**, 531 (1994).
83. Colt, J.S. & Blair, A. Parental occupational exposures and risk of childhood cancer. *Environmental health perspectives* **106**, 909-925 (1998).
84. Trasler, J.M. & Doerksen, T. Teratogen update: paternal exposures—reproductive risks. *Teratology* **60**, 161-172 (1999).
85. Fear, N., Roman, E., Reeves, G. & Pannett, B. Childhood cancer and paternal employment in agriculture: the role of pesticides. *British journal of cancer* **77**, 825 (1998).
86. Soubry, A., Hoyo, C., Jirtle, R.L. & Murphy, S.K. A paternal environmental legacy: evidence for epigenetic inheritance through the male germ line. *Bioessays* **36**, 359-371 (2014).
87. Savitz, D.A. & Chen, J. Parental occupation and childhood cancer: review of epidemiologic studies. *Environmental health perspectives* **88**, 325 (1990).
88. Shu, X.O.*, et al.* A population-based case-control study of childhood leukemia in Shanghai. *Cancer* **62**, 635-644 (1988).
89. Landrigan, P.J., Schechter, C.B., Lipton, J.M., Fahs, M.C. & Schwartz, J. Environmental pollutants and disease in American children: estimates of morbidity, mortality, and costs for lead poisoning, asthma, cancer, and developmental disabilities. *Environmental health perspectives* **110**, 721 (2002).
90. de Blank, P.M.*, et al.* Years of life lived with disease and years of potential life lost in children who die of cancer in the United States, 2009. *Cancer medicine* **4**, 608-619 (2015).
91. Ostrom, Q.T.*, et al.* CBTRUS statistical report: primary brain and central nervous system tumors diagnosed in the United States in 2007–2011. *Neuro-oncology* **16**, iv1-iv63 (2014).
92. Steliarova-Foucher, E.*, et al.* International incidence of childhood cancer, 2001–10: a population-based registry study. *The Lancet Oncology* **18**, 719-731 (2017).
93. Boonstra, A.*, et al.* Severe fatigue in childhood cancer survivors. *The Cochrane Library* (2017).
94. Hudson, M.M.*, et al.* Health status of adult long-term survivors of childhood cancer: a report from the Childhood Cancer Survivor Study. *Jama* **290**, 1583-1592 (2003).
95. Robison, L.L. & Hudson, M.M. Survivors of childhood and adolescent cancer: life-long risks and responsibilities. *Nature Reviews Cancer* **14**, 61-70 (2014).
96. Schwartz, C.L. Health status of childhood cancer survivors: Cure is more than the eradication of cancer. *JAMA* **290**, 1641-1643 (2003).
97. Sorensen, J.C.*, et al.* BGP-15 protects against Oxaliplatin-induced skeletal myopathy and mitochondrial reactive oxygen species production in mice. *Frontiers in Pharmacology* **8**, 137 (2017).
98. Glantz, J.C. Reproductive toxicology of alkylating agents. *Obstetrical & gynecological survey* **49**, 709-715 (1994).
99. Warwick, G. The mechanism of action of alkylating agents. (AACR, 1963).
100. Kaye, S.B. New antimetabolites in cancer chemotherapy and their clinical impact. *British journal of cancer* **78**, 1-7 (1998).

101. Smorenburg, C., Sparreboom, A., Bontenbal, M. & Verweij, J. Combination chemotherapy of the taxanes and antimetabolites: its use and limitations. *European Journal of Cancer* **37**, 2310-2323 (2001).
102. Peters, G.*, et al.* Basis for effective combination cancer chemotherapy with antimetabolites. *Pharmacology & therapeutics* **87**, 227-253 (2000).
103. Kothari, A., Hittelman, W.N. & Chambers, T.C. Cell cycle–dependent mechanisms underlie vincristine-induced death of primary acute lymphoblastic leukemia cells. *Cancer research* **76**, 3553-3561 (2016).
104. Moudi, M., Go, R., Yien, C.Y.S. & Nazre, M. Vinca alkaloids. *International journal of preventive medicine* **4**, 1231 (2013).
105. Gewirtz, D. A critical evaluation of the mechanisms of action proposed for the antitumor effects of the anthracycline antibiotics adriamycin and daunorubicin. *Biochemical Pharmacology* **57**, 727-741 (1999).
106. Gilliam, L.A., Moylan, J.S., Callahan, L.A., Sumandea, M.P. & Reid, M.B. Doxorubicin causes diaphragm weakness in murine models of cancer chemotherapy. *Muscle & nerve* **43**, 94-102 (2011).
107. Schelman, W.R.*, et al.* A Phase I Study of Triapine(®) in Combination with Doxorubicin in Patients with Advanced Solid Tumors. *Cancer chemotherapy and pharmacology* **63**, 1147-1156 (2009).
108. Lu, P. Monitoring Cardiac Function in Patients Receiving Doxorubicin. *Seminars in Nuclear Medicine* **35**, 197-201 (2005).
109. Agudelo, D., Bourassa, P., Bérubé, G. & Tajmir-Riahi, H.-A. Intercalation of antitumor drug doxorubicin and its analogue by DNA duplex: Structural features and biological implications. *International Journal of Biological Macromolecules* **66**, 144-150 (2014).
110. Quach, B., Birk, A. & Szeto, H. Mechanism of preventing doxorubicin-induced mitochondrial toxicity with cardiolipin-targeted peptide, SS-31 (966.1). *The FASEB Journal* **28**, 966.961 (2014).
111. Cheregi, B., Timpani, C., Nurgali, K., Hayes, A. & Rybalka, E. Chemotherapy-induced mitochondrial respiratory dysfunction, oxidant production and death in healthy skeletal muscle C2C12 myoblast and myotube models. *Neuromuscular Disorders* **25, Supplement 2**, S202 (2015).
112. Rybalka, E.*, et al.* Chemotherapeutic agents induce mitochondrial superoxide production and toxicity but do not alter respiration in skeletal muscle in vitro. *Mitochondrion* **42**, 33-49 (2018).
113. Deavall, D.G., Martin, E.A., Horner, J.M. & Roberts, R. Drug-induced oxidative stress and toxicity. *Journal of toxicology* **2012**(2012).
114. Sawyer, D.B., Peng, X., Chen, B., Pentassuglia, L. & Lim, C.C. Mechanisms of Anthracycline Cardiac Injury: Can We Identify Strategies for Cardioprotection? *Progress in Cardiovascular Diseases* **53**, 105-113 (2010).
115. Sarosiek, K.A., Ni Chonghaile, T. & Letai, A. Mitochondria: gatekeepers of response to chemotherapy. *Trends in Cell Biology* **23**, 612-619 (2013).
116. Wilne, S.*, et al.* Presentation of childhood CNS tumours: a systematic review and meta-analysis. *The lancet oncology* **8**, 685-695 (2007).
117. Parsons, D.W.*, et al.* The genetic landscape of the childhood cancer medulloblastoma. *science* **331**, 435-439 (2011).
118. Berman, D.M.*, et al.* Medulloblastoma growth inhibition by hedgehog pathway blockade. *Science* **297**, 1559-1561 (2002).

119. Huse, J.T. & Holland, E.C. Targeting brain cancer: advances in the molecular pathology of malignant glioma and medulloblastoma. *Nature reviews cancer* **10**, 319 (2010).
120. Louis, D.N.*, et al.* The 2007 WHO classification of tumours of the central nervous system. *Acta neuropathologica* **114**, 97-109 (2007).
121. Gilbertson, R.J. & Ellison, D.W. The origins of medulloblastoma subtypes. *Annu. Rev. pathmechdis. Mech. Dis.* **3**, 341-365 (2008).
122. Provias, J.P. & Becker, L.E. Cellular and molecular pathology of medulloblastoma. *Journal of neuro-oncology* **29**, 35-43 (1996).
123. Grill, J.*, et al.* Treatment of medulloblastoma with postoperative chemotherapy alone: an SFOP prospective trial in young children. *The lancet oncology* **6**, 573-580 (2005).
124. Packer, R.J.*, et al.* Treatment of children with medulloblastomas with reduced-dose craniospinal radiation therapy and adjuvant chemotherapy: A Children's Cancer Group Study. *Journal of Clinical Oncology* **17**, 2127-2127 (1999).
125. Biko, D.M., Anupindi, S.A., Hernandez, A., Kersun, L. & Bellah, R. Childhood Burkitt lymphoma: abdominal and pelvic imaging findings. *American Journal of Roentgenology* **192**, 1304-1315 (2009).
126. Wright, D., McKeever, P. & Carter, R. Childhood non-Hodgkin lymphomas in the United Kingdom: findings from the UK Children's Cancer Study Group. *Journal of clinical pathology* **50**, 128-134 (1997).
127. Voss, S.D.*, et al.* Surveillance computed tomography imaging and detection of relapse in intermediate-and advanced-stage pediatric Hodgkin's lymphoma: a report from the Children's Oncology Group. *Journal of Clinical Oncology* **30**, 2635 (2012).
128. Schwartz, C.L.*, et al.* A risk-adapted, response-based approach using ABVE-PC for children and adolescents with intermediate-and high-risk Hodgkin lymphoma: the results of P9425. *Blood* **114**, 2051-2059 (2009).
129. Pui, C.-H. *Acute lymphoblastic leukemia*, (Springer, 2011).
130. Harris, N.L.*, et al.* World Health Organization classification of neoplastic diseases of the hematopoietic and lymphoid tissues: report of the Clinical Advisory Committee meeting—Airlie House, Virginia, November 1997. *Journal of clinical oncology* **17**, 3835-3849 (1999).
131. Vardiman, J.W.*, et al.* The 2008 revision of the World Health Organization (WHO) classification of myeloid neoplasms and acute leukemia: rationale and important changes. *Blood* **114**, 937-951 (2009).
132. Skipper, H.E. & Perry, S. Kinetics of normal and leukemic leukocyte populations and relevance to chemotherapy. *Cancer Research* **30**, 1883-1897 (1970).
133. Hustu, H., Aur, R., Verzosa, M., Simone, J. & Pinkel, D. Prevention of central nervous system leukemia by irradiation. *Cancer* **32**, 585-597 (1973).
134. Gao, R.W., Dusenbery, K.E., Cao, Q., Smith, A.R. & Yuan, J. Augmenting total body irradiation with a cranial boost before stem cell transplantation protects against post-transplant central nervous system relapse in acute lymphoblastic leukemia. *Biology of Blood and Marrow Transplantation* **24**, 501-506 (2018).
135. Cohler, C.*, et al.* Evaluation and Outcome of Central Nervous System Involvement in Pediatric Acute Lymphoblastic Leukemia in Dar es Salaam, Tanzania. *Pediatric blood & cancer* **63**, 458-464 (2016).

136. Jeha, S.*, et al.* Improved CNS control of childhood acute lymphoblastic leukemia without cranial irradiation: St Jude Total Therapy Study 16. *Journal of Clinical Oncology* **37**, 3377 (2019).
137. Siva, S., MacManus, M.P., Martin, R.F. & Martin, O.A. Abscopal effects of radiation therapy: a clinical review for the radiobiologist. *Cancer letters* **356**, 82-90 (2015).
138. Green, D.M.*, et al.* Effect of cranial irradiation on sperm concentration of adult survivors of childhood acute lymphoblastic leukemia: a report from the St. Jude Lifetime Cohort Study. *Human Reproduction* **32**, 1192-1201 (2017).
139. Duffner, P.K., Cohen, M.E., Thomas, P.R. & Lansky, S.B. The long-term effects of cranial irradiation on the central nervous system. *Cancer* **56**, 1841-1846 (1985).
140. Monje, M. & Fisher, P.G. Neurological complications following treatment of children with brain tumors. *Journal of pediatric rehabilitation medicine* **4**, 31-36 (2011).
141. Bredahl, E.C., Pfannenstiel, K.B., Quinn, C.J., Hayward, R. & Hydock, D.S. Effects of Exercise on Doxorubicin-Induced Skeletal Muscle Dysfunction. *Medicine and science in sports and exercise* (2016).
142. de Lima Junior, E.A.*, et al.* Doxorubicin caused severe hyperglycaemia and insulin resistance, mediated by inhibition in AMPk signalling in skeletal muscle. *Journal of cachexia, sarcopenia and muscle* **7**, 615-625 (2016).
143. Gilliam, L.A.A.*, et al.* Doxorubicin acts through tumor necrosis factor receptor subtype 1 to cause dysfunction of murine skeletal muscle. *Journal of Applied Physiology* **107**, 1935-1942 (2009).
144. Gilliam, L.A.A. & St. Clair, D.K. Chemotherapy-Induced Weakness and Fatigue in Skeletal Muscle: The Role of Oxidative Stress. *Antioxidants & Redox Signaling* **15**, 2543-2563 (2011).
145. van Brussel, M.*, et al.* Physical function and fitness in long-term survivors of childhood leukaemia. *Pediatric rehabilitation* **9**, 267-274 (2006).
146. Adams, S.C.*, et al.* Impact of resistance and aerobic exercise on sarcopenia and dynapenia in breast cancer patients receiving adjuvant chemotherapy: a multicenter randomized controlled trial. *Breast cancer research and treatment* **158**, 497-507 (2016).
147. Zalite, I.O.*, et al.* Influence of cachexia and sarcopenia on survival in pancreatic ductal adenocarcinoma: a systematic review. *Pancreatology* **15**, 19-24 (2015).
148. Reisinger, K.W.*, et al.* Loss of skeletal muscle mass during neoadjuvant chemoradiotherapy predicts postoperative mortality in esophageal cancer surgery. *Annals of surgical oncology* **22**, 4445-4452 (2015).
149. Okumura, S.*, et al.* Impact of preoperative quality as well as quantity of skeletal muscle on survival after resection of pancreatic cancer. *Surgery* **157**, 1088-1098 (2015).
150. Andersen, K.K., Duun-Henriksen, A.K., Frederiksen, M.H. & Winther, J.F. Ninth grade school performance in Danish childhood cancer survivors. *British Journal of Cancer* (2017).
151. Yang, L.*, et al.* Hand grip strength and cognitive function among elderly cancer survivors. *PloS one* **13**, e0197909 (2018).
152. Aoyagi, T., Terracina, K.P., Raza, A., Matsubara, H. & Takabe, K. Cancer cachexia, mechanism and treatment. *World journal of gastrointestinal oncology* **7**, 17 (2015).
153. Anderson, L.J., Albrecht, E.D. & Garcia, J.M. Update on Management of Cancer-Related Cachexia. *Current Oncology Reports* **19**, 3 (2017).

154. Anker, S.D., Steinborn, W. & Strassburg, S. Cardiac cachexia. *Annals of medicine* **36**, 518-529 (2004).
155. Barton, M.K. Cancer cachexia awareness, diagnosis, and treatment are lacking among oncology providers. *CA: A Cancer Journal for Clinicians*, n/a-n/a (2017).
156. Dodson, S*., et al.* Muscle Wasting in Cancer Cachexia: Clinical Implications, Diagnosis, and Emerging Treatment Strategies. *Annual Review of Medicine* **62**, 265-279 (2011).
157. Mantovani, G*., et al.* Cancer-Related Anorexia/Cachexia Syndrome and Oxidative Stress: An Innovative Approach beyond Current Treatment. *Cancer Epidemiology Biomarkers & Prevention* **13**, 1651-1659 (2004).
158. Sakuma, K. & Yamaguchi, A. Sarcopenia and cachexia: the adaptations of negative regulators of skeletal muscle mass. *Journal of cachexia, sarcopenia and muscle* **3**, 77-94 (2012).
159. Sorensen, J.C*., et al.* BGP-15 Protects against Oxaliplatin-Induced Skeletal Myopathy and Mitochondrial Reactive Oxygen Species Production in Mice. *Frontiers in pharmacology* **8**(2017).
160. Sorensen, J.C*., et al.* Platinum-based chemotherapy induces skeletal muscle wasting and mitochondrial dysfunction in mice. *Poster session presented at the the Annual Proceedings of the Australian Society of Medical Research* (2016).
161. Barreto, R*., et al.* Cancer and Chemotherapy Contribute to Muscle Loss by Activating Common Signaling Pathways. *Frontiers in Physiology* **7**(2016).
162. Braun, T.P*., et al.* Muscle atrophy in response to cytotoxic chemotherapy is dependent on intact glucocorticoid signaling in skeletal muscle. *PloS one* **9**, e106489 (2014).
163. Gilliam, L.A.A*., et al.* The anticancer agent doxorubicin disrupts mitochondrial energy metabolism and redox balance in skeletal muscle. *Free Radical Biology and Medicine* **65**, 988-996 (2013).
164. Attar, A*., et al.* Malnutrition is high and underestimated during chemotherapy in gastrointestinal cancer: an AGEO prospective cross-sectional multicenter study. *Nutrition and cancer* **64**, 535-542 (2012).
165. Davidson, W*., et al.* Malnutrition and chemotherapy-induced nausea and vomiting: implications for practice. in *Oncology nursing forum*, Vol. 39 (2012).
166. Damrauer, J.S*., et al.* Chemotherapy-induced muscle wasting: association with NF-κB and cancer cachexia. *European Journal of Translational Myology* **28**(2018).
167. Stene, G.B*., et al.* Deterioration in muscle mass and physical function differs according to weight loss history in cancer cachexia. *Cancers* **11**, 1925 (2019).
168. Pin, F., Barreto, R., Couch, M.E., Bonetto, A. & O'Connell, T.M. Cachexia induced by cancer and chemotherapy yield distinct perturbations to energy metabolism. *Journal of cachexia, sarcopenia and muscle* **10**, 140-154 (2019).
169. Ballarò, R., Costelli, P. & Penna, F. Animal models for cancer cachexia. *Current opinion in supportive and palliative care* **10**, 281-287 (2016).
170. Weber, D.R., Leonard, M.B. & Zemel, B.S. Body composition analysis in the pediatric population. *Pediatric endocrinology reviews: PER* **10**, 130 (2012).
171. Wells, J.C. Toward Body Composition Reference Data for Infants, Children, and Adolescents–. *Advances in nutrition* **5**, 320S-329S (2014).
172. Pratesi, A., Tarantini, F. & Di Bari, M. Skeletal muscle: an endocrine organ. *Clinical cases in mineral and bone metabolism* **10**, 11 (2013).

173. Fitts, R.H. The cross-bridge cycle and skeletal muscle fatigue. *Journal of applied physiology* **104**, 551-558 (2008).
174. Sweeney, H.L. & Stull, J.T. Alteration of cross-bridge kinetics by myosin light chain phosphorylation in rabbit skeletal muscle: implications for regulation of actin-myosin interaction. *Proceedings of the National Academy of Sciences* **87**, 414-418 (1990).
175. Metzger, J.M., Greaser, M.L. & Moss, R.L. Variations in cross-bridge attachment rate and tension with phosphorylation of myosin in mammalian skinned skeletal muscle fibers. Implications for twitch potentiation in intact muscle. *The Journal of general physiology* **93**, 855-883 (1989).
176. Lieber, R.L. *Skeletal muscle structure, function, and plasticity*, (Lippincott Williams & Wilkins, 2002).
177. Bottinelli, R., Pellegrino, M., Canepari, M., Rossi, R. & Reggiani, C. Specific contributions of various muscle fibre types to human muscle performance: an in vitro study. *Journal of Electromyography and Kinesiology* **9**, 87-95 (1999).
178. Girgenrath, S., Song, K. & Whittemore, L.A. Loss of myostatin expression alters fiber-type distribution and expression of myosin heavy chain isoforms in slow-and fast-type skeletal muscle. *Muscle & nerve* **31**, 34-40 (2005).
179. Murton, A., Constantin, D. & Greenhaff, P. The involvement of the ubiquitin proteasome system in human skeletal muscle remodelling and atrophy. *Biochimica et Biophysica Acta (BBA)-Molecular Basis of Disease* **1782**, 730-743 (2008).
180. Booth, F.W., Roberts, C.K. & Laye, M.J. Lack of exercise is a major cause of chronic diseases. *Comprehensive Physiology* **2**, 1143 (2012).
181. Bloise, F.F., Cordeiro, A. & Ortiga-Carvalho, T.M. Role of thyroid hormone in skeletal muscle physiology. *Journal of Endocrinology* **236**, R57-R68 (2018).
182. De Onis, M*., et al.* Comparison of the World Health Organization (WHO) Child Growth Standards and the National Center for Health Statistics/WHO international growth reference: implications for child health programmes. *Public health nutrition* **9**, 942-947 (2006).
183. Malina, R.M., Bouchard, C. & Bar-Or, O. *Growth, maturation, and physical activity*, (Human kinetics, 2004).
184. Mouly, V*., et al.* The mitotic clock in skeletal muscle regeneration, disease and cell mediated gene therapy. *Acta Physiologica* **184**, 3-15 (2005).
185. Isaevska, E*., et al.* Cancer incidence rates and trends among children and adolescents in Piedmont, 1967–2011. *PloS one* **12**, e0181805 (2017).
186. Schiaffino, S., Dyar, K.A., Ciciliot, S., Blaauw, B. & Sandri, M. Mechanisms regulating skeletal muscle growth and atrophy. *FEBS Journal* **280**, 4294-4314 (2013).
187. Moss, F. & Leblond, C. Satellite cells as the source of nuclei in muscles of growing rats. *The Anatomical Record* **170**, 421-435 (1971).
188. Dayanidhi, S. & Lieber, R.L. Skeletal muscle satellite cells: mediators of muscle growth during development and implications for developmental disorders. *Muscle & nerve* **50**, 723-732 (2014).
189. Lemke, S.B. & Schnorrer, F. Mechanical forces during muscle development. *Mechanisms of development* **144**, 92-101 (2017).
190. Mauro, A. Satellite cell of skeletal muscle fibers. *The Journal of biophysical and biochemical cytology* **9**, 493 (1961).

191. Ciciliot, S. & Schiaffino, S. Regeneration of mammalian skeletal muscle: basic mechanisms and clinical implications. *Current pharmaceutical design* **16**, 906-914 (2010).
192. Musarò, A.*, et al.* Localized Igf-1 transgene expression sustains hypertrophy and regeneration in senescent skeletal muscle. *Nature genetics* **27**, 195 (2001).
193. Weissman, I.L. Stem cells. *cell* **100**, 157-168 (2000).
194. Schultz, E. Satellite cell behavior during skeletal muscle growth and regeneration. *Medicine and science in sports and exercise* **21**, S181-186 (1989).
195. Sanes, J.R. & Lichtman, J.W. Development of the vertebrate neuromuscular junction. *Annual review of neuroscience* **22**, 389-442 (1999).
196. Jolesz, F. & Sreter, F. Development, innervation, and activity-pattern induced changes in skeletal muscle. *Annual Review of Physiology* **43**, 531-552 (1981).
197. Charlton, C., Mohler, W. & Blau, H. Neural cell adhesion molecule (NCAM) and myoblast fusion. *Developmental biology* **221**, 112-119 (2000).
198. Goldspink, G. The proliferation of myofibrils during muscle fibre growth. *Journal of cell science* **6**, 593-603 (1970).
199. WILLIAMS, P.E. & Goldspink, G. Longitudinal growth of striated muscle fibres. *Journal of cell science* **9**, 751-767 (1971).
200. Williams, P.E. & Goldspink, G. The effect of immobilization on the longitudinal growth of striated muscle fibres. *Journal of Anatomy* **116**, 45 (1973).
201. White, R.B., Biérinx, A.-S., Gnocchi, V.F. & Zammit, P.S. Dynamics of muscle fibre growth during postnatal mouse development. *BMC developmental biology* **10**, 21 (2010).
202. Gokhin, D.S., Ward, S.R., Bremner, S.N. & Lieber, R.L. Quantitative analysis of neonatal skeletal muscle functional improvement in the mouse. *Journal of Experimental Biology* **211**, 837-843 (2008).
203. Schultz, E. A quantitative study of the satellite cell population in postnatal mouse lumbrical muscle. *The Anatomical Record* **180**, 589-595 (1974).
204. Neal, A., Boldrin, L. & Morgan, J.E. The satellite cell in male and female, developing and adult mouse muscle: distinct stem cells for growth and regeneration. *PloS one* **7**, e37950 (2012).
205. Gibson, M.C. & Schultz, E. Age-related differences in absolute numbers of skeletal muscle satellite cells. *Muscle & nerve* **6**, 574-580 (1983).
206. Oustanina, S., Hause, G. & Braun, T. Pax7 directs postnatal renewal and propagation of myogenic satellite cells but not their specification. *The EMBO journal* **23**, 3430-3439 (2004).
207. McCarthy, J.J.*, et al.* Effective fiber hypertrophy in satellite cell-depleted skeletal muscle. *Development* **138**, 3657-3666 (2011).
208. Zemel, B.S. Influence of complex childhood diseases on variation in growth and skeletal development. *American Journal of Human Biology* **29**, e22985 (2017).
209. Orsso, C.E.*, et al.* Low muscle mass and strength in pediatrics patients: Why should we care? *Clinical Nutrition* **38**, 2002-2015 (2019).
210. Frey, T.G. & Mannella, C.A. The internal structure of mitochondria. *Trends in biochemical sciences* **25**, 319-324 (2000).
211. Zamponi, N.*, et al.* Mitochondrial network complexity emerges from fission/fusion dynamics. *Scientific reports* **8**, 1-10 (2018).

212. Moore, A.S., Wong, Y.C., Simpson, C.L. & Holzbaur, E.L. Dynamic actin cycling through mitochondrial subpopulations locally regulates the fission–fusion balance within mitochondrial networks. *Nature communications* **7**, 1-13 (2016).
213. Sherratt, H. Mitochondria: structure and function. *Revue neurologique* **147**, 417-430 (1991).
214. Schwartz, M. & Vissing, J. Paternal inheritance of mitochondrial DNA. *New England Journal of Medicine* **347**, 576-580 (2002).
215. Anderson, S.*, et al.* Sequence and organization of the human mitochondrial genome. *Nature* **290**, 457 (1981).
216. Powers, S.K., Talbert, E.E. & Adhihetty, P.J. Reactive oxygen and nitrogen species as intracellular signals in skeletal muscle. *The Journal of Physiology* **589**, 2129-2138 (2011).
217. Powers, S.K., Wiggs, M.P., Duarte, J.A., Zergeroglu, A.M. & Demirel, H.A. *Mitochondrial signaling contributes to disuse muscle atrophy*, (2012).
218. Chen, Q., Vazquez, E.J., Moghaddas, S., Hoppel, C.L. & Lesnefsky, E.J. Production of reactive oxygen species by mitochondria central role of complex III. *Journal of Biological Chemistry* **278**, 36027-36031 (2003).
219. Kurihara, Y.*, et al.* Mitophagy Plays an Essential Role in Reducing Mitochondrial Production of Reactive Oxygen Species and Mutation of Mitochondrial DNA by Maintaining Mitochondrial Quantity and Quality in Yeast. *Journal of Biological Chemistry* **287**, 3265-3272 (2012).
220. Brookes, P.S., Yoon, Y., Robotham, J.L., Anders, M. & Sheu, S.-S. Calcium, ATP, and ROS: a mitochondrial love-hate triangle. *American Journal of Physiology-Cell Physiology* **287**, C817-C833 (2004).
221. Webster, K.A. Mitochondrial membrane permeabilization and cell death during myocardial infarction: roles of calcium and reactive oxygen species. *Future cardiology* **8**, 863-884 (2012).
222. Bernardi, P. & Petronilli, V. The permeability transition pore as a mitochondrial calcium release channel: a critical appraisal. *Journal of bioenergetics and biomembranes* **28**, 131-138 (1996).
223. Bonnard, C.*, et al.* Mitochondrial dysfunction results from oxidative stress in the skeletal muscle of diet-induced insulin-resistant mice. *The Journal of Clinical Investigation* **118**, 789-800 (2008).
224. Bottinger, L.*, et al.* A complex of Cox4 and mitochondrial Hsp70 plays an important role in the assembly of the cytochrome c oxidase. *Molecular biology of the cell* **24**, 2609-2619 (2013).
225. Frohnert, B.I. & Bernlohr, D.A. Protein carbonylation, mitochondrial dysfunction, and insulin resistance. *Advances in Nutrition: An International Review Journal* **4**, 157-163 (2013).
226. Green, D.R. & Kroemer, G. The pathophysiology of mitochondrial cell death. *Science* **305**, 626-629 (2004).
227. Emily, H.-Y.C.*, et al.* BCL-2, BCL-X L sequester BH3 domain-only molecules preventing BAX-and BAK-mediated mitochondrial apoptosis. *Molecular cell* **8**, 705-711 (2001).
228. Alway, S.E., Mohamed, J.S. & Myers, M.J. Mitochondria Initiate and Regulate Sarcopenia. *Exercise and Sport Sciences Reviews* (2017).

229. Yao, J.*, et al.* Mitochondrial bioenergetic deficit precedes Alzheimer's pathology in female mouse model of Alzheimer's disease. *Proceedings of the National Academy of Sciences* **106**, 14670-14675 (2009).
230. Larsen, S.*, et al.* Biomarkers of mitochondrial content in skeletal muscle of healthy young human subjects. *J Physiol* **590**, 3349-3360 (2012).
231. Argilés, J.M., López-Soriano, F.J. & Busquets, S. Muscle wasting in cancer: the role of mitochondria. *Current Opinion in Clinical Nutrition & Metabolic Care* **18**, 221-225 (2015).
232. Dobs, A.S.*, et al.* Effects of enobosarm on muscle wasting and physical function in patients with cancer: a double-blind, randomised controlled phase 2 trial. *The lancet oncology* **14**, 335-345 (2013).
233. Wallace, D.C. Mitochondria and cancer. *Nature Reviews Cancer* **12**, 685-698 (2012).
234. Zorov, D.B., Juhaszova, M. & Sollott, S.J. Mitochondrial reactive oxygen species (ROS) and ROS-induced ROS release. *Physiological reviews* **94**, 909-950 (2014).
235. Davies, K. & Doroshow, J. Redox cycling of anthracyclines by cardiac mitochondria. I. Anthracycline radical formation by NADH dehydrogenase. *Journal of Biological Chemistry* **261**, 3060-3067 (1986).
236. Doroshow, J. & Davies, K. Redox cycling of anthracyclines by cardiac mitochondria. II. Formation of superoxide anion, hydrogen peroxide, and hydroxyl radical. *Journal of Biological Chemistry* **261**, 3068-3074 (1986).
237. Chen, Y., Jungsuwadee, P., Vore, M., Butterfield, D.A. & St Clair, D.K. Collateral damage in cancer chemotherapy: oxidative stress in nontargeted tissues. *Molecular interventions* **7**, 147 (2007).
238. Dirks-Naylor, A.J., Tran, N.T.K., Yang, S., Mabolo, R. & Kouzi, S.A. The effects of acute doxorubicin treatment on proteome lysine acetylation status and apical caspases in skeletal muscle of fasted animals. *Journal of Cachexia, Sarcopenia and Muscle* **4**, 239-243 (2013).
239. Gilliam, L.A.A.*, et al. Doxorubicin acts via mitochondrial ROS to stimulate catabolism in C2C12 myotubes*, (2012).
240. Gorini, S.*, et al.* Chemotherapeutic drugs and mitochondrial dysfunction: focus on doxorubicin, trastuzumab, and sunitinib. *Oxidative medicine and cellular longevity* **2018**(2018).
241. Xu, X., Persson, H.L. & Richardson, D.R. Molecular Pharmacology of the Interaction of Anthracyclines with Iron. *Molecular Pharmacology* **68**, 261-271 (2005).
242. Finn, N.A., Findley, H.W. & Kemp, M.L. A Switching Mechanism in Doxorubicin Bioactivation Can Be Exploited to Control Doxorubicin Toxicity. *PLoS Computational Biology* **7**, e1002151 (2011).
243. Ismail, H.M.*, et al.* Inhibition of iPLA2β and of stretch-activated channels by doxorubicin alters dystrophic muscle function. *British Journal of Pharmacology* **169**, 1537-1550 (2013).
244. Conklin, K.A. Chemotherapy-Associated Oxidative Stress: Impact on Chemotherapeutic Effectiveness. *Integrative Cancer Therapies* **3**, 294-300 (2004).
245. Yang, J.-L., Weissman, L., Bohr, V.A. & Mattson, M.P. Mitochondrial DNA damage and repair in neurodegenerative disorders. *DNA repair* **7**, 1110-1120 (2008).
246. Kourie, J.I. *Interaction of reactive oxygen species with ion transport mechanisms*, (1998).

247. Leeuwenburgh, C. Role of apoptosis in sarcopenia. *J. Gerontol. Ser. A-Biol. Sci. Med. Sci.* **58**, 999-1001 (2003).
248. Powers, S.K., Kavazis, A.N. & DeRuisseau, K.C. *Mechanisms of disuse muscle atrophy: role of oxidative stress*, (2005).
249. Du, J.*, et al.* Activation of caspase-3 is an initial step triggering accelerated muscle proteolysis in catabolic conditions. *J. Clin. Invest.* **113**, 115-123 (2004).
250. Smuder, A.J., Kavazis, A.N., Min, K. & Powers, S.K. *Exercise protects against doxorubicin-induced oxidative stress and proteolysis in skeletal muscle*, (2011).
251. Lecker, S.H., Solomon, V., Mitch, W.E. & Goldberg, A.L. Muscle protein breakdown and the critical role of the ubiquitin-proteasome pathway in normal and disease states. *The Journal of nutrition* **129**, 227S-237S (1999).
252. Lecker, S.H., Goldberg, A.L. & Mitch, W.E. Protein Degradation by the Ubiquitin–Proteasome Pathway in Normal and Disease States. *Journal of the American Society of Nephrology* **17**, 1807-1819 (2006).
253. Adachi, K.*, et al.* A Deletion of Mitochondrial DNA in Murine Doxorubicin-Induced Cardiotoxicity. *Biochemical and Biophysical Research Communications* **195**, 945-951 (1993).
254. Gouspillou, G.*, et al.* Anthracycline-containing chemotherapy causes long-term impairment of mitochondrial respiration and increased reactive oxygen species release in skeletal muscle. *Scientific reports* **5**, 8717 (2015).
255. Alcindor, T. & Beauger, N. Oxaliplatin: a review in the era of molecularly targeted therapy. *Current Oncology* **18**, 18-25 (2011).
256. Raymond, E., Chaney, S., Taamma, A. & Cvitkovic, E. Oxaliplatin: a review of preclinical and clinical studies. *Annals of Oncology* **9**, 1053-1071 (1998).
257. Raymond, E., Faivre, S., Woynarowski, J.M. & Chaney, S.G. Oxaliplatin: mechanism of action and antineoplastic activity. *Semin Oncol* **25**, 4-12 (1998).
258. André, T.*, et al.* Oxaliplatin, fluorouracil, and leucovorin as adjuvant treatment for colon cancer. *New England Journal of Medicine* **350**, 2343-2351 (2004).
259. Talvensaari, K.K., Jämsen, A., Vanharanta, H. & Lanning, M. Decreased isokinetic trunk muscle strength and performance in long-term survivors of childhood malignancies: correlation with hormonal defects. *Archives of physical medicine and rehabilitation* **76**, 983-988 (1995).
260. Gourdier, I., Crabbe, L., Andreau, K., Pau, B. & Kroemer, G. Oxaliplatin-induced mitochondrial apoptotic response of colon carcinoma cells does not require nuclear DNA. *Oncogene* **23**, 7449-7457 (2004).
261. Lutsenko, S., Barnes, N.L., Bartee, M.Y. & Dmitriev, O.Y. Function and regulation of human copper-transporting ATPases. *Physiological reviews* **87**, 1011-1046 (2007).
262. Wisnovsky, Simon P.*, et al.* Targeting Mitochondrial DNA with a Platinum-Based Anticancer Agent. *Chemistry & Biology* **20**, 1323-1328 (2013).
263. Montalvo, R.N., Doerr, V., Min, K., Szeto, H.H. & Smuder, A.J. Doxorubicin-induced oxidative stress differentially regulates proteolytic signaling in cardiac and skeletal muscle. *American Journal of Physiology-Regulatory, Integrative and Comparative Physiology* **318**, R227-R233 (2020).
264. Olson, R.D. & Mushlin, P.S. Doxorubicin cardiotoxicity: analysis of prevailing hypotheses. *The FASEB journal* **4**, 3076-3086 (1990).
265. Min, K.*, et al. Mitochondrial-targeted antioxidants protect skeletal muscle against immobilization-induced muscle atrophy*, (2011).

266. Singh, K. & Hood, D.A. *Effect of denervation-induced muscle disuse on mitochondrial protein import*, (2011).
267. Min, K.*, et al.* Increased mitochondrial emission of reactive oxygen species and calpain activation are required for doxorubicin-induced cardiac and skeletal muscle myopathy. *The Journal of Physiology* **593**, 2017-2036 (2015).
268. Hyatt, H., Deminice, R., Yoshihara, T. & Powers, S.K. Mitochondrial dysfunction induces muscle atrophy during prolonged inactivity: A review of the causes and effects. *Archives of biochemistry and biophysics* **662**, 49-60 (2019).
269. Abrigo, J., Simon, F., Cabrera, D., Vilos, C. & Cabello-Verrugio, C. Mitochondrial dysfunction in skeletal muscle pathologies. *Current Protein and Peptide Science* **20**, 536-546 (2019).
270. Sena, Laura A. & Chandel, Navdeep S. Physiological Roles of Mitochondrial Reactive Oxygen Species. *Molecular Cell* **48**, 158-167 (2012).
271. Lokireddy, S.*, et al.* The Ubiquitin Ligase Mul1 Induces Mitophagy in Skeletal Muscle in Response to Muscle-Wasting Stimuli. *Cell Metabolism* **16**, 613-624 (2012).
272. Sorensen, J.C.*, et al.* Idebenone protects against chemotherapy-induced skeletal muscle wasting and mitochondrial dysfunction in mice. *Proceedings of the Australian Physiological Society* **46**, 142 (2015).
273. Jackman, R.W. & Kandarian, S.C. *The molecular basis of skeletal muscle atrophy*, (2004).
274. Jang, Y.C.*, et al.* Increased superoxide in vivo accelerates age-associated muscle atrophy through mitochondrial dysfunction and neuromuscular junction degeneration. *The FASEB Journal* **24**, 1376-1390 (2010).
275. Bonaldo, P. & Sandri, M. Cellular and molecular mechanisms of muscle atrophy. *Disease Models & Mechanisms* **6**, 25-39 (2013).
276. Lenaz, G. Mitochondria and Reactive Oxygen Species. Which Role in Physiology and Pathology? in *Advances in Mitochondrial Medicine*, Vol. 942 (eds. Scatena, R., Bottoni, P. & Giardina, B.) 93-136 (Springer Netherlands, 2012).
277. Crouch, M.-L.*, et al.* Cyclophosphamide leads to persistent deficits in physical performance and in vivo mitochondria function in a mouse model of chemotherapy late effects. *PloS one* **12**, e0181086 (2017).
278. Neel, B.A., Lin, Y. & Pessin, J.E. Skeletal Muscle Autophagy: A New Metabolic Regulator. *Trends in endocrinology and metabolism: TEM* **24**, 10.1016/j.tem.2013.1009.1004 (2013).
279. Evans, W.J.*, et al.* Cachexia: a new definition. *Clinical nutrition* **27**, 793-799 (2008).
280. Maccarrone, M., Melino, G. & Finazzi-Agro, A. Lipoxygenases and their involvement in programmed cell death. *Cell Death & Differentiation* **8**, 776-784 (2001).
281. England, K. & Cotter, T. Direct oxidative modifications of signalling proteins in mammalian cells and their effects on apoptosis. *Redox Report* **10**, 237-245 (2005).
282. Moylan, J.S. & Reid, M.B. Oxidative stress, chronic disease, and muscle wasting. *Muscle & Nerve: Official Journal of the American Association of Electrodiagnostic Medicine* **35**, 411-429 (2007).
283. Ranek, M.J. & Wang, X. Activation of the ubiquitin-proteasome system in doxorubicin cardiomyopathy. *Current hypertension reports* **11**, 389 (2009).
284. Corradetti, R. Chemotherapy-induced peripheral neuropathy. *Chemotherapy* **249**, 279 (2014).

285. Zitvogel, L., Apetoh, L., Ghiringhelli, F. & Kroemer, G. Immunological aspects of cancer chemotherapy. *Nature reviews immunology* **8**, 59-73 (2008).
286. Lynch, D.R., Perlman, S.L. & Meier, T. A phase 3, double-blind, placebo-controlled trial of idebenone in Friedreich ataxia. *Archives of Neurology* **67**, 941-947 (2010).
287. Literati-Nagy, B.*, et al.* Improvement of insulin sensitivity by a novel drug, BGP-15, in insulin-resistant patients: a proof of concept randomized double-blind clinical trial. *Hormone and metabolic research* **41**, 374-380 (2009).
288. Sourris, K.C.*, et al.* Ubiquinone (coenzyme Q10) prevents renal mitochondrial dysfunction in an experimental model of type 2 diabetes. *Free Radical Biology and Medicine* **52**, 716-723 (2012).
289. Orsucci, D., Mancuso, M., Ienco, E.C., LoGerfo, A. & Siciliano, G. Targeting mitochondrial dysfunction and neurodegeneration by means of coenzyme Q10 and its analogues. *Current medicinal chemistry* **18**, 4053-4064 (2011).
290. Lenaz, G., Fato, R., Formiggini, G. & Genova, M.L. The role of Coenzyme Q in mitochondrial electron transport. *Mitochondrion* **7**, S8-S33 (2007).
291. Mancuso, M., Orsucci, D., Volpi, L., Calsolaro, V. & Siciliano, G. Coenzyme Q10 in neuromuscular and neurodegenerative disorders. *Current drug targets* **11**, 111-121 (2010).
292. Briere, J.-J., Schlemmer, D., Chretien, D. & Rustin, P. Quinone analogues regulate mitochondrial substrate competitive oxidation. *Biochemical and biophysical research communications* **316**, 1138-1142 (2004).
293. Kerr, D.S. Treatment of mitochondrial electron transport chain disorders: A review of clinical trials over the past decade. *Molecular Genetics and Metabolism* **99**, 246-255.
294. Mangialasche, F., Solomon, A., Winblad, B., Mecocci, P. & Kivipelto, M. Alzheimer's disease: clinical trials and drug development. *The Lancet Neurology* **9**, 702-716 (2010).
295. Mariotti, C.*, et al.* Idebenone treatment in Friedreich patients: one-year-long randomized placebo-controlled trial. *Neurology* **60**, 1676-1679 (2003).
296. Geromel, V.*, et al.* Coenzyme Q 10 and idebenone in the therapy of respiratory chain diseases: rationale and comparative benefits. *Molecular genetics and metabolism* **77**, 21-30 (2002).
297. Lenaz, G.*, et al.* Role of mitochondria in oxidative stress and aging. *Annals of the New York Academy of Sciences* **959**, 199-213 (2002).
298. Giorgio, V.*, et al.* The effects of idebenone on mitochondrial bioenergetics. *Biochimica et Biophysica Acta (BBA)-Bioenergetics* **1817**, 363-369 (2012).
299. Zhao, K.*, et al.* Cell-permeable peptide antioxidants targeted to inner mitochondrial membrane inhibit mitochondrial swelling, oxidative cell death, and reperfusion injury. *The Journal of biological chemistry* **279**, 34682-34690 (2004).
300. Cho, J.*, et al.* Potent mitochondria-targeted peptides reduce myocardial infarction in rats. *Coronary artery disease* **18**, 215-220 (2007).
301. Petri, S.*, et al.* Cell-permeable peptide antioxidants as a novel therapeutic approach in a mouse model of amyotrophic lateral sclerosis. *Journal of neurochemistry* **98**, 1141-1148 (2006).
302. Oliff, A.*, et al.* Tumors secreting human TNF/cachectin induce cachexia in mice. *Cell* **50**, 555-563 (1987).
303. Zhou, X.*, et al.* Reversal of cancer cachexia and muscle wasting by ActRIIB antagonism leads to prolonged survival. *Cell* **142**, 531-543 (2010).

304. Riad, A.*, et al.* Pretreatment with statin attenuates the cardiotoxicity of Doxorubicin in mice. *Cancer research* **69**, 695-699 (2009).
305. Fardell, J.E.*, et al.* The impact of sustained and intermittent docetaxel chemotherapy regimens on cognition and neural morphology in healthy mice. *Psychopharmacology* **231**, 841-852 (2014).
306. Stoeltzing, O.*, et al.* Inhibition of integrin α5β1 function with a small peptide (ATN-161) plus continuous 5-FU infusion reduces colorectal liver metastases and improves survival in mice. *International journal of cancer* **104**, 496-503 (2003).
307. Tournigand, C.*, et al.* FOLFIRI followed by FOLFOX6 or the reverse sequence in advanced colorectal cancer: a randomized GERCOR study. *Journal of Clinical Oncology* **22**, 229-237 (2004).
308. Venook, A.P.*, et al.* CALGB/SWOG 80405: Phase III trial of irinotecan/5-FU/leucovorin (FOLFIRI) or oxaliplatin/5-FU/leucovorin (mFOLFOX6) with bevacizumab (BV) or cetuximab (CET) for patients (pts) with KRAS wild-type (wt) untreated metastatic adenocarcinoma of the colon or rectum (MCRC). (American Society of Clinical Oncology, 2014).
309. Seigers, R.*, et al.* Cognitive impact of cytotoxic agents in mice. *Psychopharmacology* **232**, 17-37 (2015).
310. Ezoe, K.*, et al.* Long-term adverse effects of cyclophosphamide on follicular growth and angiogenesis in mouse ovaries. *Reproductive biology* **14**, 238-242 (2014).
311. Rendeiro, C.*, et al.* Long-lasting impairments in adult neurogenesis, spatial learning and memory from a standard chemotherapy regimen used to treat breast cancer. *Behavioural brain research* **315**, 10-22 (2016).
312. Hydock, D., Bredahl, E., Quinn, C. & Hayward, R. Protective effects of endurance or resistance training exercise on chemotherapy-induced skeletal muscle weakness and fatigue. *The FASEB Journal* **29**, LB660 (2015).
313. Bhasin, S.*, et al.* Sarcopenia Definition: The Position Statements of the Sarcopenia Definition and Outcomes Consortium. *Journal of the American Geriatrics Society* (2020).
314. Evans, W.J. & Campbell, W.W. Sarcopenia and age-related changes in body composition and functional capacity. *The Journal of nutrition* **123**, 465-468 (1993).
315. Lang, T.*, et al.* Sarcopenia: etiology, clinical consequences, intervention, and assessment. *Osteoporosis international* **21**, 543-559 (2010).
316. Marcell, T.J. Sarcopenia: causes, consequences, and preventions. *The Journals of Gerontology Series A: Biological Sciences and Medical Sciences* **58**, M911-M916 (2003).
317. Murphy, S.B. Classification, staging and end results of treatment of childhood non-Hodgkin's lymphomas: dissimilarities from lymphomas in adults. in *Semin Oncol*, Vol. 7 332-339 (Elsevier, 1980).
318. Linet, M.S., Ries, L.A., Smith, M.A., Tarone, R.E. & Devesa, S.S. Cancer surveillance series: recent trends in childhood cancer incidence and mortality in the United States. *Journal of the National Cancer Institute* **91**, 1051-1058 (1999).
319. de Beaumais, T.A.*, et al.* Determinants of mercaptopurine toxicity in paediatric acute lymphoblastic leukemia maintenance therapy. *British journal of clinical pharmacology* **71**, 575-584 (2011).
320. Gaynon, P.S. Childhood acute lymphoblastic leukaemia and relapse. *Br J Haematol* **131**, 579-587 (2005).

321. Henze, G. The BFM 76/79 acute lymphoblastic leukemia therapy study. *Klin Padiatr* **193**, 145-154 (1981).
322. Lange, B.J.*, et al.* Double-delayed intensification improves event-free survival for children with intermediate-risk acute lymphoblastic leukemia: a report from the Children's Cancer Group. *Blood* **99**, 825-833 (2002).
323. McNeer, J.L. & Nachman, J.B. The optimal use of steroids in paediatric acute lymphoblastic leukaemia: no easy answers. *Br J Haematol* **149**, 638-652 (2010).
324. Matloub, Y.*, et al.* Escalating intravenous methotrexate improves event-free survival in children with standard-risk acute lymphoblastic leukemia: a report from the Children's Oncology Group. *Blood*, blood-2010-2012-322909 (2011).
325. Packer, R.J., Sutton, L.N., D'Angio, G., Evans, A.E. & Schut, L. Management of children with primitive neuroectodermal tumors of the posterior fossa/medulloblastoma. *Pediatric Neurosurgery* **12**, 272-282 (1985).
326. Christie, D., Leiper, A., Chessells, J. & Vargha-Khadem, F. Intellectual performance after presymptomatic cranial radiotherapy for leukaemia: effects of age and sex. *Archives of Disease in Childhood* **73**, 136-140 (1995).
327. Abayomi, O.K. Pathogenesis of irradiation-induced cognitive dysfunction. *Acta oncologica* **35**, 659-663 (1996).
328. Keime-Guibert, F., Napolitano, M. & Delattre, J.-Y. Neurological complications of radiotherapy and chemotherapy. *Journal of neurology* **245**, 695-708 (1998).
329. Silverman, C.L.*, et al.* Late effects of radiotherapy on patients with cerebellar medulloblastoma. *Cancer* **54**, 825-829 (1984).
330. Pollack, I.F. & Jakacki, R.I. Childhood brain tumors: epidemiology, current management and future directions. *Nature Reviews Neurology* **7**, 495 (2011).
331. Packer, R.J.*, et al. Phase III Study of Craniospinal Radiation Therapy Followed by Adjuvant Chemotherapy for Newly Diagnosed Average-Risk Medulloblastoma*, (2006).
332. Packer, R.J.*, et al.* Outcome for children with medulloblastoma treated with radiation and cisplatin, CCNU, and vincristine chemotherapy. *Journal of neurosurgery* **81**, 690-698 (1994).
333. Evans, A.E., Anderson, J.R., Lefkowitz-Boudreaux, I.B. & Finlay, J.L. Adjuvant chemotherapy of childhood posterior fossa ependymoma: Cranio-spinal irradiation with or without adjuvant CCNU, vincristine, and prednisone: A Childrens Cancer Group study. *Medical and Pediatric Oncology* **27**, 8-14 (1996).
334. Robertson, P.L.*, et al.* Survival and prognostic factors following radiation therapy and chemotherapy for ependymomas in children: a report of the Children's Cancer Group. **88**, 695 (1998).
335. Lefkowitz, I.B.*, et al.* Results of treatment of children with recurrent medulloblastoma/primitive neuroectodermal tumors with lomustine, cisplatin, and vincristine. *Cancer* **65**, 412-417 (1990).
336. Spreafico, F.*, et al.* Survival of adults treated for medulloblastoma using paediatric protocols. *European Journal of Cancer* **41**, 1304-1310 (2005).
337. Fuller, L., Banker, F., Butler, J., Gamble, J. & Sullivan, M. The natural history of non-Hodgkin's lymphomata stages I and II. *The British journal of cancer. Supplement* **2**, 270 (1975).

338. Gerrard, M.*, et al.* Excellent survival following two courses of COPAD chemotherapy in children and adolescents with resected localized B-cell non-Hodgkin's lymphoma: results of the FAB/LMB 96 international study. *Br J Haematol* **141**, 840-847 (2008).
339. Aydin, B.*, et al.* FAB LMB 96 Regimen for Newly Diagnosed Burkitt Lymphoma in Children: Single-center Experience. *Journal of Pediatric Hematology/Oncology* **41**, e7-e11 (2019).
340. Cairo, M.*, et al.* Overall survival of children and adolescents with mature B cell non-Hodgkin lymphoma who had refractory or relapsed disease during or after treatment with FAB/LMB 96: a report from the FAB/LMB 96 study group. *Br J Haematol* **182**, 859-869 (2018).
341. Cairo, M.S.*, et al.* Advanced stage, increased lactate dehydrogenase, and primary site, but not adolescent age (≥ 15 years), are associated with an increased risk of treatment failure in children and adolescents with mature B-cell non-Hodgkin's lymphoma: results of the FAB LMB 96 study. *Journal of Clinical Oncology* **30**, 387 (2012).
342. Gerrard, M.*, et al.* Outcome and pathologic classification of children and adolescents with mediastinal large B-cell lymphoma treated with FAB/LMB96 mature B-NHL therapy. *Blood, The Journal of the American Society of Hematology* **121**, 278-285 (2013).
343. Attias, D., Hodgson, D. & Weitzman, S. Primary mediastinal B-cell lymphoma in the pediatric patient: Can a rational approach to therapy be based on adult studies? *Pediatric blood & cancer* **52**, 566-570 (2009).
344. Hochberg, J., Waxman, I.M., Kelly, K.M., Morris, E. & Cairo, M.S. Adolescent non-Hodgkin lymphoma and Hodgkin lymphoma: state of the science. *Br J Haematol* **144**, 24-40 (2009).
345. Giulino-Roth, L. How I treat primary mediastinal B-cell lymphoma. *Blood* **132**, 782-790 (2018).
346. Thacker, N.*, et al.* Management of non-Hodgkin lymphoma: ICMR consensus document. *The Indian Journal of Pediatrics* **84**, 382-392 (2017).
347. Dunleavy, K. & Gross, T.G. Management of aggressive B-cell NHLs in the AYA population: an adult vs pediatric perspective. *Blood* **132**, 369-375 (2018).
348. Abla, O., Batchelor, T.T. & Attarbaschi, A. Primary Central Nervous System Lymphoma. in *Non-Hodgkin's Lymphoma in Childhood and Adolescence* 229-238 (Springer, 2019).
349. Fukano, R. Mature B-Cell Acute Lymphoblastic Leukemia. in *Pediatric Acute Lymphoblastic Leukemia* 73-80 (Springer, 2020).
350. Lange, J., Lenz, G. & Burkhardt, B. Mature aggressive B-cell lymphoma across age groups–molecular advances and therapeutic implications. *Expert review of hematology* **10**, 123-135 (2017).
351. Helwick, C. & Cairo, M.S. For High-Grade and Aggressive Non-Hodgkin Lymphomas, Treat Adults Like Children. (2016).
352. Molyneux, E.*, et al.* The use of anthracyclines in the treatment of endemic Burkitt lymphoma. *Br J Haematol* **177**, 984-990 (2017).
353. Hesseling, P.*, et al.* The 2000 Burkitt lymphoma trial in Malawi. *Pediatric blood & cancer* **44**, 245-250 (2005).
354. Hesseling, P.B.*, et al.* Treating burkitt's lymphoma in Malawi, Cameroon, and Ghana. (2008).

355. Hesseling, P., Molyneux, E., Kamiza, S. & Broadhead, R. Rescue chemotherapy for patients with resistant or relapsed endemic Burkitt's lymphoma. *Transactions of the Royal Society of Tropical Medicine and Hygiene* **102**, 602-607 (2008).
356. Hesseling, P., Molyneux, E., Kamiza, S., Israels, T. & Broadhead, R. Endemic Burkitt lymphoma: a 28-day treatment schedule with cyclophosphamide and intrathecal methotrexate. *Annals of tropical paediatrics* **29**, 29-34 (2009).
357. Depani, S.*, et al.* Outcome is unchanged by adding vincristine upfront to the Malawi 28-day protocol for endemic Burkitt lymphoma. *Pediatric blood & cancer* **62**, 1929-1934 (2015).
358. Perel, P.*, et al.* Comparison of treatment effects between animal experiments and clinical trials: systematic review. *Bmj* **334**, 197 (2007).
359. Sams-Dodd, F. Target-based drug discovery: is something wrong? *Drug discovery today* **10**, 139-147 (2005).
360. Bruggeman, A.R.*, et al.* Cancer cachexia: beyond weight loss. *Journal of oncology practice* **12**, 1163-1171 (2016).
361. Prado, C.M.*, et al.* Prevalence and clinical implications of sarcopenic obesity in patients with solid tumours of the respiratory and gastrointestinal tracts: a population-based study. *The lancet oncology* **9**, 629-635 (2008).
362. Palmela, C.*, et al.* Body composition as a prognostic factor of neoadjuvant chemotherapy toxicity and outcome in patients with locally advanced gastric cancer. *Journal of gastric cancer* **17**, 74-87 (2017).
363. Shachar, S.S.*, et al.* Skeletal muscle measures as predictors of toxicity, hospitalization, and survival in patients with metastatic breast cancer receiving taxane-based chemotherapy. *Clinical Cancer Research* **23**, 658-665 (2017).
364. Wendrich, A.W.*, et al.* Low skeletal muscle mass is a predictive factor for chemotherapy dose-limiting toxicity in patients with locally advanced head and neck cancer. *Oral oncology* **71**, 26-33 (2017).
365. Versteeg, K.S.*, et al.* Higher muscle strength is associated with prolonged survival in older patients with advanced cancer. *The oncologist* **23**, 580 (2018).
366. Ota, T.*, et al.* Skeletal muscle mass as a predictor of the response to neo-adjuvant chemotherapy in locally advanced esophageal cancer. *Medical Oncology* **36**, 15 (2019).
367. Shahrasbi, A., Armin, A., Ardebili, A., Rafie, K. & Ansari, M. Hematologic Adverse Effects following Systemic Chemotherapy. *Journal of Oncology Medicine and Practice* **2**, 110 (2017).
368. Elias, L., Portlock, C.S. & Rosenberg, S.A. Combination chemotherapy of diffuse histiocytic lymphoma with cyclophosphamide, adriamycin, vincristine and prednisone (CHOP). *Cancer* **42**, 1705-1710 (1978).
369. Limat, S.*, et al.* Early cardiotoxicity of the CHOP regimen in aggressive non-Hodgkin's lymphoma. *Annals of Oncology* **14**, 277-281 (2003).
370. Tilly, H.*, et al.* Intensive conventional chemotherapy (ACVBP regimen) compared with standard CHOP for poor-prognosis aggressive non-Hodgkin lymphoma. *Blood* **102**, 4284-4289 (2003).
371. Nakayama, S.*, et al.* Multiple cytokine-producing aggressive EBV-positive diffuse large B cell lymphoma, not otherwise specified with hemophagocytic syndrome. *Annals of Hematology* **99**, 381-383 (2020).

372. Yokoyama, M*., et al.* Incidence and risk factors for febrile neutropenia in Japanese patients with non-Hodgkin B cell lymphoma receiving R-CHOP: 2-year experience in a single center (STOP FN in NHL 2). *Supportive Care in Cancer* **28**, 571-579 (2020).
373. Liao, X., Guo, Y., Shen, Y. & Xiao, J. Recurrent Gastrointestinal Hemorrhage in Children with Philadelphia-Positive B-Cell Acute Lymphoblastic Leukemia Treated with Dasatinib. *Case Reports in Hematology* **2020**(2020).
374. Sasaki, K*., et al.* Phase 2 study of hyper-CMAD with liposomal vincristine for patients with newly diagnosed acute lymphoblastic leukemia. *American journal of hematology* (2020).
375. Daneshfard, B., Shahriari, M., Heiran, A., Nimrouzi, M. & Yarmohammadi, H. Effect of chamomile on chemotherapy-induced neutropenia in pediatric leukemia patients: A randomized triple-blind placebo-controlled clinical trial. *Avicenna Journal of Phytomedicine* **10**, 58 (2020).
376. Khan, S., Anwar, S., Latif, M.F., Farooq, A. & Faizan, M. Induction-remission response in peadiatric acute lymphoblastic leukaemia, Lahore protocol versus UKALL 2011 interim guidelines. *JPMA. The Journal of the Pakistan Medical Association* **70**, 591-596 (2020).
377. van der Heyden, B*., et al.* Automated CT-derived skeletal muscle mass determination in lower hind limbs of mice using a 3D U-Net deep learning network. *Journal of Applied Physiology* **128**, 42-49 (2020).
378. Pauwels, E., Van Loo, D., Cornillie, P., Brabant, L. & Van Hoorebeke, L. An exploratory study of contrast agents for soft tissue visualization by means of high resolution X-ray computed tomography imaging. *Journal of microscopy* **250**, 21-31 (2013).
379. Moreau, J*., et al.* Correlation between muscle mass and handgrip strength in digestive cancer patients undergoing chemotherapy. *Cancer medicine* (2019).
380. Rogers, B.H., Brown, J.C., Gater, D.R. & Schmitz, K.H. Association between maximal bench press strength and isometric handgrip strength among breast cancer survivors. *Archives of physical medicine and rehabilitation* **98**, 264-269 (2017).
381. Visovsky, C. Muscle strength, body composition, and physical activity in women receiving chemotherapy for breast cancer. *Integrative cancer therapies* **5**, 183-191 (2006).
382. Fanny, P.-R*., et al.* Physical capability markers used to define sarcopenia and their association with cardiovascular, respiratory and cancer outcomes: A prospective study from UK Biobank. *Maturitas* (2020).
383. Hayes, A., Scott, D. & Dorgo, S. EFFECTS OF ETHNICITY AND GEOGRAPHICAL LOCATION ON SARCOPENIA AND HAND GRIP STRENGTH: A PILOT STUDY. *Innovation in Aging* **1**, 1014 (2017).
384. Hogrel, J.-Y*., et al.* Normalized grip strength is a sensitive outcome measure through all stages of Duchenne muscular dystrophy. *Journal of Neurology*, 1-7 (2020).
385. Duong, T. Nova Southeastern University (2020).
386. Bulut, N., Gürbüz, I., Yilmaz, Ö., Aydin, G. & Karaduman, A. The association of hand grip strength with functional measures in non-ambulatory children with Duchenne muscular dystrophy. *Arquivos de Neuro-Psiquiatria* **77**, 792-796 (2019).
387. Agelaki, S*., et al.* Cancer cachexia, sarcopenia and hand-GRIP strength (HGS) in the prediction of outcome in patients with metastatic non-small cell lung cancer (NSCLC) treated with immune checkpoint inhibitors (ICIs): A prospective, observational study. (American Society of Clinical Oncology, 2019).

388. Blauwhoff-Buskermolen, S., Langius, J.A., Becker, A., Verheul, H.M. & de van der Schueren, M.A. The influence of different muscle mass measurements on the diagnosis of cancer cachexia. *Journal of cachexia, sarcopenia and muscle* **8**, 615-622 (2017).
389. Goodman, C.A.*, et al.* Taurine supplementation increases skeletal muscle force production and protects muscle function during and after high-frequency in vitro stimulation. *Journal of Applied Physiology* **107**, 144-154 (2009).
390. Hayes, A. & Williams, D.A. Long-term clenbuterol administration alters the isometric contractile properties of skeletal muscle from normal and dystrophin-deficient mdx mice. *Clinical and experimental pharmacology and physiology* **21**, 757-765 (1994).
391. Hayes, A. & Williams, D.A. Contractile properties of clenbuterol-treated mdx muscle are enhanced by low-intensity swimming. *Journal of Applied Physiology* **82**, 435-439 (1997).
392. Hayes, A. & Williams, D.A. Contractile function and low-intensity exercise effects of old dystrophic (mdx) mice. *American Journal of Physiology-Cell Physiology* **274**, C1138-C1144 (1998).
393. Altarawneh, M.M.*, et al.* Effects of testosterone suppression, hindlimb immobilization, and recovery on [3H] ouabain binding site content and Na+, K+-ATPase isoforms in rat soleus muscle. *Journal of Applied Physiology* **128**, 501-513 (2020).
394. Rand, M.S. Selection of biomedical animal models. in *Sourcebook of models for biomedical research* 9-15 (Springer, 2008).
395. Hau, J. & Schapiro, S.J. *Handbook of laboratory animal science: Essential Principles and Practices, Volume I*, (CRC press, 2002).
396. Conn, P.M. *Sourcebook of models for biomedical research*, (Springer Science & Business Media, 2008).
397. Eppig, J.T. & Strivens, M. Finding a mouse: the international mouse strain resource (IMSR). *Trends in Genetics* **15**, 81-82 (1999).
398. Eppig, J.T., Motenko, H., Richardson, J.E., Richards-Smith, B. & Smith, C.L. The International Mouse Strain Resource (IMSR): cataloging worldwide mouse and ES cell line resources. *Mammalian Genome* **26**, 448-455 (2015).
399. Eppig, J.T.*, et al.* The Mouse Genome Database (MGD): from genes to mice—a community resource for mouse biology. *Nucleic acids research* **33**, D471-D475 (2005).
400. Davidson, M., Lindsey, J. & Davis, J. Requirements and selection of an animal model. *Israel journal of medical sciences* **23**, 551-555 (1987).
401. Hariri, N. & Thibault, L. High-fat diet-induced obesity in animal models. *Nutrition research reviews* **23**, 270-299 (2010).
402. Hendrickson, E.A. The SCID mouse: relevance as an animal model system for studying human disease. *The American journal of pathology* **143**, 1511 (1993).
403. Mathe, D. Dyslipidemia and diabetes: animal models. *Diabete & metabolisme* **21**, 106-111 (1995).
404. Muschler, G.F., Raut, V.P., Patterson, T.E., Wenke, J.C. & Hollinger, J.O. The design and use of animal models for translational research in bone tissue engineering and regenerative medicine. *Tissue Engineering Part B: Reviews* **16**, 123-145 (2010).
405. Rees, D. & Alcolado, J. Animal models of diabetes mellitus. *Diabetic medicine* **22**, 359-370 (2005).

406. Stokes, W.S. Selecting appropriate animal models and experimental designs for endocrine disruptor research and testing studies. *ILAR journal* **45**, 387-393 (2004).
407. Williams, J.P.*, et al.* Animal models for medical countermeasures to radiation exposure. *Radiation research* **173**, 557-578 (2010).
408. Wood, M.W. & Hart, L.A. Selecting appropriate animal models and strains: making the best use of research, information and outreach. *AATEX* **14**, 303-306 (2007).
409. Lelovas, P.P., Xanthos, T.T., Thoma, S.E., Lyritis, G.P. & Dontas, I.A. The laboratory rat as an animal model for osteoporosis research. *Comparative medicine* **58**, 424-430 (2008).
410. Vandamme, T.F. Use of rodents as models of human diseases. *Journal of pharmacy & bioallied sciences* **6**, 2 (2014).
411. Albus, U. Guide for the Care and Use of Laboratory Animals (8th edn). (SAGE Publications Sage UK: London, England, 2012).
412. Fox, J.G.*, et al. The mouse in biomedical research: normative biology, husbandry, and models*, (Elsevier, 2006).
413. Workman, P.*, et al.* Guidelines for the welfare and use of animals in cancer research. *British journal of cancer* **102**, 1555 (2010).
414. Kilkenny, C., Browne, W., Cuthill, I.C., Emerson, M. & Altman, D.G. Animal research: reporting in vivo experiments—the ARRIVE guidelines. (SAGE Publications Sage UK: London, England, 2011).
415. Xia, Y.-P.*, et al.* Transgenic delivery of VEGF to mouse skin leads to an inflammatory condition resembling human psoriasis. *Blood* **102**, 161-168 (2003).
416. Lee, J.-S.*, et al.* Application of comparative functional genomics to identify best-fit mouse models to study human cancer. *Nature genetics* **36**, 1306 (2004).
417. Hinrichs, S.H., Nerenberg, M., Reynolds, R.K., Khoury, G. & Jay, G. A transgenic mouse model for human neurofibromatosis. *Science* **237**, 1340-1343 (1987).
418. Seok, J.*, et al.* Genomic responses in mouse models poorly mimic human inflammatory diseases. *Proceedings of the National Academy of Sciences* **110**, 3507-3512 (2013).
419. Tatar, M., Bartke, A. & Antebi, A. The endocrine regulation of aging by insulin-like signals. *Science* **299**, 1346-1351 (2003).
420. FDA, U.S. Product Development Under the Animal Rule: Guidance for Industry. (ed. Services, U.S.D.o.H.a.H.) 3 (Center for Drug Evaluation and Research (CDER), Center for Biologics Evaluation and Research (CBER), 2015).
421. McQuade, R.M.S., J. C.; Timpani, C. A.; Nurgali, K.; Rybalka, E. Idebenone therapy protects against Oxaliplatin-induced gastrointestinal dysfunction. *Proceedings of the Australian Physiological Society* **46**, 90 (2015).
422. Stojanovska, V.M., R. M.; Stweart, M.; Timpani, C. A.; Sorensen, J. C; Orbell, J.; Rybalka, E.; Nurgali, K. Platinum accumulation and changes in mitochondrial function of the longitudinal muscle & myenteric plexus following oxaliplatin administration. *Proceedings of the Australian Physiological Society* **46**, 91 (2015).
423. Guo, T.*, et al.* Myostatin inhibition in muscle, but not adipose tissue, decreases fat mass and improves insulin sensitivity. *PloS one* **4**, e4937 (2009).
424. Northrup, R.*, et al.* Effect of ghrelin and anamorelin (ONO-7643), a selective ghrelin receptor agonist, on tumor growth in a lung cancer mouse xenograft model. *Supportive Care in Cancer* **21**, 2409-2415 (2013).

425. Zuber, J.*, et al.* Mouse models of human AML accurately predict chemotherapy response. *Genes & development* **23**, 877-889 (2009).
426. Pasetto, L.*, et al.* Micro-computed tomography for non-invasive evaluation of muscle atrophy in mouse models of disease. *PloS one* **13**(2018).
427. Constantinou, C.*, et al.* Nuclear magnetic resonance in conjunction with functional genomics suggests mitochondrial dysfunction in a murine model of cancer cachexia. *International journal of molecular medicine* **27**, 15-24 (2011).
428. Schneeberger, A.L., Thompson, R.T., Driedger, A.A., Finley, R.J. & Inculet, R.I. Effect of cancer on the in vivo energy state of rat liver and skeletal muscle. *Cancer research* **49**, 1160-1164 (1989).
429. Kavirayani, A., Sundberg, J. & Foreman, O. Primary neoplasms of bones in mice: retrospective study and review of literature. *Veterinary pathology* **49**, 182-205 (2012).
430. Franchi, A. Epidemiology and classification of bone tumors. *Clinical Cases in mineral and bone metabolism* **9**, 92 (2012).
431. Demetrius, L. Of mice and men: When it comes to studying ageing and the means to slow it down, mice are not just small humans. *EMBO reports* **6**, S39-S44 (2005).
432. Schmidt-Nielsen, K. *Scaling: why is animal size so important?*, (Cambridge university press, 1984).
433. Goldsmith, M.A., Slavik, M. & Carter, S.K. Quantitative prediction of drug toxicity in humans from toxicology in small and large animals. *Cancer Research* **35**, 1354-1364 (1975).
434. FDA. Estimating the Maximum Safe Starting Dose in Initial Clinical Trials for Therapeutics in Adult Healthy Volunteers. (ed. Services, U.S.D.o.H.a.H.) (Center for Drug Evaluation and Research (CDER), 2005).
435. Siegel, R.L., Miller, K.D. & Jemal, A. Cancer statistics, 2016. *CA: a cancer journal for clinicians* **66**, 7-30 (2016).
436. Laboratory, T.J. (Mouse) Lifespan as a biomarker. Vol. 2016 (The Jackson Laboratory, https://www.jax.org/research-and-faculty/research-labs/the-harrison-lab/gerontology/life-span-as-a-biomarker#, 2016).
437. Flurkey, K., Currer, J.M. & Harrison, D. Mouse models in aging research. in *The mouse in biomedical research* 637-672 (Elsevier, 2007).
438. Agriculture, V. Example Animal Monitoring Sheet. Vol. 2017 (Australian Government, agriculture.vic.gov.au, 2017).
439. Jordan, K.*, et al.* Supportive treatments for patients with cancer. *Deutsches Ärzteblatt International* **114**, 481 (2017).
440. Lin, M.L.M., Robinson, P.D., Flank, J., Sung, L. & Dupuis, L.L. The safety of prochlorperazine in children: a systematic review and meta-analysis. *Drug safety* **39**, 509-516 (2016).
441. Patel, M.P.*, et al.* Randomized open-label phase II trial of 5-day aprepitant plus ondansetron compared to ondansetron alone in the prevention of chemotherapy-induced nausea-vomiting (CINV) in glioma patients receiving adjuvant temozolomide. *Supportive Care in Cancer* **28**, 2229-2238 (2020).
442. Kang, H.J.*, et al.* Aprepitant for the prevention of chemotherapy-induced nausea and vomiting in paediatric subjects: An analysis by age group. *Pediatric blood & cancer* **65**, e27273 (2018).

443. Mehra, N.*, et al.* Effectiveness of olanzapine in patients who fail therapy with aprepitant while receiving highly emetogenic chemotherapy. *Medical Oncology* **35**, 12 (2018).
444. Giagnuolo, G.*, et al.* Single center experience on efficacy and safety of Aprepitant for preventing chemotherapy-induced nausea and vomiting (CINV) in pediatric Hodgkin Lymphoma. *PloS one* **14**, e0215295 (2019).
445. Gao, J.J., Tan, M., Pohlmann, P.R. & Swain, S.M. HALT-D: a phase II evaluation of crofelemer for the prevention and prophylaxis of diarrhea in patients with breast cancer on pertuzumab-based regimens. *Clinical breast cancer* **17**, 76-78 (2017).
446. Jaćević, V.*, et al.* The efficacy of amifostine against multiple-dose doxorubicin-induced toxicity in rats. *International journal of molecular sciences* **19**, 2370 (2018).
447. Tahover, E.*, et al.* Dexrazoxane added to doxorubicin-based adjuvant chemotherapy of breast cancer: a retrospective cohort study with a comparative analysis of toxicity and survival. *Anti-cancer drugs* **28**, 787-794 (2017).
448. Jang, J.H.*, et al.* Efficacy of intravenous iron treatment for chemotherapy-induced anemia: A prospective Phase II pilot clinical trial in South Korea. *Plos Medicine* **17**, e1003091 (2020).
449. Ghidini, M.*, et al.* New developments in the treatment of chemotherapy-induced neutropenia: focus on balugrastim. *Therapeutics and clinical risk management* **12**, 1009 (2016).
450. Bellini, G.*, et al.* The role of mifamurtide in chemotherapy-induced osteoporosis of children with osteosarcoma. *Current cancer drug targets* **17**, 650-656 (2017).
451. Essex, A.L.*, et al.* Bisphosphonate treatment ameliorates chemotherapy-induced bone and muscle abnormalities in young mice. *Frontiers in Endocrinology* **10**, 809 (2019).
452. Feld, L.G.*, et al.* Clinical practice guideline: maintenance intravenous fluids in children. *Pediatrics* **142**(2018).
453. Saito, S.*, et al.* Prophylactic piperacillin administration in pediatric patients with solid tumors following different intensities of chemotherapy. *Pediatrics International* **62**, 158-168 (2020).
454. Sulis, M.L.*, et al.* Effectiveness of antibacterial prophylaxis during induction chemotherapy in children with acute lymphoblastic leukemia. *Pediatric blood & cancer* **65**, e26952 (2018).
455. Hyltander, A.*, et al.* Supportive nutrition on recovery of metabolism, nutritional state, health-related quality of life, and exercise capacity after major surgery: a randomized study. *Clinical Gastroenterology and Hepatology* **3**, 466-474 (2005).
456. Sturgeon, K.M., Mathis, K.M., Rogers, C.J., Schmitz, K.H. & Waning, D.L. Cancer-and Chemotherapy-Induced Musculoskeletal Degradation. *JBMR plus* **3**, e10187 (2019).
457. Paviglianiti, A. A Review on the Impact of Body Mass Index on Outcomes in Pediatric Leukemia. *Journal of Blood Medicine* **11**, 205 (2020).
458. Esbenshade, A.J. & Ness, K.K. Dietary and exercise interventions for pediatric oncology patients: the way forward. *JNCI Monographs* **2019**, 157-162 (2019).
459. O'Quigley, J., Pepe, M. & Fisher, L. Continual reassessment method: a practical design for phase 1 clinical trials in cancer. *Biometrics*, 33-48 (1990).
460. OECD. *Test No. 425: Acute Oral Toxicity: Up-and-Down Procedure*, (2008).
461. Bruce, R.D. An up-and-down procedure for acute toxicity testing. *Fundamental and Applied Toxicology* **5**, 151-157 (1985).

462. Nijmeijer, B.A.*, et al.* Monitoring of engraftment and progression of acute lymphoblastic leukemia in individual NOD/SCID mice. *Experimental Hematology* **29**, 322-329 (2001).
463. Teitz, T.*, et al.* Preclinical models for neuroblastoma: establishing a baseline for treatment. *PloS one* **6**, e19133 (2011).
464. Wu, X., Northcott, P.A., Croul, S. & Taylor, M.D. Mouse models of medulloblastoma. *Chinese journal of cancer* **30**, 442 (2011).
465. Kerbel, R.S. Human tumor xenografts as predictive preclinical models for anticancer drug activity in humans: better than commonly perceived—but they can be improved. *Cancer biology & therapy* **2**, 133-138 (2003).
466. Ledford, H. Translational research: 4 ways to fix the clinical trial. *Nature News* **477**, 526-528 (2011).
467. Mak, I.W., Evaniew, N. & Ghert, M. Lost in translation: animal models and clinical trials in cancer treatment. *American journal of translational research* **6**, 114 (2014).
468. Berry, D.*, et al.* Comparison of prednisolone, vincristine, methotrexate, and 6-mercaptopurine vs. vincristine and prednisone induction therapy in childhood acute leukemia. *Cancer* **36**, 98-102 (1975).
469. Peterson, B.A. & Bloomfield, C.D. High-dose methotrexate for the remission induction of refractory adult acute lymphocytic leukemia. *Medical and pediatric oncology* **5**, 79-84 (1978).
470. Rodriguez, V.*, et al.* POMP combination chemotherapy of adult acute leukemia. *Cancer* **32**, 69-75 (1973).
471. Simone, J.V. Factors that influence haematological remission duration in acute lymphocytic leukaemia. *Br J Haematol* **32**, 465-472 (1976).
472. Armitage, J.O., Corder, M., Leimert, J., Dick, F. & Elliot, T. Advanced diffuse histiocytic lymphoma treated with cyclophosphamide, doxorubicin, vincristine, and prednisone (CHOP) without maintenance therapy. *Cancer treatment reports* **64**, 649-654 (1980).
473. Winick, N.J.*, et al.* Unexpected acute neurologic toxicity in the treatment of children with acute lymphoblastic leukemia. *JNCI: Journal of the National Cancer Institute* **84**, 252-256 (1992).
474. Howard, S.C., McCormick, J., Pui, C.-H., Buddington, R.K. & Harvey, R.D. Preventing and managing toxicities of high-dose methotrexate. *The oncologist* **21**, 1471-1482 (2016).
475. Saracco, P.*, et al.* Steroid withdrawal syndrome during steroid tapering in childhood acute lymphoblastic leukemia: a controlled study comparing prednisone versus dexamethasone in induction phase. *Journal of pediatric hematology/oncology* **27**, 141-144 (2005).
476. Lennard, L. The clinical pharmacology of 6-mercaptopurine. *European journal of clinical pharmacology* **43**, 329-339 (1992).
477. Brooks, S.V. & Faulkner, J.A. Contractile properties of skeletal muscles from young, adult and aged mice. *The Journal of physiology* **404**, 71-82 (1988).
478. Hayes, A.*, et al.* The Effect of Yearly-Dose Vitamin D Supplementation on Muscle Function in Mice. *Nutrients* **11**, 1097 (2019).
479. Foundation, A.C.R. Acute Lymphoblastic Leukaemia. Vol. 2016 (2016).
480. Harrison, C.J. Acute lymphoblastic leukemia. *Clinics in laboratory medicine* **31**, 631-647 (2011).

481. Pui, C.-H.*, et al.* Treating childhood acute lymphoblastic leukemia without cranial irradiation. *New England Journal of Medicine* **360**, 2730-2741 (2009).
482. Pui, C.-H. & Evans, W.E. Treatment of acute lymphoblastic leukemia. *New England Journal of Medicine* **354**, 166-178 (2006).
483. Thivat, E.*, et al.* Weight change during chemotherapy changes the prognosis in non metastatic breast cancer for the worse. *BMC cancer* **10**, 648 (2010).
484. Prat, F.*, et al.* Predictive factors for survival of patients with inoperable malignant distal biliary strictures: a practical management guideline. *Gut* **42**, 76-80 (1998).
485. Kiss, N., Isenring, E., Gough, K. & Krishnasamy, M. The prevalence of weight loss during (chemo) radiotherapy treatment for lung cancer and associated patient-and treatment-related factors. *Clinical nutrition* **33**, 1074-1080 (2014).
486. Einhorn, L.H. & Donohue, J. Cis-diamminedichloroplatinum, vinblastine, and bleomycin combination chemotherapy in disseminated testicular cancer. *Annals of internal medicine* **87**, 293-298 (1977).
487. Brinksma, A.*, et al.* Malnutrition in childhood cancer patients: a review on its prevalence and possible causes. *Critical reviews in oncology/hematology* **83**, 249-275 (2012).
488. Ward, E.*, et al.* Nutritional problems in children treated for medulloblastoma: Implications for enteral nutrition support. *Pediatric blood & cancer* **53**, 570-575 (2009).
489. Mittelman, A., Albert, D.J. & Murphy, G.P. Lomustine treatment of metastatic renal cell carcinoma. *JAMA* **225**, 32-35 (1973).
490. Costa, A.L.*, et al.* Prevention of nausea and vomiting in patients undergoing oral anticancer therapies for solid tumors. *BioMed research international* **2015**(2015).
491. Butte, N.F., Garza, C. & De Onis, M. Evaluation of the feasibility of international growth standards for school-aged children and adolescents. *The Journal of nutrition* **137**, 153-157 (2007).
492. Olshan, J.S.*, et al.* The effects of adjuvant chemotherapy on growth in children with medulloblastoma. *Cancer* **70**, 2013-2017 (1992).
493. Samuelsson, B.O., Márky, I., Rosberg, S. & Albertsson-Wikland, K. Growth and growth hormone secretion after treatment for childhood non-Hodgkin's lymphoma. *Medical and Pediatric Oncology: The Official Journal of SIOP—International Society of Pediatric Oncology (Societé Internationale d'Oncologie Pédiatrique* **28**, 27-34 (1997).
494. Thun-Hohenstein, L., Frisch, H. & Schuster, E. Growth after radiotherapy and chemotherapy in children with leukemia or lymphoma. *Hormone Research in Paediatrics* **37**, 91-95 (1992).
495. Langer, H.T.*, et al.* Muscle atrophy due to nerve damage is accompanied by elevated myofibrillar protein synthesis rates. *Frontiers in physiology* **9**, 1220 (2018).
496. Quasthoff, S. & Hartung, H.P. Chemotherapy-induced peripheral neuropathy. *Journal of neurology* **249**, 9-17 (2002).
497. Maynard, L.M.*, et al.* Childhood body composition in relation to body mass index. *Pediatrics* **107**, 344-350 (2001).
498. Gargiulo, S.*, et al.* Evaluation of growth patterns and body composition in C57Bl/6J mice using dual energy X-ray absorptiometry. *BioMed research international* **2014**(2014).
499. Flombaum, C.D. & Meyers, P.A. High-dose leucovorin as sole therapy for methotrexate toxicity. *Journal of clinical oncology* **17**, 1589-1589 (1999).

500. Kintzel, P.E. Anticancer drug—induced kidney disorders. *Drug safety* **24**, 19-38 (2001).
501. Ramsey, L.B.*, et al.* Consensus guideline for use of glucarpidase in patients with high-dose methotrexate induced acute kidney injury and delayed methotrexate clearance. *The oncologist* **23**, 52-61 (2018).
502. Magee, C.C. Acute Kidney Injury and Cancer: Incidence, Pathophysiology, Prevention/Treatment, and Outcomes. in *Core Concepts in Acute Kidney Injury* 133-143 (Springer, 2018).
503. Cody, E.M. & Dixon, B.P. Hemolytic uremic syndrome. *Pediatric Clinics* **66**, 235-246 (2019).
504. Salvadori, M. & Bertoni, E. Update on hemolytic uremic syndrome: diagnostic and therapeutic recommendations. *World journal of nephrology* **2**, 56 (2013).
505. Benz, K. & Amann, K. Thrombotic microangiopathy: new insights. *Current opinion in nephrology and hypertension* **19**, 242-247 (2010).
506. Padovani, L., Horan, G. & Ajithkumar, T. Radiotherapy advances in paediatric medulloblastoma treatment. *Clinical Oncology* **31**, 171-181 (2019).
507. Taran, S., Taran, R., Malipatil, N. & Haridas, K. Paediatric Medulloblastoma: An Updated Review. *West Indian Medical Journal* **65**(2016).
508. Kieffer, V.*, et al.* Intellectual, educational, and situation-based social outcome in adult survivors of childhood medulloblastoma. *Developmental neurorehabilitation* **22**, 19-26 (2019).
509. Ness, K.K.*, et al.* Physical performance limitations among adult survivors of childhood brain tumors. *Cancer* **116**, 3034-3044 (2010).
510. Harten, G.*, et al.* Slight impairment of psychomotor skills in children after treatment of acute lymphoblastic leukemia. *European journal of pediatrics* **142**, 189-197 (1984).
511. Vainionpää, L. Clinical neurological findings of children with acute lymphoblastic leukaemia at diagnosis and during treatment. *European journal of pediatrics* **152**, 115-119 (1993).
512. Wilson, C., Gawade, P. & Ness, K. Impairments that influence physical function among survivors of childhood cancer. *Children* **2**, 1-36 (2015).
513. Oeffinger, K.C. & Hudson, M.M. Long-term complications following childhood and adolescent cancer: Foundations for providing risk-based health care for survivors. *CA: a cancer journal for clinicians* **54**, 208-236 (2004).
514. Barreto, R.*, et al.* Chemotherapy-related cachexia is associated with mitochondrial depletion and the activation of ERK1/2 and p38 MAPKs. *Oncotarget* (2016).
515. Hirschey, M.D.*, et al.* SIRT3 deficiency and mitochondrial protein hyperacetylation accelerate the development of the metabolic syndrome. *Molecular cell* **44**, 177-190 (2011).
516. Ren, J., Pulakat, L., Whaley-Connell, A. & Sowers, J.R. Mitochondrial biogenesis in the metabolic syndrome and cardiovascular disease. *Journal of molecular medicine* **88**, 993-1001 (2010).
517. Bugger, H. & Abel, E.D. Molecular mechanisms for myocardial mitochondrial dysfunction in the metabolic syndrome. *Clinical science* **114**, 195-210 (2008).
518. James, A.M., Collins, Y., Logan, A. & Murphy, M.P. Mitochondrial oxidative stress and the metabolic syndrome. *Trends in endocrinology & metabolism* **23**, 429-434 (2012).

519. Schreurs, M., Kuipers, F. & Van Der Leij, F. Regulatory enzymes of mitochondrial β-oxidation as targets for treatment of the metabolic syndrome. *obesity reviews* **11**, 380-388 (2010).
520. Nicolson, G.L. Metabolic syndrome and mitochondrial function: molecular replacement and antioxidant supplements to prevent membrane peroxidation and restore mitochondrial function. *Journal of cellular biochemistry* **100**, 1352-1369 (2007).
521. De Haas, E.C*., et al.* The metabolic syndrome in cancer survivors. *The lancet oncology* **11**, 193-203 (2010).
522. Chueh, H.W. & Yoo, J.H. Metabolic syndrome induced by anticancer treatment in childhood cancer survivors. *Annals of pediatric endocrinology & metabolism* **22**, 82 (2017).
523. Oudin, C*., et al.* Prevalence and risk factors of the metabolic syndrome in adult survivors of childhood leukemia. *Blood, The Journal of the American Society of Hematology* **117**, 4442-4448 (2011).
524. thanga Tamilselvan, S., Scott, J.X. & Sneha, L. Metabolic syndrome in childhood cancer survivors. (American Society of Clinical Oncology, 2017).
525. Laker, R.C*., et al.* Short-term exercise training early in life restores deficits in pancreatic β-cell mass associated with growth restriction in adult male rats. *American Journal of Physiology-Endocrinology and Metabolism* **301**, E931-E940 (2011).
526. Kazemi-Bajestani, S.M.R., Mazurak, V.C. & Baracos, V. Computed tomography-defined muscle and fat wasting are associated with cancer clinical outcomes. in *Seminars in cell & developmental biology*, Vol. 54 2-10 (Elsevier, 2016).
527. Charles, J.P., Cappellari, O., Spence, A.J., Hutchinson, J.R. & Wells, D.J. Musculoskeletal geometry, muscle architecture and functional specialisations of the mouse hindlimb. *PloS one* **11**(2016).
528. Wang, L. & Kernell, D. Fibre type regionalisation in lower hindlimb muscles of rabbit, rat and mouse: a comparative study. *Journal of anatomy* **199**, 631-643 (2001).
529. Shortreed, K.E*., et al.* Muscle-specific adaptations, impaired oxidative capacity and maintenance of contractile function characterize diet-induced obese mouse skeletal muscle. *PloS one* **4**, e7293 (2009).
530. Bioscience, S. XF24 Extracellular Flux Analyzer and Prep Station Installation and Operation manual. **3**(2010).
531. Technologies, A. Agilent Seahorse XF Cell Mito Stress Test Kit; User Guide Kit 103015-100. (2019).
532. Bennett, J.M*., et al.* Proposals for the Classification of the Acute Leukaemias French-American-British (FAB) Co-operative Group. *Br J Haematol* **33**, 451-458 (1976).
533. Schultz, K.R*., et al.* Risk-and response-based classification of childhood B-precursor acute lymphoblastic leukemia: a combined analysis of prognostic markers from the Pediatric Oncology Group (POG) and Children9s Cancer Group (CCG). *Blood* **109**, 926-935 (2007).
534. Båvenholm, P.N., Pigon, J., Östenson, C.-G. & Efendic, S. Insulin sensitivity of suppression of endogenous glucose production is the single most important determinant of glucose tolerance. *Diabetes* **50**, 1449-1454 (2001).
535. Stefan, N*., et al.* Plasma adiponectin and endogenous glucose production in humans. *Diabetes care* **26**, 3315-3319 (2003).

536. Kowalski, G.M., Moore, S.M., Hamley, S., Selathurai, A. & Bruce, C.R. The effect of ingested glucose dose on the suppression of endogenous glucose production in humans. *Diabetes* **66**, 2400-2406 (2017).
537. Lund, A.*, et al.* Higher endogenous glucose production during OGTT vs isoglycemic intravenous glucose infusion. *The Journal of Clinical Endocrinology & Metabolism* **101**, 4377-4384 (2016).
538. Alatrach, M., Agyin, C., Adams, J., DeFronzo, R.A. & Abdul-Ghani, M.A. Decreased basal hepatic glucose uptake in impaired fasting glucose. *Diabetologia* **60**, 1325-1332 (2017).
539. Shannon, C.*, et al.* Effect of chronic hyperglycemia on glucose metabolism in subjects with normal glucose tolerance. *Diabetes* **67**, 2507-2517 (2018).
540. Cubeddu, L.X., Hoffmann, I.S., Fuenmayor, N.T. & Finn, A.L. Efficacy of ondansetron (GR 38032F) and the role of serotonin in cisplatin-induced nausea and vomiting. *New England Journal of Medicine* **322**, 810-816 (1990).
541. McQuade, R.M.*, et al.* OXALIPLATIN-INDUCED ENTERIC NEURONAL LOSS AND GASTROINTESTINAL DYSFUNCTION IS ALLEVIATED BY CO-TREATMENT WITH BGP-15 *Under Submission* (2016).
542. McQuade, R.M.*, et al.* Role of oxidative stress in oxaliplatin-induced enteric neuropathy and colonic dysmotility in mice. *British journal of pharmacology* **173**, 3502-3521 (2016).
543. Austin, J. & Marks, D. Hormonal regulators of appetite. *International journal of pediatric endocrinology* **2009**, 1-9 (2008).
544. Rickard, K.A., Coates, T.D., Grosfeld, J.L., Weetman, R.M. & Baehner, R.L. The value of nutrition support in children with cancer. *Cancer* **58**, 1904-1910 (1986).
545. Donaldson, S.S., Wesley, M.N., DeWys, W.D., Suskind, R.M. & Jaffe, N. A study of the nutritional status of pediatric cancer patients. *American Journal of Diseases of Children* **135**, 1107-1112 (1981).
546. Tandon, S., Moulik, N.R., Kumar, A., Mahdi, A.A. & Kumar, A. Effect of pre-treatment nutritional status, folate and vitamin B12 levels on induction chemotherapy in children with acute lymphoblastic leukemia. *Indian pediatrics* **52**, 385-389 (2015).
547. Goddard, E., Cohen, J., Bramley, L., Wakefield, C.E. & Beck, E.J. Dietary intake and diet quality in children receiving treatment for cancer. *Nutrition reviews* **77**, 267-277 (2019).
548. Leong, D.P.*, et al.* Prognostic value of grip strength: findings from the Prospective Urban Rural Epidemiology (PURE) study. *The Lancet* **386**, 266-273 (2015).
549. Tyrovolas, S.*, et al.* Factors associated with skeletal muscle mass, sarcopenia, and sarcopenic obesity in older adults: a multi-continent study. *Journal of cachexia, sarcopenia and muscle* **7**, 312-321 (2016).
550. Yoo, J.-I., Choi, H. & Ha, Y.-C. Mean hand grip strength and cut-off value for sarcopenia in Korean adults using KNHANES VI. *Journal of Korean medical science* **32**, 868-872 (2017).
551. Naito, T.*, et al.* Skeletal muscle depletion during chemotherapy has a large impact on physical function in elderly Japanese patients with advanced non–small-cell lung cancer. *BMC cancer* **17**, 571 (2017).
552. Extermann, M.*, et al.* Impact of chemotherapy on medium-term physical function and activity of older breast cancer survivors, and associated biomarkers. *Journal of geriatric oncology* **8**, 69-75 (2017).

553. Morishita, S.*, et al.* Assessment of the Mini-Balance Evaluation Systems Test, Timed Up and Go test, and body sway test between cancer survivors and healthy participants. *Clinical Biomechanics* **69**, 28-33 (2019).
554. Mangia, A.S.*, et al.* What clinical, functional, and psychological factors before treatment are predictors of poor quality of life in cancer patients at the end of chemotherapy? *Revista da Associação Médica Brasileira* **63**, 978-987 (2017).
555. Ness, K.K.*, et al.* Frailty in childhood cancer survivors. *Cancer* **121**, 1540-1547 (2015).
556. McQuade, R.M.*, et al.* Role of Oxidative Stress in Oxaliplatin-Induced Enteric Neuropathy and Colonic Dysmotility in Mice. *British Journal of Pharmacology* (2016).
557. Renn, C.L.*, et al.* Multimodal assessment of painful peripheral neuropathy induced by chronic oxaliplatin-based chemotherapy in mice. *Molecular pain* **7**, 1 (2011).
558. Trivedi, M.S., Hershman, D.L. & Crew, K.D. Management of chemotherapy-induced peripheral neuropathy. *American Journal of Hematology/Oncology®* **11**(2015).
559. Dolan, M.E.*, et al.* Clinical and genome-wide analysis of cisplatin-induced peripheral neuropathy in survivors of adult-onset cancer. *Clinical Cancer Research* **23**, 5757-5768 (2017).
560. Starobova, H. & Vetter, I. Pathophysiology of chemotherapy-induced peripheral neuropathy. *Frontiers in molecular neuroscience* **10**, 174 (2017).
561. Brackenbury, J. & Holloway, S. Age and exercise effects on mitochondrial density and capillary fibre ratio in bird leg muscle. *British poultry science* **32**, 645-653 (1991).
562. Passos, J.F., von Zglinicki, T. & Kirkwood, T.B. Mitochondria and ageing: winning and losing in the numbers game. *Bioessays* **29**, 908-917 (2007).
563. Allen, R.E. & Rankin, L.L. Regulation of satellite cells during skeletal muscle growth and development. *Proceedings of the Society for Experimental Biology and Medicine* **194**, 81-86 (1990).
564. Ogawa, S., Yakabe, M. & Akishita, M. Age-related sarcopenia and its pathophysiological bases. *Inflammation and regeneration* **36**, 1-6 (2016).
565. Bluhm, E.C.*, et al.* Cause-specific mortality and second cancer incidence after non-Hodgkin lymphoma: a report from the Childhood Cancer Survivor Study. *Blood, The Journal of the American Society of Hematology* **111**, 4014-4021 (2008).
566. Cairo, M.S.*, et al.* Results of a randomized international study of high-risk central nervous system B non-Hodgkin lymphoma and B acute lymphoblastic leukemia in children and adolescents. *Blood* **109**, 2736-2743 (2006).
567. Park, S.-S.*, et al.* Treadmill exercise ameliorates chemotherapy-induced muscle weakness and central fatigue by enhancing mitochondrial function and inhibiting apoptosis. *International neurourology journal* **23**, S32 (2019).
568. Twist, C.J.*, et al.* Defining risk factors for chemotherapeutic intervention in infants with stage 4S neuroblastoma: a report from Children's Oncology Group Study ANBL0531. *Journal of Clinical Oncology* **37**, 115 (2019).
569. Bartels, H.C.*, et al.* A meta-analysis of morbidity and mortality in primary cytoreductive surgery compared to neoadjuvant chemotherapy in advanced ovarian malignancy. *Gynecologic oncology* **154**, 622-630 (2019).
570. Dulloo, A.G., Jacquet, J., Seydoux, J. & Montani, J.-P. The thrifty 'catch-up fat'phenotype: its impact on insulin sensitivity during growth trajectories to obesity and metabolic syndrome. *International journal of obesity* **30**, S23 (2006).
571. Burke, A., Krueger, J. & Wistinghausen, B. Novel Therapies in Paediatric NHL. in *Non-Hodgkin's Lymphoma in Childhood and Adolescence* 315-335 (Springer, 2019).

572. Swain, S.M., Whaley, F.S. & Ewer, M.S. Congestive heart failure in patients treated with doxorubicin: a retrospective analysis of three trials. *Cancer: Interdisciplinary International Journal of the American Cancer Society* **97**, 2869-2879 (2003).
573. Von Hoff, D.D*., et al.* Risk factors for doxorubicin-lnduced congestive heart failure. *Annals of internal medicine* **91**, 710-717 (1979).
574. Rigacci, L*., et al.* Liposome-encapsulated doxorubicin in combination with cyclophosphamide, vincristine, prednisone and rituximab in patients with lymphoma and concurrent cardiac diseases or pre-treated with anthracyclines. *Hematological oncology* **25**, 198-203 (2007).
575. Sonis, S.T. Mucositis: the impact, biology and therapeutic opportunities of oral mucositis. *Oral oncology* **45**, 1015-1020 (2009).
576. Peterson, D.E., Jones, J.B. & Petit, R.G. Randomized, placebo-controlled trial of Saforis for prevention and treatment of oral mucositis in breast cancer patients receiving anthracycline-based chemotherapy. *Cancer* **109**, 322-331 (2007).
577. Peterson, D., Bensadoun, R.-J., Roila, F. & Group, E.G.W. Management of oral and gastrointestinal mucositis: ESMO Clinical Practice Guidelines. *Annals of oncology* **22**, vi78-vi84 (2011).
578. Liang, R., Chen, G.-Y., Fu, S.-X., Zhong, J. & Ma, Y. Benefit of oral nutritional supplements for children with acute lymphoblastic leukaemia during remissioninduction chemotherapy: A quasi-experimental study. *Asia Pacific journal of clinical nutrition* **27**, 144 (2018).
579. Rathe, M*., et al.* Bovine Colostrum Against Chemotherapy-Induced Gastrointestinal Toxicity in Children With Acute Lymphoblastic Leukemia: A Randomized, Double-Blind, Placebo-Controlled Trial. *Journal of Parenteral and Enteral Nutrition* (2019).
580. Jameson, J.L. & De Groot, L.J. *Endocrinology-E-Book: Adult and Pediatric,(Expert Consult Premium Edition-Enhanced Online Features and Print)*, (Elsevier Health Sciences, 2010).
581. Halton, J.M., Atkinson, S.A. & Barr, R.D. Growth and body composition in response to chemotherapy in children with acute lymphoblastic leukemia. *International Journal of Cancer* **78**, 81-84 (1998).
582. Kerpel-Fronius, E. & Kaiser, E. Hypoglycaemia in infantile malnutrition. *Acta Pædiatrica* **56**, 119-127 (1967).
583. Bandsma, R.H*., et al.* Mechanisms behind decreased endogenous glucose production in malnourished children. *Pediatric research* **68**, 423 (2010).
584. Mittelman, S.D., Fu, Y.-Y., Rebrin, K., Steil, G. & Bergman, R.N. Indirect effect of insulin to suppress endogenous glucose production is dominant, even with hyperglucagonemia. *The Journal of clinical investigation* **100**, 3121-3130 (1997).
585. Kavazis, A.N., Smuder, A.J. & Powers, S.K. *Effects of short-term endurance exercise training on acute doxorubicin-induced FoxO transcription in cardiac and skeletal muscle*, (2014).
586. Campbell, T.L. & Quadrilatero, J. Data on skeletal muscle apoptosis, autophagy, and morphology in mice treated with doxorubicin. *Data in brief* **7**, 786-793 (2016).
587. Al-Majid, S. & McCarthy, D.O. Cancer-induced fatigue and skeletal muscle wasting: the role of exercise. *Biological research for nursing* **2**, 186-197 (2001).
588. Groninger, E., Boer, M.-D., De Graaf, S., Kamps, W. & De Bont, E. Vincristine induced apoptosis in acute lymphoblastic leukaemia cells: a mitochondrial controlled

pathway regulated by reactive oxygen species? *International journal of oncology* **21**, 1339-1345 (2002).
589. Espinosa, A., Henríquez-Olguín, C. & Jaimovich, E. Reactive oxygen species and calcium signals in skeletal muscle: a crosstalk involved in both normal signaling and disease. *Cell Calcium* **60**, 172-179 (2016).
590. Sakellariou, G.K.*, et al.* Mitochondrial ROS regulate oxidative damage and mitophagy but not age-related muscle fiber atrophy. *Scientific reports* **6**(2016).
591. Wang, H.-w.*, et al.* Mitochondrial respiratory chain dysfunction mediated by ROS is a primary point of fluoride-induced damage in Hepa1-6 cells. *Environmental Pollution* **255**, 113359 (2019).
592. Peoples, J.N., Saraf, A., Ghazal, N., Pham, T.T. & Kwong, J.Q. Mitochondrial dysfunction and oxidative stress in heart disease. *Experimental & Molecular Medicine* **51**, 1-13 (2019).
593. Pérez-Carreras, M.*, et al.* Defective hepatic mitochondrial respiratory chain in patients with nonalcoholic steatohepatitis. *Hepatology* **38**, 999-1007 (2003).
594. Powers, S.K., Kavazis, A.N. & McClung, J.M. Oxidative stress and disuse muscle atrophy. *Journal of Applied Physiology* **102**, 2389-2397 (2007).
595. Sandri, M. *Signaling in Muscle Atrophy and Hypertrophy*, (2008).
596. Ventadour, S. & Attaix, D. Mechanisms of skeletal muscle atrophy. *Current opinion in rheumatology* **18**, 631-635 (2006).
597. Speth, P., Van Hoesel, Q. & Haanen, C. Clinical pharmacokinetics of doxorubicin. *Clinical pharmacokinetics* **15**, 15-31 (1988).
598. Lizcano, J.M. & Alessi, D.R. The insulin signalling pathway. *Current biology* **12**, R236-R238 (2002).
599. Kim, J.-a., Wei, Y. & Sowers, J.R. Role of mitochondrial dysfunction in insulin resistance. *Circulation research* **102**, 401-414 (2008).
600. Celichowski, J.*, et al.* Changes in contractile properties of motor units of the rat medial gastrocnemius muscle after spinal cord transection. *Experimental physiology* **91**, 887-895 (2006).
601. Uchida, T.*, et al.* Reactive oxygen species upregulate expression of muscle atrophy-associated ubiquitin ligase Cbl-b in rat L6 skeletal muscle cells. *American Journal of Physiology-Cell Physiology* **314**, C721-C731 (2018).
602. Jackson, M.*, et al.* Oxidative stress in skeletal muscle: Unraveling the potential beneficial and deleterious roles of reactive oxygen species. in *Oxidative Stress* 713-733 (Elsevier, 2020).
603. Huang, L.-s., Cobessi, D., Tung, E.Y. & Berry, E.A. Binding of the respiratory chain inhibitor antimycin to the mitochondrial bc1 complex: a new crystal structure reveals an altered intramolecular hydrogen-bonding pattern. *Journal of molecular biology* **351**, 573-597 (2005).
604. Sebastián, D. & Zorzano, A. Self-Eating for Muscle Fitness: Autophagy in the Control of Energy Metabolism. *Developmental Cell* **54**, 268-281 (2020).
605. Bagherniya, M., Butler, A.E., Barreto, G.E. & Sahebkar, A. The effect of fasting or calorie restriction on autophagy induction: A review of the literature. *Ageing research reviews* **47**, 183-197 (2018).
606. Kola, B. Role of AMP-activated protein kinase in the control of appetite. *Journal of neuroendocrinology* **20**, 942-951 (2008).

607. Di Prospero, N.A*., et al.* Safety, tolerability, and pharmacokinetics of high-dose idebenone in patients with Friedreich ataxia. *Arch Neurol* **64**, 803-808 (2007).
608. Tomilov, A., Allen, S., Hui, C.K., Bettaieb, A. & Cortopassi, G. Idebenone is a cytoprotective insulin sensitizer whose mechanism is Shc inhibition. *Pharmacological Research* **137**, 89-103 (2018).
609. Rhea, E.M. & Banks, W.A. Role of the blood-brain barrier in central nervous system insulin resistance. *Frontiers in neuroscience* **13**, 521 (2019).
610. Feng, Z., Smith, J.A., Gueven, N. & Quirino, J.P. Metabolic Stability of New Mito-Protective Short-Chain Naphthoquinones. *Pharmaceuticals* **13**, 29 (2020).
611. Grattagliano, I., Calamita, G., Cocco, T., Wang, D.Q. & Portincasa, P. Pathogenic role of oxidative and nitrosative stress in primary biliary cirrhosis. *World Journal of Gastroenterology: WJG* **20**, 5746 (2014).
612. Shearn, C.T., Orlicky, D.J. & Petersen, D.R. Dysregulation of antioxidant responses in patients diagnosed with concomitant primary sclerosing cholangitis/inflammatory bowel disease. *Experimental and molecular pathology* **104**, 1-8 (2018).
613. Simůnek, T*., et al.* Anthracycline-induced cardiotoxicity: overview of studies examining the roles of oxidative stress and free cellular iron. *Pharmacol Rep* **61**, 154-171 (2009).
614. Cappetta, D*., et al.* Oxidative stress and cellular response to doxorubicin: a common factor in the complex milieu of anthracycline cardiotoxicity. *Oxidative medicine and cellular longevity* **2017**(2017).
615. Rocca, C., Pasqua, T., Cerra, M.C. & Angelone, T. Cardiac damage in anthracyclines therapy: focus on oxidative stress and inflammation. *Antioxidants & Redox Signaling* **32**, 1081-1097 (2020).
616. Fuentes, E.N*., et al.* IGF-I/PI3K/Akt and IGF-I/MAPK/ERK pathways in vivo in skeletal muscle are regulated by nutrition and contribute to somatic growth in the fine flounder. *American Journal of Physiology-Regulatory, Integrative and Comparative Physiology* **300**, R1532-R1542 (2011).
617. Ji, L.L. Modulation of skeletal muscle antioxidant defense by exercise: role of redox signaling. *Free Radical Biology and Medicine* **44**, 142-152 (2008).
618. Mattson, M.P. Hormesis defined. *Ageing research reviews* **7**, 1-7 (2008).
619. Eshima, H*., et al.* Dysfunction of muscle contraction with impaired intracellular Ca2+ handling in skeletal muscle and the effect of exercise training in male db/db mice. *Journal of Applied Physiology* **126**, 170-182 (2019).
620. Allen, D.G., Whitehead, N.P. & Froehner, S.C. Absence of dystrophin disrupts skeletal muscle signaling: roles of Ca2+, reactive oxygen species, and nitric oxide in the development of muscular dystrophy. *Physiological reviews* **96**, 253-305 (2016).
621. Di Meo, S., Napolitano, G. & Venditti, P. Mediators of physical activity protection against ROS-linked skeletal muscle damage. *International journal of molecular sciences* **20**, 3024 (2019).
622. Vallejo-Illarramendi, A., Toral-Ojeda, I., Aldanondo, G. & de Munain, A.L. Dysregulation of calcium homeostasis in muscular dystrophies. *Expert reviews in molecular medicine* **16**(2014).
623. Miyata, H., Lakatta, E.G., Stern, M.D. & Silverman, H.S. Relation of mitochondrial and cytosolic free calcium to cardiac myocyte recovery after exposure to anoxia. *Circulation research* **71**, 605-613 (1992).

624. Qiu, J.*, et al.* Mechanistic role of reactive oxygen species and therapeutic potential of antioxidants in denervation-or fasting-induced skeletal muscle atrophy. *Frontiers in physiology* **9**, 215 (2018).
625. Talvensaari, K. Growth impairment in long-term survivors of childhood cancer. *Reactions* **592**, 16 (1996).
626. Bhakta, N.*, et al.* The cumulative burden of surviving childhood cancer: an initial report from the St Jude Lifetime Cohort Study (SJLIFE). *The Lancet* **390**, 2569-2582 (2017).
627. Santilli, V., Bernetti, A., Mangone, M. & Paoloni, M. Clinical definition of sarcopenia. *Clinical cases in mineral and bone metabolism* **11**, 177 (2014).